INVESTIGATIONS ON LOW-VALENT GROUP 8 AND 9 METALLORADICALS

Thesis by

Ayumi Takaoka

In Partial Fulfillment of the Requirements for the Degree of

Doctor of Philosophy

California Institute of Technology

Pasadena, CA

2012

(Defended January 17, 2012)

Acknowledgments

I would like to first and foremost thank my research advisor, Professor Jonas C. Peters, for taking me into his group in 2007 and advising me throughout my graduate career. In addition to being a truly brilliant principle investigator, Jonas has always been incredibly patient in teaching me the fundamental process of research, and I am extremely grateful for this. As previous graduates of this research group have also stated, much of my scientific thought process operates according to how I believe Jonas would proceed in solving difficult problems. Indeed, I believe that I have been able to conduct research most efficiently by thinking about the types of questions Jonas would ask during our group meetings. Simply put, I could not have asked for a better advisor. Jonas also gave me the opportunity to pursue my graduate studies at two of the best research institutions in the world, for which I feel very fortunate. This unique experience gave me a chance to work at two very distinct environments and provided me with the confidence in taking an industrial position in Japan, which is a place where I have not lived for over 13 years and expect to be quite different from both MIT and Caltech.

Professors Dick Schrock and Theo Agapie were the chairs of my thesis committee at MIT and Caltech, respectively. Dick was always supportive of the chemistry I was pursuing at MIT, and was especially excited about the dinitrogen complexes that I was synthesizing at the time. He was always available for scientific discussion, and he even spent time with me for our annual thesis chair meeting before our group left for Caltech, even through he no longer had any obligations to do so. Theo was also very supportive of my research at Caltech and was a great thesis chair to have. His criticism was extremely constructive, and his assessment of my research was always positive, regardless of

content. Many of the questions that he raised during our meetings helped me think more deeply about my research. Theo also happens to be married to one of my very good friends, Smaranda, and was kind enough to invite me to their wedding. I wish the best to both Theo and Smaranda in the future. Other members of my two committees, Professors Steve Lippard at MIT and Harry Gray and Mitchio Okumura at Caltech, were also instrumental in providing me with great advice through the years.

I owe a tremendous amount to my classmates, Samantha MacMillan, Seth Mickenberg, Daniel Suess, and Charlene Tsay, who joined the Peters group with me in 2007. Each and every member of this group has been a great friend and has helped me keep my sanity through tough times. I will greatly miss them. I have also been fortunate to overlap with a large number of brilliant co-workers. I would like to name a few in detail that have particularly been helpful. Aside from Jonas, Dr. Neal Mankad probably influenced my approach to research the most, and I am honored to coauthor a publication with him. He also introduced me to fantasy football, which has been one of my favorite pastimes outside of research. Dr. Arjun Mendiratta and Laura Gerber also coauthored publications with me. Professor Yunho Lee was an incredible boxmate who taught me many experimental techniques. Dr. Marc-Etienne Moret was one of my best sources of chemical knowledge, and was also a great lunch buddy. Kenny Lotito and Jon Rittle were my other boxmates who had to endure my presence while conducting research inside the glovebox. Dr. Hill Harman, Alicia Chang, and Henry Fong are friends from my undergraduate research group, and I will miss not seeing them everyday. John Anderson was my fantasy football rival and was kind enough to invite me to his residence for multiple football games. I would also like to thank my other co-workers over the years,

Professor Nate Sczymczak, Professor Louise Berben, Dr. Ning Jin, Dr. Caroline Sauoma, Dr. Chris Uyeda, Dr. Charles McCrory, and Sid Creutz.

I could not have performed my research without the competence of the technical staff at both MIT and Caltech. Dr. Peter Müller and Larry Henling were the X-ray crystallographers that helped me at the two institutions, respectively. Dr. Jeff Simpson, Anne Gorham, and Dr. David Vandervelde were staff at the NMR facilities and were always helpful in setting up NMR experiments that were beyond my understanding. Dr. Angelo DiBilio taught me how to measure an EPR spectrum.

I have been very fortunate to be surrounded by a great group of friends outside the Peters group at both MIT and Caltech. Julia Kozhukh and Shuang Liu were my friends at MIT, and I wish the best for both of them in their future. Rachel Klet was a person I first met at the Caltech visiting weekend, and she introduced me to numerous delicious cuisines throughout this area. Hidehiko Inagaki, Akihisa Goban, and Taisuke Imai are members of the Japanese community at Caltech whom I have had a great time with. In addition to these people, countless others have been kind and helpful to me.

I would also like to thank the entire MIT and Caltech community. Both institutions were incredible research environments. In fact, I had such a nice time at MIT that I was somewhat hesitant to move from Cambridge to Pasadena because I thought it could only get worse. I am fortunate that I was wrong and that the Caltech community as a whole has been extremely welcoming and friendly.

Finally, I could not have accomplished anything that I have these past few years without the support of my parents, Jun and Tomoko Takaoka, and my sister, Haruka

Takaoka. I look forward to living closer to my family in the coming years. Last but not least, I am indebted to Hazuki Nakatani for providing moral support over the years.

The past few years have been absolutely incredible. This experience will probably be one of the biggest highlights of my life.

Abstract

Tetradentate, monoanionic, tris(phosphino)silyl ligands were chelated to group 8 and 9 transition metals to stabilize complexes with unusual oxidation states and/or geometries. Initial studies with the $[SiP^{Ph}_3]^-$ ligand on ruthenium established the flexibility of this ancillary ligand in stabilizing complexes with strongly *trans* influencing ligands in *trans* dispositions. A related ligand scaffold, $[SiP^{iPr}_3]^-$, was subsequently used to stabilize mononuclear complexes of Ru(I) and Os(I), the first examples to be isolated and thoroughly chracterized. EPR spectroscopy and DFT calculations supported their metalloradical character, and further studies highlighted their reactivity in both one- and two-electron redox processes. The ability of the $[SiP^{iPr}_3]^-$ scaffold to stabilize d^7 metalloradicals of group 8 metals was extended to group 9 metals, and a series of d^7 complexes of cobalt, rhodium, and iridium were synthesized in which their ancillary ligands, oxidation states, spin states, and geometry are conserved. Similar to the previously reported $[SiP^{iPr}_3]Fe(N_2)$ complex, the related $[SiP^{iPr}_3]Ru(N_2)$ complex was shown to exhibit N−N coupling of organic azides to yield azoarenes catalytically. Detailed mechanistic studies conclusively showed that the Ru(III) imide species, whose iron analog is the key intermediate in the $[SiP^{iPr}_3]Fe$ system, is not involved in the mechanism for the $[SiP^{iPr}_3]Ru$ system. Instead, a mechanism in which free nitrene is released during the catalytic cyle is favored. Finally, hybrid ligands with multiple thioether donors in place of phosphine donors on the $[SiP^{R}_3]^-$ scaffold were synthesized to stabilize a number of dinitrogen complex of iron. These complexes featured rare examples of S−Fe−N_2 linkages.

Table of Contents

List of Figures

List of Table

List of Abbreviations

Ad	1-Adamantyl
Anal	Analysis
Ar	Generic aryl group
Ar^F	3,5-$(CF_3)C_6H_3$
ArN=NAr	Azoarene
atm	Atmosphere
br	Broad
calcd	Calculated
cat	Catecholate
CCD	Charge-coupled device
cm	Centimeter
cm^{-1}	Wave number
COD	Cyclooctadiene
Cp	Cyclopentadienyl
Cp*	Pentamethylcyclopentadienyl
CV	Cyclic voltammetry
Cy	Cyclohexyl
d	Doublet *or* deuterium
D	deuterium
d^x	d-electron count of x
d_x	Compound with x deuterium atoms
dd	Doublet of doublets

deg	Degree
DFT	Density Functional Theory
dtbpe	1,2-Bis(di-*tert*-butylphosphino)ethane
E	Generic main-group element
e	Electron
EPR	Electron paramagnetic resonance
equiv	Equivalents
esp	α,α,α’,α’-tetramethyl-1,3-benzenedipropionate
eu	Entropy units
Et	Ethyl
F	Structure factor
Fc	Ferrocene
FeMoco	Iron-Molybdenum cofactor
G	Gauss
g	Gram
g	g-factor
g_{iso}	Isotropic g-factor
g_{max}	Maximum anisotropic g-tensor
g_{min}	Minimum anisotropic g-tensor
GHz	Gigahertz
HOMO	Highest occupied molecular orbital
Hz	Hertz
I	Nuclear Spin

Inc	Incorporated
*i*Pr	*iso*-Propyl
IR	Infrared
ISC	Intersystem crossing
J	NMR coupling constant
J_{xy}	NMR coupling constant between nuclei x and y
K	Kelvin
Kcal	Kilocalorie
KIE	Kinetic isotope effect
L	Generic neutral ligand
LUMO	Lowest unoccupied molecular orbital
M	Generic transition metal *or* molar
m	Multiplet
m	*meta*
Me	Methyl
Mes	Mesityl
MeTHF	Methyltetrahydrofuran
mg	Milligram
MHz	Megahertz
min	Minutes
mL	Milliliter
mM	Millimolar
mm	Millimeter

mmol	Millimole
MO	Molecular orbital
mol	Mole
ms	Millisecond
*n*Bu	*n*-Butyl
NIR	Near infrared
nm	Nanometer
NMR	Nuclear magnetic resonance
N_xH_y	General nitrogenous ligand with x N and y H atoms
o	*ortho*
p	*para*
Ph	Phenyl
$PhBP^{Ph}_3$	$PhB(CH_2PPh_2)_3^-$
PP3	$P(CH_2CH_2PPh_2)_3$
ppm	Parts per million
q	Quartet
R	Generic organic group *or* R-factor
ref	Reference
RT	Room temperature
S	Spin
s	Singlet *or* second
SD	Spin density
SiP^R_3	$(2\text{-}R_2PC_6H_4)_3Si^-$

SOMO	Singly occupied molecular orbital
t	Triplet
T_{1min}	Minimum relaxation time
TBA	Tetra-*n*-butyl ammonium
TBP	Trigonal bipyramidal
*t*Bu	*tert*-Butyl
td	Triplet of doublets
Tf	SO_2CF_3
THF	Tetrahydrofuran
TPB	$(2\text{-}i\text{Pr}_2\text{C}_6\text{H}_4)_3\text{B}$
UV	Ultraviolet
V	Volt
VIS	Visible
vs	Versus
wR	Weighted R-factor
X	Generic anionic ligand
XRD	X-ray diffraction
HSQC	Heteronuclear single-quantum correlation spectroscopy
δ	Chemical shift
ε	Extinction coefficient in units of M^{-1} cm^{-1}
η^x	Hapticity of order x
μ-X	Bridging X ligand
μ_B	Bohr magneton

μ_{eff}	Effective magnetic moment
μL	Microliter
ν_{xy}	Frequency between atoms x and y
Σ	Summation
τ	Index of trigonality for 5-coordinate complexes
°	Degree
Δ	Heat *or* difference
°C	Degrees Celsius
Å	Angstrom
σ	Sigma symmetry orbital
π	Pi symmetry orbital
^{1}H	Hydrogen-1
^{11}B	Boron-11
^{13}C	Carbon-13
^{15}N	Nitrogen-15
^{19}F	Fluorine-19
^{29}Si	Silicon-29
^{31}P	Phosphorus-31
$\{^{1}H\}$	Proton-decoupled
6-311G, etc.	Basis sets for DFT
B3LYP, etc.	DFT functionals

Chapter 1: Introduction

1.1 Opening Remarks

Low-valent metalloradicals of the late 2nd and 3rd row transition metals are reactive species that generally cannot be isolated and require *in situ* characterization.[1] To date, these S = ½ species have largely been treated as chemical curiosities, exhibiting interesting spectroscopic properties but rarely displaying controlled reactivity. Several examples in the literature that exhibit well-defined behavior, however, point to the potential that these reactive species possess in undergoing challenging chemical transformations.[2] By virtue of possessing a metal-centered radical, these species tend to undergo one-electron transformations, highlighting reactivity that is orthogonal to the two-electron pathways that their closed-shell analogs typically proceed through. Thus, controlling the reactivity of these species may lead to transformations that cannot be realized with their more common diamagnetic congeners.

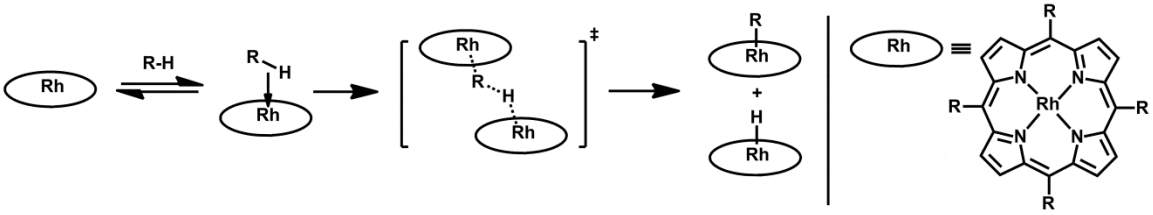

Scheme 1.1.

A classic example of well-defined reactivity exhibited by low-valent 2nd and 3rd row metalloradicals is the activation of C−H bonds by Rh(II) porphyrin complexes.[3] These metalloradicals, which exist in equilibrium with their dimers to a degree that is dependent on the substituent on the *meso* position of the porphyrin macrocycle, cooperatively act with a second species to bimolecularly cleave unactivated C−H bonds, including those of methane (Scheme 1.1). The stability of the resulting Rh(III) species, however, limits the usefulness of this transformation towards catalysis. Similarly, while other well-defined

stoichiometric transformations by related metalloradicals have been demonstrated previously[1] these species have rarely been invoked in catalytic reactions.[4]

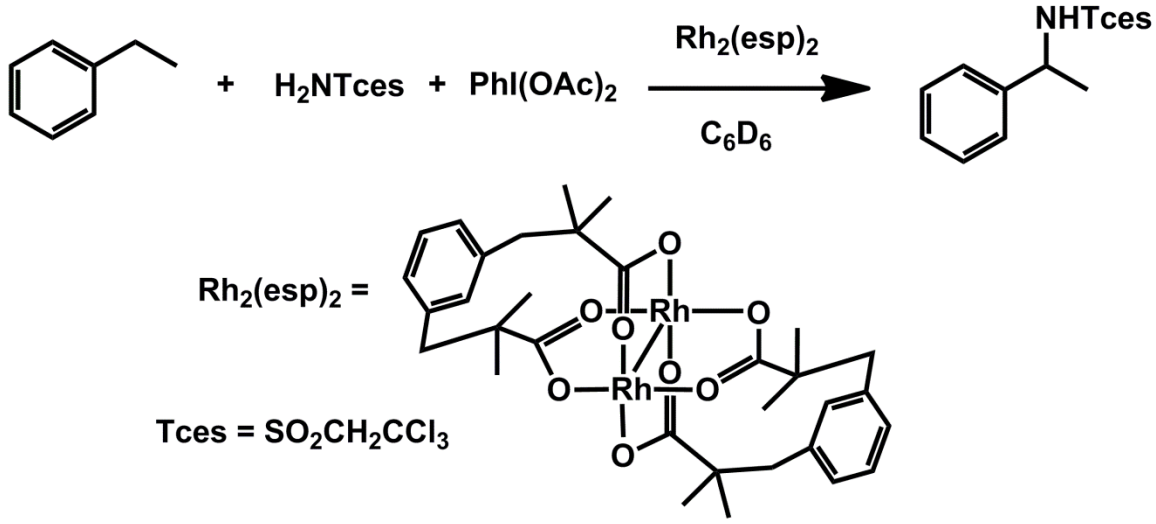

Scheme 1.2.

A more recent example that proposes the intermediacy of a low-valent Rh metalloradical in catalysis has been reported by Berry.[5] These researchers followed the initial studies of intermolecular C−H amination by Du Bois,[6] who utilized a chelating dicarboxylate to prepare the dirhodium tetracarboxylate complex, $Rh_2(esp)_2$ (esp = α,α,α',α'-tetramethyl-1,3-benzenedipropionate). In Berry's studies, two distinct reaction regimes were noticed in the C−H amination of ethylbenzene using the $Rh_2(esp)_2$ catalyst (Scheme 1.2). The first regime occurred during the early stages of the reaction and was characterized by a fast rate of product formation. The rate of product formation rapidly dropped after about 30% conversion, however, at which point the second reaction regime continued to yield product, albeit at a slower rate. Through careful mechanistic studies, Berry concluded that the two reaction regimes underwent distinct mechanisms to access a common rhodium nitrene intermediate, which is responsible for insertion of the nitrene group into a C−H bond. Specifically, the fast regime was proposed to involve the well

recognized nitrene transfer mechanism,[7] in which the *in situ* generated compound, PhI=NR, reacts with the catalyst to yield the rhodium nitrene complex (Scheme 1.3). In contrast, the second regime was proposed to involve successive proton/electron loss from a coordinated amine ligand to yield the same nitrene intermediate through one-electron transformations that involves the intermediacy of a Rh(II)/Rh(III) species.

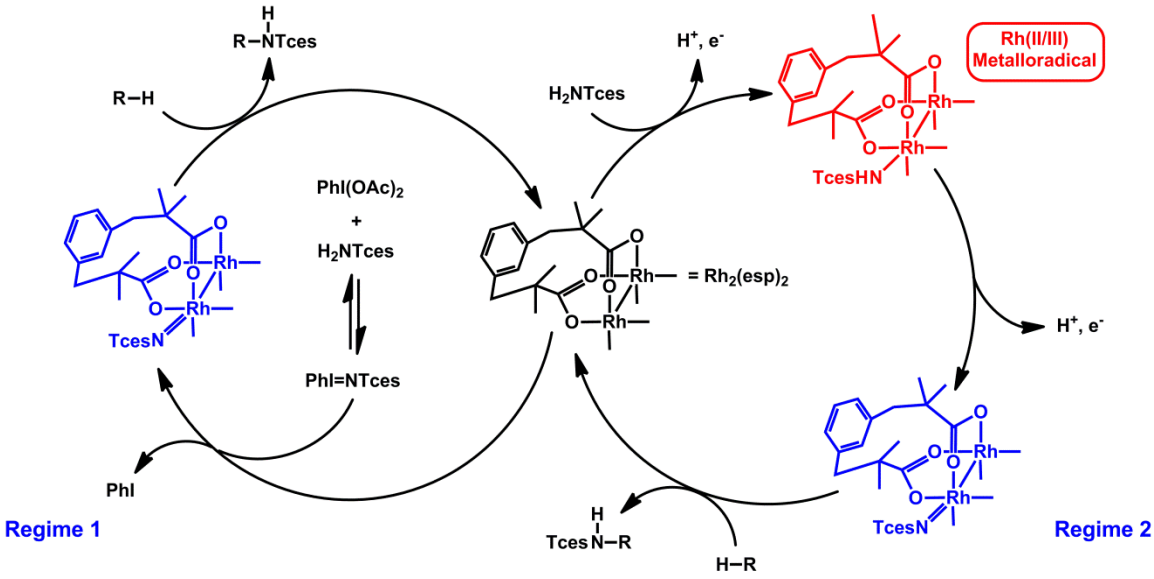

Scheme 1.3.

In support of these arguments, the Rh(II)/Rh(III) intermediate was characterized by a number of spectroscopic techniques. Further, the amination reaction was found to proceed in the absence of the hypervalent iodine compound if a one electron oxidant, $Ce(SO_4)_2$, was added to the catalyst and free amine; this observation suggests the involvement of a pathway that involves successive one-electron steps. The second reaction regime is notable in that this pathway does not necessitate the use of the PhI=NR reagent, which releases iodobenzene as a by-product, and that the reaction would likely work under electrocatalytic conditions. Thus, in addition to the promise of discovering new reactivity, metalloradicals may react analogously to their related diamagnetic

complexes, but proceed through different chemical pathways, to allow for more atom economical and less stringent reaction conditions in catalysis.

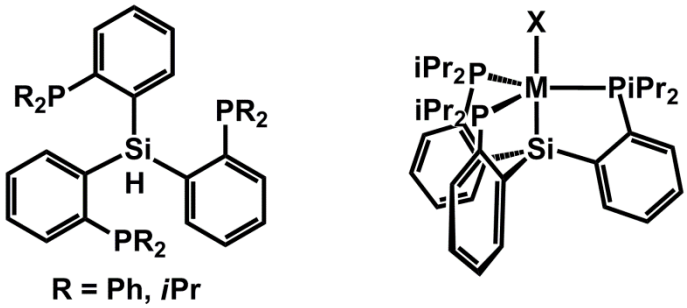

Figure 1.1. (Left) The $[SiP^{R}_{3}]^{-}$ class of ligands. (Right) A generic metal complex, $[SiP^{R}_{3}]MX$, where X is a ligand *trans* to the silyl anchor.

1.2 The Tris(phosphino)silyl Ligand

Our group recently introduced a class of tetradentate, tris(phosphino)silyl ligands, $[SiP^{R}_{3}]^{-}$ ($[SiP^{R}_{3}] = (2\text{-}R_2PC_6H_4)_3Si^{-}$), R = Ph, *i*Pr], to stabilize five coordinate complexes of late transition metals.[8] These ligands feature a strongly *trans* influencing silyl anchor in the ligand backbone, which was designed to strongly coordinate to the metal center and maintain the metal center in the plane of the three phosphine ligands. The ligand scaffold thus enforces a trigonal planar $[SiP^{R}_{3}]M$ core with an apical site available for an additional coordination site. Initial studies with this scaffold demonstrated its unique electronic flexibility in accommodating transition metal complexes with unusual geometries and oxidation states. For example, iron complexes with a strongly *trans* influencing methyl ligand opposite the silyl anchor were synthesized; these complexes were the first species to feature these two strongly *trans* influencing ligands in *trans* dispositions.[8,9] Subsequent studies on ruthenium, detailed in chapter 2, demonstrated that

this scaffold could stabilize related complexes where *trans* influencing silyl, silylene, germylene, and phosphido complexes could be placed opposite the silyl anchor. On the other hand, the same report that introduced these ligands also described the synthesis of unusual Fe(I) complexes, $[SiP^{R}_{3}]Fe(N_2)$ (R = Ph, *i*Pr). Subsequent studies showed that these complexes could be oxidized and reduced to yield a series of iron dinitrogen complexes with the same ancillary ligand that differ only by charge.[9] This class of dinitrogen complexes comprised the first example of such series to be isolated and crystallographically characterized, showcasing the electronic plasticity of metal centers chelated by the $[SiP^{R}_{3}]^{-}$ scaffolds.

1.3 d^7 Complexes of Group 8 and 9

As demonstrated by the stability of the Fe(I) complex,[8] $[SiP^{R}_{3}]Fe(N_2)$, the $[SiP^{R}_{3}]^{-}$ ligands seemed capable of stabilizing unusual low-valent metalloradicals of their chelated metal centers. This feature is not specific for these ancillary ligands, however; literature precendent exists for related tetradentate tripodal ligands that were shown to stabilize similar complexes of the late transition metals. Work by Bianchini, in particular, showed that the topologically related tris(phosphino)phosphine ligand, PP3 (PP3 = $P(CH_2CH_2PPh_2)_3$, could be coordinated to iron,[10] ruthenium,[11] and rhodium[12] to yield open-shell d^7 complexes. The latter two complexes were noteworthy as late metalloradicals of the heavier metals are still exceptionally rare.[1,13] Thus, the strongly coordinating $[SiP^{R}_{3}]^{-}$ ligands appeared as reasonable candidates for stabilizing analogous d^7 group 8 and 9 metalloradicals of the 2nd and 3rd row metals.

Chapters 3 and 4 detail the synthesis and characterization of group 8 and group 9 metalloradicals chelated by the $[SiP^{iPr}_3]^-$ ligand, respectively. The *i*Pr groups on the ancillary ligand provide enough steric bulk to allow for isolation of these metalloradicals. These complexes were characterized by a number of spectroscopic techniques and by single-crystal X-ray diffraction studies. Importantly, with the recent increase of reports on the redox non-innocence of many ancillary ligands,[14] emphasis was placed on ensuring that the isolated d^7 complexes were indeed metalloradical in character. In this context, EPR spectroscopy was an invaluable tool in assessing the location of spin on a metal complex. The deviation of the isotropic g-value, g_{iso}, from that of the free electron value of 2.0023 and large anisotropy in the g-tensors that is observed in the spectrum of frozen solution samples have been used as crude indicators of metalloradical character.[15] The EPR parameters, obtained by spectral simulation, were further complemented by spin density values from DFT calculations to provide strong evidence for the location of spin. As described in chapter 3, the EPR spectra and the DFT calculations qualitatively agree and suggest that the location of predominant spin is on the metal center for the formally d^7 (M = Ru, Os) group 8 complexes, confirming our assignment of the species as *bona fide* metalloradicals. Likewise, an analogous series of d^7 complexes of group 9 is detailed in chapter 4, and similar analysis also points to metalloradical character for these speceies.

1.4 Reactivity of a Ru(I) Metalloradical

Low-valent metalloradicals, by virtue of featuring a metal-centered radical, often exhibit one-electron reactivity; two-electron reactivity can be observed in some cases,

especially if two metalloradicals are involved in the process.[3] Accordingly, the Ru(I) metalloradical, [SiP$^{iPr}_3$]Ru(N_2), is found to undergo one-electron transformations with oxidants such as iodine and diphenyldisulfide (chapter 3). The same species, however, is also found to effect a formal two electron nitrene transfer from an organic azide to yield a formally Ru(III) imide species. A number of organic azides are found to yield related imide species, but the reaction is found to proceed only for aryl azides with electron withdrawing substituents.

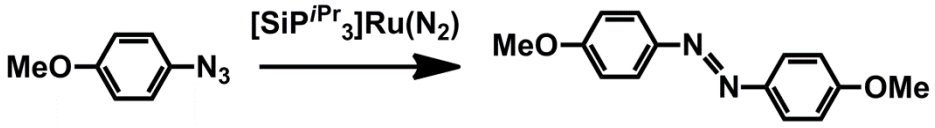

Scheme 1.4.

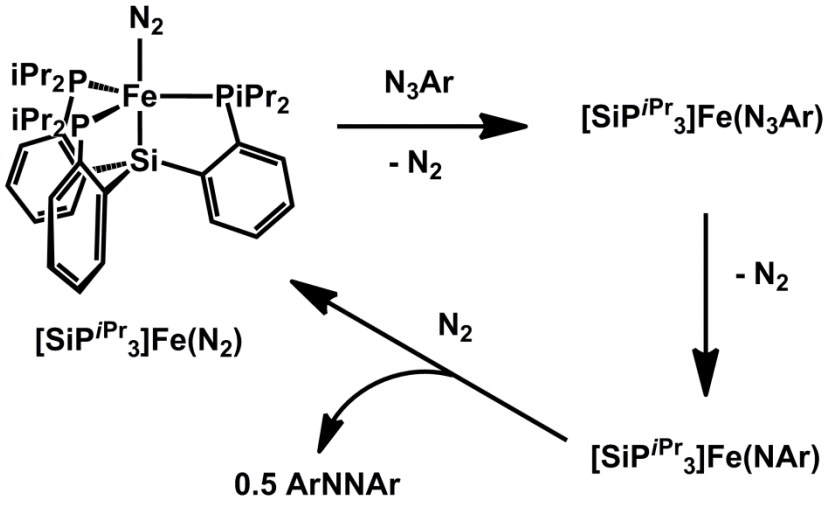

Scheme 1.5.

In contrast, catalytic N−N coupling of two aryl azides is observed when aryl azides with electron donating substituents, such as *p*-methoxy and *p*-ethoxy groups (Scheme 1.4). Such N−N coupling of two organic azides to yield azoarenes has rarely been observed, especially catalytically.[16] A notable example is the related catalytic N−N coupling of aryl azides by the Fe(I) complex, [SiP$^{iPr}_3$]Fe(N_2) complex.[17] Careful studies

have provided a detailed mechanistic picture of this transformation, as shown in Scheme 1.5. Briefly, an aryl azide initially displaces the dinitrogen ligand on [SiP$^{i\mathrm{Pr}}_3$]Fe(N_2) to yield an unstable azide adduct complex, [SiP$^{i\mathrm{Pr}}_3$]Fe(N_3Ar). Subsequently dinitrogen extrusion results in a transient Fe(III) imide complex, [SiP$^{i\mathrm{Pr}}_3$]Fe(NAr), which undergoes bimolecular coupling to yield the azoarene product. While a similar mechanistic picture can be proposed for the [SiP$^{i\mathrm{Pr}}_3$]Ru(N_2) catalyzed reaction, studies described in chapter 5 conclusively show that the corresponding imide species, [SiP$^{i\mathrm{Pr}}_3$]Ru(NAr), is not involved in the catalytic cycle.

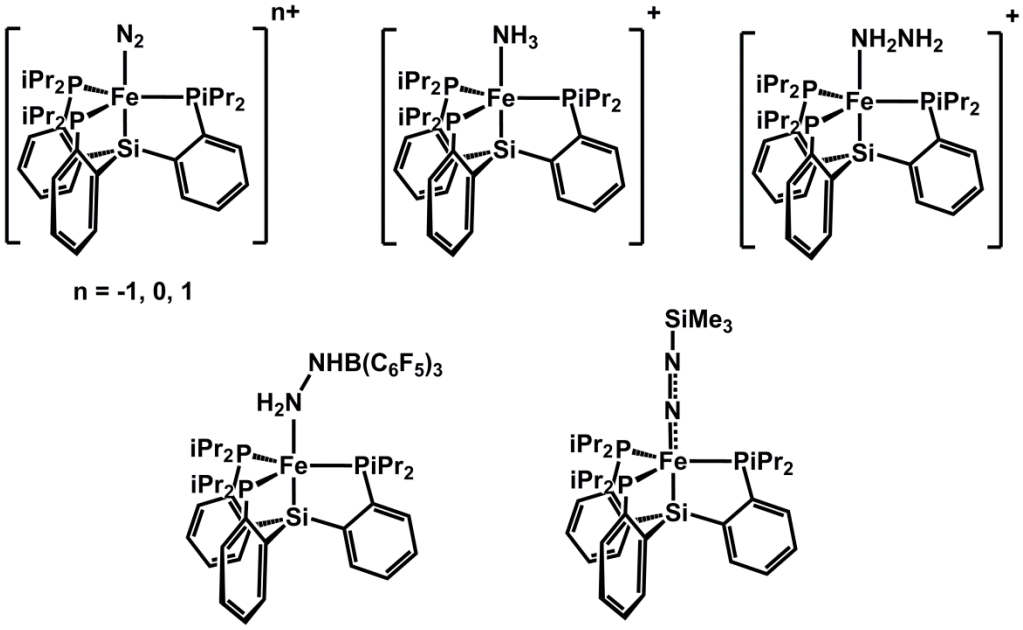

Figure 1.2. Example model complexes of the generic formula [SiP$^{i\mathrm{Pr}}_3$]Fe(N_xH_y).

1.5 Hybrid Phosphine/Thioether Ligands

Complexes of the [SiP$^{i\mathrm{Pr}}_3$]$^-$ ligand have been found to exhibit an unusual aptitude towards the binding of N_2. So far, dinitrogen complexes of iron, ruthenium, osmium,

cobalt, rhodium, and iridium have been prepared, with some examples in multiple oxidation states.[8,9] Importantly, the iron dinitrogen complexes, which can be prepared in three distinct oxidation states, have been used to further functionalize the dinitrogen ligand with trimethylsilyl groups to yield silyldiazenido complexes.[9] Other nitrogenous ligands (N_xH_y) such as ammonia, hydrazine, and borane-capped hydrazido ligands have also been stabilized with the [SiP^{iPr}_3]Fe scaffold (Figure 1.2). Together with the dinitrogen and silyldiazenido complexes, this class of complexes serves as interesting model complexes of intermediates that are postulated along a proposed mechanism for dinitrogen activation at iron by the iron-molybdenum nitrogenase enzyme, which is known to transform dinitrogen to ammonia at a metallocluster called the iron-molybdenum cofactor (FeMoco) (Figure 1.3, left).[18] Assuming initial dinitrogen coordination at one of the four iron centers along the belt of the cluster, the local geometry of the dinitrogen coordinated iron center would approximate a trigonal bipyramid, as the iron center in [SiP^{iPr}_3]Fe(N_2).

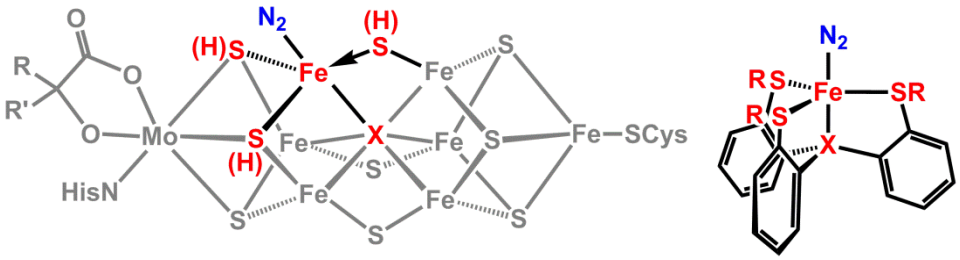

Figure 1.3. Hypothetical binding mode of N2 at the FeMoco (left) and a hypothetical model complex (right). Whether any of the S-atoms shown in red for FeMoco (left) are protonated during catalysis is unknown.

An obvious difference between the coordination environment of iron in [SiP$^{iPr}_3$]Fe(N_2) and the proposed N_2 bound iron center in FeMoco is the presence of sulfur donors in the latter. In general, transition metal complexes coordinated by sulfur donors are not found to bind N_2;[19] only one structurally characterized example for iron was known prior to the work in chapter 6.[20] Taking advantage of the tendency of the [SiP$^{iPr}_3$]Fe scaffold to bind N_2, hybrid thioether/phosphine ligands in which one or multiple phosphine donors have been replaced with thioethers in the [SiP$^{iPr}_3$]$^-$ scaffold have been synthesized. As detailed in chapter 6, these hybrid ligands have been coordinated to iron to stabilize a number of both mononuclear and dinuclear dinitrogen complexes of iron featuring multiple sulfur donors.

References Cited

1 de Bruin, B; Hetterscheid, D. G. H.; Koekkoek, A. J. J., Grützmacher, H. *Prog. Inorg. Chem*. **2007**, *55*, 247.

2 Cui, W.; Li, S.; Wayland, B. B. *J. Organomet. Chem.* **2007**, *692*, 3198.

3 a) Sherry, A. E.; Wayland, B. B. *J. Am. Chem. Soc.* **1990**, *112*, 1259. b) Wayland, B. B.; Ba, S.; Sherry, A. E. *J. Am. Chem. Soc.* **1991**, *113*, 5305.

4 a) Padhye, S.; Yerande, R.; Patil, R. P.; Kelkar, A. A.; Chaudhari, R. V. *Inorg. Chim. Acta.* **1989**, *156*, 23. b) Hetterscheid, D. G. H.; Smits, J. M. M.; de Bruin, B. *Organometallics* **2004**, *23*, 4236. c) Krumper, J. R.; Gerisch, M.; Suh, J. M.; Bergman, R. G.; Tilley, T. D. *J. Org. Chem.* **2003**, *68*, 9705.

5 Kornecki, K. P.; Berry, J. F. *Chem. –Eur. J.* **2011**, *17*, 5827.

6 Williams, K.; Du Bois, J. *J. Am. Chem. Soc.* **2007**, *129*, 562.

7 Li, Zhen; Quan, R. W.; Jacobsen, E. N. *J. Am. Chem. Soc.* **1995**, *117*, 5889.

8 a) Mankad, N. P.; Whited, M. T.; Peters, J. C. *Angew. Chem. Int. Ed.* **2007**, *129*, 5768. b) Whited, M. T.; Mankad, N. P.; Lee, Y.; Oblad, P. F.; Peters, J. C. *Inorg. Chem.* **2009**, *48*, 2507.

9 Lee, Y.; Mankad, N. P.; Peters, J. C. *Nat. Chem.* **2010**, *2*, 558.

10 Bianchini, C.; Laschi, F.; Masi, D.; Ottaviani, F. M.; Pastor, A.; Peruzzini, M.; Zanello, P.; Zanobini, F. *J. Am. Chem. Soc.* **1993**, *115*, 2723.

11 Bianchini, C.; Laschi, F.; Peruzzini, M.; Zanello, P. *Gazz. Chim. Ital.* **1994**, *124*, 271.

12 Bianchini, C.; Laschi, F.; Masi, D.; Ottaviani, F. M.; Pastor, A.; Peruzzini, P.; Zanobini, F. *J. Am. Chem. Soc.* **1993**, *115*, 2723.

13 Poli, R. *Angew. Chem., Int. Ed.* **2011**, *50*, 43.

14 a) C. C. Lu, E. Bill, T. Weyhermüller, E. Bothe, K. Wieghardt, *J. Am. Chem. Soc.* **2008**, *130*, 3181. b) D. Adhikari, S. Mossin, F. Basuli, J. C. Huffman, R. K. Szilagyi, K. Meyer, D. J. Mindiola, *J. Am. Chem. Soc.* **2008**, *130*, 3676. c) S. B. Harkins, N. P. Mankad, A. J. Miller, R. K. Szilagyi, J. C. Peters, *J. Am. Chem. Soc.* **2008**, *130*, 3478. d) M. R. Haneline, A. F. Heyduk, *J. Am. Chem. Soc.* **2006**, *128*, 8410.

15 de Bruin, B.; Hetterscheid, D. G. H. *Eur. J. Inorg. Chem.* **2007**, 211.

16 a) Ragaini, F.; Penoni, A.; Gallo, E.; Tollari, S.; Gotti, C. L.; Lapadula, M.; Mangioni, E.; Cenini, S. *Chem. -Eur. J.* **2003**, *9*, 249. b) Heyduk, A. F.; Zarkesh, R. A.; Nguyen, A. I. *Inorg. Chem.* **2011**, *50*, 9849.

17 Mankad, N. P.; Müller, P.; Peters, J. C. *J. Am. Chem. Soc.* **2010**, *132*, 4083.

18 Hoffman, B. M.; Dean, D. R.; Seefeldt, L. C. *Acc. Chem. Res.* **2009**, *42*, 609.

19 Selected examples; a) Mori, H.; Seino, H.; Hidai, M.; Mizobe, Y. *Angew. Chem. Int. Ed.* **2007**, *46*, 5431. b) Dilworth, J. R.; Henderson, R. A.; Hills, A.; Hughes, D. L.; Macdonald, C.; Stephens, A. N.; Walton, D. R. M. *J. Chem. Soc., Dalton Trans.* **1990**, 1077. c) Yoshida, T.; Adachi, T.; Kaminaka, M.; Ueda, T. *J. Am. Chem. Soc.* **1988**, *110*, 4872. d) Morris, R. H.; Ressner, J. M.; Sawyer, J. F.; Shiralian, M. *J. Am. Chem. Soc.* **1984**, *106*, 3683.

20 Bart, S.; Lobkovsky, E.; Bill, E.; Wieghardt, K.; Chirik, P. J. *Inorg. Chem.* **2007**, *46*, 7055.

Chapter 2: E-H Bond Activation Reactions (E = H, C, Si, Ge) at Ruthenium: Terminal Phosphides, Silylenes, and Germylenes

Reproduced in part with permission from

Takaoka, A.; Mendiratta, A.; Peters, J. C. *Organometallics* **2009**, *28*, 3744-3753.

2.1 Introduction

Tetradentate, tripodal ligands have a long-standing history in inorganic chemistry and continue to be exploited to prepare new types of coordination complexes and catalyst auxiliaries. [1] Recently, we reported the synthesis of the tripodal monoanionic tris(phosphino)silyl ligands $[SiP^{R}_{3}]^{-}$ ($[SiP^{R}_{3}]$ = $[(2\text{-}R_2PC_6H_4)_3Si]$, R = Ph and ^{i}Pr) and several corresponding iron complexes, including a terminal N_2 adduct of iron(I).[2] A conspicuous feature of this ligand scaffold is the presence of a strongly *trans*-influencing silyl anchor,[3] which is unlikely to be labile due to its anionic nature. This feature contrasts that of several topologically related ligands such as Sacconi's tris(phosphino)amine $N(CH_2CH_2PR_2)_3$ systems[4] and Meyer's more recently developed tris(carbene)amine system,[5] in which the apical amine donor can be hemilabile as a function of the ligand that occupies the site opposite the N atom. This article examines the properties of the $[SiP^{Ph}_{3}]^{-}$ ligand by studying a family of ruthenium complexes in which synthetic attempts are made to place strongly *trans*-influencing donor ligands at the site opposite the silyl anchor. Our studies have revealed interesting E−H bond activation transformations (E = H, C, Si, Ge). We also report the isolation and structural characterization of unusual coordination complexes including examples of terminal phosphide, silylene, and germylene complexes. These functionalities occupy positions *trans* to the silyl anchor and to our knowledge are structurally unique in this context.

2.2 Results and Discussion

2.2.1 Alkyl and Phosphide Complexes

Alkyl and phosphide ligands were initially targeted as candidates for the *trans*-influencing ligands opposite the silyl anchor. Heating $[SiP^{Ph}_3]H$, $Ru(PPh_3)_4Cl_2$, and excess triethylamine at 60 °C affords purple crystals of $[SiP^{Ph}_3]RuCl$ (**2.1**) in 95% yield after workup (Scheme 2.1). The solid-state structure of **2.1** reveals a structure midway between a square pyramid and a trigonal bipyramid (τ = 0.47; Figure 2.1)[6] with a Si−Ru−Cl angle of 174.35(3)°. At room temperature the phosphines are equivalent on the ^{31}P NMR time scale. Addition of methyllithium at −78 °C to a THF solution of **2.1**, followed by warming to room temperature, leads to an orange solution of the thermally unstable methyl complex $[SiP^{Ph}_3]RuMe$ (**2.2**). A ^{1}H NMR spectrum of the solution at room temperature, taken shortly after addition of methyllithium at −78 °C, features a quartet at δ = −0.98 ppm corresponding to the methyl protons coupled to three equivalent phosphines on the NMR timescale. The corresponding $^{31}P\{^{1}H\}$ NMR spectrum shows a singlet at δ = 63.7 ppm. Both spectra indicate 3-fold symmetry for dissolved **2.2** on the NMR timescale, whereas its diamagnetism suggests a structure similar to **2.1**.

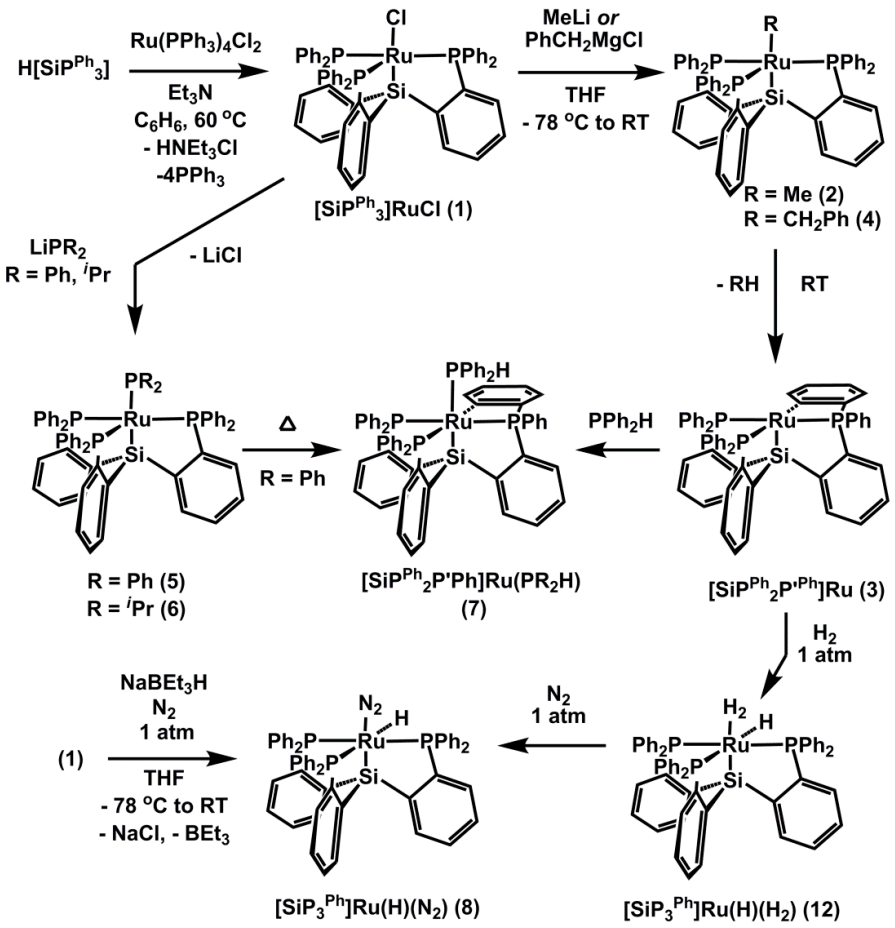

Scheme 2.1

Solutions of **2.2** cleanly convert over approximately 30 min at room temperature to the new species [SiP$^{Ph}_2$P'^{Ph}]Ru (**2.3**) via cyclometalation of an *ortho* phenyl C−H bond with concomitant loss of methane. The solid-state structure of **2.3**, shown in Figure 2.1, shows a square-pyramidal geometry ($\tau = 0.07$) with the silicon atom occupying the apical position and an open coordination site *trans* to the silyl anchor. The Ru−Si bond length in **2.3** is shorter than that in **2.1** (2.2592(6) vs 2.3222(11) Å), which is in accordance with the absence of a *trans* ligand opposite the silyl anchor in **2.3**. The $^{31}P\{^{1}H\}$ NMR spectrumof **2.3** features three sets of peaks, with the resonance of the phosphine in the metallacycle shifted significantly upfield at $\delta = -11.3$ ppm relative to the others at $\delta =$

64.9 and 62.0 ppm. Upfield shifts for the $^{31}P\{^{1}H\}$ NMR spectrum of cyclometalated phosphine complexes are well precedented.[7]

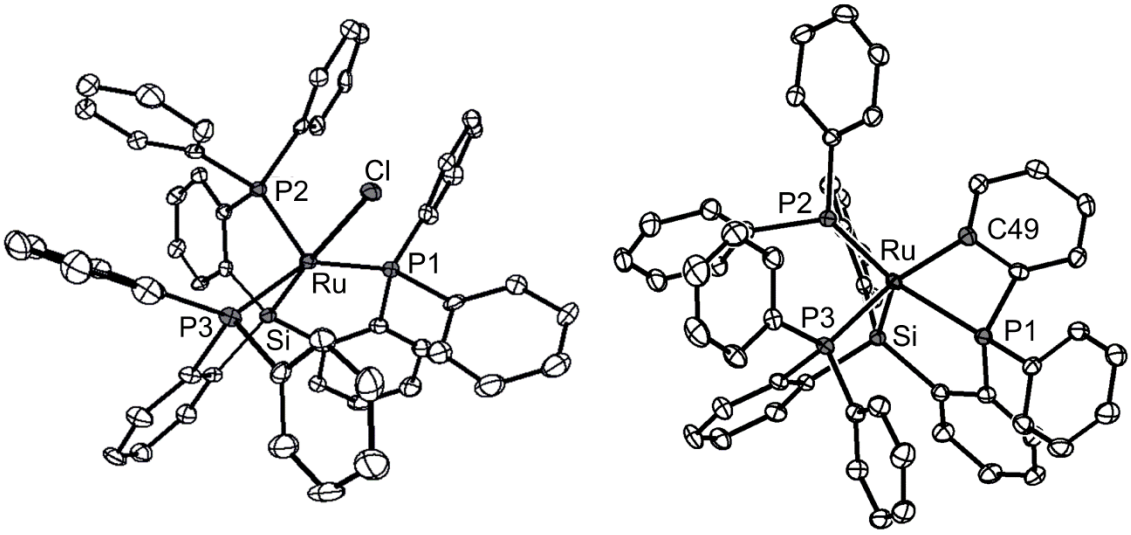

Figure 2.1. Left: Solid-state structure of **2.1**. Right: Solid-state structure of **2.3**. Thermal ellipsoids are set at 50% probability, and solvent molecules and hydrogen atoms are removed for clarity. Selected bond lengths (Å) and angles (°): **2.1**: Ru−Si, 2.3222(11); Ru−P(1), 2.3284(11); Ru−P(2), 2.2027(11); Ru−P(3), 2.3214(12); Ru−Cl, 2.5117(10), Si−Ru−Cl, 174.35(3). **2.3**: Ru−Si, 2.2592(6), Ru−C(49), 2.137(2); Ru−P(1), 2.3447(6); Ru−P(2), 2.3240(6); Ru−P(3), 2.3186(6).

The reaction between benzyl magnesium chloride and **2.1** results in the corresponding benzyl complex $[SiP^{Ph}_3]Ru(CH_2Ph)$ (**2.4**). NMR spectroscopy suggests that the benzyl moiety is not bound in an η^1 fashion. At room temperature complex **2.4** exhibits two broad resonances at δ = 81.4 and 58.3 ppm in a 1:2 ratio in the $^{31}P\{^{1}H\}$ spectrum in addition to several broad $[SiP^{Ph}_3]^-$ resonances in the ^{1}H and $^{13}C\{^{1}H\}$ spectra.

An η^3 assignment of the benzyl ligand in **2.4** is suggested by the large $^1J_{CH}$ value of 145 Hz at the benzylic carbon in the ^{13}C spectrum of **2.4**, though η^2 coordination cannot be rigorously excluded from the NMR data available.[8] The upfield resonance of the *ortho* hydrogens of the benzyl ligand in the ^1H NMR spectrum, which appears as a doublet at δ = 5.97 (J = 7.6 Hz) in d8-THF, provides strong evidence against η^1 coordination.[8] Although broadening of the *ortho* hydrogen resonance is observed upon cooling, decoalescence is not observed at temperatures as low as −90 °C. Decoalescence of the *ortho* carbons on the benzyl ligand is likewise not attained in the $^{13}C\{^1H\}$ spectrum at −90 °C. The benzyl species shows thermal instability akin to **2.2** and decays to **2.3** via loss of toluene over several days at 22 °C.

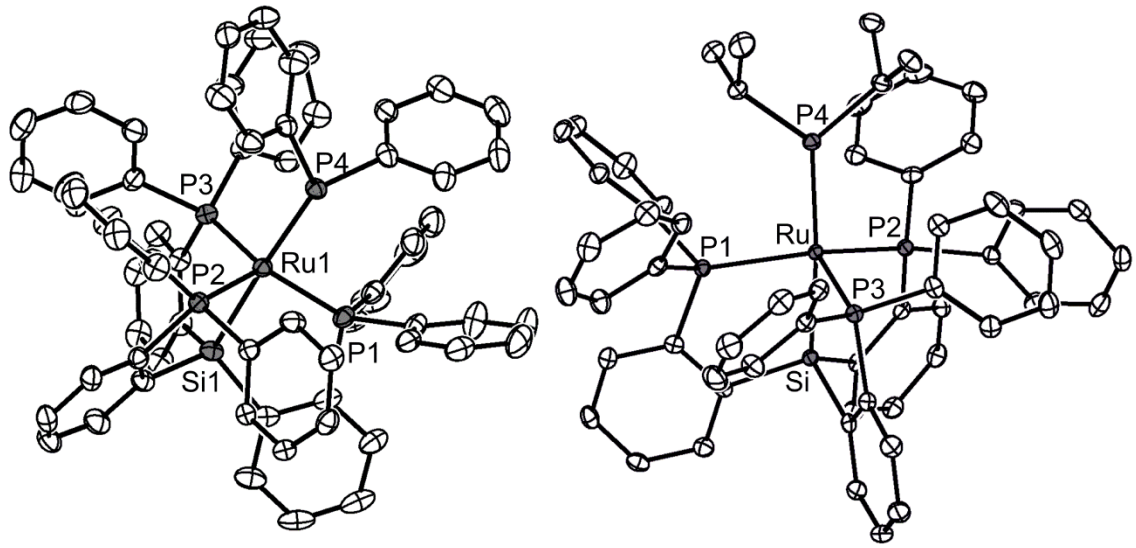

Figure 2.2. Left: Solid-state structure of **2.5**. Right: Solid-state structure of **2.6**. Thermal ellipsoids are set at 50% probability, and solvent molecules and hydrogen atoms are removed for clarity. Selected bond lengths (Å) and angles (°): **2.5**: Ru(1)−Si(1), 2.3783; Ru(1)−P(4), 2.2700; Si(1) –Ru(1) –P(4), 176.42(1). **2.6**: Ru−Si, 2.3690(4), Ru−P(4), 2.2592(4); Si−Ru−P(4), 161,88(2).

The addition of lithium diphenylphosphide to **2.1** at −78 °C immediately leads to a dark green solution of the phosphidecomplex [SiP^{Ph}_3]$RuPPh_2$ (**2.5**). The $^{31}P\{^1H\}$ spectrum exhibits one species with resonances at δ = 214.1 and 75.0 ppm corresponding to the phosphide and phosphine P nuclei, respectively. The highly downfield chemical shift of the phosphide P nucleus indicates the presence of a terminal phosphide ligand with a planar geometry about the phosphorus atom,[9] a rare feature for ruthenium phosphide complexes; there is only one other structurally characterized example.[10] The solid-state structure (Figure 2.2) contains two molecules in the asymmetric unit and shows that the angles about the terminal phosphide ligand sum to average values of 357°. In contrast to **2.1**, the geometry of **2.5** more closely approximates a trigonal bipyramid, with an average τ value of 0.74. Notably, the Ru−P (phosphide) bond lengths of 2.2700(3) and 2.2525(3) Å are significantly shorter than the Ru−P (phosphine) bond lengths that average to 2.32 Å, despite the presence of the *trans*-silyl group. This observation points to multiple-bond character between the phosphide ligand and the ruthenium center, especially in light of the planar geometry about the phosphide P atom. Complex **2.5** is also structurally distinctive in that the terminal phosphide and silyl ligands are *trans* disposed in the solid state with Si−Ru−P angles of 176° and 174° for the two molecules in the asymmetric unit. The diisopropyl phosphide complex, [SiP^{Ph}_3]RuP^{iPr}_2 (**2.6**), is prepared analogously to **2.5** and exhibits similar spectroscopic characteristics but different structural parameters, with a geometry closer to that of **2.1** (Figure 2.2). The Ru−Si bond in **2.6** is appreciably longer than in **2.1** (2.369 vs 2.322 Å), reflecting the stronger *trans* influence of the phosphide ligand. Similarly to solutions of **2.2** and **2.4**, solutions of **2.5** decay to an isolable cyclometalated phosphine adduct

complex, **2.7** (Scheme 2.1). The identity of **2.7** is confirmed by elemental analysis, an (ν_{P-H}) IR stretch at 2288 cm^{-1}, and a J_{PH} of 302 Hz in the ^{31}P NMR spectrum for the coordinated PPh_2H. Complex **2.7** is also accessible via addition of diphenylphosphine to **2.3**.

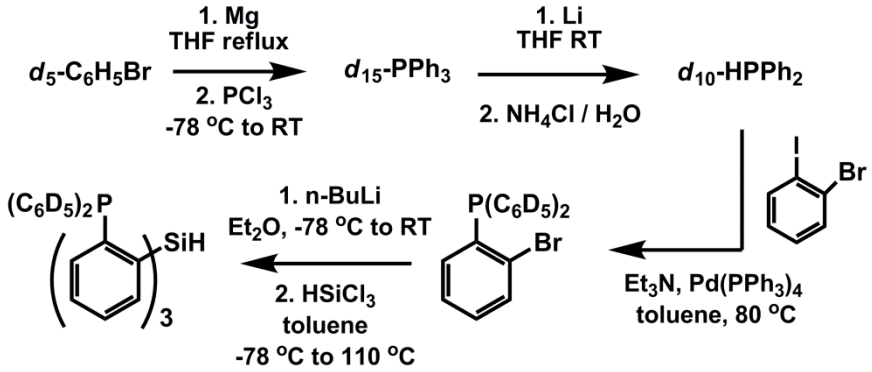

Scheme 2.2

The decay of **2.5** follows clean first-order kinetics with activation parameters of $\Delta H^{\ddagger}$ = 20(2) kcal/mol and $\Delta S^{\ddagger}$ = 16(4) eu. A kinetic isotope effect was obtained by the use of a deuterated ligand, d_{30}-[SiP^{Ph}_3]H, in which the phenyl substituents on the phosphine arms are fully deuterated. The synthesis of d_{30}-[SiP^{Ph}_3]H is outlined in Scheme 2.2 and is accomplished in four steps in an overall yield of 42%. d_{10}-PPh_2H,[11] prepared in 81% yield by lithium metal reduction of d_{15}-PPh_3 followed by acidic workup, is coupled with 2-iodobromobenzene through a palladium-catalyzed reaction to yield d_{10}-[2-(diphenylphosphino)phenylbromide] in 95% yield. Lithiation of d_{10}-[2-(diphenylphosphino)phenylbromide], followed by addition of trichlorosilane, yields the desired deuterated product in 85% yield. The ^1H NMR spectrum of the prepared d_{30}-[SiP^{Ph}_3]H shows resonances attributable to the protons on the ligand backbone with very little (<3%) incorporation of ^1H nuclei in the phenyl substituents of the phosphine. d_{30}-[SiP^{Ph}_3]Ru(PPh_2) was prepared analogously to **2.5**, and its thermal decay behavior at

35 °C shows a kinetic isotope effect of 5.5(3). Collectively, the kinetic data suggest a highly ordered transition state with significant C-H bond cleavage.

2.2.2 Silane, Silylene, and Germylene Complexes

The clean conversion of **2.2** to **2.3** and **2.5** to **2.7** via C−H activation of a phenyl ring inspired us to examine the installation of a silyl ligand trans to the $[SiP^{Ph}_3]^-$ silyl anchor. Structurally characterized mononuclear complexes with trans silyl ligands are not known for group 8 metals, with a small number reported for the earlier metals[12] and the rest comprised of group 10 or later metals.[13] The first approach we examined involved addition of silanes to the dinitrogen hydride complex $[SiP^{Ph}_3]Ru(H)(N_2)$ (**2.8**). Complex **2.8** is readily prepared by addition of sodium triethylborohydride to **2.1**. Our assignment of **2.8** is based upon the presence of a hydride resonance at δ = −7.95 ppm in the ^1H NMR spectrum and an ($_{\nu N-N}$) IR stretch at 2167 cm^{-1}, which shifts to 2095 cm^{-1} upon use of $^{15}N_2$ (calcd: 2093 cm^{-1}). The Ru-H stretch is not observed in the IR spectrum. In accordance with the high-frequency N_2 stretch, the N_2 ligand is appreciably labile. Solutions of **2.8** change color from yellow to orange under reduced pressure, and the ^{15}N NMR spectrum of an isotopically enriched sample features a single broad resonance centered at δ = −65 ppm (ref to$MeNO_2$) with no signal for free N_2, indicating facile exchange. Judging from the $^2J_{PH}$ values of 60 and 28 Hz, the structure of **2.8** is most consistent with a pseudooctahedral complex featuring a dinitrogen ligand *trans* disposed to the silyl anchor. Such an arrangement is rare and renders the N_2 ligand labile, as has been observed by our group for the iron complex [SiPPh3]Fe(N_2).[2]

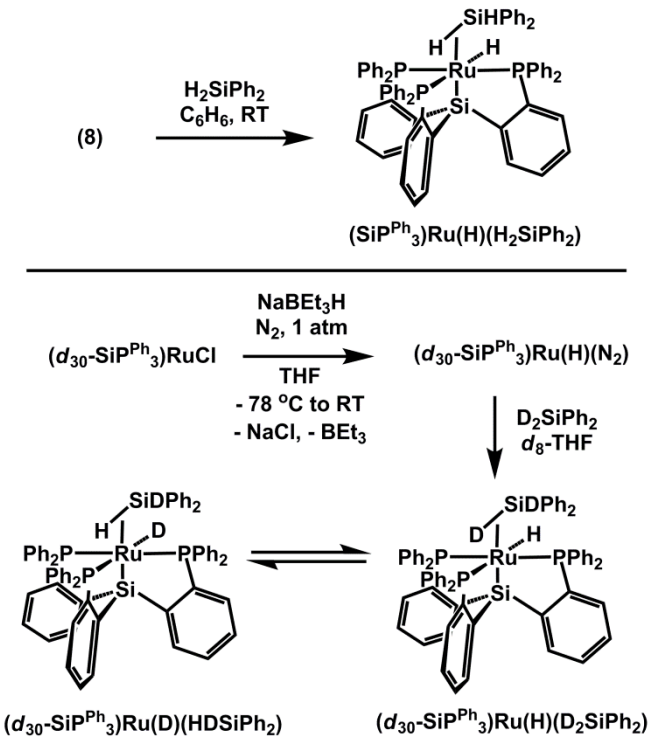

Scheme 2.3

As outlined in Scheme 2.3, the addition of diphenylsilane to **2.8** cleanly leads to one species by ^{1}H NMR spectroscopy. The solid-state structure of the product[14] reveals Ru-Si bond lengths of 2.4808(4) and 2.4103(4) Å for the silicon derived from diphenylsilane and that from the [SiP$^{Ph}_{3}$]− ligand, respectively. Although a signature resonance in the hydride region of the ^{1}H NMR spectrum is easily discerned, hydrogen atom(s) bound to the ruthenium center could not be assigned from the XRD data (see Supporting Information). At −20 °C, a resonance at δ = 5.46 ppm is observed that integrates in a 1:2 ratio against the hydridic resonance at δ = −7.18 ppm. The former resonance appears close to the silicon hydride resonance of diphenylsilane in the same solvent (δ = 4.88 ppm, d_8-THF) and is assigned to a terminal silicon hydride. The latter resonance could be assigned to two hydride ligands, giving a dihydride/silyl formulation for the product **2.9**, or alternatively to a resonance arising from a terminal Ru hydride and

a bridging Ru−H−Si hydride in rapid exchange. Further cooling of 9 to −80 °C does not lead to decoalescence of this resonance. To establish the possibility of a direct hydride interaction with the new silicon-containing ligand, a $^{1}H–^{29}Si$ HSQC experiment was undertaken. The spectrum at −20 °C reveals coupling constants of $^{1}J_{SiH}$ = 80 Hz at δ = −7.18 ppm[15] and $^{1}J_{SiH}$ = 210 Hz at δ = 5.46 ppm at −20 °C. These data suggest the most reliable assignment to be a terminal hydride/η^2−silane adduct complex, [SiP^{Ph}_3]Ru(H)(η^2−H_2SiPh_2) (**2.9**), instead of a dihydride/silyl complex. While **2.9** is six-coordinate, the $^{31}P\{^{1}H\}$ NMR spectrum features a single resonance even at −80 °C, indicative of fluxional behavior and potential scrambling of the hydride and silane hydrogen atoms. Scrambling in **2.9** was examined through ^{1}H NMR analysis of a deuterated analogue synthesized by the addition of D_2SiPh_2 to a solution of d_{30}-[SiP^{Ph}_3]Ru(H)(N_2).[16] The presence of a single exchangeable ^{1}H nucleus enables facile examination of scrambling. The ^{1}H NMR spectrum at −20 °C indeed shows resonances at both 5.46 and −7.18 ppm in a 1:2.8 ratio, pointing to facile scrambling between the three hydrogen atoms in **2.8** (Scheme 2.3) and to the slight preference for deuterium to occupy the position on the silane that is not interacting with the metal.[17]

To explore related Si−H bond activation processes, the reaction between diphenylsilane and the cyclometalated species **2.3** was examined. While many cyclometalated complexes are stable to ring opening under a variety of conditions, several systems have been found to ring open upon addition of substrates.[18] Accordingly, the addition of diphenylsilane to **2.3** at −78 °C quantitatively produces a single product according to the ^{1}H NMR spectrum. The spectrum features an upfield singlet resonance at δ = −8.97 ppm. Moreover, the $^{29}Si\{^{1}H\}$ spectrum shows a singlet resonance at δ = 374

ppm, which is significantly downfield of known silyl complexes,[19] in addition to the quartet resonance for the $[SiP^{Ph3}]^-$ ligand at δ = 104 ppm ($^2J^{SiP}$ = 15 Hz). Taken together, the spectra support the formulation of the silylene complex $[SiP^{Ph}_3]Ru(H)(SiPh_2)$ (**2.10a**).

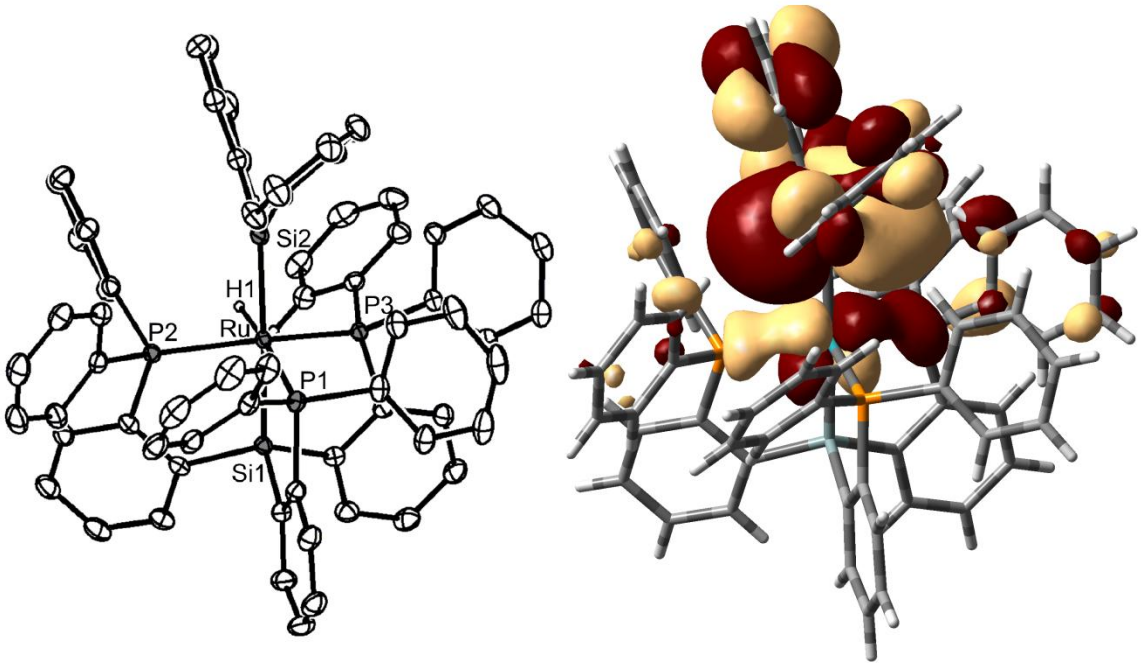

Figure 2.3. Left: Solid-state structure of **2.10a**. Right: LUMO of 2.10a. Thermal ellipsoids are set at 50% probability, and hydrogens on the phenyl rings and solvent molecules have been removed for clarity. Selected bond lengths (Å) and angles (°): Ru−Si(2), 2.2842(5); Ru−P(1), 2.3698(5); Ru−P(2), 2.2920(5); Ru−P(3), 2.3130(5); Si(1) −Ru−Si(2), 175.58(2).

The solid-state structure, shown in Figure 2.3, corroborates this assignment and reveals a terminal silylene ligand trans disposed to the silyl anchor of the $[SiP^{Ph}_3]^-$ ligand, providing a Si1-Ru-Si2 angle of 175.58(2)°. As for the case of the phosphide complex **2.5**, this arrangement of ligands is to our knowledge unprecedented.[20] The angles about the silylene silicon sum to 359.9(1)°, confirming sp^2 hybridization at the Si atom. The

hydride ligand can be located in the difference map and resides at a position that is nearly coplanar with the plane defined by the silylene moiety, providing evidence against direct Si−H interactions. The Ru−Si bond length between the metal and the silylene moiety is 2.2842(5) Å and is slightly longer than other base-free ruthenium silylene complexes,[21] manifesting the *trans* influence of the silyl donor. The addition of methylphenylsilane to **2.3** similarly results in the facile conversion to the silylene complex [SiP^{Ph}_3]Ru(H)(SiMePh) (**2.10b**), featuring $^{29}Si\{^1H\}$ resonances at δ = 359 and 101 ppm ($^2J_{SiP}$ = 18 Hz). As in **2.10a**, the hydride resonance at δ = −9.21 ppm in the ^1H spectrum shows no coupling with the phosphines. Both **2.10a** and **2.10b** exhibit a single resonance in the $^{31}P\{^1H\}$ NMR spectrum at 22 °C despite being six coordinate, as in **29**. We presume that complexes **2.10a** and **2.10b** result from α-hydrogen migration from a five-coordinate silyl intermediate, [SiP^{Ph}_3]Ru($SiHR_2$), by analogy with the proposed manner by which several other silylenes derived from silanes are thought to be formed.[22]

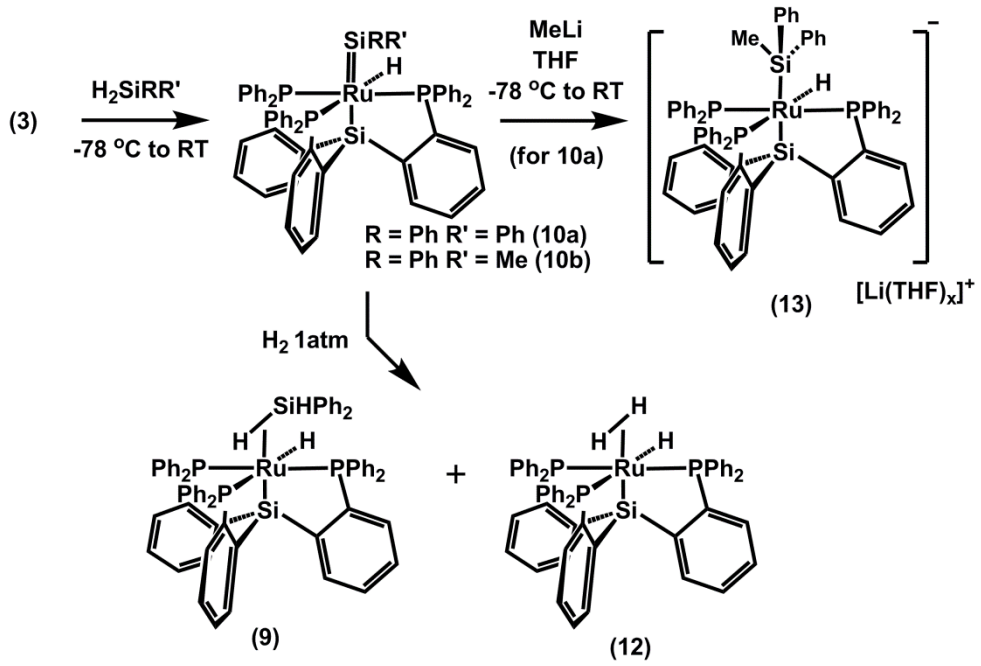

Scheme 2.4

The germylene analogue of **2.10a** is similarly obtained through the addition of diphenylgermane to **2.3** (Scheme **2.4**). Such a reaction cleanly affords $[SiP^{Ph}_3]Ru(H)(GePh_2)$ (**2.11**). As expected, complex **2.11** exhibits spectroscopic characteristics closely resembling that of **2.10a**, and an XRD study establishes that it is nearly isostructural. The only significant difference arises from the Ru−Ge bond length of 2.3579(3) Å. This bond length is difficult to compare with other systems due to the dearth of ruthenium germylene complexes, but is similar to the reported bond length of 2.339(1) Å in the related iridium complex, $[PhB(CH_2PPh_2)_3]Ir(H)_2(GeMes_2)$.[23]

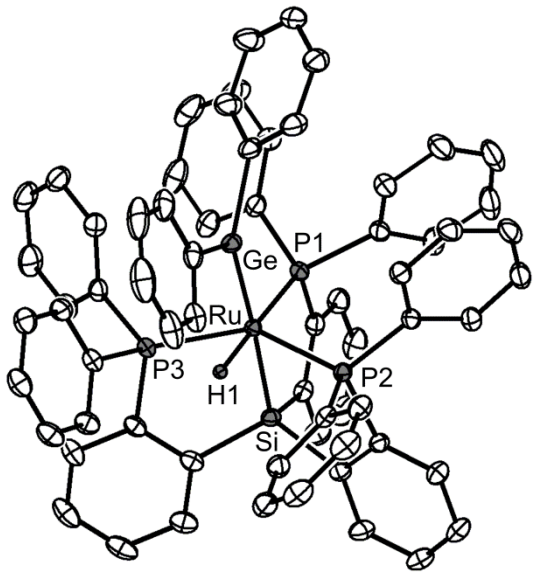

Figure 2.4. Solid-state structure of **2.11**. Thermal ellipsoids are set at 50% probability, and hydrogen atoms on phenyl rings and solvent molecules are removed for clarity. Selected bond lengths (Å) and angles (°): Ru−Ge, 2.3579(3); Ru−P(1), 2.3709(5); Ru−P(2), 2.2955(5); Ru−P(3), 2.3136(5); Si−Ru−Ge, 176.25(1).

While bona fide examples of terminal silylene complexes have gained increasing prominence in the literature,[24] those that feature a strongly donating ligand *trans* to the silylene moiety are quite rare[25] and may be expected to be unstable. Typical examples of complexes featuring a strong donor *trans* to a silylene ligand possess two heteroatom-stabilized cyclic silylenes opposite one another.[26] Accordingly, solutions of **2.10a** and **2.10b** decompose slowly to unknown products at room temperature over a few days but are stable in the solid state at −35 °C. For comparison, the related six-coordinate iridium silylene complexes $[PhBP^{Ph}_3]Ir(H)_2(SiR_2)$ (R = Mes, Ph, Et, Me)[22,23] are prepared at elevated temperatures and are appreciably more stable ($[PhBP^{Ph}_3]=[PhB(CH_2PPh_2)_3]^-$).

The addition of excess H_2 gas to **2.10a** affords two products, with the silane adduct **2.9** being the major species present. The minor product is obtained quantitatively via an independent route through the addition of excess H_2 gas to **2.3** and is assigned as the dihydrogen hydride complex $[SiP^{Ph}_3]Ru(H)(H_2)$ (**2.12**). Complex **2.12** features a broad upfield resonance at δ = −4.3 ppm that exhibits coalescence even at −80 °C, making a specific structural assignment difficult. However, the short T_{1min} value of 33 ms recorded at 0 °C (500 MHz ^{1}H NMR) is consistent with a dihydrogen/hydride formulation.[27,28] The dihydrogen ligand is labile, and **2.12** can hence be converted to **2.8** upon prolonged exposure to dinitrogen. The formation of **2.12** likely results from silane displacement by dihydrogen, as exposure of excess H_2 gas to **2.9** results in partial conversion of **2.9** to **2.12** with loss of free silane. Addition of approximately 1 equiv of H_2 gas to **2.10a** further results in formation of **2.9** with very little concomitant generation of **2.12**.

The addition of methyllithium to **2.10a** at −78 °C was examined to try to generate a species exhibiting *trans* disposition of silyl ligands. The LUMOof **2.10a**, obtained from a

single-point DFT calculation and shown in Figure 2.3, reveals significant contribution from the p orbital on the silicon of the silylene moiety,[29] which suggests it should have electrophilic character. Our data for the addition of methyllithium to **2.10a** is consistent with nucleophilic attack at the silylene to generate a $MePh_2Si^-$ ligand, as opposed to deprotonation of the metal-bound hydride. The ^{1}H NMR spectrum of the product formed shows a singlet hydride resonance at $\delta = -9.77$ ppm, which exhibits no coupling to the phosphine P atoms as in **2.10a** and **2.10b**, and a resonance at $\delta = 0.21$ that is assigned to the methyl group. The absence of satellites at the upfield resonance indicates little interaction between the hydride and either silyl Si atom, suggesting the hydride silyl product $\{[SiP^{Ph}_3]Ru(H)(SiMePh_2)\}\{Li(THF)_x\}$ (**2.13**). The structure of **2.13** is presumed to feature the silyl ligand *trans* to the $[SiP^{Ph}_3]^-$ silyl anchor on the basis of variable temperature NMR analysis. As shown in Figure 2.5, upon cooling to −90 °C, partial decoalescence of the hydride resonance to a broad five-line pattern with a coupling constant of $J_{HP} = 28$ Hz is observed. This splitting pattern is reminiscent of that observed for the hydride resonance in **2.8**, with $^2J_{HP} = 60$ Hz, 28 Hz due to coupling with the *cis* and *trans* phosphines, respectively. We rationalize the broad five-line pattern of **2.13** as resulting from the superposition of a doublet of triplets with similar coupling constants.

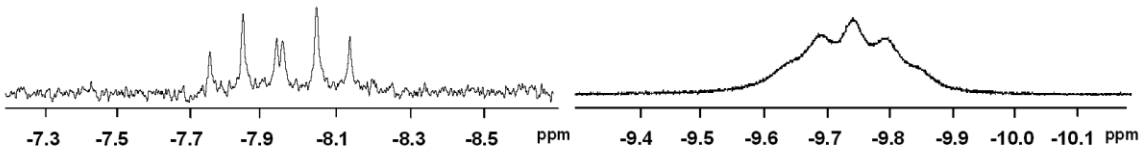

Figure 2.5. Left: ^{1}H NMR (300 MHz) of the hydride resonance of 2.8 at RT. Right: ^{1}H NMR (500 MHz) of **2.13** in the hydride region at −90 °C.

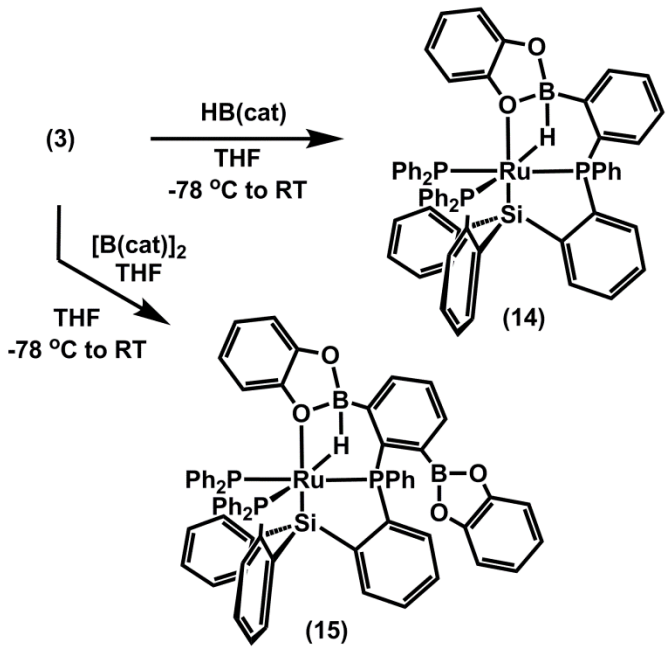

Scheme 2.5

2.2.3 Attempts to Synthesize Boryl Complexes

We have also attempted the installation of a boryl ligand opposite the silyl anchor. While unsuccessful, the reaction products (Scheme 2.5) are interesting and worthy of brief comment. Addition of catecholborane at −78 °C to **2.3** followed by warming gives rise to a light orange solution. Its ^{1}H NMR spectrum shows clean formation of one product featuring a broad resonance at δ = −6.24 ppm, and a broad resonance at δ = 12 ppm is observed in the ^{11}B{^{1}H} spectrum. The solid-state structure for complex **2.14**, shown in Figure 2.6, depicts formal insertion of the B−H bond into the M−C bond of the metallacycle, revealing a bridging B−(μ−H)−Ru hydride.[30] The Ru−B distance of 2.468(2) Å indicates very little, if any, direct interaction between the boron atom with the metal. One of the oxygen atoms from the catecholborane is coordinated to the metal, with a Ru−O distance of 2.376(2) Å, completing the coordination sphere. The above reaction

suggested to us that replacement of the bridging hydride unit with a boryl ligand might be possible through addition of bis(catecholato)diboron. However, such a reaction instead affords a product with a ^{1}H NMR spectrum closely resembling **2.14**. The solid-state structure of the product, **2.15**, indeed reveals an analogous structure to **2.14**, but moreover shows that a phenyl ring has been selectively borylated at the ortho position. A number of mechanisms are conceivable for this transformation,[31] and a plausible intermediate might be the intended boryl complex, which subsequently activates the aryl C-H bond.

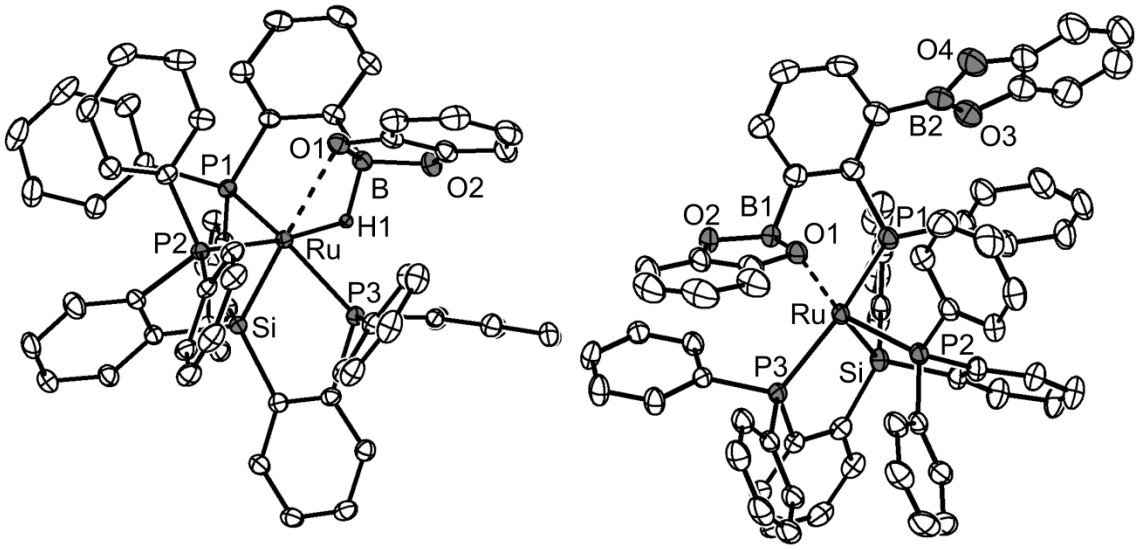

Figure 2.6. Left: Solid-state structure of **2.14**. Right: Solid-state structure of **2.15**. Thermal ellipsoids are set at 50% probability, and hydrogens on phenyl rings and solvent molecules have been removed for clarity. The bridging hydride was not found in **2.15**. Selected bond lengths (Å) and angles (°): **2.14**: Ru−Si, 2.2913(6); Ru−P(1), 2.3288(5); Ru−P(2) 2.3250(5); Ru−P(3), 2.3382(6); Ru−O(1), 2.3757(15); Ru−B, 2.4684(2); Si−Ru−O(1), 167.47(4). **2.15**: Ru−Si, 2.2952(3); Ru−P(1), 2.3400(3); Ru−P(2), 2.3108(3); Ru−P(3), 2.3497(3); Ru−O(1), 2.3265(6); Ru−B, 2.449(1); Si−Ru−O(1), 167.65(2).

2.3 Conclusion

The tetradentate $[SiP^{Ph}_3]^-$ ligand has been exploited in the preparation of a family of new ruthenium complexes. Most notably, the cyclometalated derivative **2.3** is a reactive synthon that activates E−H bonds, allowing the preparation of structurally distinctive silylene and germylene complexes. In addition, phosphide/silyl and disilyl complexes can be prepared using the $[SiP^{Ph}_3]$Ru scaffold. All of these complexes are unusual by virtue of the placement of two strongly *trans*-influencing ligands in approximate *trans* positions to one another. As such, these species are thermally unstable, as is manifest in the thermal conversion of phosphide **2.5** to phosphine **2.7**. Studies in our lab continue to map the reactivity patterns of this $[SiP_3]$Ru system and to exploit its propertiesin the context of homogeneous catalysis.

2.4 Experimental Section

2.4.1 General Considerations

All manipulations were carried out using standard Schlenk or glovebox techniques under an atmosphere of dinitrogen. Unless otherwise noted, solvents were degassed and dried by thoroughly sparging with N_2 gas followed by passage through an activated alumina column. Pentane, benzene, toluene, tetrahydrofuran, and diethyl ether were tested with a standard purple solution of sodium benzophenone ketyl in tetrahydrofuran. All reagents were purchased from commercial vendors and used without further purification unless otherwise noted. Celite (Celite 545) was dried at 150 °C overnight before use. Methyllithium was purchased in a solution form and concentrated, redissolved in tetrahydrofuran, and titrated. $Ru(PPh_3)_4Cl_2$, [32] tris(2-

(diphenylphosphino)phenyl)silane ([SiP$^{Ph}_3$]H),[2] and diphenylphosphine were synthesized according to literature procedures.[11] d_{15}-Triphenylphosphine was prepared by a modification of a literature procedure[33] in which purification was attained by column chromatography (eluent 1:1 hexane/EtOAc). d_{10}-Diphenylphosphine was prepared analogously to diphenylphosphine. d_{30}-[SiP$^{Ph}_3$]H was synthesized analogously to [SiP$^{Ph}_3$]H using d_{10}-[2-(diphenylphosphino)phenyl bromide] (prepared analogously to 2-(diphenylphosphino)phenyl bromide[34]). LiP*i*Pr$_2$·3THF was synthesized by the addition of lithium pellets to a THF solution of chlorodiisopropylphosphine. LiPPh$_2$·3Et$_2$O was synthesized by the addition of butyllithium to a diethyl ether solution of diphenylphosphine. Triethylamine was dried over calcium hydride and distilled. Deuterated solvents were purchased from Cambridge Isotope Laboratories, Inc., degassed, and stored over 3 Å molecular sieves prior to use. Elemental analyses were performed by Desert Analytics, Tuscon, AZ, and by Columbia Analytical Services, Tuscon, AZ (formerly Desert Analytics).

2.4.2 X-ray Diffraction Details

X-ray diffraction studies were carried out at the Beckman Institute Crystallography Facility and at the MIT Department of Chemistry X-ray Diffraction Facility on a Bruker Smart 1000 CCD diffractometer or Bruker three-circle Platform diffractometer, equipped with a CCD detector. Data were collected at 100 Kusing Mo Kα (λ = 0.71073 Å) radiation for all structures except for **2.6** and Cu Kα (λ=1.54178 Å) for **2.6** and solved using SHELXL.[35] X-ray quality crystals were grown as described in the

experimental procedures. The crystals were mounted on a glass fiber or nylon loop with Paratone N oil.

2.4.3 Spectroscopic Measurements

Varian Mercury-300, Bruker Avance-400, and Varian Inova-500 were used to collect ^{1}H, $^{11}B\{^{1}H\}$, $^{13}C\{^{1}H\}$, $^{29}Si\{^{1}H\}$, and $^{31}P\{^{1}H\}$ spectra at room temperature unless otherwise noted. ^{1}H and $^{13}C\{^{1}H\}$ spectra were referenced to residual solvent resonances. $^{11}B\{^{1}H\}$ spectra were referenced to external boron trifluoride etherate (δ = 0 ppm), $^{15}N\{^{1}H\}$ spectra were referenced to external neat nitromethane (δ = 0 ppm), $^{29}Si\{^{1}H\}$ spectra were referenced to external tetramethylsilane (δ = 0 ppm), and $^{31}P\{^{1}H\}$ spectra were referenced to external 85% phosphoric acid (δ = 0 ppm).

2.4.4 Kinetic Measurements

In a typical experiment, 0.5 mL of a solution of **2.5** (approximately 50 mM) was added to a J. Young tube containing a sealed internal integration standard (PPh_3), and the sealed tube was heated on a temperature-equilibrated hot plate, which was kept to within 0.5 °C at all times. The reaction was followed by $^{31}P\{^{1}H\}$ NMR, and the ratio of **2.5** to PPh_3 was obtained through comparison of the peak height of **2.5** (peak at 75.0 ppm) to that of PPh_3. The resulting data were fit to first-order decay. The rate constants reported are the average of two experiments, and the error reported is the standard deviation of the two rate constants obtained. A kinetic isotope effect was obtained by performing an analogous reaction at 35 °C using d_{30}-[SiP^{Ph}_3]Ru(PPh_2) (prepared similarly to **2.5**) and comparing the rate constants of the decay of **2.5** and d_{30}-[SiP^{Ph}_3]Ru(PPh_2).

2.4.5 DFT Calculations

A single-point calculation on **2.10a** was run on the Gaussian03[36] suite of programs with the B3LYP[37] level of theory with the LANL2DZ basis set for Ru,[38] Si, and P with diffuse and polarization functions for Si and P.[39] The 6-31G(d,p) basis set was used for C and H.

2.4.6 Synthesis

Synthesis of [SiP$^{Ph}_3$]RuCl (2.1). [SiP$^{Ph}_3$]H (1.90 g, 2.34 mmol) and $Ru(PPh_3)_4Cl_2$ (2.86 g, 2.34 mmol) were charged into a flask, and benzene (120 mL) was added. Triethylamine (1.01 mL, 7.26 mmol) was added, and the flask was heated at 60 °C for 18 h. The mixture was filtered through Celite, and the volatiles were removed *in vacuo*. Layering diethyl ether over a concentrated CH_2Cl_2 solution resulted in large purple blocks. The crystals were dissolved in benzene, and lyophilization yielded an analytically pure, red-purple solid (2.12 g, 95.6%). Crystals suitable for X-ray diffraction were grown by vapor diffusion of pentane into a concentrated benzene solution. ^{1}H NMR (C_6D_6, δ): 8.38 (d, *J* = 7.5 Hz, 3H), 7.38 (m, 11H), 7.24 (t, 3H), 7.15 (m, 7H), 6.87 (t, 3H), 6.77 (t, 5H), 6.66 (t, 10H). ^{13}C{^{1}H} NMR (C_6D_6, δ): 155.0, 154.9, 147.9, 135.7, 134.2, 132.7, 132.5, 129.8, 129.2, 128.8. ^{31}P{^{1}H} NMR (C_6D_6, δ): 68.1 (s). ^{29}Si{^{1}H} NMR ($CDCl_3$, δ): 77.6 (q, J = 16 Hz). Anal. Calcd for $C_{54}H_{42}SiP_3ClRu$: C, 68.38; H, 4.46. Found: C, 68.44; H, 4.23.

Synthesis of [SiP$^{Ph}_3$]RuMe (2.2). [SiP$^{Ph}_3$]RuCl (10 mg, 0.011 mmol) was charged into a J. Young tube and dissolved in d_8-THF. The tube was cooled to −78 °C, and MeLi (11 μL, 0.011 mmol) was syringed in. The tube was quickly capped, and a NMR spectrum of the

sample was taken immediately afterward. ^{1}H NMR(d_8-THF, δ): 8.34 (d, J = 7.2 Hz, 3H), 7.36-6.71 (m, 39H), −0.98 (q, *J* = 4.8 Hz, 3H, Ru−CH_3). ^{31}P{^{1}H} NMR (d_8-THF, δ): 63.7

Synthesis of [SiP$^{Ph}_2$P'^{Ph}]Ru (2.3). [SiP$^{Ph}_3$]RuCl (0.93 g, 0.98 mmol) was dissolved in THF (60 mL) in a flask and cooled to −78 °C. MeLi (0.95 mL, 0.98 mmol) was added dropwise via syringe. The red solution was warmed to room temperature, yielding an orange solution. The solvent was removed in vacuo, and benzene (50 mL) was added to the resulting orange solid. The resulting solution was stirred for 1 h, and the mixture was filtered through Celite and concentrated. Recrystallization from layering diethyl ether over a concentrated THF solution yielded orange needles that analyzed for [SiP$^{Ph}_2$P'^{Ph}]Ru·Et2O. These crystals were suitable for X-ray diffraction, and the solid-state structure includes one molecule of diethyl ether, consistent with the elemental analysis. The diethyl ether could be removed by prolonged exposure of the crushed crystals to vacuum (0.76 g, 85%). ^{1}H NMR(C_6D_6, δ): 8.32 (m, 2H), 8.16 (d, *J* = 7.5 Hz, 1H), 8.03 (d, *J* = 6.6 Hz, 1H), 7.73 (m, 3H), 7.53 (t, *J* = 7.5 Hz, 1H),7.27-6.38 (m, 31H), 6.22 (td, *J* = 13.0 Hz, 1.8 Hz, 2H). ^{13}C{^{1}H} NMR (*d*8-THF, δ): 167.8, 167.2, 157.0, 156.6, 153.8, 153.3, 151.6, 151.3, 149.7, 149.3, 146.8, 146.5, 146.4, 146.3, 145.9, 140.0, 139.8, 137.6, 136.5, 136.4, 135.7, 135.6, 135.0, 134.9, 132.3, 132.1, 131.3, 131.3, 131.2, 131.1, 131.1, 130.8, 129.9, 128.8, 129.7, 128.4, 128.2, 127.8, 127.6, 127.5, 127.2, 127.0, 126.8, 126.7, 126.4, 126.2, 126.0, 125.9, 125.7, 125.6, 125.4, 125.2, 124.7, 124.3, 124.2, 122.5, 119.7. ^{29}Si{^{1}H} NMR (d_8-THF, δ): 71.4. ^{31}P{^{1}H} NMR (C_6D_6, δ): 64.9 (dd, *J* = 19 Hz, 14 Hz), 62.0 (dd, *J* = 235 Hz, 14 Hz), −11.3 (dd, *J* = 235 Hz, 19 Hz). Anal. Calcd for $C_{58}H_{51}OSiP_3Ru$: C, 70.65; H, 5.21. Found: C, 70.77; H, 5.40.

Synthesis of [SiP$^{Ph}_3$]Ru(η^3−CH$_2$Ph) (2.4). [SiP$^{Ph}_3$]RuCl (50 mg, 0.053 mmol) was dissolved in THF(5 mL) and cooled to −78 °C. BnMgCl (27 μL, 0.053 mmol) was added by syringe, and the resulting solution was allowed to warm to room temperature. The solvent was removed in vacuo, the residue was redissolved in benzene, and the resulting solution was filtered through Celite. Pentane was added to a concentrated solution to precipitate out the product, which was pure by NMR(48 mg, 91%). ^{1}H NMR (d_8-THF, δ): 7.8-6.5 (br, overlapping peaks), 6.96 (t, *J* = 7.2 Hz, 1H), 6.63 (t, *J* = 7.6 Hz, 2H), 5.97 (d, *J* = 7.6 Hz, 2H), 2.52 (q, *J* = 4.4 Hz, 2H). ^{1}H NMR(d_8-THF, δ, −20 °C): 7.93 (d, *J* = 7.2 Hz, 2H), 7.63 (s, 4H), 7.45-7.12 (m, 12H), 6.97-6.85 (m, 10H), 6.72-6.6 (m, 8H), 6.41 (s, 4H), 6.40 (d, *J* = 8.4 Hz, 4H), 5.88 (d, *J* = 8 Hz, 2H), 2.49 (br, 2H). ^{13}C{^{1}H} NMR (C_6D_6, δ): 152.1 (br), 139.3 (br), 134.4, 132.5, 131.1 (br), 129.2, 127.7, 126.1, 121.3, 38.4. ^{13}C{^{1}H} NMR (d_8-THF, δ, −20 °C): 157.9, 157.4, 152.4 (m), 147.0, 146.7, 140.0 (br), 139.4 (br), 136.9, 135.6, 134.4, 134.3, 133.8, 132.8, 132.6, 132.4, 130.7, 129.8, 128.9, 128.6, 128.5, 128.3, 128.2, 128.0, 127.9, 127.7, 125.7, 38.2 (m). ^{31}P{^{1}H} NMR (C_6D_6, δ): 81.4 (br), 58.3 (br).

Synthesis of [SiP$^{Ph}_3$]Ru(PPh$_2$) (2.5). [SiP$^{Ph}_3$]RuCl (0.30 g, 0.32 mmol) was dissolved in THF (5 mL) and cooled to −78 °C. LiPPh$_2$·Et$_2$O (84 mg, 0.32 mmol) was added in one portion, resulting in an immediate color change to dark green. Solvent was removed, and the resulting solid was redissolved in benzene, followed by filtration through Celite. The dark green solution was lyophilized to yield a green solid (0.34 g, 97%). Crystals suitable for X-ray diffraction were grown from layering diethyl ether over a concentrated solution of dichloromethane at −35 °C. ^{1}H NMR (C_6D_6, δ): 8.48 (d, *J* = 7.2 Hz, 3H), 7.25-6.67 (m, 52H). ^{13}C{^{1}H} NMR(C_6D_6, δ): 156.0 (m), 151.6, 150.9 (m), 143.2 (m), 133.6, 132.8,

132.5, 132.3 (m), 129.4, 128.9, 128.7, 128.5, 128.3, 128.1, 128.0, 128.0, 127.9, 126.9. $^{31}P\{^{1}H\}$ NMR (C_6D_6, δ): 214.1 (q, *J* = 15 Hz, 1P), 75.0 (d, *J* = 15 Hz).

Synthesis of [SiPPh3]Ru(PiPr2) (2.6). [SiP^{Ph}_3]RuCl (0.20 g, 0.21 mmol) was suspended in benzene (10 mL), and an excess of Li*P*iPr_2·THF (0.082 g, 0.42 mmol) was added in one portion. The resulting mixture was stirred for 7 h, at which time the color of the solution had turned from purple to dark green. The mixture was filtered through Celite, and pentane was layered over a concentrated solution to yield green crystals that analyzed for [SiP^{Ph}_3]Ru(P*i*Pr_2)·1.5C_6H_6 (0.17 g, 71%). These crystals were suitable for X-ray diffraction and showed the correct number of benzene molecules, as indicated by the elemental analysis. ^{1}H NMR(C_6D_6, δ): 8.36 (d, *J* = 6.9 Hz, 3H), 7.24-7.20 (m, 15H), 6.96 (m, 3H), 6.82 (q, *J* = 7.5 Hz, 21H), 3.04 (2H, *J* = 7.2 Hz, 2H), 1.18 (d, *J* = 7.2 Hz, 6H), 1.15 (d, *J* = 7.2 Hz, 6H). $^{13}C\{^{1}H\}$ NMR (C_6D_6, δ): 155.6 (m), 151.2 (m), 143.7 (m), 133.5, 133.3(m), 132.1, 129.0, 128.9, 128.7, 128.5, 128.3, 128.0, 127.9, 46.3 (d, *J* = 8.0 Hz), 21.7, 21.6. $^{31}P\{^{1}H\}$ NMR (C_6D_6, δ): 295.0 (q, *J* = 18 Hz, Ru−*P*iPr_2), 77.0 (d, *J* = 18 Hz). Anal. Calcd for $C_{69}H_{65}SiP_4Ru$: C, 72.23; H, 5.71. Found: C, 72.45; H, 5.72.

Synthesis of [$SiP^{Ph}_2P'^{Ph}$]Ru($PHPh_2$) (2.7). [$SiP^{Ph}_2P'^{Ph}$]Ru (0.025 g, 0.027 mmol) was dissolved in THF (4 mL) and cooled to −78 °C. To the stirring solution was added diphenylphosphine via syringe. The resulting yellow solution was warmed to room temperature, and the solvent was removed to yield a yellow solid. Analytically pure material was obtained by recrystallization from layering pentane over a concentrated THF solution to yield yellow microcrystals (0.023 g, 76%). ^{1}H NMR(C_6D_6, δ): 8.44 (d, *J* = 7.0 Hz, 1H), 8.26 (d, *J* = 7.0 H, 1H), 8.10 (m, 3H), 7.65 (t, *J* = 7.5 Hz, 1H), 7.59 (t, *J* = 7.5 Hz, 2H), 7.56 (dt, *J* = 303 Hz, 9.5 Hz, 1H, *P*HPh_2), 7.40 (t, *J* = 8.0 Hz, 2H), 7.33-

6.39 (m, 38H), 5.65 (t, *J* = 8.0 Hz, 2H). $^{13}C\{^{1}H\}$ NMR (C_6D_6, δ): 161.3, 160.8, 158.0, 157.6, 154.9, 154.5, 152.2, 151.8, 151.5, 150.8, 150.5, 150.3, 149.9, 145.7, 145.3, 142.4, 142.1, 141.5, 140.1, 139.4, 139.3, 137.6, 137.4, 135.4, 135.3, 135.1, 134.9, 134.2, 134.0, 133.9, 133.4, 133.3, 132.6, 132.5, 130.5, 130.3, 129.7, 129.4, 129.3, 129.3, 129.2, 128.9, 128.0, 127.9, 127.8, 127.5, 127.4, 127.1, 127.0, 126.4, 126.3. $^{31}P\{^{1}H\}$ NMR (C_6D_6, δ): 67.6 (dm, *J* = 226 Hz), 62.3 (m), 8.4 (q, *J* = 21 Hz), −13.0 (dm, *J* = 226 Hz). IR (KBr, cm^{-1}): 3046, 2956, 2924, 2869, 2288 (ν[P−H]), 1954, 1558, 1479, 1434, 1309, 1273, 1183, 1156, 1090. Anal. Calcd for $C_{66}H_{52}SiP_4Ru$: C, 72,18; H, 4.77. Found: C, 71.59; H, 4.82. Alternatively, a solution of $[SiP^{Ph}_3]Ru(PPh_2)$ can be left standing at room temperature for several days and cleanly decays to **2.7**.

Synthesis of $[SiP^{Ph}_3]Ru(H)(N_2)$ (2.8). $[SiP^{Ph}_3]RuCl$ (0.60 g, 0.63 mmol) was dissolved in THF (60 mL) and cooled to −78 °C. Sodium triethylborohydride (1M in THF, 0.63 mL, 0.63 mmol) was added dropwise to the solution, and the resulting solution was warmed to room temperature. The solvent was removed, and the resulting solid was redissolved in benzene, followed by filtration through Celite. Pentane was layered over a concentrated benzene solution to yield white needles (0.53 g, 88%). ^{1}H NMR(C_6D_6, δ): 8.59 (d, *J* = 7.2 Hz, 2H), 8.32 (d, *J* = 7.5 Hz, 1H), 7.87 (m, 4H), 7.44 (m, 2H), 7.31 (td, *J* = 6.0 Hz, 1.2 Hz, 2H), 7.20-6.46 (m, 32H), −7.95 (dt, *J* = 60.9 Hz, 27.6 Hz, 1H, Ru−*H*). $^{13}C\{^{1}H\}$ NMR (C_6D_6, δ): 156.8, 156.2, 155.8, 155.4, 155.0, 150.8, 150.5, 150.1, 149.1, 148.5, 147.4, 142.1, 141.8, 141.5, 140.3, 140.0, 137.5 (t), 134.4 (t), 133.7, 133.2, 133.1 (d), 132.9, 132.5, 132.3, 129.3 (d), 129.2, 127.7, 127.4 (d). $^{15}N\{^{1}H\}$ NMR (C_6D_6, δ): −65.1. $^{31}P\{^{1}H\}$ NMR (C_6D_6, δ): 67.5 (d, *J* = 12 Hz, 2P), 59.4 (t, *J* = 12 Hz, 1P). IR (KBr, cm^{-1}): 3050, 2929, 2869, 2167 (ν[N_2]), 1896, 1482, 1436, 1118.

Synthesis of [SiP$^{Ph}_3$]Ru(H)(η^2-H$_2$SiPh$_2$) (2.9). [SiP$^{Ph}_3$]Ru(H)(N$_2$) (0.15 g, 0.16 mmol) was dissolved in benzene (7 mL), and diphenylsilane (0.030 mL, 0.16 mmol) was added dropwise to the stirring solution. The mixture was stirred for 5 min, and the solvent was removed. Layering pentane over a concentrated benzene solution yielded yellow crystals suitable for X-ray diffraction (0.15 g, 85%). ^{1}H NMR (d_8-THF, δ): 8.43 (d, *J* = 7.0 Hz, 3H), 7.33 (t, *J* = 7.0 Hz, 3H), 7.03-6.70 (m, 46H), 5.49 (br, 1H, Ru−Si*H*Ph$_2$), −7.18 (br, 2H, Ru(H)(*H*Si*H*Ph$_2$). ^{13}C{^{1}H} NMR(C$_6$D$_6$, δ): 153.9 (m), 150.7 (m), 143.3, 143.1, 143.0, 135.5, 133.6, 133.4, 132.8, 132.8, 132.7, 132.5, 128.8, 128.7, 128.1, 127.9, 127.7, 127.6, 127.4. ^{29}Si{^{1}H} NMR (C$_6$D$_6$, δ): 90.3, −5.4. ^{31}P{1H} NMR(C$_6$D$_6$, δ): 66.0. IR (KBr, cm^{-1}): 3055, 2086 (ν[Si−H]) 1961, 1891, 1813, 1479, 1307, 1250, 1187, 1102. Anal. Calcd for C$_{66}$H$_{55}$Si$_2$P$_3$Ru: C, 72.18; H, 5.04. Found: C, 72.79; H, 5.01.

Synthesis of [SiP$^{Ph}_3$]Ru(H)(SiPh$_2$) (2.10a). [SiP$^{Ph}_2$P'^{Ph}]Ru (0.20 g, 0.22 mmol) was dissolved in THF (10 mL) and cooled to −78 °C. Diphenylsilane (40 μL, 0.22 mmol) was added via syringe, and the resulting red solution was allowed to warm to room temperature. The solvent was removed, and lyophilization of a benzene solution resulted in an analytically pure red solid (0.22 g, 91%). Crystals suitable for X-ray diffraction were grown from layering pentane over a concentrated benzene solution. ^{1}H NMR (d_8-THF, δ): 8.66 (d, *J* = 7.0 Hz, 3H), 7.32 (t, *J* = 7.2 Hz, 3H), 7.26-6.57 (m, 46H), −8.97 (s, 1H, Ru−*H*). ^{13}C{^{1}H} NMR (d_8-THF, δ): 154.9 (m), 153.9 (m), 143.3, 143.1, 143.0, 135.5, 133.6, 133.4, 132.8, 132.8, 132.7, 132.5, 128.8, 128.7, 128.1, 127.9, 127.7, 127.6, 127.4. ^{29}Si{^{1}H} NMR (C$_6$D$_6$, δ): 373.9 (s, Ru−SiPh$_2$), 103.5 (q, *J* = 15 Hz). ^{31}P{^{1}H} NMR (C$_6$D$_6$, δ): 73.6. Anal. Calcd for C$_{66}$H$_{55}$Si$_2$P$_3$Ru: C, 72.31; H, 4.87. Found: C, 72.29; H, 4.97.

Synthesis of [SiP$^{Ph}_3$]Ru(H)(SiMePh) (2.10b). [SiP$^{Ph}_2$P'^{Ph}]Ru (0.040 g, 0.044 mmol) was dissolved in THF (5 mL) and cooled to −78 °C. Methylphenylsilane (6.0 μL, 0.044 mmol) was added via syringe, and the resulting orange solution was allowed to warm to room temperature. The solvent was removed, and lyophilization of a benzene solution resulted in an orange solid (0.043 g, 95%). ^{1}H NMR (C_6D_6, δ): 8.51 (d, *J* = 7.0 Hz, 3H), 7.29-7.09 (m, 20H), 6.98 (t, *J* = 7.5 Hz, 3H), 6.90 (t, *J* = 7.5 Hz, 3H), 6.80 (t, *J* = 7.5 Hz, 6H), 6.68 (t, *J* = 7.5 Hz, 12H), 1.04 (s, Ru−SiC*H*$_3$Ph, 3H), −9.21 (s, Ru−H, 1H). ^{13}C{1H} NMR(C_6D_6, δ): 154.5 (m), 153.3 (m), 152.3, 142.8 (m), 134.3, 132.8, 132.3 (m), 132.0, 129.1, 128.3, 127.6, 127.4, 127.3, 19.4 (Ru−Si*C*H$_3$Ph). ^{29}Si{^{1}H} NMR (d_8-THF, δ): 359.5 (s, Ru−SiMePh), 101.7 (q, *J* = 18 Hz). ^{31}P{^{1}H} NMR (C_6D_6, δ): 73.2.

Synthesis of [SiP$^{Ph}_3$]Ru(H)(GePh$_2$) (2.11). [SiP$^{Ph}_2$P'^{Ph}]Ru (0.10 g, 0.11 mmol) was dissolved in THF (7 mL) and cooled to −78 °C. Diphenylgermane (21 μL, 0.11 mmol) was added via syringe, and the resulting dark red solution was warmed to room temperature. The solvent was removed, and recrystallization from layering pentane over a concentrated benzene solution yielded red crystals suitable for X-ray diffraction. The crystals were washed with pentane, crushed, and dried under vacuum to yield an analytically pure solid (0.93 g, 74%). ^{1}H NMR (C_6D_6, δ): 8.60 (d, *J* = 7.5 Hz, 3H), 7.3-6.9(m, 31H), 6.73 (t, *J* = 7.5 Hz, 7H), 6.58 (t, *J* = 7.5 Hz, 11H), −8.95 (s, 1H, Ru−H). ^{13}C{^{1}H} NMR (d_8-THF, δ): 163.0, 155.1, 154.7, 152.3, 151.9, 142.6 (br), 133.5 (br), 132.5, 128.7, 128.3, 127.9, 127.6 (br), 127.5, 127.4. ^{31}P{^{1}H} NMR (C_6D_6, δ): 76.2 (br). Anal. Calcd for $C_{66}H_{53}SiP_3GeRu$: C, 69.49; H, 4.68. Found: C, 69.23; H, 4.53.

Synthesis of [SiP$^{Ph}_3$]Ru(H)(H$_2$) (2.12). [SiP$^{Ph}_2$P'^{Ph}]Ru was charged into a J. Young tube and freeze-pump-thawed three times. Excess H_2 gas (1 atm) was introduced. Analysis by

NMR indicated clean conversion to product. ^{1}H NMR(C_6D_6, δ): 8.58 (d, *J* = 7.5 Hz, 3H), 7.31-7.24 (m, 18H), 6.96 (t, *J* = 7.5 Hz, 3H), 6.77 (t, *J* = 7.5 Hz, 6H), 6.63 (t, *J* = 7.5 Hz, 12H), −4.23 (s, 3H, Ru−(*H*)(*H*$_2$)). ^{13}C{^{1}H} NMR (C_6D_6, δ): 155.6 (m), 150.3 (m), 140.7 (m), 133.2, 133.2, 133.1, 132.9, 129.1, 128.9, 128.7, 128.1, 127.9, 127.8. ^{31}P{^{1}H} NMR (C_6D_6, δ): 71.2.

Synthesis of {[SiP$^{Ph}_3$]Ru(H)(SiMePh$_2$)}Li(THF)*x* (2.13). [SiP$^{Ph}_3$]Ru(H)(SiPh$_2$) (0.040 g, 0.037 mmol) was dissolved in THF (4 mL) and cooled to −78 °C. MeLi (0.035 mL, 0.037 mmol) was added dropwise and allowed warm to room temperature. The resulting red solution was lyophilized to give an orange-red solid that was pure by ^{1}H NMR. ^{1}H NMR(*d*$_8$-THF, δ): 8.18 (d, *J* = 7.0 Hz, 3H), 7.02 (t, *J* = 7.0 Hz, 3H), 6.88 (d, *J* = 7.0 Hz, 4H), 6.80-6.48 (m, 32H), 0.21 (s, 3H, Si−C*H*$_3$), −9.77 (s, 1H, Ru−H). ^{13}C{^{1}H} NMR (*d*$_8$-THF, δ): 158.4, 155.6 (m), 154.8 (m), 144.0, 134.9, 131.7, 129.5, 127.8, 124.2, 123.9, 123.6, 123.5, 121.1, 7.2. ^{29}Si{1H} NMR(*d*$_8$-THF, δ): 102.4 (q, *J* = 19.8 Hz), 9.6 (q, *J* = 12.2 Hz). ^{31}P{^{1}H} NMR (*d*$_8$-THF, δ): 70.4

Synthesis of [SiP$^{Ph}_2$P^{Ph}–B(cat)]Ru(μ−H) (2.14). [SiP$^{Ph}_2$P'^{Ph}]Ru (0.12 g, 0.13 mmol) was dissolved in THF (7 mL) and cooled to −78 °C. Catecholborane (14 μL, 0.13 mmol) was added via syringe, and the resulting orange solution was allowed to warm to room temperature. The solvent was removed, and crystals suitable for X-ray diffraction were grown from layering pentane over a concentrated benzene solution to yield orange crystals that analyzed as [SiP$^{Ph}_2$P^{Ph}–BH(O$_2$C$_6$H$_4$)]Ru·1.5C6H6 (0.10 g, 69%). These crystals were suitable for X-ray diffraction, and the solid-state structure shows the correct number of solvent molecules. ^{1}H NMR(C_6D_6, δ): 8.43 (d, *J* = 7.5 Hz, 1H), 8.28 (d, *J* = 7.2 Hz, 1H), 8.14 (m, 2H), 7.98 (m, 2H), 7.72-7.60 (m, 2H), 7.21-6.00 (m, 38H), −6.24

(br, 1H, Ru−H−B). ^{11}B{1H} NMR(d_8-THF, δ): 12 (br). ^{13}C{^{1}H} NMR(d_8-THF, δ): 157.8, 157.5, 157.;1, 156.8, 156.1, 154.6, 151.2, 150.9, 150.3, 149.9, 147.8, 147.4, 144.7, 144.5, 141.6, 141.3, 139.6, 139.3, 136.6, 136.5, 136.2 (d, *J* = 3.4 Hz), 136.1, 135.8, 134.8 (d, *J* = 3.0 Hz), 134.2 (d, *J* = 4.3 Hz), 134.0 (d, *J* = 3.9 Hz), 133.8 (d, *J* = 20.8), 133.5 (m), 133.2, 132.8 (d, *J* = 10.4 Hz), 132.7, 132.5 (d, *J* = 15.3 Hz), 132.2, 131.6 (d, *J* = 3.4 Hz), 130.7, 130.5, 130.4, 130.3 (d, *J* = 3.4 Hz), 129.8, 129.1(d, *J* = 21.5 Hz), 128.9, 128.8, 128.7, 128.6, 128.5, 128.5, 128.4, 128.3, 128.2, 128.0, 128.0, 127.9, 127.8, 127.5 (d, *J* = 8.9 Hz), 121.8, 119.0, 117.6, 113.5, 112.1, 108.6. ^{29}Si{^{1}H} NMR (C_6D_6, δ): 75.7. ^{31}P{^{1}H} NMR (C_6D_6, δ): 72.7 (dd, *J* = 20.0, 15.7 Hz), 63.8 (dd, *J* = 233.0, 20.0 Hz), 54.1 (dd, *J* = 233.0, 15.7 Hz). Anal. Calcd for $C_{69}H_{54}BO_2SiP_3Ru$: C, 72.12; H, 4.74. Found: C, 72.48; H, 4.65.

Synthesis of [SiP$^{Ph}_2$P$^{C6H3B(cat)}$ −B(cat)]Ru(μ−H) (2.15). [SiP$^{Ph}_2$P'^{Ph}]Ru (0.10 g, 0.11 mmol) was dissolved in toluene (30 mL) and cooled to −78 °C. Biscatecholatodiboron (0.026 g, 0.11 mmol) was added in one portion, and the resulting orange solution was allowed to warm to room temperature. The solvent was removed, and the residue was recrystallized twice from layering pentane over a concentrated benzene solution to yield yellow crystals suitable for X-ray diffraction (0.081 g, 64%). ^{1}H NMR (d_8-THF, δ): 8.50 (d, *J* = 7.5 Hz, 1H), 8.22 (d, *J* = 7.0 Hz, 1H), 8.10 (t, *J* = 8.5 Hz, 2H), 8.00-7.95 (m, 2H), 7.76 (d, *J* = 7.5 Hz, 1H), 7.71 (d, *J* = 6 Hz, 1H), 7.43-5.81 (m, 40H), −6.25 (br, 1H). ^{11}B{1H} NMR(d_8-THF, δ): 30 (br), 11(br). ^{13}C{^{1}H} NMR (d_8-THF, δ): 156.5, 156.2, 155.8, 155.6, 154.7, 151.1, 150.7, 149.9, 149.5, 149.2, 149.0, 148.5, 148.1, 144.7, 144.4, 144.7, 144.4, 142.4, 142.2, 141.8, 137.2, 137.1, 136.6, 136.5, 136.1, 135.8, 135.5, 135.4, 134.8, 134.5, 134.3, 134.2, 134.0, 133.7, 133.6, 133.4, 133.3, 133.2, 133.0, 132.9, 132.8,

132.2, 132.1, 130.8, 130.6, 130.5, 129.7, 129.5, 129.3, 128.9, 128.9, 128.8, 128.7, 128.5, 128.4, 128.3, 128.0, 128.0, 127.9, 127.6, 127.6, 127.4, 127.1, 127.0. $^{31}P\{^{1}H\}$ NMR (d_8-THF, δ): 72.6 (dd, J = 19.5 Hz, 16.1 Hz), 68.8 (dd, J = 232.8 Hz, 19.5 Hz), 54.8 (dd, J = 232.7 Hz, 16.1 Hz). Anal. Calcd for $C_{66}H_{49}B_2O_4SiP_3Ru$: C, 68.94; H, 4.30. Found: C, 69.02; H, 3.84.

References Cited

1 a) Macbeth, C. E.; Golombek, A. P.; Young, V. G. Jr.; Yang, C.; Kuczera, K.; Hendrich, M. P.; Borovik, A. S. *Science* **2000**, *289*, 938. b) Lim, M. H.; Rohde, J.; Stubna, A.; Bukowski, M. R.; Costas, M.; Ho, R. Y. N.; Münck, E.; Nam, W.; Que, L. Jr. *Proc. Natl. Acad. Sci. U.S.A.***2003**, *100*, 3665. c) Yandulov, D. V.; Schrock, R. R. *Science* **2003**, *301*, 76.

2 a) Mankad, N. P.; Whited, M. T. *Angew. Chem., Int. Ed.* **2007**, *46*, 5768. b) Whited, M. T.; Mankad, N. P.; Lee, Y.; Peters, J. C. *Inorg. Chem.* **2009**, *48*, 2507.

3 Joslin et al. have previously reported a similar scaffold. See: Joslin, F. L.; Stobart, S. R. *Chem. Commun.* **1989**, 504.

4 a) Sacconi, L.; Bertini, I. *J. Am. Chem. Soc.* **1967**, *89*, 2235. b) Stoppioni, P.; Mani, F.; Sacconi, L. *Inorg. Chem.* **1974**, *11*, 227. c) Di Vaira, M.; Ghilardi, C. A.; Sacconi, L. *Inorg. Chem.* **1976**, *15*, 1555.

5 a) Hu, X.; Castro-Rodriguez, I.; Meyer, K. *J. Am. Chem. Soc.* **2003**, *125*, 12237. b) Hu, X.; Castro-Rodriguez, I.; Meyer, K. *J. Am. Chem. Soc.* **2004**, *126*,13464.

6 Addison, A. W.; Rao, T. N.; Van Rihn, J. J.; Verschoor, G. C. *J. Chem. Soc., Dalton Trans.* **1984**, 1349.

7 a) Cole-Hamilton, D. J.; Wilkinson, G. J. *J. Chem. Soc., Dalton Trans.* **1977**, 797. b) Pez, G. P.; Grey, R. A.; Corsi, J. *J. Am. Chem. Soc.* **1981**, *103*, 7528.

8 a) Cámpora, J.; López, J. A.; Palma, P.; Ruíz, C.; Carmona, E. *Organometallics* **1997**, *16*, 2709. b) Brookhart, M.; Buck, R. C.; Danielson, E. III *J. Am. Chem. Soc.* **1989**, *111*, 567. c) Winter, M. J.; Woodward, S. J. *J. Chem. Soc., Chem. Commun.* **1989**, 457. d) Braun, T.; Münch, G.; Windmüller, B.; Gevert, O.; Laubender, M.; Werner, H.

Chem. –Eur. J. **2003**, *9*, 2516. e) Boardman, B. M.; Valderrama, J. M.; Muñoz, F.; Wu, G.; Bazan, B. C.; Rojas, R. *Organometallics* **2008**, *27*, 1671. f) Gielens, E. E. C. G.; Tiesnitsch, J. Y.; Hessen, B.; Teuben, J. H. *Organometallics* **1998**, *17*, 1652.

9 a) Baker, R. T.; Whitney, J. F.; Breford, S. S. *Organometallics* **1983**, *2*, 1049. b) Rocklage, S. M.; Schrock, R. R.; Churchill, M. R.; Wasserman, H. J. *Organometallics* **1982**, *1*, 1332.

10 Derrah, E. J.; Pantazis, D. A.; McDonald, R.; Rosenberg, L. *Organometallics* **2007**, *26*, 1473.

11 Gulyás, H.; Benet-Buchholz, J.; Escudero-Adan, E. C.; Freixa, Z.; van Leeuwen, P. W. N. M. *Chem. –Eur. J.* **2007**, *13*, 3424.

12 a) Wu, Z.; Diminnie, J. B.; Xue, Z. *J. Am. Chem. Soc.* **1999**, *121*, 4300. b) Qiu, H.; Woods, J. B.; Wu, Z.; Chen, T.; Yu, X.; Xue, Z. *Organometallics* **2005**, *24*, 4190.

13 Selected examples: a) Ilsley, W. H.; Sadurski, E. A.; Schaaf, T. F.; Albright, M. J.; Anderson, T. J.; Glick, M. D.; Oliver, J. P. *J. Organomet. Chem.* **1980**, *190*, 257. b) Biershenk, T. R.; Guerra, M. A.; Juhlke, T. J.; Larson, S. B.; Lagow, R. J. *J. Am. Chem. Soc.* **1987**, *109*, 4855. c) Arnold, J.; Tilley, T. D.; Rheingold, A. L.; Geib, S. J.; *Inorg. Chem.* **1987**, *26*, 2106. d) Suginome, M.; Oike, H.; Shuff, P. H.; Ito, Y. *J. Organomet. Chem.* **1996**, *521*, 405.

14 See appendix 1.

15 J_{SiH} = 40 Hz from the spectrum, but this value is doubled to account for the rapid exchange with the hydride, which is assumed to have a J_{SiH} = 0 Hz. See Taw, F. L.; Bergman, R. G.; Brookhart, M. *Organometallics* **2004**, *23*, 886 for further details.

16 d_{30}-[SiP^{Ph}_3]Ru(H)(N_2) is prepared analogously to **2.8**.

17 A small amount of free diphenylsilane is also observed in the spectrum. This indicates that free diphenyl silane can exchange with the η^2-coordinated silane.

18 a) Selected examples: a) Leucke, H. F.; Bergman, R. G. *J. Am. Chem. Soc.* **1997**, *119*, 11538. b) Mork, B. V.; Tilley, T. D. *J. Am. Chem. Soc.* **2001**, *123*, 9702.

19 Corey, J. Y.; Braddock-Wilking, J. *Chem. Rev.* **1999**, *99*, 175.

20 Okazaki et al. have reported a complex in which a base-stabilized silylene and a silyl ligand are at an angle of 160.34(2)° and 159.89(3)° from each other. See Okazaki, M.; Minglana, J. J. G.; Yamahira, N.; Tobita, H.; Ogino, H. *Can. J. Chem.* **2003**, *81*, 1350.

21 a) Ochiai, M.; Hashimoto, H.; Tobita, H. *Angew. Chem., Int. Ed.* **2007**, *46,* 8192. b) Grumbine, S. K.; Tilley, T. D. *J. Am. Chem. Soc.* **1994**, *116*, 5495.

22 Peters, J. C.; Feldman, J. D.; Tilley, T. D. *J. Am. Chem. Soc.* **1999**, *121*, 9871

23 Feldman, J. D.; Peters, J. C.; Tilley, T. D. *Organometallics* **2002**, *21*, 4065.

24 Waterman, R.; Hayes, P. G.; Tilley, T. D. *Acc. Chem. Res.* **2007**, *40*, 712.

25 An example of a base-stabilized silylene complex with a *trans* hydride ligand has been reported. See: Grumbine, S. D.; Tilley, T. D.; Arnold, F. P.; Rheingold, A. L. *J. Am. Chem. Soc.* **1993**, *115*, 7884.

26 a) Haaf, M.; Schmedake, T. A.; West, R. *Acc. Chem. Res.* **2000**, *33*, 704. b) Gehrhus, B.; Hitchcock, P. B.; Lappert, M. F.; Maciejewski, H. *Organometallics* **1998**, *17*, 5599.

27 a) Hamilton, D. G.; Crabtree, R. J. *J. Am. Chem. Soc.* **1988**, *110*, 4126. b) Desrosiers, P. J.; Cai, L.; Lin, Z.; Richards, R.; Halpern, J. *J. Am. Chem. Soc.* **1991**, *113*, 4173.

28 A partial deuteration experiment of **2.12** using HD has been performed in attempts obtain the H−D coupling constant, but overlap of H_3 and H_2D isotopomer resonances

at 0 °C complicates the analysis. Further cooling results in the gradual merging of the resonances until at −50 °C a single broad resonance is observed. This method of analysis follows Oldham, W. J. Jr.; Hinkle, A. S.; Heinekey, D. M. *J. Am. Chem.. Soc.* **1997**, *119*, 11028.

29 Tilley and co-workers have reported related results: a) Hayes, P. G.; Beddie, C.; Hall, M. B. *J. Am. Chem. Soc.* **2006**, *128*, 428. b) Calimano, E.; Tilley, T. D. *J. Am. Chem. Soc.* **2008**, *130*, 9226.

30 Such an insertion has been observed previously. See Baker, R. T.; Calabrese, J. C.; Wescott, S. A.; Marder, T. B. *J. Am. Chem. Soc.* **1995**, *117*, 8777.

31 a) Hartwig, J. F.; Cook, K. S.; Hapke, M.; Incarvito, C. D.; Fan, Y.; Webster, C. E. ; Hall, M. B. *J. Am. Chem. Soc.***2005**, *127*, 2538. b) Wan, X.; Wang, X.; Luo, Y.; Takami, S.; Kubo, M.; Miyamoto, A. *Organometallics* **2002**, *21*, 3703. c) Ishiyama, T.; Miyaura, N. *J. Organomet. Chem.* **2003**, *680*, 3. d) Tamura, H.; Yamazaki, H.; Sato, H.; Sakaki, S. *J. Am. Chem. Soc.* **2003**, *125*, 16114.

32 Hallman, P. S.; Stephenson, T. A.; Wilkinson, W. C. *Inorg. Synth.* **1970**, *12*, 237.

33 Baldwin, J. E.; Barden, T. C.; Pugh, R. L.; Widdison, W. C. *J. Org. Chem.* **1987**, *52*, 3303.

34 Whited, M. T.; Rivard, E.; Peters, J. C. *Chem. Commun.* **2006**, 1613.

35 Sheldrick, G. M. *Acta Crystallogr. A* **2008**, *64*, 112.

36 Gaussian 03, Revision C.02, Frisch, M. J.; Trucks, G. W.; Schlegel, H. B.; Scuseria, G. E.; Robb, M. A.; Cheeseman, J. R.; Montgomery, Jr., J. A.; Vreven, T.; Kudin, K. N.; Burant, J. C.; Millam, J. M.; Iyengar, S. S.; Tomasi, J.; Barone, V.; Mennucci, B.; Cossi, M.; Scalmani, G.; Rega, N.; Petersson, G. A.; Nakatsuji, H.; Hada, M.; Ehara,

M.; Toyota, K.; Fukuda, R.; Hasegawa, J.; Ishida, M.; Nakajima, T.; Honda, Y.; Kitao, O.; Nakai, H.; Klene, M.; Li, X.; Knox, J. E.; Hratchian, H. P.; Cross, J. B.; Bakken, V.; Adamo, C.; Jaramillo, J.; Gomperts, R.; Stratmann, R. E.; Yazyev, O.; Austin, A. J.; Cammi, R.; Pomelli, C.; Ochterski, J. W.; Ayala, P. Y.; Morokuma, K.; Voth, G. A.; Salvador, P.; Dannenberg, J. J.; Zakrzewski, V. G.; Dapprich, S.; Daniels, A. D.; Strain, M. C.; Farkas, O.; Malick, D. K.; Rabuck, A. D.; Raghavachari, K.; Foresman, J. B.; Ortiz, J. V.; Cui, Q.; Baboul, A. G.; Clifford, S.; Cioslowski, J.; Stefanov, B. B.; Liu, G.; Liashenko, A.; Piskorz, P.; Komaromi, I.; Martin, R. L.; Fox, D. J.; Keith, T.; Al-Laham, M. A.; Peng, C. Y.; Nanayakkara, A.; Challacombe, M.; Gill, P. M. W.; Johnson, B.; Chen, W.; Wong, M. W.; Gonzalez, C.; and Pople, J. A.; Gaussian, Inc., Wallingford CT, 2004.

37 a) Becke, A. D. *J. Chem. Phys.* **1993**, *98*, 5648. b) Lee, C.; Yang, W.; Parr, R. G. *Phys. Rev. B* **1988**, *37*, 785.

38 a) Hay, P. J.; Wadt, W. R.; *J. Chem. Phys.* **1985**, *82*, 270. b) Wadt, W. R.; Hay, P. J. *J. Chem. Phys.* **1985**, *82*, 284. c) Hay, P. J.; Wadt, W. R. *J. Chem. Phys.* **1985**, *82*, 299.

39 Check, C. E.; Faust, T. O.; Bailey, J. M.; Wright, B. J.; Gilbert, T. M.; Sunderlin, L. S. *J. Chem. Phys.* **2001**, *105*, 8111.

Chapter 3: Access to Well-Defined Ruthenium(I) and Osmium(I) Metalloradicals

Reproduced in part with permission from

Takaoka, A.; Gerber, L. C. H.; Peters, J. C. *Angewandte Chemie, International Edition*

2010, *49*, 4088-4091.

3.1 Introduction

Low-valent metalloradicals of the late 2nd and 3rd row transition metals have garnered recent attention in the context of their interesting spectroscopic properties and potential applicability in catalysis.[1] Mononuclear Ru(I) and Os(I) compounds of such types are particularly sparse.[2] Due to the inherent instability of these species, studies that extend beyond attempts to rapidly characterize them *in situ* are not available. As a consequence the chemistry of mononuclear Ru(I) and Os(I) complexes is essentially unexplored.[3]

Recently we reported the first mononuclear complexes of Fe(I) with terminal dinitrogen ligands.[4] The iron centers in these complexes are chelated by bulky tetradentate tris(phosphino)silyl ligands, $[SiP^{R}_{3}]^{-}$ ($[SiP^{R}_{3}]^{-}$ = $(2\text{-}R_2PC_6H_4)_3Si^{-}$, R = Ph, *i*Pr), that favor mono- rather than dinuclear species. The steric influence provided by this scaffold and its ability to accommodate the Fe(I) oxidation state made it a plausible candidate for exploring access to the unusual oxidation states Ru(I) and Os(I). Herein we report structural, spectroscopic, and theoretical studies of well-defined and mononuclear Ru(I) and Os(I) complexes, $[SiP^{iPr}_{3}]M(L)$ (M = Ru, Os; L = N_2, Pme_3). To our knowledge, these are the first such examples to be isolated and thoroughly characterized, including characterization by X-ray diffraction. Moreover, initial reactivity studies with $[SiP^{iPr}_{3}]M(N_2)$ (M = Ru, Os) complexes expose both one- and two-electron reactivity. The latter type affords unusual M(III) imido (M = Ru, Os) complexes, $[SiP^{iPr}_{3}]M(Nar)$ (M = Ru, Os; Ar = $C_6H_4CF_3$), that display substantial "imidyl" radical character. In contrast to its highly unstable and structurally related Fe(III) imido derivative, which can

only be observed in a frozen glass,[5] these imidyl radicals are sufficiently long-lived to isolate in pure form.

3.2 Results and Discussion

Precursors to the M(I) (M = Ru, Os) complexes, [SiP$^{iPr}_3$]MCl (M = Ru (**3.1**), Os (**3.2**)), are prepared by heating a mixture of HsiP$^{iPr}_3$, [(η^6-C_6H_6)M(Cl)(μ-Cl)]$_2$, and Et_3N in toluene to yield red **3.1** and brown **3.2** in 94% and 95% yield, respectively (Scheme 3.1). Chemical reduction of **3.1** and **3.2** with KC_8 results in green [SiP$^{iPr}_3$]M(N_2) (M = Ru (**3.3**), Os(**3.4**)) in 85% and 70% yield. The ^{1}H NMR spectra of **3.3** and **3.4** are similar and show broad features between δ = −1~11 ppm, consistent with their expected paramagnetism (S = 1/2). The IR spectra of **3.3** and **3.4** depict strong vibrations at 2088 and 2052 cm^{-1} for the nitrogen ligands.

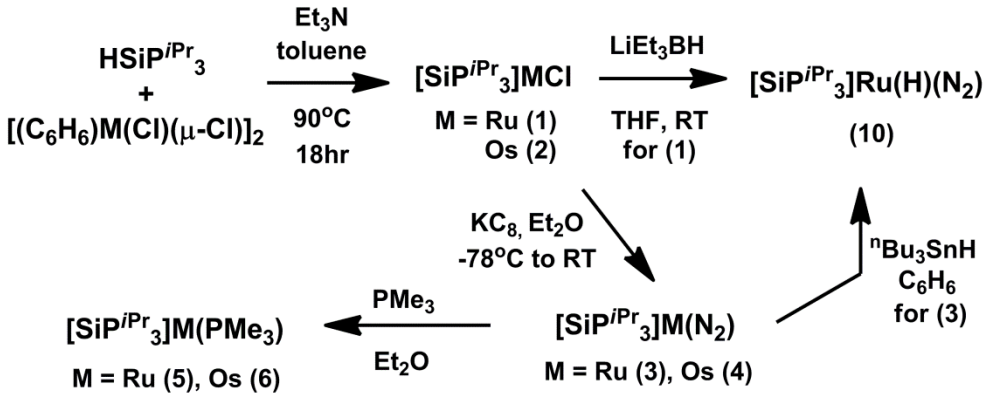

Scheme 3.1.

Crystals of **3.3** and **3.4** suitable for X-ray diffraction are grown from slow evaporation of a concentrated pentane solution. Unlike [SiP$^{iPr}_3$]Fe(N_2), which is rigorously trigonal bipyramidal (TBP),[4] the solid-state structures of **3.3** (Figure 3.2) and **3.4** (see appendix) feature substantive distortions from TBP geometries (τ = 0.76 (**3.3**), 0.70(**3.4**))[6] with one of the P−M−P angles notably larger than the others. The N−N bond lengths are short

(1.097(5) (**3.3**), 1.101(6) (**3.4**) Å) and consistent with the high ν_{N2} values. The N_2 ligands in **3.3** and **3.4** are labile, and addition of one equivalent of Pme_3 results in formation of the phosphine adducts, $[SiP^{iPr}_3]M(Pme_3)$ (M = Ru (**3.5**), Os(**3.6**)). Compound **3.5** has been crystallographically characterized (see appendix) and has a geometry similar to **3.3** ($\tau = 0.86$).

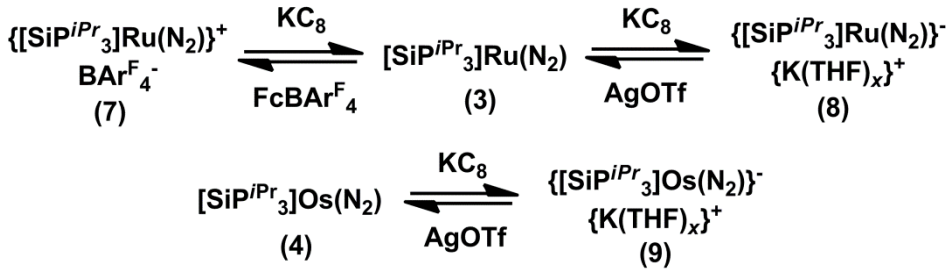

Scheme 3.2.

The cyclic voltammogram of **3.3** shows one oxidation event at −1.24 V (vs Fc/Fc^+), and one reduction event at −2.14 V, which are assigned to the formal $Ru^{II/I}$ and $Ru^{I/0}$ couples, respectively. Chemical oxidation and reduction of **3.3** with $FcBAr^F_4$ (BAr^F_4 = tetrakis(3,5-bis(trifluoromethyl)phenyl)borate) and KC_8 leads to the corresponding Ru(II) and Ru(0) dinitrogen complexes, $\{[SiP^{iPr}_3]Ru(N_2)\}^+BAr^F_4{}^-$ (**3.7**) and $\{[SiP^{iPr}_3]Ru(N_2)\}^-K(THF)_x^+$ (**3.8**), respectively, which have also been crystallographically characterized (see appendix). Complexes **3.3**, **3.7**, and **3.8** represent a rare series of mononuclear N_2 complexes spanning three distinct states of oxidation (Scheme 3.2); the analogous Fe system also stabilizes the corresponding N_2 series.[7] The N_2 ligand in **3.7** is very labile and appears to be in equilibrium with an N_2 free species,[8] as evidenced by the shift in the $Ru^{II/I}$ couple under argon and its $^{15}N\{^1H\}$ NMR spectrum, which only shows resonances for the coordinated N_2 at low temperature.[9] While the cyclic voltammogram of **3.4** also displays a reduction event at −1.94 V, an irreversible oxidation event at −1.17 V is

observed. The reduction product, $\{[SiP^{iPr}_3]Os(N_2)\}^-K(THF)_x^+$ (**3.9**) was accessed similarly to **3.8** and its solid-state structure is isostructural (see appendix).

Although **3.3**-**3.6** are formally Ru(I) and Os(I) complexes, the possibility of a ligand-centered radical cannot be excluded based on structural studies alone, especially in light of the growing recognition of redox non-innocence of many auxiliary ligands.[10] To investigate the distribution of spin density in **3**-**6**, their EPR spectra were measured at 77 K in toluene glass (Figure 3.1 and appendix). Each spectrum exhibits rhombic features with large hyperfine coupling to one phosphorus atom, consistent with unpaired spin density localized in an orbital of the equatorial plane of the TBP.

In assessing metal radical character, the anisotropy of g-values ($\Delta g = g_{max} - g_{min}$) is particularly noteworthy, since large Δg has been noted as a crude indication of metalloradical character for $S = 1/2$ systems.[11,12] Overall the Δg values for **3**-**6**, which are 0.135, 0.257, 0.166, and 0.318 respectively, are significantly larger than complexes that have been assigned as ligand centered radicals.[13,14] The noticeably larger Δg values for the Os relative to the Ru complexes are largely due to the greater spin-orbit coupling constant for the heavier metal.[15] Although g-values alone cannot be used as a quantitative measure of spin density, the simulated EPR parameters support our formulations of **3.3**-**3.6** as *bona fide* metalloradicals. As a test of our assignment, Mülliken spin densities (SD) were calculated for **3.3**-**3.6** (Figure 3.2 and appendix). These calculations place 76% (**3.3**), 69% (**3.4**), 84% (**3.5**), and 79% (**3.6**) of the SD at the metal center. In addition 16% (**3.3**), 15% (**3.4**), 13% (**3.5**), and 13% (**3.6**) of the SD is located at the phosphines.[16] In each complex, one of the P atoms possesses a greater value relative to the other two, consistent with the EPR simulations that suggest an unpaired spin in the equatorial plane.

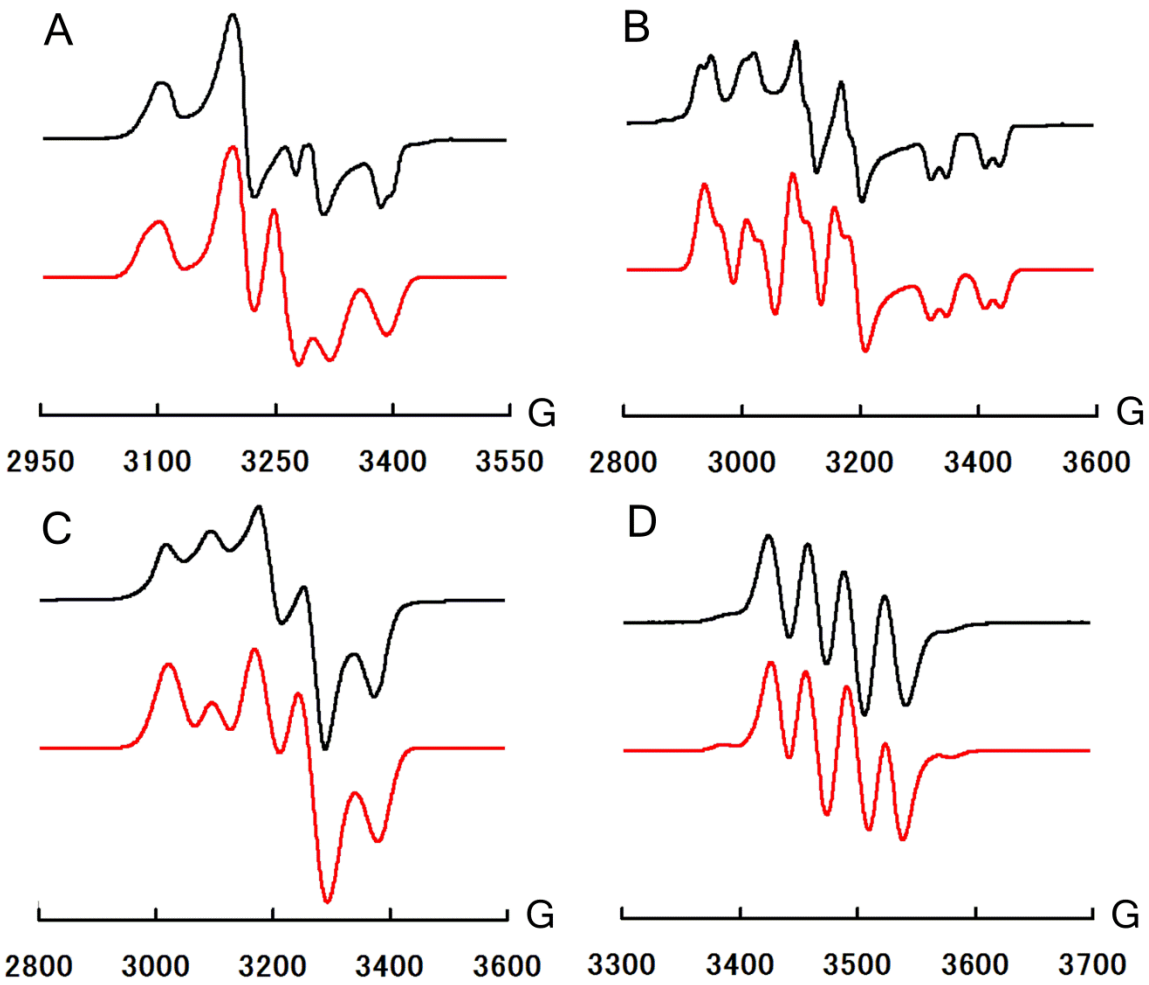

Figure 3.1. A) EPR specrum of **3.3** (77 K). (g_x, g_y, g_z) = (2.130, 2.076, 1.995). B) EPR specrum of **3.4** (77 K). (g_x, g_y, g_z) = (2.239, 2.133, 1.982). C) EPR specrum of **3.5** (77 K). (g_x, g_y, g_z) = (2.175, 2.075, 2.009). D) EPR specrum of **3.11** (RT). g_{iso} = 2.020. The lower curves are simulations. See the appendix for other parameters.

Chemical evidence consistent with the metalloradical character of **3.3** is obtained by its treatment with $^{n}Bu_3SnH$, which cleanly affords the hydride complex [SiP$^{iPr}_3$]Ru(H)(N_2), (**3.10**), over 24 h; this is similar to the reactivity of other metal-

centered radicals towards $^{n}Bu_3SnH$.[17a] In addition, **3.3** reacts cleanly with I_2 and PhS-SPh to afford the corresponding Ru(II) iodide and thiolate complexes, [SiP$^{iPr}_3$]RuI and [SiP$^{iPr}_3$]RuSPh (see experimental section).

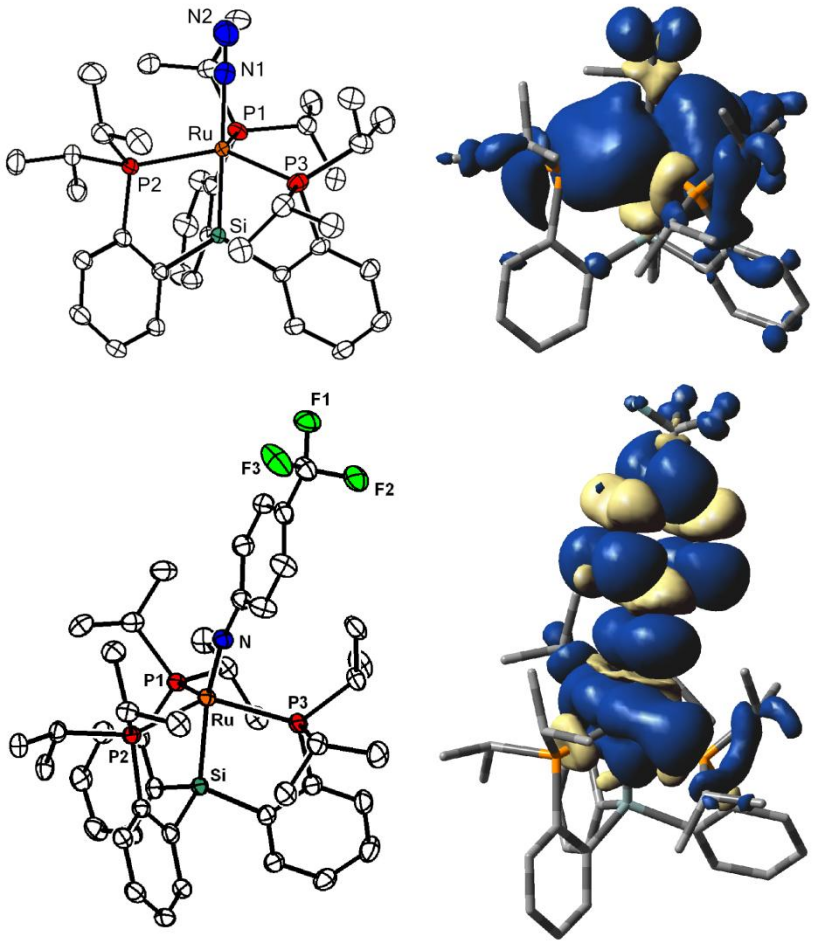

Figure 3.2. Solid-state structures (thermal ellipsoids set at 50% probability) and spin density plots (0.0004 isocontours) for **3.3** (top) and **3.11** (bottom). Selected bond lengths (Å) and angles (°) for **3.3**: Ru−N(1), 2.049(3); Ru−P(1), 2.3221(9); Ru−P(2), 2.3743(9); Ru−P(3), 2.3253(9); Ru−Si, 2.2187(9); N(1)−N(2), 1.097(5); Si−Ru−N(1), 177.0(1). **3.11**: Ru−N, 1.869(2); Ru−P(1), 2.2968(7); Ru−P(2), 2.4242(6); Ru−P(3), 2.3756(7); Ru−Si, 2.3949(6); Si−Ru−N, 162.4(1); Ru−N−C(Ar), 172.0(2).

The reactivity of late second and third row metalloradicals often follows one-electron processes.[1,17] Having observed one-electron reactivity in **3.3** we sought, in turn, to investigate whether two-electron processes might also be feasible. To this end, complex **3.3** was treated with organoazides to see if metal imido/nitrene species would be formed through loss of N_2, akin to the recently observed reactivity of related Fe(I) complexes.[18] Treatment of **3.3** with *para*-CF_3 substituted phenylazide led to formation of the formally Ru(III) imido species, [SiP^{iPr}_3]Ru(Nar) Ar = $C_6H_4CF_3$ (**3.11**). The solid-state structure of **3.11** (Figure 3.2) reveals a geometry midway between a TBP (τ = 0.54) and SQP with a Ru−N bond length of 1.869(2) Å. While this bond length is significantly shorter than Ru−N bonds between typical ruthenium anilides (Ru−N > 1.95 Å),[19] it is appreciably longer than prototypical ruthenium imido complexes (Ru-N < 1.80 Å).[20] Treatment of **3.4** with *para*-CF_3 substituted phenylazide also leads to the corresponding Os(III) imido species [SiP^{iPr}_3]Os(Nar) Ar = $C_6H_4CF_3$ (**3.12**). Crystallographic characterization establishes that **3.12** is isostructural to its ruthenium analogue **3.11** (see appendix).

Complexes **3.11** and **3.12** represent interesting examples of 5-coordinate, formally d^5 imido complexes. Qualitative molecular orbital diagrams predict low bond orders (less than or equal to 1.5) due to the occupation of π^* orbitals.[21] It is worth underscoring that TBP complexes with metal-ligand multiple bonds and d-electron configurations >1 are virtually unknown. Que and co-workers have provided a noteworthy recent exception.[22] The stability of **3.11** and **3.12** is, therefore, surprising and distinct from its chemically related and highly unstable iron derivative [SiP^{iPr}_3]Fe(N-*p*-tolyl), which has a calculated geometry[23] close to **3.11** and **3.12**. [SiP^{iPr}_3]Fe(N-*p*-tolyl) is only observable by EPR when

generated photolytically in a frozen glass, decomposing rapidly *via* presumed bimolecular nitrene coupling to yield azobenzenes.[5] While complexes **3.11** and **3.12** decompose in solution at room temperature over several days, they are stable at −35 ^{o}C as solids for extended periods.

The difference in stability/reactivity between [SiP$^{i\text{Pr}}_3$]Fe(Nar) and complexes **3.11** and **3.12** could potentially be attributed to differences in electronic configuration. Though they are formally M(III) imido complexes, close examination of their EPR spectra indicate that they possess significant nitrogen centered radical character. Unlike the RT spectra of **3.3**-**3.6**, which show broad features, the spectra of **3.11** and **3.12** (Figure 3.1 and appendix) show relatively sharp four line patterns with isotropic g-values of 2.02 and 2.01, respectively, which are much closer in value to that of a free electron (g_e = 2.0023) compared to the corresponding metalloradicals **3.3**-**3.6**. Ruthenium and osmium hyperfine coupling are also observed (A^{Ru} = 48 MHz (**3.11**), A^{Os} = 150 MHz (**3.12**)) and the spectra are best simulated by assigning hyperfine coupling to one nitrogen atom (A^{N} = 98 MHz (**3.11**), A^{N} = 93 MHz (**3.12**)) and smaller coupling to one phosphorus atom (A^{P} = 64 MHz (**3.11**), A^{P} = 58 MHz (**3.12**)). These isotropic A^{N} values are surprisingly large. For comparison, the similarly sp-hybridized NO radical has a nitrogen hyperfine coupling constant of A^{N} = 77 MHz.[24] In addition, the Ru hyperfine coupling constant, A^{Ru}, in **3.11** is smaller than a spectroscopically detected Ru(III) imido complex that was suggested to possess considerable ligand radical character.[25] Further supporting the largely ligand-centered radical character of **3.11** and **3.12**, the EPR spectra at 77 K reveal much smaller g-anisotropies (Δg = 0.072 (**3.11**), 0.128 (**3.12**)) relative to their corresponding Ru(I) and Os(I) metalloradicals, **3.3**-**3.6**. DFT calculations are consistent

with the EPR parameters and show that 54% (**3.11**) and 54% (**3.12**) of the SD is distributed throughout the Nar moiety, of which 27% (**3.11**) and 24% (**3.12**) is on the nitrogen atom and 40% (**3.11**) and 39% (**3.12**) is located at the metal center (see appendix). While delocalization of the spin density along the M−Nar moiety is evident, both EPR and DFT data suggest that perhaps **3.11** and **3.12** are best considered M(II) complexes with a ligand-localized radical (Scheme 3.3). This ligand radical is a one-electron oxidized imido ligand $(\cdot Nar)^{-}$ and exhibits properties of a rare imidyl radical that has only very recently been described in coordination chemistry.[25, 26] The electronic configurations of **3.11** and **3.12** distinguish themselves from $[SiP^{iPr}_3]Fe(Nar)$,[5] whose DFT-predicted ground state (S = ½) is calculated to consist of a largely metal-centered radical.

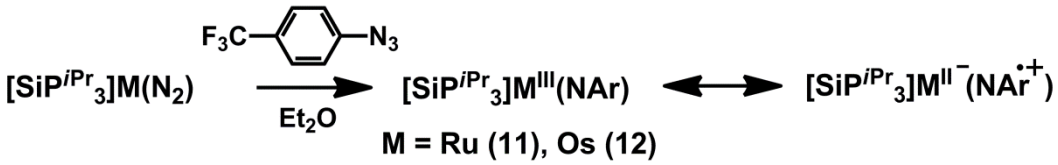

Scheme 3.3.

3.3 Conclusion

In conclusion, we have introduced several well-defined examples of mononuclear Ru(I) and Os(I) complexes. These unusual complexes have been shown, through EPR simulations and DFT calculations, to consist of predominantly metal-centered radical character with a minority of the spin density delocalized onto the chelated phosphines. The reactivity of the dinitrogen adduct derivatives **3.3** and **3.4** were shown to exhibit

formal M(I/III) group transfer reactivity. Detailed analysis of the imido/nitrene products suggests that they possess substantial imidyl radical character at the "ArN" moiety.

3.4 Experimental Section

3.4.1 General Considerations

All manipulations were carried out using standard Schlenk or glovebox techniques under an atmosphere of dinitrogen. Unless otherwise noted, solvents were degassed and dried by thoroughly sparging with N_2 gas followed by passage through an activated alumina column. Hexamethyldisiloxane was dried over CaH_2 and distilled. Pentane, hexamethyldisiloxane, benzene, toluene, tetrahydrofuran, and diethylether were tested with a standard purple solution of sodium benzophenone ketyl in tetrahydrofuran. Unless noted otherwise, all reagents were purchased from commercial vendors and used without further purification. Celite (Celite® 545) was dried at 150 °C overnight before use. $[(C_6H_6)RuCl_2]_2$,[27] $[(\eta^6\text{-}C_6H_6)OsCl_2]_2$,[28] tris(2-(diisopropylphosphino)phenyl)silane ($[SiP^{iPr}_3]H$),[4] *para*-CF_3 substituted phenyl aizde ($N_3C_6H_4CF_3$),[29] and KC_8 [30] were synthesized according to literature procedures. Triethylamine was dried over calcium hydride and distilled. Deuterated solvents were purchased from Cambridge Isotope Laboratories, Inc., degassed, and stored over 3 Å molecular sieves prior to use. Elemental analyses were performed by Midwest Microlabs and by Columbia Analytical Services, Tuscon, AZ (formerly Desert Analytics). Combustion analysis for dinitrogen compounds, **3.3**, **3.4**, **3.7**, and **3.10**, could not be obtained due to the labile N_2 ligand. Similar behavior has been observed for dinitrogen complexes supporting by this ligand scaffold.

3.4.2 X-ray Crystallography Procedures

X-ray diffraction studies were carried out at the MIT Department of Chemistry X-Ray Diffraction Facility on a Bruker three-circle Platform diffractometer, equipped with a CCD detector. Data wer collected at 100 K using Mo Kα (λ = 0.71073 Å) radiation for **3.3**, **3.7**, **3.8**, **3.9**, **3.10** and Cu Kα (λ =1.54178 Å) for **3.4**, **3.5**, and **3.11** and solved using SHELXS [31] and refined against F^2 on all data by full-matrix least squares with SHELXL.[31] X-ray quality crystals were grown as described in the experimental procedures.

3.4.3 Spectroscopic Measurements

Varian Mercury-300 and Varian Inova-500 were used to collect ^{1}H, ^{13}C{^{1}H}, ^{29}Si{^{1}H}, and ^{31}P{^{1}H} spectra at room temperature (^{15}N{^{1}H} for compound **3.7** was recorded at −90 ^{o}C) unless otherwise noted. ^{1}H and ^{13}C{^{1}H} spectra were referenced to residual solvent resonances. The ^{15}N{^{1}H} spectrum of **3.7** was referenced to neat $H_3CC^{15}N$ (δ = 245 ppm) in comparison to liquid NH_3 (δ = 0 ppm). ^{29}Si{^{1}H} spectra were referenced to external tetramethylsilane (δ = 0 ppm), and ^{31}P{^{1}H} spectra were referenced to external 85% phosphoric acid (δ = 0 ppm). IR measurements were obtained on samples prepared as KBr pellets using a Bio-Rad Excalibur FTS 3000 spectrometer. X-band EPR spectra were obtained on a Bruker EMX spectrometer. Room temperature spectra were simulated using WINEPR SimFonia program,[32] and low temperature spectra were simulated using W95EPR program.[33] SQUID measurements were obtained using Quantum Designs MPMS XL magnetometer at 1000 G. The samples were prepared

under a dinitrogen atmosphere in a polycarbonate capsule wrapped with Teflon tape and suspended in the magnetometer in a plastic straw.

3.4.4 Electrochemistry

Electrochemical measurements were carried out in a glovebox under a dinitrogen atmosphere in a one-compartment cell using a CH Instruments 600B electrochemical analyzer. A glassy carbon electrode was used as the working electrode and platinum wire was used as the auxillary electrode. The reference electrode was $Ag/AgNO_3$ in THF. The ferrocene couple Fc^+/Fc was used as an external reference. Solutions (THF) of electrolyte (0.3 M tetra-*n*-butylammonium hexafluorophosphate) and analyte were also prepared under an inert atmosphere.

3.4.5 DFT Calculations

Geometry optimizations for **3.3**-**3.6, 3.11**, and **3.12** were run on the Gaussian03[34] suite of programs starting from solid-state coordinates with the B3LYP[35] level of theory with the LANL2TZ(f)[36] basis set for Ru and Os, 6-31G(d)[37] basis set for Si, P, and N, and LANL2DZ [38] basis set for C, F, and H atoms. For optimization of compound **3.5**, convergence criteria were slightly relaxed from the default values to meet convergence (Maximum force: 0.000450 to 0.000540, RMS force: 0.000300 to 0.000360, Maximum displacement: 0.001800 to 0.002160, RMS displacement: 0.001200 to 0.001440). Frequencies calculations on **3.3**-**3.6** confirmed the optimized structures to be minima. Although convergence was met with default convergence criteria for the optimization of **3.11** and **3.12**, subsequent frequency calculations revealed them to be a transition states

(1 imaginary frequency), each with a low energy vibration that features small movement of mainly the CF_3 group. Optimization with different starting coordinates with a pruned (99,590) grid instead of the default pruned (75,302) grid also resulted in the same transition state. Using tighter convergence criteria did not lead to convergence on a reasonable timescale. Use of a different functional, PBE1PBE, with default criteria with the same basis set, however, led to convergence for **3.11**, but not for **3.12**, with no imaginary frequencies and very similar structure. Use of the BP86 functional also lead to a converged structure with 1 imaginary frequency for **3.12**. The spin densities calculated from these transition state structures for **3.11** and **3.12** are very similar to those values calculated from X-ray coordinates. For consistency and owing to its widespread use, for **3.11** and **3.12** we report the spin density values calculated from an optimized structure using the B3LYP functional in the maintext. Spin density calculated from x-ray coordinates are listed in the appendix, along with spin densities from optimized structures. Additional energy calculations were run using the same functional as the optimizations with the LANL2TZ(f) for the transition metals, and 6-311G(d,p)[39] basis set for all other atoms. Energy calculations on solid-state structures were run using the same functional and basis set as the energy calculations for the optimized structures.

The optimization resulted in structures in good agreement to bond lengths and angles of those observed in the solid-state structure, except for overestimation of the metal-phosphorus bond lengths, which is typical for the B3LYP functional. Since spin delocalization onto the phosphorus atoms is present in our system, however, we believe that overestimated metal-phosphorus bond lengths result in a reduced spin density on the P atoms, and an increase in the metal spin density. Energy calculations on compounds

calculated using solid-state coordinates, indeed, place approximately 10% greater spin density on the metal and 10% less on the phosphorus atoms relative to those derived from the optimized structures. The results from these calculations, however, do not change the conclusions drawn from this study. See the appendix for a table with spin densities derived both from geometry optimized structures and from solid-state structures.

3.4.6 Synthesis

Synthesis of [SiP$^{iPr}_3$]RuCl (**3.1**). H[SiP$^{iPr}_3$] (0.82 g, 1.3 mmol), [(C_6H_6)$OsCl_2$]$_2$ (0.44 g, 0.88 mmol), and Et_3N (0.93 mL, 6.7 mmol) were charged into a 100 mL Schlenk tube and 25 mL of toluene was added. The flask was sealed, and heated at 90 ^oC for 18 h. The reaction mixture was filtered through Celite, and the volatiles were removed in vacuo to yield analytically pure material (0.95 g, 95%). ^1H NMR (C_6D_6, δ): 8.26 (d, *J* = 7.2 Hz, 3H), 7.23-7.16 (m, 6H), 7.01 (t, *J* = 7.2 Hz, 3H), 2.44 (m, 6H), 1.19 (m, 18H), 0.97 (s, 18H). $^{13}C\{^1H\}$ NMR ($CDCl_3$, δ): 156.0 (m), 144.8 (m), 132.4 (m), 129.6, 128.7, 126.8, 29.5 (m), 20.0, 19.9. $^{29}Si\{^1H\}$ NMR ($CDCl_3$, δ): 75.5 (q, *J* = 16.7 Hz).$^{31}P\{^1H\}$ NMR (C_6D_6, δ): 72.6 (s). Anal. Calcd for $C_{36}H_{54}SiP_3ClRu$: C, 58.09; H, 7.31 Found: C, 58.43; H, 6.99.

Synthesis of [SiP$^{iPr}_3$]OsCl (**3.2**). H[SiP$^{iPr}_3$] (0.50 g, 0.82 mmol) and [(C_6H_6)$OsCl_2$]$_2$ (0.36g, 0.53 mmol) were charged into a flask and toluene (50 mL) was added. Triethylamine (0.50 mL, 2.5 mmol) was added and the flask was heated at 90 °C for 18 h. The mixture was filtered through Celite, and the volatiles were removed in vacuo to yield analytically pure material (0.64g, 94%). ^1H NMR (C_6D_6, δ): 8.29 (d, *J* = 6.9 Hz, 3H), 7.26-7.16 (m, 6H), 6.99 (t, *J* = 6.9 Hz, 3H), 2.62 (m, 6H), 1.19 (m, 18H), 1.00 (s, 18H).

$^{13}C\{^{1}H\}$ NMR ($CDCl_3$, δ): 156.9 (m), 146.3 (m), 132.6 (m), 130.0, 129.1, 127.1, 30.9 (m), 20.7, 20.4. $^{29}Si\{^{1}H\}$ NMR ($CDCl_3$, δ): 53.5 (m).$^{31}P\{^{1}H\}$ NMR (C_6D_6, δ): 45.2 (s). Anal. Calcd for $C_{36}H_{54}SiP_3ClOs$: C, 51.88; H, 6.52; N. 0.00. Found: C, 52.33; H, 6.68; N, < 0.05.

Synthesis of [SiP$^{i\mathrm{Pr}}_3$]RuN$_2$ (3.3). [SiP$^{i\mathrm{Pr}}_3$]RuCl (0.10 g, 0.13 mmol) was suspended in 8 mL of Et_2O in a scintillation vial and placed inside a cold well that was cooled in a dry ice/acetone bath. KC_8 (20. Mg, 0.15 mmol) was added in one portion. The resulting mixture was stirred inside the cold well for 15 min The brown mixture was taken out of the well, and stirred for an additional 20 min at room temperature, at which time a color change to dark green resulted. Volatiles were removed, and the product was extracted with benzene and filtered through Celite. Lyophilization of the benzene solution resulted in 0.18 g (91%) of green **3.3**. Crystals suitable for X-ray diffraction were obtained through slow evaporation of a concentrated pentane solution. ^{1}H NMR (C_6D_6, δ): 10.1, 8.7, 7.8, 3.1, 1.0. IR (KBr, cm^{-1}): 2088 (ν[N_2]). μ_{eff} (SQUID) = 1.69 μ_B.

Synthesis of [SiP$^{i\mathrm{Pr}}_3$]OsN$_2$ (3.4). [SiP$^{i\mathrm{Pr}}_3$]OsCl (0.10 g, 0.12 mmol) was suspended in 8 mL Et_2O in a scintillation vial and placed inside a cold well that was cooled in a dry ice/acetone bath. KC_8 (21 mg, 0.15 mmol) was added in one portion and the mixture was stirred for 15 min inside the cold well. The mixture was stirred for an additional 20 min at room temperature. Volatiles were removed, and benzene was added. The mixture was filtered through celite and the resulting benzene solution was lyophilized to yield green **3.4** (0.14 mg, 70%). Crystals suitable for X-ray diffraction were obtained by slow evaporation of a concentrated pentane solution of **3.4** out into hexamethyldisiloxane at

−35 °C. ^{1}H NMR (C_6D_6, δ): 9.6, 9.1, 8.5, 3.3, 2.4. IR (KBr, cm^{-1}): 2052 (ν[N_2]). μ_{eff} (Evans' method, C_6D_6, 23 °C) = 1.6 μ_B

Synthesis of [SiP$^{iPr}_3$]Ru(Pme$_3$) (3.5). [SiP$^{iPr}_3$]RuCl (0.20 g, 0.27 mmol) was dissolved in 10 mL of THF in a scintillation vial and Pme_3 (84 μL, 0.81 mmol) was syringed in. The red/purple solution was placed inside a cold well cooled in a dry ice/acetone bath. KC_8 (36 mg, 0.27 mmol) was added in one portion, and the resulting mixture was stirred inside the cold well for 10 min The mixture was stirred for an additional 15 min at room temperature. The volatiles were removed, and the product was extracted into benzene and filtered through Celite. The resulting benzene solution was lyophilized to yield 0.19 g (90%) of orange **3.5**. Crystals suitable for X-ray diffraction were obtained by slow evaporation of a concentrated pentane solution. ^{1}H NMR (C_6D_6, δ): 16.1, 9.0, 8.3, 8.2, 5.2, −2.3. μ_{eff} (Evans' method, C_6D_6, 23 °C) = 1.6 μ_B. Anal. Calcd for $C_{39}H_{63}SiP_4Ru$: C, 59.67; H, 8.03; N, 0.00. Found: C, 59.67; H, 7.30; N, 0.24.

Alternative synthesis of 3.5. [SiP$^{iPr}_3$]RuN_2 was dissolved in benzene and one equivalent of Pme_3 was added via syringe. An immediate color change to yellow/orange with effervescence resulted, and the resulting solution was concentrated. Analysis by NMR showed only **3.5** with no **3.3** remaining.

Synthesis of [SiP$^{iPr}_3$]Os(Pme$_3$) (3.6). [SiP$^{iPr}_3$]OsN_2 (24 mg, 0.030 mmol) was dissolved in 5 mL Et_2O in a scintillation vial and Pme_3 (3.1 μL, 0.030 mmol) was syringed in, resulting in a lightening of color. After stirring for 2 min, volatiles were removed, and the resulting green film was triturated with hexamethyldisiloxane, resulting in a light green powder. The green solid was washed with a minimum amount of cold pentane and dried to yield green **3.6** (20. Mg, 78%). ^{1}H NMR (C_6D_6, δ): 22.8, 9.4, 7.8, 5.8, 1.1, −1.9. μ_{eff}

(Evans' method, C_6D_6, 23 ^oC) = 1.8 μ_B. Anal. Calcd for $C_{39}H_{63}SiP_4Os$: C, 53.59; H, 7.26; N, 0.00. Found: C, 53.73; H, 6.57; N, < 0.05.

Synthesis of {[SiP$^{iPr}_3$]Ru(N$_2$)}$^+$BAr$^F_4$$^-$ (3.7). [SiP$^{iPr}_3$]RuCl (0.10 g, 0.13 mmol) was dissolved in 16 mL of C_6H_6 and NaBAr$^F_4$ (0.12 g, 0.13 mmol) was added in one portion. A gradual color change from dark red/purple to orange took place over 1 hr. The mixture was stirred for an additional 3 hr and the reaction mixture was filtered through celite and lyophilized to yield orange **3.7** (0.18 g, 84%). Crystals suitable for X-ray diffraction were obtained from layering pentane over a concentrated CH_2Cl_2 solution of **3.7** at −35^{o}C. Layering pentane over a concentrated THF solution at RT alternatively resulted in crystals that yielded a solid-state structure with no N_2 nor THF bound. Complex **3.7** could also be prepared by addition of AgOTf to an Et_2O solution of **3.3**. ^{1}H NMR (d^8-THF, δ): 8.21 (d, *J* = 7.6 Hz, 3H), 7.82 (s, 8H), 7.77 (d, *J* = 7.6 Hz, 3H), 7.59 (s, 4H), 7.46 (t, *J* = 7.6 Hz, 3H), 7.37 (t, *J* = 7.6 Hz, 3), 2.32 (m, 6H), 1.15 (s, 18H), 0.95 (s, 18H). ^{15}N{^{1}H, −90 ^{o}C} NMR (d^8-THF, δ): 337.5, 300.0. ^{31}P{^{1}H} NMR (CD_2Cl_2, δ): 69.1 (s).

Synthesis of {[SiP$^{iPr}_3$]Ru(N$_2$)}$^-$K$^+$(THF)$_2$ (3.8). [SiP$^{iPr}_3$]RuCl (0.10 g, 0.13 mmol) was dissolved in 8 mL of THF and placed inside a cold well cooled in a dry ice/acetone bath. KC_8 (21 mg, 0.15 mmol) was added in one portion, and the mixture was stirred inside the well for 10 min The reaction mixture was stirred for an additional 10 min at room temperature and the volatiles were removed. Benzene was added to the mixture and the mixture was filtered through celite. Volatiles were removed and the resulting [SiP$^{iPr}_3$]RuN$_2$ was redissolved in THF and placed inside the cold well. A second batch of KC_8 (36 mg, 0.27 mmol) was added in one portion, resulting in a color change to dark red. The reaction mixture was stirred for 10 min inside the cold well and stirred for an

additional 10 min at room temperature. The dark red mixture was filtered through celite, and concentrated. Layering pentane over a concentrated THF solution resulted in dark crystals of **3.8** (85 mg, 73%) suitable for X-ray diffraction. ^{1}H NMR (d_8-THF, δ): 7.96 (d, J = 7.6 Hz, 3H), 6.88 (d, J = 8.0 Hz, 3H), 6.80 (t, J = 8.0 Hz, 3H), 2.41 (m, 6H), 0.97 (s, 18H), 0.71 (s, 18H). ^{13}C{^{1}H} NMR (d_8-THF, δ): 151.9, 130.0, 124.8, 123.6, 121.9, 31.7, 18.4. ^{29}Si{^{1}H} NMR (d_8-THF, δ): 90.7 (q, J = 20 Hz). ^{31}P{^{1}H} NMR (d_8-THF, δ): 82.8 (s). IR (KBr, cm^{-1}): 1960 (ν[N_2]). Despite repeated attempts, satisfactory combustion analysis could not be obtained for this complex. However, combustion analysis was obtained for the 18-crown-6 complex, {[SiP$^{i\text{Pr}}_3$]Ru(N_2)}$^{-}$K^{+}(18-c-6) (**3.8'**).

Synthesis of {[SiP$^{i\text{Pr}}_3$]Ru(N_2)}$^{-}$K^{+}(18-c-6) (3.8'). {[SiP$^{i\text{Pr}}_3$]Ru(N_2)}$^{-}$K^{+}(THF)$_2$ (50. Mg, 0.054 mmol) was dissolved in 5 mL of THF and a THF solution of 18-crown-6 (22 mg, 0.082 mmol) was added dropwise. The resulting solution was stirred for 30 min, and volatiles were removed. The residue was washed with Et_2O (2 x 1 mL) and C_6H_6 (2 x 1 mL). Recrystallization from layering pentane over a concentrated THS solution resulted in dark crystals of {[SiP$^{i\text{Pr}}_3$]Ru(N_2)}$^{-}$K^{+}(18-c-6) (45 mg, 80%) that analyzed with one molecule of THF. ^{1}H NMR (d_8-THF, δ): 7.88 (d, J = 8.1 Hz, 3H), 7.18 (d, J = 7.8 Hz, 3H), 6.79 (m, 6H), 3.58 (s, 24H), 2.49 (br, 6H), 0.90 (s, 18H), 0.64 (s, 18H). ^{31}P{^{1}H} NMR (d_8-THF, δ): 79.7 (br) (s). IR (KBr, cm^{-1}): 1992 (ν[N_2]). Anal. Calcd. for $C_{52}H_{86}N_2O_7KsiP_3Ru$: C, 56.14; H, 7.79; N, 2.52. Found: C, 56.21; H, 7.84; N, 2.78.

Synthesis of {[SiP$^{i\text{Pr}}_3$]Os(N_2)}$^{-}$K^{+}(THF)$_2$ (3.9). [SiP$^{i\text{Pr}}_3$]OsN_2 (57 mg, 0.069 mmol) was dissolved in 4 mL of THF in a scintillation vial. The vial was placed inside a cold well cooled in a dry ice/acetone bath and KC_8 (14 mg, 0.10 mmol) was added in one portion. The resulting mixture was stirred for 15 min, and stirred for an additional 15 min at room

temperature. The dark red mixture was filtered through celite and volatiles were removed. Pentane was layered over a concentrated THF solution of **3.9** to yield dark crystals (40 mg, 57%). ^{1}H NMR (d_8-THF, δ): 7.97 (d, J = 6.6 Hz, 3H), 7.20 (d, J = 6.9 Hz, 3H), 6.78 (m, 6H), 2.8 (br, 6H), 0.87 (s, 18H), 0.67 (s, 18H). ^{31}P NMR (d_8-THF, δ): 49.9 (br). Crystals suitable for X-ray diffraction were obtained by layering pentane over a concentrated THF solution of **3.9**. In light of the difficulties encountered in obtaining satisfactory combustion analysis for **3.9**, the 18-crown-6 complex for **3.9**, {[SiP$^{i\mathrm{Pr}}_3$]Os(N_2)}$^-$K$^+$(18-c-6) (**3.9'**), was synthesized.

Synthesis of {[SiP$^{i\mathrm{Pr}}_3$]Os(N_2)}$^-$K$^+$(18-c-6) (3.9'). {[SiP$^{i\mathrm{Pr}}_3$]Os(N_2)}$^-$K$^+$(THF)$_2$ (20. mg, 0.020 mmol) was dissolved in 4 mL of THF in a scintillation vial. 18-crown-6 (6.1 mg, 0.023 mmol) was dissolved in 1 mL of THF and added dropwise to the dark red solution, resulting in no change in color. The resulting solution was stirred for 15 min, and the volatiles were removed, resulting in a dark red film. Triturating with Et_2O resulted in the precipitation of red microcrystals, and the crystalline material was washed with Et_2O, pentane, and dried (19 mg, 90%) to yield **3.9'** that analyzed with one molecule of THF. ^{1}H NMR (d_8-THF, δ): 7.94 (d, J = 7.0 Hz, 3H), 7.17 (d, J = 7.0 Hz, 3H), 6.81 (m, 3H), 6.72 (m, 3H), 3.52 (s, 24H), 2.40 (br, 6H), 0.83 (s, 18H), 0.65 (s, 18H). ^{13}C{^{1}H} NMR (d_8-THF, δ): 158.7 (m), 154.1 (m), 130.0 (m), 125.3, 123.8, 122.1, 69.3, 33.5 (br), 18.9, 18.7. ^{29}Si{^{1}H} NMR (d_8-THF, δ): 85.2 (q, J = 16 Hz). ^{31}P{^{1}H} NMR (d_8-THF, δ): 50.0. Anal. Calcd. for $C_{52}H_{86}N_2O_7KsiP_3Os$: C, 51.98; H, 7.21; N, 2.33. Found: C, 51.68; H, 6.97; N, 1.77.

Synthesis of [SiP$^{i\mathrm{Pr}}_3$]Ru(H)(N_2) (3.10). [SiP$^{i\mathrm{Pr}}_3$]RuCl (51 mg, 0.068 mmol) was dissolved in 5 mL of THF and the reaction mixture was placed inside a cold well cooled

in a dry ice/acetone bath. $LiEt_3BH$ (68 μL, 0.068 mmol) was added dropwise. The resulting solution was stirred for 15 min inside the cold well. The reaction mixture was stirred for an additional 20 min at room temperature and volatiles were removed. Benzene was added to the mixture and the mixture was filtered through Celite. Lyophilization of the benzene solution resulted in pale red **3.10** (48 mg, 96%). Crystals suitable for X-ray diffraction were obtained by vapor diffusion of pentane into a concentrated benzene solution of **3.10**. ^{1}H NMR (C_6D_6, δ): 8.19 (d, *J* = 7.2 Hz, 2H), 8.00 (d, *J* = 7.2 Hz, 1H), 7.43 (m, 2H), 7.22-7.01 (m, 7H), 2.69 (br, 2H), 2.43 (sep, *J* = 6.3 Hz, 2H), 2.26 (sep, *J* = 6.6 Hz, 2H), 1.43-1.11 (m, 18H), 0.90-0.62 (m, 18H), -10.3 (dt, *J* = 62 Hz, 35 Hz). ^{13}C{^{1}H} NMR (C_6D_6, δ): 158.6 (d, *J* = 48 Hz), 155.9 (m), 150.0 (m), 147.1 (d, *J* = 35 Hz), 133.6 (d, *J* = 20 Hz), 132.9 (t, *J* = 10 Hz), 130.0-129.0 (m), 127.7, 127.1, 126.2, 32.2, 29.8 (m), 28.5 (d, *J* = 12 Hz), 22.6, 20.5, 20.4, 20.0, 19.9, 19.7, 19.6, 19.2. ^{29}Si{^{1}H} NMR (C_6D_6, δ): 80.0 (q, *J* = 13 Hz). ^{31}P{^{1}H} NMR (C_6D_6, δ): 73.0 (br, 2P), 65.8 (s, 1P). IR (KBr, cm^{-1}): 2140 (ν[N_2]).

Synthesis of [SiP$^{iPr}_3$]Ru(Nar) Ar = $C_6H_4CF_3$ (3.11). [SiP$^{iPr}_3$]RuN_2 (43 mg, 0.058 mmol) was dissolved in 6 mL Et_2O in a scintillation vial and the vial was placed inside a cold well cooled in a dry ice/acetone bath. ArN_3 (11 mg, 0.058 mmol) was dissolved in 1 mL Et_2O in a 4 mL vial and also cooled inside the cold well. The azide solution was added dropwise to the solution of [SiP$^{iPr}_3$]RuN_2, resulting in a rapid color changed to dark red/purple. The solution was stirred for 10 min inside the cold well, and stirred for an additional 10 min at room temperature. Volatiles were removed, and the residue was washed with a small portion of cold pentane. Crystals suitable for X-ray diffraction were obtained by slow evaporation of a 1:1 = Et_2O:pentane solution out into

hexamethyldisiloxane (23 mg, 46%). ^{1}H NMR (C_6D_6, δ): 9.1, 7.3, 7.0, 5.8. μ_{eff} (Evans' method, C_6D_6, 23 ^oC) = 1.5 μ_B

Synthesis of [SiP$^{iPr}_3$]Os(Nar) Ar = $C_6H_4CF_3$ (3.12). [SiP$^{iPr}_3$]OsN_2 (47 mg, 0.057 mmol) was dissolved in 10 mL Et_2O in a scintillation vial, and the vial was placed inside a cold well cooled in a dry ice/acetone bath. ArN_3 (11 mg, 0.057 mmol) was dissolved in 1 mL Et_2O in a 4 mL vial and also cooled inside the cold well. The azide solution was added dropwise to the solution of [SiP$^{iPr}_3$]RuN_2, resulting in a gradual color chang from dark green dark red/orange. The solution was stirred for 10 min inside the cold well, and stirred for an additional 5 min at room temperature. Volatiles were removed, and crystals suitable for X-ray diffraction were obtained by slow evaporation of a 1:1 = Et_2O: pentane solution out into hexamethyldisiloxane (22 mg, 41%). ^{1}H NMR (C_6D_6, δ): 9.9, 6.1, 5.8 (very broad). μ_{eff} (Evans' method, C_6D_6, 23 ^oC) = 1.5 μ_B

Reaction of 3 with I_2. [SiP$^{iPr}_3$]RuN_2 (22 mg, 0.030 mmol) was dissolved in 4 mL of Et_2O in a scintillation vial and placed inside a cold well cooled in a dry ice/acetone bath. Iodine (3.8 mg, 0.015 mmol) was added to the solution in one portion, and the resulting mixture was allowed to stir for 10 min inside the well. A gradual color change to a red/purple solution resulted, and the solution was allowed to stir for ten additional minutes. Volatiles were removed to yield a red solid (21 mg, 85%). The identity of the product, [SiP$^{iPr}_3$]RuI, was confirmed through ^{1}H, ^{31}P{^{1}H}, and by x-ray crystallography. ^{1}H NMR (C_6D_6, δ): 8.26 (d, *J* = 7.0 Hz, 3H), 7.24-7.18 (m, 6H), 7.01(t, 3H), 2.50 (m, 6H), 1.17 (m, 18H), 0.88 (s, 18H). ^{31}P NMR (C_6D_6, δ): 70.1 (s).

Reaction of 3 with PhS-SPh. [SiP$^{iPr}_3$]RuN_2 (22 mg, 0.029 mmol) was dissolved in 4 mL Et_2O in a scintillation vial, and the vial was placed inside a cold well cooled in a dry

ice/acetone bath. Diphenyldisulfide (3.2 mg, 0.015 mmol) was added in one portion. The color of the reaction mixture turned to a bright purple color after several minutes. The reaction vial was stirred for 15 min inside the cold well and 15 min at room temperature, resulting in precipitation of a purple solid. Volatiles were removed, which resulted in a purple solid. The solid was washed with cold Et_2O and dried (19 mg, 80%). The identity of the product, [SiP$^{i\text{Pr}}_3$]Ru(SPh), was confirmed through ^{1}H, ^{31}P{^{1}H}, and by x-ray crystallography. ^{1}H NMR (C_6D_6, δ): 8.11 (d, J = 6.5 Hz, 3H), 7.98(d, J = 7.5 Hz, 2H), 7.35-7.01(m, 12H), 2.68 (m, 6H), 1.13 (m, 18H), 0.93 (s, 18H). ^{31}P{^{1}H} NMR (C_6D_6, δ): 70 (br).

References Cited

1 de Bruin, B; Hetterscheid, D. G. H.; Koekkoek, A. J. J.; Grützmacher, H. *Prog. Inorg. Chem.* **2007**, *55* 247.

2 a) Ru(I): Bianchini, C.; Laschi, F.; Peruzzini, M.; Zanello, P. *Gazz. Chim. Ital.* **1994**, *124*, 271. b) Angelici, R. J.; Zhu, B.; Fedi, S.; Laschi, F.; Zanello, P. *Inorg. Chem.* **2007**, *46*, 10901. c) Mulazzani, Q. G.; Emmi, S.; Fuochi, P. G.; Hoffman, M. Z.; Venturi, M. *J. Am. Chem. Soc.* **1978**, *100*, 981. d) Robinson, S. D.; Uttley, M. F.; *J. Chem. Soc., Dalton Trans.* **1972**, 1. e) Zotti, G.; Pilloni, G.; Bressan, M.; Martelli, M.; *J. Electroanal. Chem.* **1977**, *75*, 607. Os(I): f) Bianchini, C.; Peruzzini, M.; Ceccanti, A.; Laschi, F.; Zanello, P. *Inorg. Chim. Acta.* **1997**, *259*, 61. g) Vugman, N. V.; Rossi, A. M.; Danon, J. *J. Chem. Phys.* **1978**, *68*, 3152. h) Zotti, G.; Pilloni, G.; Bressan, M.; Martelli, M. *Inorg. Chim. Acta.* **1978**, *30*, L311.

3 a) Schröder, M.; Stephenson, T. A in *Comprehensive Coordination Chemistry,* Vol. 4 (Eds: Wilkinson, G.), Permagon Books Ltd., Oxford, **1987**, pp. 277-519. b) Griffith, W. P. in *Comprehensive Coordination Chemistry*, Vol. 4 (Eds: Wilkinson, G.), Permagon Books Ltd., Oxford, **1987**, pp. 519-635. c) Housecroft, C. E. in *Comprehensive Coordination Chemistry II,* Vol. 5 (Eds: McCleverty, J. A.; Meyer, T. J.), Elsevier Ltd., Oxford, **2004**, pp. 555-733.

4 a) Mankad, N. P.; Whited, M. T.; Peters, J. C. *Angew. Chem. Int. Ed.* **2007**, *46*, 5768. b) Whited, M. T.; Mankad, N. P.; Lee, Y.; Oblad, P. F.; Peters, J. C. *Inorg. Chem.* **2009**, *48*, 2507.

5 Mankad, N. P.; Peters, J. C. *J. Am. Chem. Soc.* **2010**, *132*, 4083.

6 $\tau = (\beta-\alpha)/60$ where β and α represent the two largest angles. $\tau = 1$ for TBP, 0 for square pyramid. See Addison, A. W.; Rao, T. N.; Van Rijn, J. J.; Veschoor, G. C. *J. Chem. Soc. Dalton Trans*. **1984**, 1349.

7 An analogous series for the corresponding Fe complexes is reported. See Lee, Y.; Mankad, N. P.; Peters, J. C. *Nat. Chem.*, **2010**, *2*, 558.

8 A crystal grown in a THF/pentane mixture at RT, in contrast to the crystals grown from a CH_2Cl_2/pentane mixture at −35 ^oC that yielded the N_2 bound structure of **3.7**, reveals a solid state structure with neither N_2 nor THF bound. Both structures show an agostic interaction, which is also seen in a number of other Ru(II) complexes in this work. See appendix 2.

9 This sample was prepared from an independent route involving salt metathesis of complex **1** with $NaBAr^F_4$, ruling out any exchange process with impurities of **3** that would broaden out the spectrum.

10 a) Lu, C. C.; Bill, E.; Weyhermüller, T.; Bothe, E.; Wieghardt, K. *J. Am. Chem. Soc.* **2008**, *130*, 3181. b) Adhikari, D.; Mossin, S.; Basuli, F.; Huffman, J. C.; Szilagyi, R. K.; Meyer, K.; Mindiola, D. J. *J. Am. Chem. Soc.* **2008**, *130*, 3676. c) Harkins, S. B.; Mankad, N. P.; Miller, A. J.; Szilagyi, R. K.; Peters, J. C. *J. Am. Chem. Soc.* **2008**, *130*, 3478. d) Haneline, M. R.; Heyduk, A. F. *J. Am. Chem. Soc.* **2006**, *128*, 8410.

11 de Bruin, B.; Hetterscheid, D. *Eur. J. Inorg. Chem.* **2007**, 211.

12 Some complexes with large Δg have been found to be mainly ligand-based radicals. See Miyazato, Y.; Wada, T.; Muckerman, J. T.; Fujita, E.; Tanaka, K. *Angew. Chem. Int. Ed.* **2007**, *46*, 5728.

13 a) Büttner, T.; Geier, J.; Frison, G.; Harmer, J.; Calle, C.; Schweiger, A.; Schönberg, H.; Grützmacher, H. *Science* **2005**, *307*, 235. b) Cataldo, L.; Choua, S.; Berclaz, T.; Geoffroy, M.; Mézailles, N.; Avarvari, N.; Mathey, F.; Le Floch, P. *J. Phys. Chem. A.* **2002**, *106*, 3017.

14 Two mixed-valent dinuclear Ru complexes, each with one Ru(I) center, exhibit Δg values of 0.20 and 0.26. See: Sarkar, B.; Kaim, W.; Fiedler, J.; Duboc, C. *J. Am. Chem. Soc.* **2004**, *126*, 14706.

15 Kober, E. M.; Meyer, T. J. *Inorg. Chem.* **1984**, *23*, 3877.

16 Calculated from DFT optimized structures. See experimental section for details.

17 a) Baird, M. C. *Chem. Rev.* **1988**, *88*, 1217. b) Paonessa, R. S.; Thomas, N. C.; Halpern, J. *J. Am. Chem. Soc.* **1985**, *107*, 4333.

18 a) Brown, S. D.; Betley, T. A.; Peters, J. C. *J. Am. Chem. Soc.* **2003**, *125*, 322. b) Nieto, I.; Ding, F.; Bontchev, R. P.; Wang, H.; Smith, J. M. *J. Am. Chem. Soc.* **2008**, *130*, 2716. c) Cowley, R. E.; Eckert, N. A.; Lehaïk, J.; Holland, P. L. *Chem Commun*. **2009**, 1760.

19 Selected examples: a) Jayaprakash, K. N.; Gunnoe, T. B.; Boyle, P. D. *Inorg. Chem.* **2001**, *40*, 6481. b) Liang, J. L.; Huang, J. S.; Zhou, Z. Y.; Cheung, K. K.; Che, C. M. *Chem. Eur. J.* **2001**, *7*, 2306.

20 Selected examples: a) Burell, A. K.; Steedman, A. J. *J. Chem. Soc., Chem. Commun.* **1995**, 2109.; b) Danopoulos, A. A.; Wilkinson, G.; Hussain-Bates, B.; Hursthouse, M. B. *Polyhedron* **1992**, *11*, 2961.

21 Betley, T. A.; Wu, Q.; Van Voorhis, T.; Nocera, D. G. *Inorg. Chem.* **2008**, *47*, 1849.

22 For a d^4 multiply bonded species in TBP geometry see England, J.; Martinho, M.; Farquhar, E. R.; Frisch, J. R.; Bominaar, E. L.; Münck, E.; Que, L., Jr. *Angew. Chem. Int. Ed.* **2009**, *48*, 3622.

23 The calculated structure has *i*Pr groups replaced with Me groups and Ar = Ph instead of PhMe. $\tau = 0.49$ for this compound. See reference 5.

24 Ashford, N. A.; Jarke, F. H.; Solomon, I. J. *J. Chem. Phys.* **1972**, *57*, 3867.

25 Walstrom, A. N.; Fullmer, B. C.; Fan, H.; Pink, M.; Buschhorn, D. T.; Caulton, K. G. *Inorg. Chem.* **2008**, *47*, 9002.

26 Lu, C. C.; George, S. D.; Weyhermüller, T.; Bill, E.; Bothe, E.; Wieghardt, K. *Angew. Chem. Int. Ed.* **2008**, *47*, 6384.

27 Palmer, M. J.; Kenny, J. A.; Walsgrove, T.; Kawamoto, A. M.; Wills, M. *J. Chem. Soc., Perkin Trans. 1* **2002**, 416.

28 Peacock, A. F. A.; Habtemariam, A.; Fernández, R.; Walland, V.; Fabbiani, F. P. A.; Parsons, S.; Aird, R. E.; Jodrell, D. I.; Sadler, P. J. *J. Am. Chem. Soc.* **2006**, *128*, 1739.

29 Hu, M.; Li, J.; Yao, S. Q. *Org. Lett.* **2008**, *10*, 5529.

30 Weitz, I. S.; Rabinovitz, M.; *J. Chem. Soc., Perkin Trans. 1* **1993**, 117.

31 Sheldrick, G. M. *Acta. Cryst.* **2008**, *A64*, 112.

32 WINEPR SimFonia Version 1.25, Bruker Analytische Messtechnik GmbH, 1996.

33 F. Neese, *QCPE Bull.* **1995**, *15*, 5.

34 Gaussian 03, Revision C.02, Frisch, M. J.; Trucks, G. W.; Schlegel, H. B.; Scuseria, G. E.; Robb, M. A.; Cheeseman, J. R.; Montgomery, Jr., J. A.; Vreven, T.; Kudin, K. N.; Burant, J. C.; Millam, J. M.; Iyengar, S. S.; Tomasi, J.; Barone, V.; Mennucci, B.; Cossi, M.; Scalmani, G.; Rega, N.; Petersson, G. A.; Nakatsuji, H.; Hada, M.; Ehara, M.;

Toyota, K.; Fukuda, R.; Hasegawa, J.; Ishida, M.; Nakajima, T.; Honda, Y.; Kitao, O.; Nakai, H.; Klene, M.; Li, X.; Knox, J. E.; Hratchian, H. P.; Cross, J. B.; Bakken, V.; Adamo, C.; Jaramillo, J.; Gomperts, R.; Stratmann, R. E.; Yazyev, O.; Austin, A. J.; Cammi, R.; Pomelli, C.; Ochterski, J. W.; Ayala, P. Y.; Morokuma, K.; Voth, G. A.; Salvador, P.; Dannenberg, J. J.; Zakrzewski, V. G.; Dapprich, S.; Daniels, A. D.; Strain, M. C.; Farkas, O.; Malick, D. K.; Rabuck, A. D.; Raghavachari, K.; Foresman, J. B.; Ortiz, J. V.; Cui, Q.; Baboul, A. G.; Clifford, S.; Cioslowski, J.; Stefanov, B. B.; Liu, G.; Liashenko, A.; Piskorz, P.; Komaromi, I.; Martin, R. L.; Fox, D. J.; Keith, T.; Al-Laham, M. A.; Peng, C. Y.; Nanayakkara, A.; Challacombe, M.; Gill, P. M. W.; Johnson, B.; Chen, W.; Wong, M. W.; Gonzalez, C.; and Pople, J. A.; Gaussian, Inc., Wallingford CT, 2004.

35 a) Becke, A.D. *J. Chem. Phys.* **1993**, *98*, 5648. b) Lee, C.; Yang, W.; Parr, R. G. *Phys. Rev. B.* **1988**, *37*, 785.

36 a) Hay, P. J.; Wadt, W. R. *J. Chem. Phys.* **1985**, *82*, 299. b) Roy, L. E.; Hay, P. J.; Martin, R. L. *J. Chem. Theory Comput.* **2008**, *4*, 1029. c) Ehlers, A. W.; Bohme, M.; Dapprich, S.; Gobbi, A.; Hollwarth, A.; Jonas, V.; Kohler, K. F.; Stegmann, R.; Veldkamp, A.; Frenking, G. *Chem. Phys. Lett.* **1993**, *208*, 111.

37 a) Hariharan, P. C.; Pople, J. A. *Theoret. Chimica Acta.* **1973**, *28*, 213. b) Francl, M. M.; Petero, W. J.; Hehre, W. J.; Binkley, J. S.; Gordon, M. S.; DeFrees, D. J.; Pople, J. A. *J. Chem. Phys.* **1982**, *77*, 3654. c) Rassolov, V.; Pople, J. A.; Ratner, M.; Windus, T. L. *J. Chem. Phys.* **1998**, *109*, 1223.

38 Dunning, T. H.; Hay, P. J. in Methods of Electronic Structure Theory, Vol. 2, Schaefer III, ed., Plenum Press **1977**.

39 a) Krishnan, R.; Binkley, J. S.; Seeger, R.; Pople, J. A. *J. Chem. Phys.* **1980**, *72*, 650.

b) McLean, A. D.; Chandler, G. S. *J. Chem. Phys.* **1980**, *72*, 5639.

Chapter 4: A Homologous Series of Cobalt, Rhodium, and Iridium Metalloradicals

Reproduced in part with permission from

Takaoka, A.; Peters, J. C.

Inorganic Chemistry **2012**, *51*, 16-18.

4.1 Introduction

Low-valent metalloradicals of the late 2nd and 3rd row transition metals are, in general, reactive species that have often necessitated *in situ* characterization.[1] There are a small number of well-defined examples of these $S = ½$ metal-centered radicals, however, that point to their interesting spectroscopic properties and reactivity patterns.[1, 2] Wayland's classic studies of methane activation by Rh(II) porphyrin complexes nicely illustrates the latter point.[3] The relative instability of these 2nd and 3rd row metalloradicals in comparison with their 1st row congeners constitutes an interesting dichotomy in the chemistry of late transition metals.[4] Few studies, however, have compared the properties of late metalloradicals within a group that possess similar geometries and ancillary ligands.[5]

We have recently employed a tripodal, tris(phosphino)silyl ligand, $[SiP^{iPr}_3]H$ ($[SiP^{iPr}_3] = (2\text{-}iPr_2PC_6H_4)_3Si^-$),[6] to stabilize a number of group 8 metalloradicals, including unusual examples of mononuclear Ru(I) and Os(I) complexes.[7] These metalloradicals included a series of dinitrogen complexes of iron(I), ruthenium(I), and osmium(I). We herein report on the synthesis and thorough characterization of a related series of isoelectronic PMe_3 adduct complexes of the group 9 metals, $\{[SiP^{iPr}_3]M(PMe_3)\}BAr^F_4$ (M = Co (**4.1**), Rh (**4.2**), Ir (**4.3**), BAr^F_4 = tetrakis(3,5-bis(trifluoromethyl)phenyl)borate)). This family of group 9 complexes constitutes a rare instance wherein a series of metalloradicals within a group can be isolated, and for which their ancillary ligands, oxidation states, spin states, and geometries are conserved.

4.2 Results and Discussion

Entry to the desired d^7, group 9 complexes begins with the dinitrogen complexes, [SiP$^{iPr}_3$]M(N_2) (M = Co (**4.4**), Rh(**4.5**), Ir(**4.6**)) (Scheme 4.1). While complexes **4.4** and **4.6** have been reported,[6b] complex **4.5** has not been previously synthesized. Briefly, **4.5** is prepared through dehydrodehalogenation of a hydrido chloride complex, [SiP$^{iPr}_3$]Rh(H)(Cl) (**7**), with MeMgBr in 97% yield. Complex **4.7**, in turn, is prepared via Si-H bond activation by addition of [SiP$^{iPr}_3$]H to $[Rh(COD)Cl]_2$ in 87% yield. As previously described for **4.6**,[6b] complex **4.5** features a high N_2 stretching frequency (ν_{N2} = 2159 cm^{-1}) and a labile N_2 ligand whose lability can be monitored by UV-Vis spectroscopy on removal and reintroduction of N_2 atmosphere (See the appendix).

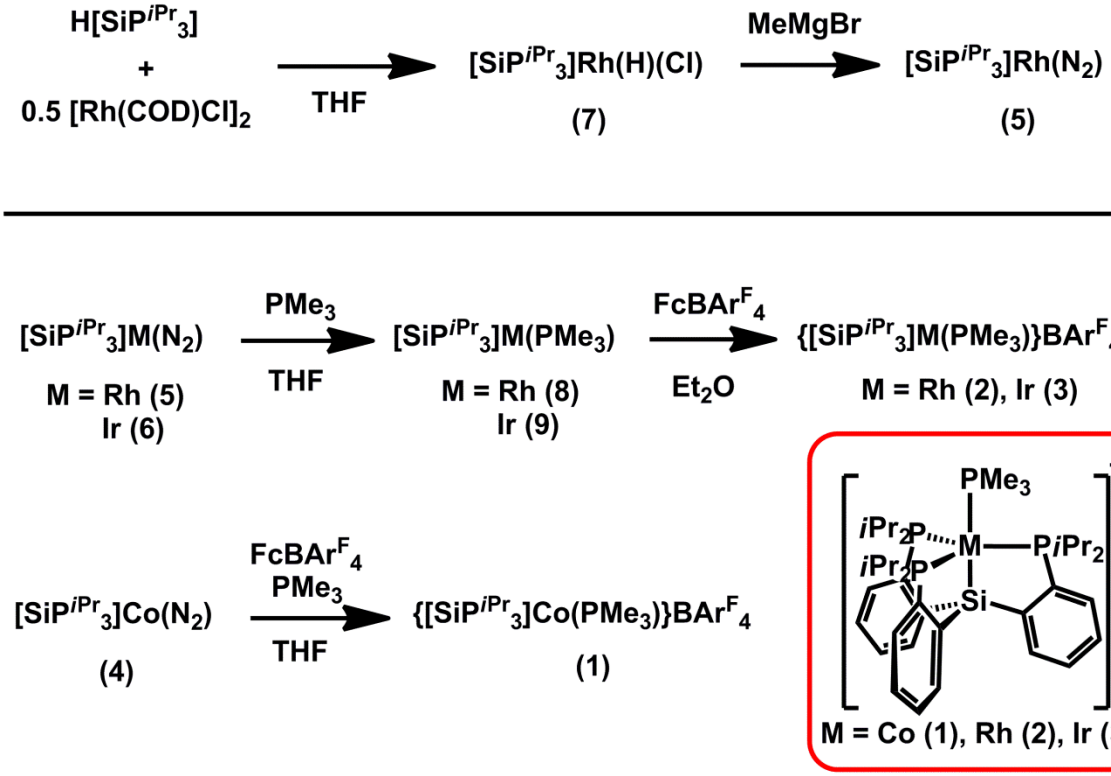

Scheme 4.1

For the Rh and Ir systems, addition of excess PMe_3 to the dinitrogen complexes **4.5** and **4.6** leads to clean and facile substitution to afford the yellow PMe_3 complexes, $[SiP^{iPr}_3]M(PMe_3)$ (M = Rh (**4.8**), Ir(**4.9**)). Complexes **4.8** and **4.9** reveal reversible oxidation waves at −0.78 and −0.76 V (vs Fc/Fc^+, THF), respectively. Accordingly, oxidation of **4.8** and **4.9** with $FcBAr^F_4$ (Fc = $Fe(C_5H_5)_2$) results in color changes to blue and purple, respectively, and affords the desired 17 e^-, S = ½ complexes, **4.2** (66%) and **4.3** (88%).

In contrast to **4.2** and **4.3**, the cobalt metalloradical **4.1** is synthesized by the addition of $FcBAr^F_4$ to a solution containing **4.4** and excess PMe_3, which yields orange, S = ½, complex **4.1** in 58% after workup. Interestingly, the reduction of isolated **4.1** by $CoCp^*_2$ under an N_2 atmosphere cleanly regenerates the Co(I)−N_2 adduct **4.4** with quantitative loss of PMe_3. Further, complex **4.4** exhibits no tendency to bind PMe_3 under an atmosphere of N_2 upon excess addition of PMe_3. Hence, the apparent stronger preference of Co(I) for N_2 over PMe_3 in comparison to the related Rh(I) and Ir(I) fragments appears to be thermodynamic rather than kinetic in origin.

The solid-state structures of **4.1**, **4.2**, and **4.3** have been obtained through X-ray diffraction studies (Figure 4.1). The geometries about the metal centers are similar, exhibiting distorted trigonal bipyramidal geometries (τ = 0.81 (**4.1**), 0.75 (**4.2**), 0.73 (**4.3**)).[8] This correspondence allows for a comparison of their chemical and spectroscopic properties. For reference, the series of group 8 dinitrogen complexes chelated by the same ancillary scaffold, $[SiP^{iPr}_3]M(N_2)$ (M = Fe, Ru, Os), exhibits τ values of 0.99 (0.84) (Fe, **4.10**),[9] 0.76 (Ru, **4.11**), 0.70 (Os, **4.12**).[6ac,7] Complexes **4.1**-**4.3** each exhibit one P−M−P angle (129.54(4) (**4.1**), 131.99(3) (**4.2**), 133.51(4) (**4.3**)) that is substantially

larger than the other two, a feature that was also observed in the solid-state structures of the Ru−N_2 and Os−N_2 metalloradicals, **4.11** and **4.12**. The doubly degenerate ^{2}E ground state of an idealized TPB structure whereby the d_{xy}/d_{x2-y2} orbital is triply occupied is subject to a Jahn-Teller distortion, consistent with the distorted structural parameters of **4.1**-**4.3**. A topologically related Rh(II) complex chelated by a tetradentate tetrakis(phosphine) ligand has recently been reported.[10]

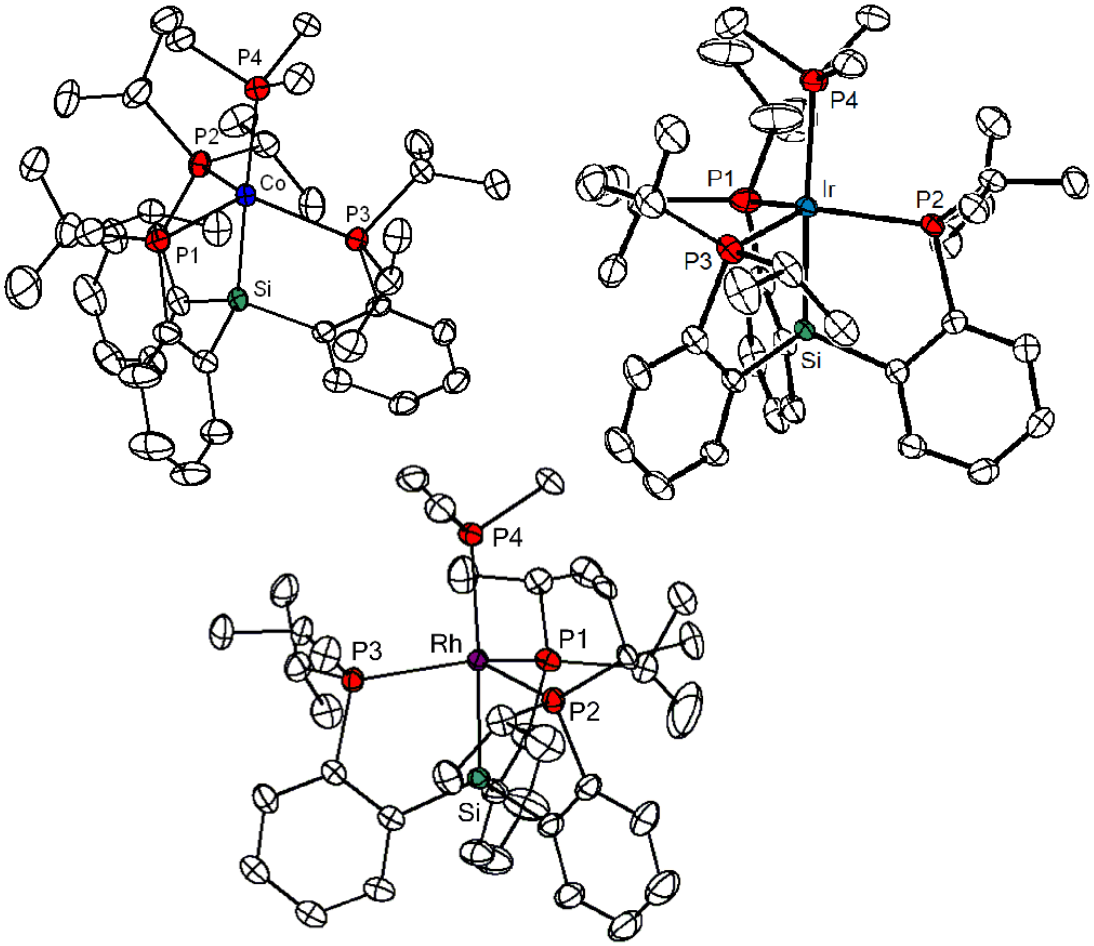

Figure 4.1. Solid-state structures of {[SiP$^{i\text{Pr}}_3$]M(PMe$_3$)}{BAr$^F_4$} (M = Co (**4.1**, top left), Rh (**4.2**, bottom)) and {[SiP$^{i\text{Pr}}_3$]Ir(PMe$_3$)}{OTf} (top right). Thermal ellipsoids are at 50% probability. BAr$^F_4$ anion, hydrogen atoms and solvent molecules are removed for clarity.

To assess the metalloradical character of complexes **4.1**-**4.3**, their EPR spectra were measured at X-band frequency. Deviations of the isotropic *g*-value from the free electron value of 2.0023 and the *g*-anisotropy in frozen solution, Δg ($\Delta g = g_{max} - g_{min}$, where g_{max} and g_{min} are the largest and smallest g-tensors), have been used as crude indicators in assessing metalloradical character; large deviations from $g = 2.0023$ at RT and higher values of Δg in frozen solution typically point to predominant spin on the metal.[1] The room temperature EPR spectra of **4.2** and **4.3** are rather featureless (see the appendix). For **4.1**, a signal could not be observed at RT, likely due to the rapid relaxation induced by the metal center. Complexes **4.2** and **4.3** exhibit spectra reminiscent of **4.11** and **4.12**, showing broad doublet signals. The splitting pattern indicates strong coupling to one P atom, while coupling to the other P atoms is smaller and unresolved. The observation of asymmetry in the P atoms even at room temperature is due to the faster timescale of the EPR experiment relative to the NMR experiment, where an averaged three-fold symmetry is suggested. The *g*-values for **4.2** and **4.3**, which are 2.100 and 2.145 respectively, are similar to the values of **4.11** (2.078) and **4.12** (2.147).

The 77 K X-band EPR spectra taken in 2-MeTHF are shown in Figure 4.2 and are more revealing. All three spectra are rhombic, with significant anisotropy (Table 4.1). The Δg values for **4.1**-**4.3** are 0.61, 0.18, 0.33 and together with the RT isotropic *g*-values, suggest significant metalloradical character. While the spectrum of **4.1** does not show resolvable hyperfine coupling with either the Co or P atoms, the spectra of **4.2** and **4.3** exhibit sharp splitting. Both spectra have been simulated by assigning a large hyperfine coupling to one P atom, with smaller coupling to either the P, Rh, or Ir atoms. Large

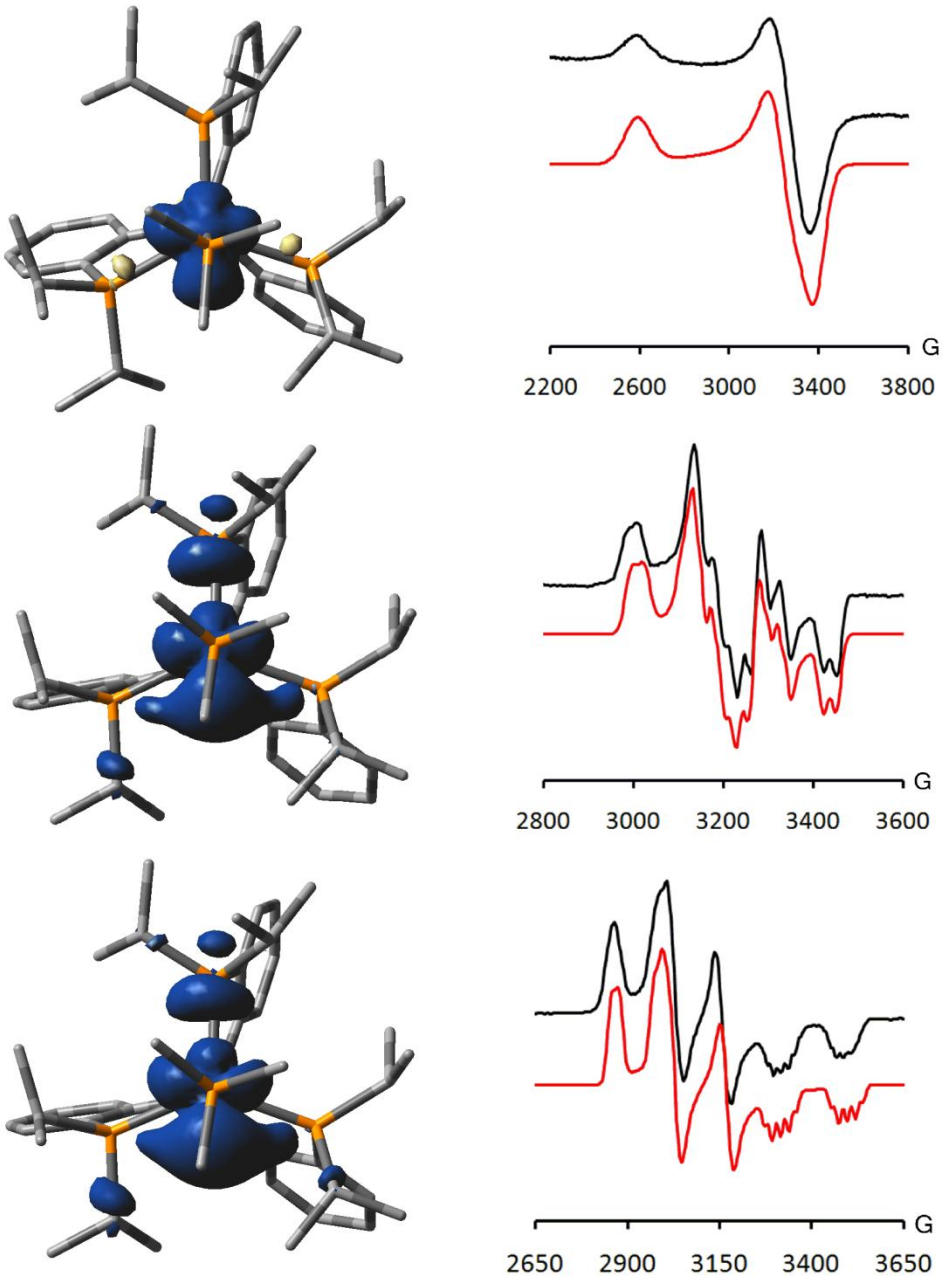

Figure 4.2. Spin density plots (left) and X-Band 77 K EPR spectra (right) in 2-MeTHF of **4.1** (top), **4.2** (center), and **4.3** (bottom). The spin density plots are shown as looking down the Me_3P-M-Si axis with the P atom opposite to the largest P−M−P angle at the top. The lower curves in each EPR spectra represent simulations.

coupling to only one P atom is also seen in the EPR spectra of **4.11** and **4.12** at 77 K, and is ascribed to coupling to the P atom opposite the largest P−M−P angle that is observed in the solid-state structure. Similar characteristics have been previously proposed for spectroscopically characterized Rh(II) complexes featuring poly(phosphine) ligands.[11] This large coupling is consistent with the doublet resonance observed at room temperature. The magnitude of this hyperfine coupling, however, is roughly twofold greater for **4.2** and **4.3** relative to **4.11** and **4.12** (Table 4.1). While hyperfine coupling to the Ir atom is resolved in **4.3**, and is assigned a value of 65 MHz for one of the *g*-tensors,[12] that to Rh is not readily assigned due to the equal nuclear spin *I* of Rh and P. Note that although complexes **4.1-4.3** are metalloradical in character, large hyperfine coupling constants for the P atoms are observed in Rh and Ir due to the large relative gyromagnetic ratio of P compared to Rh (P:Rh = −12.9) and Ir (P:^{191}Ir = 22.6, P:^{193}Ir = 20.9). Lack of observation of coupling in complex **4.1** is likely due to the broadness of the signal.

Table 4.1. EPR parameters for complexes, **4.1-4.3** and **4.11**, **4.12**.

	Co(1)	**Rh(2)**	**Ir(3)**	**Ru(11)**[#]	**Os(12)**[#]
g_x	**2.600**	**2.205**	**2.300**	**2.175**	**2.290**
g_y	**2.080**	**2.087**	**2.170**	**2.075**	**2.200**
g_z	**1.990**	**2.025**	**1.975**	**2.009**	**1.978**
Δg	**0.61**	**0.18**	**0.33**	**0.17**	**0.31**
***A*(P)x**	**N/A**	**360**	**370**	**220**	**190**
***A*(P)y**	**N/A**	**430**	**430**	**230**	**190**
***A*(P)z**	**N/A**	**550**	**500**	**250**	**230**

Hyperfine coupling constants are in MHz and represent values for the largest coupled P atom. For full set of experimental and simulation parameters, see SI.

#: Parameters from ref 7.

Table 4.2. Mulliken spin densities from DFT calculations.

	Co(1)	Rh(2)	Ir(3)	Ru(11)[#]	Os(12)[#]
M	**1.167**	**0.746**	**0.732**	**0.836**	**0.786**
P(total)	**-0.042**	**0.233**	**0.198**	**0.135**	**0.129**
P_{max}	**-0.032**	**0.170**	**0.161**	**0.086**	**0.073**
P_{PMe3}	**-0.025**	**-0.009**	**-0.009**	**-0.009**	**-0.005**

P(total) represents the total spin density from the [SiP^{iPr}_3] scaffold. P_{max} represents the values from the phosphine possessing the greatest spin density.* Values from reference 7.

The conclusions from the EPR data are corroborated by DFT calculations (Table 4.2.). These calculations place Mulliken spin densities of 1.17,[13] 0.74, and 0.73e− at the metal centers for **4.1**, **4.2**, and **4.3**, respectively. While small in **4.1**, delocalization of spin density onto the phosphines is evident for **4.2** and **4.3** with values of 0.23 and 0.19e− distributed among the P atoms of the [SiP^{iPr}_3] scaffold. The greater spin delocalization for **4.2** and **4.3** relative to **4.1** is likely due to the greater covalency of the M−P bonds in the latter. In constrast, the apical PMe_3 P atom possesses negligible spin for all three complexes. The small degree of delocalization onto the phosphines in **4.1** may also explain its featureless 77 K spectrum. Importantly, one P atom in **4.2** and **4.3** possesses a notably greater value (0.17 for **4.2**, 0.16e− for **4.3**) relative to the other two P atoms. This P atom lies opposite the largest P−M−P angle in the equatorial plane of these complexes, and this observation is consistent with the EPR simulations that assign a large hyperfine coupling to this atom. The numbers are roughly double the value observed for the P atom with the largest spin density in **4.11** (0.09 e−) and **4.12** (0.07e−), and suggest a greater spin delocalization for the group 9 complexes, in agreement with the EPR parameters

(Table 4.1). Thus, both the EPR simulations and DFT calculations are qualitatively consistent and point to metalloradical character for **4.1**-**4.3**, with a greater degree of spin leakage for the 2nd and 3rd row derivatives **4.2** and **4.3**.

The frontier orbitals of complexes **4.1**-**4.3** are also of interest. For all three complexes, the LUMO is ligand based and the SOMO and SOMO-1 are of d_{xy}/d_{x2-y2} parentage (see the appendix). While the (LUMO, SOMO) energy difference remains relatively constant throughout the three complexes, the (SOMO, SOMO−1) energy difference increases from **4.1** to **4.3**, from 5.7 to 16.9 kcal/mol. Observation of the largest g-anisotropy in complex **4.1**, despite the smaller spin-orbit coupling constant for Co relative to Rh and Ir, is thus not only a result of greater spin density on the metal center, as suggested by DFT calculations, but also of greater admixture of the SOMO with filled orbitals (mostly SOMO−1).

4.3 Conclusion

To conclude, a series of d^7 complexes of group 9 metals have been synthesized and thoroughly characterized. The electronic structures of these complexes have been probed through both EPR spectroscopy and DFT calculations, and these results suggest metalloradical character. These complexes represent a rare series of d^7 complexes with the same coordination sphere, in which all metals within the group have been isolated. Comparison of the complexes within the series indicates greater spin delocalization onto the phosphines for Rh and Ir relative to Co. This observation is consistent with the greater degree of covalency of the M−P bonds in the heavier metals. Further, comparison of the Rh and Ir complexes, **4.2** and **4.3**, with their isoelectronic group 8 analogs, complexes

4.11 and **4.12**, points to similar electronic structures for the two sets of complexes but with increased spin delocalization onto the phosphines for **4.2** and **4.3**. The degree of covalency observed in the M−P bonds in complexes **4.2**, **4.3**, **4.11**, and **4.12** may explain the unusual stability of these 2nd and 3rd row low-valent metalloradicals with respect to other reported examples, for which few are isolable and structurally characterized.[14]

4.4 Experimental Section

4.4.1 General Considerations

All manipulations were carried out using standard Schlenk or glovebox techniques under an atmosphere of dinitrogen. Unless otherwise noted, solvents were degassed and dried by thoroughly sparging with N_2 gas followed by passage through an activated alumina column. Hexamethyldisiloxane was dried over CaH_2 and distilled. Pentane, hexamethyldisiloxane, benzene, methylcyclohexane, toluene, tetrahydrofuran, and diethylether were tested with a standard purple solution of sodium benzophenone ketyl in tetrahydrofuran. Unless noted otherwise, all reagents were purchased from commercial vendors and used without further purification. Celite (Celite® 545) was dried at 150 °C overnight before use. $FcBAr^F_4$,[15] $[SiP^{iPr}_3]Co(N_2)$,[6] and $[SiP^{iPr}_3]Ir(N_2)$[6] were prepared according to literature procedures. Deuterated solvents were purchased from Cambridge Isotope Laboratories, Inc., degassed, and stored over 3 Å molecular sieves prior to use. Elemental analyses were performed by Midwest Microlabs, IN.

4.4.2 X-ray Crystallography Procedures

X-ray diffraction studies were carried out at the Beckman Institute Crystallography Facility on a Brüker KAPPA APEX II diffractometer and at the MIT Department of Chemistry X-Ray Diffraction Facility on a Bruker three-circle Platform APEX II diffractometer solved using SHELX v. 6.14. The crystals were mounted on a glass fiber with Paratone-N oil. Data were collected at 100 K using Mo Kα (λ = 0.710 73 Å) radiation and solved using SHELXS[16] and refined against F^2 on all data by full-matrix least squares with SHELXL.[16] X-ray quality crystals were grown as described in the experimental procedures.

4.4.3 Electrochemistry

Electrochemical measurements were carried out in a glovebox under a dinitrogen atmosphere in a one-compartment cell using a CH Instruments 600B electrochemical analyzer. A glassy carbon electrode was used as the working electrode, and platinum wire was used as the auxillary electrode. The reference electrode was Ag/AgNO3 in THF. The ferrocene couple Fc+/Fc was used as an external reference. Solutions (THF) of electrolyte (0.3 M tetra-*n*-butylammonium hexafluorophosphate) and analyte were also prepared under an inert atmosphere.

4.4.4 DFT Calculations.

Geometry optimization for **4.1**, **4.2**, and **4.3** were run on the Gaussian03[17] suite of programs with the B3LYP[18] level of theory with the LANL2TZ(f)[19] basis set for Co, Rh and Ir, 6-31G(d)[20] basis set for Si and P, and LANL2DZ[21] basis set for C and H atoms. Frequency calculations on **4.2** and **4.3** confirmed the optimized structures to be minima.

For complex **4.1**, frequency calculations on the optimized structure yielded one imaginary frequency that involved a vibrational mode that depicts a slight rocking motion about the molecule. Using a pruned (99,590) grid instead of the default pruned (75,302) grid also resulted in the same transition state. Because the spin densities calculated from the optimized structure are similar to the values calculated from energy calculations on complex **4.1** using x-ray coordinates, we believe the values from the optimized structure are reliable and report these values in the maintext for consistency with the other calculated values. Spin density calculated from x-ray coordinates for **4.1** are listed in the appendix, along with spin densities from optimized structures.

Additional energy calculations were run using the same functional as the optimizations with the LANL2TZ(f) for the transition metals, and 6-311G(d,p)[22] basis set for all other atoms. Energy calculations on solid-state structures were run using the same functional and basis set as the energy calculations for the optimized structures.

4.4.5 Other Spectroscopic Measurements

Varian Mercury-300 and Varian Inova-500 were used to collect ^{1}H, ^{13}C, ^{29}Si, and ^{31}P spectra at room temperature unless otherwise noted. ^{1}H and ^{13}C spectra were referenced to residual solvent resonances. ^{29}Si spectra were referenced to external tetramethylsilane (δ = 0 ppm), and ^{31}P spectra were referenced to external 85% phosphoric acid (δ = 0 ppm). IR measurements were obtained on samples prepared as KBr pellets using a Bio-Rad Excalibur FTS 3000 spectrometer. X-band EPR spectra were obtained on a Bruker EMX spectrometer. Spectra were simulated using *Easyspin*[23] program.

4.4.6 Synthesis

Synthesis of {[SiP$^{iPr}_3$]Co(PMe$_3$)}BAr$^F_4$ (4.1). [SiP$^{iPr}_3$]Co(N_2) (30 mg, 0.043 mmol) was dissolved in 8 mL THF. FcBAr$^F_4$ (45.4 mg, 0.043 mmol) was dissolved in 2 mL THF. Both were cooled to −78 ^{o}C. PMe_3 (13 μL, 0.043 mmol) was syringed into the [SiP$^{iPr}_3$]Co(N_2) solution. The FcBAr$^F_4$ solution was subsequently added to the reaction mixture. The orange solution was stirred at −78 ^{o}C for 10 min, and concentrated. The residues were washed with pentane to removed the ferrocene, and the product was extracted into ether, and filtered through celite. Recrystallization by layering pentane over a concentrated ether solution yielded analytically pure product (40 mg, 58%). Recrystallization by slow evaporation of a concentrated ether/methylcyclohexane solution into methylcyclohexane yielded crystals suitable for X-ray diffraction. ^{1}H NMR (C_6D_6, δ): 18.0, 14.8, 8.7, 7.9, 7.5, 5.6, 4.4, −4.9, −6.6.]). μ_{eff} (Evans' method, C_6D_6:d_8-THF = 10:1, 23 ^{o}C) = 1.8 μ_B. Anal. Calcd for $C_{71}H_{75}SiP_4BF_{24}Co$: C, 53.10; H, 4.71; N. 0.00. Found: C, 52.88; H, 4.42; N, 0.00. UV-VIS (in THF): (nm, ε [mol^{-1} cm^{-1}]), 368 (3100), 403 (2030, sh), 567 (220).

Synthesis of [SiP$^{iPr}_3$]Rh(H)(Cl) (4.7). [SiP$^{iPr}_3$]H (220 mg, 0.36 mmol) and [RhCl(COD)] (88 mg, 0.18 mmol) were dissolved in 15 mL of THF and stirred for 3 h. The solution was concentrated, and the products were extracted into benzene and filtered through celite. The resulting solution was concentrated, washed with pentane (4 x 1 mL), and dried to yield the pale yellow product (232 mg, 87%). ^{1}H NMR (C_6D_6, δ): 7.99 (d, *J* = 7.2 Hz, 2H), 7.82 (d, *J* = 7.2 Hz, 1H), 7.38-6.99 (m, 9H), 2.72 (s, 2H), 2.58 (m, *J* = 6.6 Hz, 2H), 2.46 (m, *J* = 7.2 Hz, 2H), 1.82 (q, *J* = 7.2 Hz, 6H), 1.42 (q, *J* = 6.9 Hz, 6H), 1.30 (m,

6H), 1.09-0.95 (m, 12H), 0.54 (q, *J* = 6.9 Hz, 6H), −10.4 (dm, *J* = 143 Hz, 1H). $^{13}C\{^{1}H\}$ NMR (C_6D_6, δ): 155.4 (d, *J* = 46 Hz), 152.7 (t, *J* = 22 Hz), 146.4 (t, *J* = 22 Hz), 143.8 (d, *J* = 32 Hz), 133.2 (d, *J* = 19 Hz), 133.1 (t, *J* = 9.6 Hz), 128.8, 128.6, 128.2, 128.0, 126.6 (d, *J* = 5.0 Hz), 29.7 (m), 28.9 (m), 21.4, 19.8, 19.2, 18.8, 18.5. $^{31}P\{^{1}H\}$ NMR (C_6D_6, δ): 57.2 (d, *J* = 109 Hz, 2P) 47.9 (br, 1P). IR (KBr, cm^{-1}): 2037 (ν[Rh−H]).

Synthesis of [SiP$^{iPr}_3$]Rh(N$_2$) (4.5). [SiP$^{iPr}_3$]Rh(H)(Cl) (150 mg, 0.20 mmol) was dissolved in 12 mL of THF. MeMgCl (75 μL, 0.22 mmol, 3M sln) was diluted with 3 mL of THF. Both were cooled to −78 ^{o}C. The MeMgCl solution was added dropwise to the pale yellow solution of the complex, resulting in a color change to red/orange. The resulting mixture was stirred for 15 min at −78 ^{o}C, and then stirred at RT for 1.5 h, yielding a dark green solution. The solution was concentrated, and the product was extracted into a 2:1 solution of benzene:pentane, and filtered through celite. Concentration of the solution yielded the product (141 mg, 97%). ^{1}H NMR (C_6D_6, δ): 7.98 (d, *J* = 7.2 Hz, 3H), 7.30 (d, *J* = 7.5 Hz, 3H), 7.19-7.04 (m, 6H), 2.44 (m, 6H), 1.06 (m, 18H), 0.72 (m, 18H). ^{13}C NMR (C_6D_6, δ): 155.6 (m), 145.3 (m), 132.5 (m), 128.0, 128.0, 126.2, 28.9, 18.8, 18.7. ^{31}P NMR (C_6D_6, δ): 59.5 (d, *J* = 160 Hz).

Synthesis of [SiP$^{iPr}_3$]Rh(PMe$_3$) (4.8). [SiP$^{iPr}_3$]Rh(N$_2$) (90 mg, 0.13 mmol) was dissolved in 10 mL THF. The solution was cooled to −78 ^{o}C and PMe_3 (26 μL, 0.25 mmol) was syringed in. The solution was stirred at room temperature for 5 min, and concentrated. Trituration with hexamethyldisiloxane yielded a yellow powder (95 mg, 95%). ^{1}H NMR (C_6D_6, δ): 8.17 (d, *J* = 6.9 Hz, 3H), 7.45 (d, *J* = 7.8 Hz, 3H), 7.23 (t, *J* = 7.2 Hz, 3H), 7.11 (t, *J* = 7.2 Hz, 3H), 2.30 (br, 6H), 1.65 (d, *J* = 4.8 Hz, 3H), 0.97 (br, 18H), 0.80 (br, 18H). ^{13}C NMR (C_6D_6, δ): 156.6 (m), 148.3 (m), 132.3, 128.4 (br), 128.0, 126.1, 29.9, 28.9,

20.2, 18.6. ^{31}P NMR (C_6D_6, δ): 54.3 (dd, *J* = 153, 39 Hz, 3P), −29.5 (dq, *J* = 106 Hz, 39 Hz, 1P).

Synthesis of {[SiP$^{iPr}_3$]Rh(PMe$_3$)}BAr$^F_4$ (4.2). [SiP$^{iPr}_3$]Rh(PMe$_3$) (50 mg, 0.064 mmol) was dissolved in 8 mL THF. FcBAr$^F_4$ (67 mg, 0.064 mmol) was dissolved in 3 mL THF. Both were cooled to −78 ^{o}C. The FcBAr$^F_4$ solution was added dropwise to the [SiP$^{iPr}_3$]Rh(PMe$_3$) solution, causing a color change to green. The reaction mixture was stirred for 10 min, after which the reaction mixture was stirred for 30 min The mixture was concentrated, and the residues were washed with pentane. The product was extracted into ether, and filtered through celite. Recrystallization from layering pentane over a concentrated ether solution yielded crystals suitable for x-ray diffraction (69 mg, 66%). ^{1}H NMR (C_6D_6:d^8-THF = 10:1, δ): 12.0, 9.8, 8.4, 7.7, 5.3, −0.1.]). μ_{eff} (Evans' method, C_6D_6: d_8-THF = 10:1, 23 ^{o}C) = 1.6 μ_B. Anal. Calcd for $C_{71}H_{75}SiP_4BF_{24}Rh$: C, 51.68; H, 4.58; N. 0.00. Found: C, 51.33; H, 4.48; N, 0.00. UV-VIS (in THF): (nm, ε [mol^{-1} cm^{-1}]), 307 (5900, sh), 639 (320).

Synthesis of [SiP$^{iPr}_3$]Ir(PMe$_3$) (4.9). [SiP$^{iPr}_3$]Ir(N_2) (90 mg, 0.11 mmol) was dissolved in 6 mL THF. The solution was cooled to −78 ^{o}C and PMe$_3$ (34 μL, 0.033 mmol) was syringed into the reaction mixture. The reaction mixture was stirred for 5 min at −78 ^{o}C and concentrated. The residues were extracted into ether, filtered through celite, and concentrated. Trituration with hexamethyldisiloxane resulted in a yellow powder (95 mg, 99%). ^{1}H NMR (C_6D_6, δ): 8.25 (d, *J* = 7.5 Hz, 3H), 7.42 (d, *J*= 8 Hz, 3H), 7.20 (t, *J* = 7 Hz, 3H), 7.07 (t, *J* = 7.5 Hz, 3H), 2.38 (s, 6H), 1.88 (d, *J* = 6.0 Hz, 3H), 0.94 (s, 18H), 0.75 (s, 18H). ^{13}C NMR (C_6D_6, δ): 155.5 (m), 149.8 (m), 131.9 (q, *J* = 6.3 Hz), 127.7,

126.0, 31.6 (d, J = 22.1 Hz), 31.4 (br), 20.0, 18.6. ^{31}P NMR (C_6D_6, δ): 27.8 (br, 3P), −74.0 (q, J = 27.2 Hz, 1P).

Synthesis of {[SiP$^{iPr}_3$]Ir(PMe$_3$)}BAr$^F_4$ (4.3). [SiP$^{iPr}_3$]Ir(PMe$_3$) (30 mg, 0.038 mmol) was dissolved in 5 mL Et_2O. FcBAr$^F_4$ (40 mg, 0.038 mmol) was dissolved in 2 mL Et_2O. Both were cooled to −78 ^{o}C. The FcBAr$^F_4$ solution was added dropwise to the [SiP$^{iPr}_3$]Ir(PMe$_3$) solution. An immediate color change from yellow to purple resulted. The reaction mixture was stirred for 2 min at −78 ^{o}C, and was stirred at 5 min, at RT. The reaction mixture was concentrated and the residues were washed with pentane. The solids were extracted into ether, filtered through celite, and concentrated to yield the purple product. Layering pentane over a concentrated ether solution resulted in purple crystals (58 mg, 87%). Crystals of the product with OTf^- as the anion, [SiP$^{iPr}_3$]Ir(PMe$_3$)}OTf (**4.3'**), which was synthesized by the addition of AgOTf to [SiP$^{iPr}_3$]Ir(PMe$_3$) in THF, were obtained from recrystallization by layering pentane over a concentrated dichloromethane solution. These crystals were amenable to X-ray diffraction. ^{1}H NMR (C_6D_6:d^8-THF = 10:1, δ): 15.9, 10.9, 9.1, 8.3, 7.7, 5.9, −0.5.]). μ_{eff} (Evans' method, C_6D_6: d_8-THF = 10:1, 23 ^{o}C) = 1.7 μ_B. Anal. Calcd for $C_{71}H_{75}SiP_4BF_{24}Ir$: C, 49.03; H, 4.35; N. 0.00. Found: C, 49.47; H, 4.56; N, 0.00. UV-VIS (in THF): (nm, ε [mol^{-1} cm^{-1}]), 366 (138, sh), 482 (360, sh), 566 (470).

References Cited

1 de Bruin, B; Hetterscheid, D. G. H.; Koekkoek, A. J. J., Grützmacher, H. *Prog. Inorg. Chem*. **2007**, *55*, 247.

2 Cui, W.; Li, S.; Wayland, B. B. *J. Organomet. Chem.* **2007**, *692*, 3198.

3 a) Sherry, A. E.; Wayland, B. B. *J. Am. Chem. Soc.* **1990**, *112*, 1259. b) Wayland, B. B.; Ba, S.; Sherry, A. E. *J. Am. Chem. Soc.* **1991**, *113*, 5305.

4 Poli, R. *Angew. Chem. Int. Ed.* **2010**, *49*, 2.

5 a) Palmer, J. H.; Mahammed A.; Lancaster K. M.; Gross, Z.; Gray, H. B. *Inorg. Chem.* **2009**, *48*, 9308. b) Zhai, H.; Bunn, A.; Wayland, B. *Chem. Commun.* **2001**, 1294. c) Deblon, S.; Liesum, L.; Harmer, J.; Schönberg, H.; Schweiger, A.; Grützmacher, H. *Chem. –Eur. J.* **2002**, *8*, 601.

6 a) Mankad, N. P.; Whited, M. T.; Peters, J. C. *Angew. Chem. Int. Ed.* **2007**, *129*, 5768. b) Whited, M. T.; Mankad, N. P.; Lee, Y.; Oblad, P. F.; Peters, J. C. *Inorg. Chem.* **2009**, *48*, 2507. c) Lee, Y.; Mankad, N. P.; Peters, J. C. *Nat. Chem.* **2010**, *2*, 558.

7 Takaoka, A.; Gerber, L. C. H.; Peters, J. C. *Angew. Chem. Int. Ed.* **2010**, *49*, 4088.

8 $\tau = (b-a)/60$ where b and a represent the two largest angles. $\tau = 1$ for TBP, 0 for square pyramid. See; Addison, A. W.; Rao, T. N.; Van Rijn, J. J.; Verschoor, G. C. *J. Chem. Soc., Dalton Trans.* **1984**, 1349.

9 This complex has been crystallized in two different polymorphs (monoclinic or orthorhombic) depending on the conditions. Both τ values are reported, with the number in parentheses belonging to the orthorhombic structure.

10 Wassenaar, J.; Siegler, M. A.; Spek, A. L.; de Bruin, B.; Reek, J. N. H.; van der Vlugt, J. I. *Inorg. Chem.* **2010**, *49*, 6495.

11 Bianchini, C.; Meli, A.; Peruzzini, M.; Vacca, A. *Organometallics* **1990**, *9*, 360.

12 a) Zecchin, S.; Zotti, G.; Pilloni, G. *J. Organomet. Chem.* **1985**, *294*, 379. b) Dzik, W. I.; Arruga, L. F.; Siegler, M. A.; Spek, A. L.; Reek, J. N. H.; de Bruin, B. *Organometallics* **2011**, *30*, 1902. c) Vugman, N. V.; Caride, A. O.; Danon, J. *J. Chem. Phys.* **1973**, *59*, 4418.

13 Some negative spin due to spin polarization is observed on the Si (−0.09e¯).

14 Representative examples of structurally characterized Rh(II) and Iridium(II) metalloradicals: a) Danopoulos, A. A.; Wilkinson, G.; Hussain-Bates, B.; Hursthouse, M. B. *J. Chem. Soc., Dalton Trans.* **1992**, 3165. b) García, M. P.; Jiménez, M. V.; Oro, L. A.; Lahoz, F. J. *Organometallics* **1993**, *12*, 4660. c) de Bruin, B.; Peters, T. P. J.; Thewissen, S.; Blok, A. N. J.; Wilting, J. B. M.; de Gelder, R.; Smits, J. M. M.; Gal, A. W. *Angew. Chem. Int. Ed.* **2002**, *41*, 2135. d) García, M. P.; Jiménez, M. V.; Oro, L. A.; Lahoz, F. J.; Casas, J. M.; Alonso, P. J. *Organometallics* **1993**, *12*, 3257. e) Dunbar, K. R.; Haefner, S. C. *Organometallics* **1992**, *11*, 1431. f) Connely, N. G.; Emslie, D. J. H.; Metz, B.; Orpen, A. G.; Quayle, M. J. *Chem. Commun.* **1996**, 2289.

15 J. Le Bras, H. Jiao, W. E. Meyer, F. Hampel, J. A. Gladysz, *J. Organomet. Chem.* **2000**, *616*, 54.

16 Sheldrick, G. M. *Acta. Cryst.* **2008**, *A64*, 112.

17 Gaussian 03, Revision C.02, M. J. Frisch, G. W. Trucks, H. B. Schlegel, G. E. Scuseria, M. A. Robb, J. R. Cheeseman, J. A. Montgomery, Jr., T. Vreven, K. N. Kudin, J. C. Burant, J. M. Millam, S. S. Iyengar, J. Tomasi, V. Barone, B. Mennucci, M. Cossi, G. Scalmani, N. Rega, G. A. Petersson, H. Nakatsuji, M. Hada, M. Ehara, K. Toyota, R. Fukuda, J. Hasegawa, M. Ishida, T. Nakajima, Y. Honda, O. Kitao, H. Nakai, M. Klene,

X. Li, J. E. Knox, H. P. Hratchian, J. B. Cross, V. Bakken, C. Adamo, J. Jaramillo, R. Gomperts, R. E. Stratmann, O. Yazyev, A. J. Austin, R. Cammi, C. Pomelli, J. W. Ochterski, P. Y. Ayala, K. Morokuma, G. A. Voth, P. Salvador, J. J. Dannenberg, V. G. Zakrzewski, S. Dapprich, A. D. Daniels, M. C. Strain, O. Farkas, D. K. Malick, A. D. Rabuck, K. Raghavachari, J. B. Foresman, J. V. Ortiz, Q. Cui, A. G. Baboul, S. Clifford, J. Cioslowski, B. B. Stefanov, G. Liu, A. Liashenko, P. Piskorz, I. Komaromi, R. L. Martin, D. J. Fox, T. Keith, M. A. Al-Laham, C. Y. Peng, A. Nanayakkara, M. Challacombe, P. M. W. Gill, B. Johnson, W. Chen, M. W. Wong, C. Gonzalez, and J. A. Pople, Gaussian, Inc., Wallingford CT, 2004.

18 a) Becke, A.D. *J. Chem. Phys.* **1993**, *98*, 5648. b) Lee, C.; Yang, W.; Parr, R. G. *Phys. Rev. B.* **1988**, *37*, 785.

19 a) Hay, P. J.; Wadt, W. R. *J. Chem. Phys.* **1985**, *82*, 299. b) Roy, L. E.; Hay, P. J.; Martin, R. L. *J. Chem. Theory Comput.* **2008**, *4*, 1029. c) Ehlers, A. W.; Bohme, M.; Dapprich, S.; Gobbi, A.; Hollwarth, A.; Jonas, V.; Kohler, K. F.; Stegmann, R.; Veldkamp, A.; Frenking, G. *Chem. Phys. Lett.* **1993**, *208*, 111.

20 a) Hariharan, P. C.; Pople, J. A. *Theoret. Chimica Acta.* **1973**, *28*, 213. b) Francl, M. M.; Petero, W. J.; Hehre, W. J.; Binkley, J. S.; Gordon, M. S.; DeFrees, D. J.; Pople, J. A. *J. Chem. Phys.* **1982**, *77*, 3654. c) Rassolov, V.; Pople, J. A.; Ratner, M.; Windus, T. L. *J. Chem. Phys.* **1998**, *109*, 1223.

21 a) Krishnan, R.; Binkley, J. S.; Seeger, R.; Pople, J. A. *J. Chem. Phys.* **1980**, *72*, 650. b) McLean, A. D.; Chandler, G. S. *J. Chem. Phys.* **1980**, *72*, 5639.

22 Dunning, T. H.; Hay, P. J. in Methods of Electronic Structure Theory, Vol. 2, Schaefer III, ed., Plenum Press **1977**.

23 S. Stoll, A. Schweiger, *J. Magn. Reson.* **2006**, *178*, 42.

Chapter 5: Catalytic N-N Coupling of Aryl Azides to Yield Azoarenes with a Ru(I) Metalloradical

Reproduced in part with permission from

Takaoka, A.; Peters, J. C. *Submitted*.

5.1 Introduction

Organic azides are valuable sources of nitrenes (NR). They are easily synthesized for a wide array of R substitutents and release N_2 as the only by-product. These aspects make organic azides preferable for nitrene transfer/insertion in organic synthesis over hypervalent iodine compounds (PhI=NTs, etc.) and N-halogenated sulfonamides (chloramine-T, bromamine-T),[1,2,3] which have received more attention but are less flexible with respect to substituent variability and/or release of undesirable by-products. As a result, recent efforts have increasingly focused on developing metal catalyzed nitrene transfer reactions with organic azides.[4] Because the commonly invoked intermediate in these reactions is the metal nitrene/imide species, its reactivity and mechanism of formation from the precursor metal azide adduct have been an important topic of study.

Well-defined metal azide complexes are relatively uncommon species and their decay has been mechanistically examined in limited cases. Bergman and Cummins were the first to report such studies. Bergman's $Cp_2Ta(CH_3)(N_3Ar)$ complexes were found to decay cleanly in a unimolecular fashion to afford the corresponding imide complexes, $Cp_2Ta(CH_3)(NAr)$,[5] akin to N_2 extrusion in phosphazides (ArN_3PR_3) that proceeds through a four-membered transition state to yield iminophosphoranes.[6] Cummins' $V(N_3Mes)(I)(NRAr_F)_2$ (Ar_F = 2,5-C_6H_3FMe) system, in contrast, followed bimolecular decay to the corresponding imide complex, $V(NMes)(I)(NRAr_F)_2$.[7] In both studies, the γ-N atom of the azide ligand is bound to the metal center in the precursor complex and, indeed, this is the most commonly observed binding mode for structurally characterized azide complexes.[5,7,8,10] A more recent mechanistic study by Hillhouse described an

unusual η^2 bound azide complex, (dtbpe)Ni(N_3R) (dtbpe = bis(ditert-butylphosphino)ethane, R = adamantyl) that decayed unimolecularly to the imide complex, (dtbpe)Ni(NR). In this study, a large and negative entropy of activation was observed, consistent with a highly ordered transition state.[9]

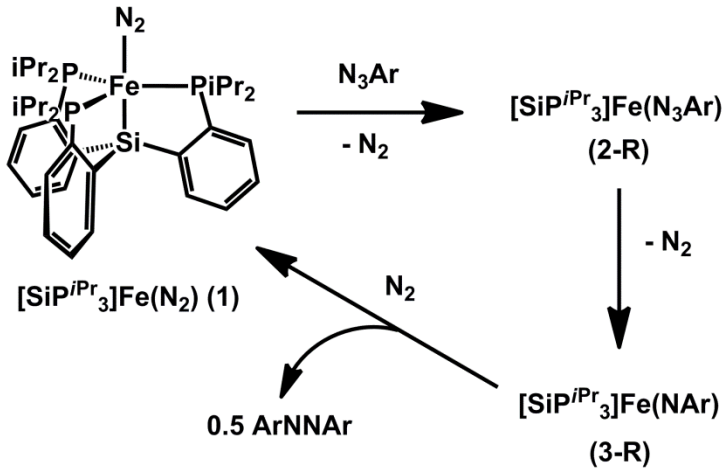

Scheme 5.1.

Our group has recently studied the interaction between aryl azides and the Fe(I) complex, [SiP$^{i\text{Pr}}_3$]Fe(N_2) (**5.1**).[10,11] This reaction was found to initially form an Fe(I) azide adduct, [SiP$^{i\text{Pr}}_3$]Fe(N_3Ar) (**5.2**), which subsequently exhibited clean unimolecular decay as in the Bergman and Hillhouse systems. Interestingly, the major product of this decay was shown to be azoarene and **5.1**, and use of excess aryl azide demonstrated catalytic azoarene formation from **5.1**. While several stoichiometric reactions had been known,[12] this example was noteworthy in that it represented a rare example of catalytic N−N coupling to yield azoarene from organic azides; the first in which azoarene was the major product.[13] Mechanistic studies suggested the formation of a transient Fe(III) imide complex, [SiP$^{i\text{Pr}}_3$]Fe(NAr) (**5.3**), following decay of **5.2**, which subsequently underwent $4e^-$ reductive N−N coupling to produce azoarene (Scheme 5.1).[14]

Complex **5.3** is a reactive species that was only observable by EPR spectroscopy in a frozen glass. While the EPR features of **5.3** were indicative of an S = ½ ground state, DFT calculations predicted a small doublet-quartet gap of 2.8 kcal/mol, perhaps suggesting that two-state reactivity[15] may be responsible for its rich reactivity; this included hydrogen atom abstraction from 9,10-dihydroanthracene and carbodiimide formation with *t*-butylisocyanide.[10] In this regard, the recent isolation of the Ru(I) metalloradical, [SiP$^{i\text{Pr}}_3$]Ru(N_2) (**5.4**), and its interaction with *p*-$CF_3C_6H_4N_3$ to yield the formally Ru(III) imide complex, [SiP$^{i\text{Pr}}_3$]Ru($NC_6H_4CF_3$) (**5.5-CF$_3$**), is noteworthy (Scheme 5.2).[16] This work highlighted the first reaction chemistry of an unusual mononuclear ruthenium(I) complex. Although **5.5-CF$_3$** did not yield azoarene upon decay, it was stable enough for thorough characterization. We thus envisioned that use of other substituted aryl azides might yield similar metal imide species (**5.5-R**) that would retain some stability for characterization, yet also exhibit N−N coupling reactivity as observed in the Fe system. Further, because the doublet-quartet gap in the heavier congeners of **5.1** is expected to be much greater than **5.1**, any azoarene formation in the Ru system could also be used as indirect support for doublet state involvement in **5.3**,[17] provided that the same mechanism is operative in both systems.

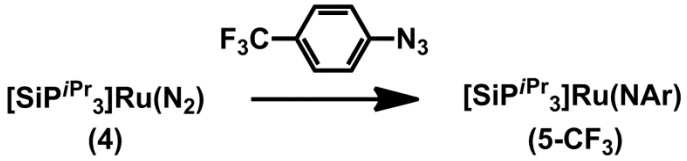

Scheme 5.2.

We herein report the results of our studies on **5.4** with substituted aryl azides. The key compounds involved are shown in Figure 5.1 for reference. The tendency of the aryl azide to degrade in the presence of **5.4** to azoarene product, either stoichiometrically or

catalytically, is dependent on the aryl-ring substitution pattern. Ternimally bonded [SiP$^{iPr}_3$]Ru(NAr) complexes **5.5-R** were observed in some stoichiometric reactions and independent synthesis of **5.5-OMe** allowed thorough characterization and detailed mechanistic studies. Contrary to our initial expectation, we establish that species **5.5-R** is not responsible for the observed reactivity and instead determine that a dramatic change in mechanism occurs in moving from Fe to Ru within the [SiP$^{iPr}_3$]M(N_2) system.

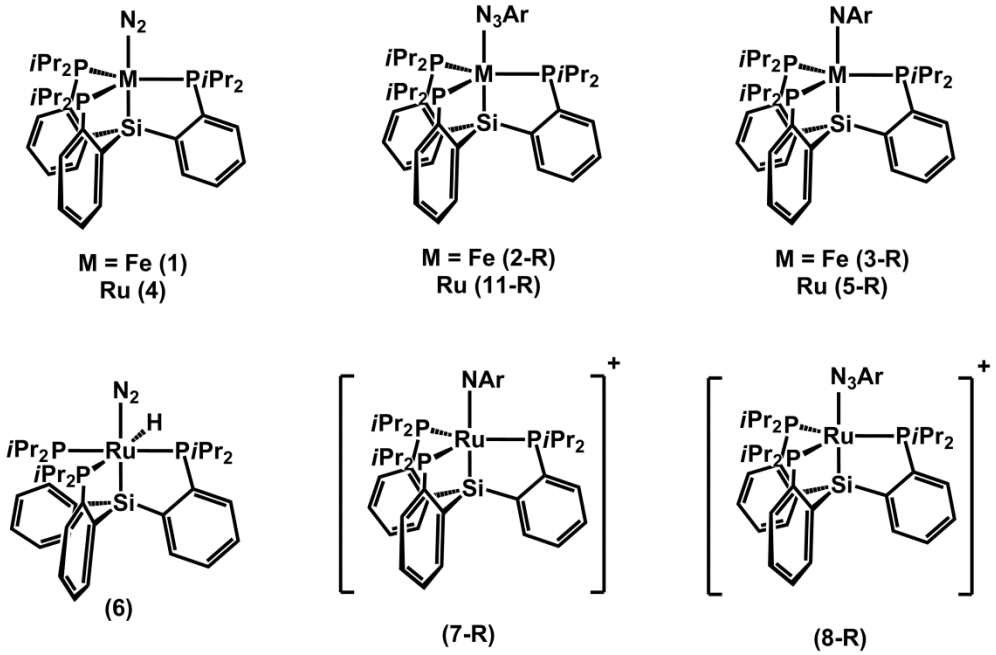

Figure 5.1. Key compounds involved in this work. Lines between core atoms only denote connectivity.

5.2. Results and Discussion

5.2.1 Reaction between 5.4 and *p*-MeOC$_6$H$_4$N$_3$ and Other Aryl Azides

Addition of one equivalent of *p*-MeOC$_6$H$_4$N$_3$ to **5.4** in Et_2O yielded the substituted azoarene, ArN=NAr (Ar = *p*-MeOC$_6$H$_4$), in 93(7)% yield as judged by ^{1}H

NMR spectroscopy with ferrocene (Fc) as an internal standard (Scheme 5.3). The major metal containing product was **5.4**, with small amounts of previously reported[16] [SiP$^{i\text{Pr}}_3$]Ru(H)(N_2) (**5.6**) and a minor paramagnetic product, which will be shown below to be the imide species, **5.5-OMe**. In contrast to the Fe system, which required heating at 70 °C, the reaction between *p*-$MeOC_6H_4N_3$ and **5.4** was complete within seconds at room temperature. As **5.4** was the major metal containing product in the stoichiometric reaction, catalysis could be expected and addition of 10 equivalents of *p*-$MeOC_6H_4N_3$ led to catalytic generation of roughly 50% yield of azoarene with catalyst decomposition. Low temperature ^{1}H NMR studies showed that azoarene began to form at about −65 ^{o}C, and no obvious buildup of intermediates was observed; the broadness of the paramagnetic resonances prevented our ability to draw any definitive conclusions about the metal containing species present in solution at these temperatures. Performing the reaction in the presence of excess elemental mercury (>500 equivalents) had little effect, suggesting that colloidal metal is unlikely to be responsible for the catalysis.

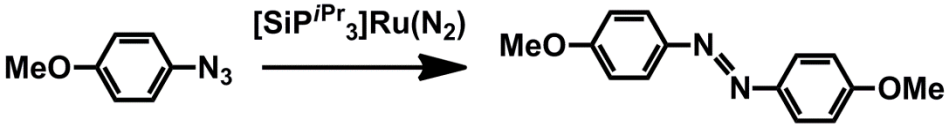

Scheme 5.3.

Use of other *para* substituted aryl azides showed that the electronic influence of the substituent, R, on the phenyl group greatly affected the yield of azoarene. Similar to R = OMe, use of azide with R = OEt led to near quantitative yield of azoarene (Table 5.1). Use of aryl azides where the aryl group is either a mesityl or a *p*-tolyl substituent, in contrast, led to diminished yields of azoarene with greater amounts of **5.6**. Finally, as previously reported, R = CF_3 did not yield any azoarene but exclusively provided **5-CF_3**.

Thus, electron donating groups increase the yield of azoarene formation. Because the aryl azide *para*-substituted by R = OMe gave the highest yield of azoarene, this aryl azide provided the main focus of subsequent mechanistic studies.

R =	***p*-OEt**	***p*-OMe**	**Mes**	***p*-Me**	***p*-CF_3**
ArNNAr	91(9)	93(7)	42(3)	29(1)	0

Table 5.1. Yield (%) of ArNNAr from **5.4** from one equivalent of substituted ArN_3.

5.2.2 A Strategy Towards the Synthesis of 5.5-OMe

We have previously concluded that Fe(III) imide complexes bimolecularly couple to yield azoarenes in the [SiP^{iPr}_3]Fe system.[10] We thus conducted experiments to probe whether such species were also responsible for azoarene formation in this Ru system. Mechanistic analysis in this study, however, was complicated by the presence of multiple paramagnetic species. Since no buildup of intermediates was observed during low temperature NMR experiments, attempts to independently synthesize **5.5-OMe** were made to assess the viability of **5.5-OMe** as a chemically and kinetically competent species for the nitrene coupling process. In this context, it is noteworthy that **5.5-CF_3** features a reversible oxidation event at −1.0 V (vs Fc/Fc^+, see SI). Chemical oxidation of **5.5-CF_3** with AgOTf cleanly led to the Ru(IV) imide complex, {[SiP^{iPr}_3]Ru(NAr)}OTf (**5.7-CF_3**). This compound is thermally robust and represents an unusual example of a structurally characterized (see SI) terminal imide of Ru(IV).[18] The increased thermal stability of **5.7-CF_3** relative to **5.5-CF_3** pointed to increased stability of **5.7-OMe** relative to **5.5-OMe**. We thus aimed at first synthesizing **5.7-OMe**, which would enable chemical

reduction to **5.5-OMe**. Since the stoichiometric reactions in this Ru system were complete within seconds at room temperature, complex **5.5-OMe** would be expected to rapidly yield azoanisole upon reduction from **5.7-OMe** if the same mechanism as in the Fe system were at play (Scheme 5.4).

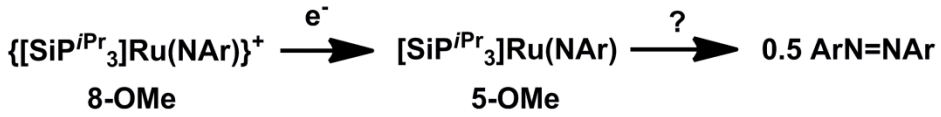

Scheme 5.4.

Addition of one equivalent of *p*-$MeOC_6H_4N_3$ to previously reported[16] {[SiP$^{i\text{Pr}}_3$]Ru(N_2)}BAr^F_4 (**5.9-BAr$^F_4$**) resulted in a rapid color change from orange to red, yielding the diamagnetic Ru(II) azide adduct, {[SiP$^{i\text{Pr}}_3$]Ru(N_3Ar)}BAr^F_4 (**5.8-OMe**) (Scheme 5.5). Both the ^{1}H and ^{31}P{^{1}H} NMR spectra are consistent with a threefold symmetric structure on the NMR timescale. The diamagnetic spectra are suggestive of a distorted 5-coordinate structure that lies between a square pyramid (SP) and trigonal bipyramid (TBP) (*vide infra*), as seen in other structurally characterized d^6 ruthenium complexes of [SiP$^R_3$] (R = *i*Pr, Ph).[16,19] The IR spectrum of **5.8-OMe** exhibits a strong N−N stretch at 2106 cm^{-1}. This value is close to the value of free *p*-$MeOC_6H_4N_3$ (2103 cm^{-1}), and is in accord with an unactivated azide ligand as expected for a cationic Ru(II) complex. Upon photolysis of **5.8-OMe** with a mercury lamp in the presence of excess azide, a color change from red to green took place, and the ^{31}P{^{1}H} signal of **5.8-OMe** at 72 ppm decreased as a new peak at 106 ppm gained in intensity. Monitoring the complete decay of the signal at 72 ppm and following with workup yielded diamagnetic and green **5.7-OMe** in good yield. Consistent with N_2 loss, the IR spectra of **5.7-OMe** showed no significant stretch near 2100 cm^{-1} after photolysis.

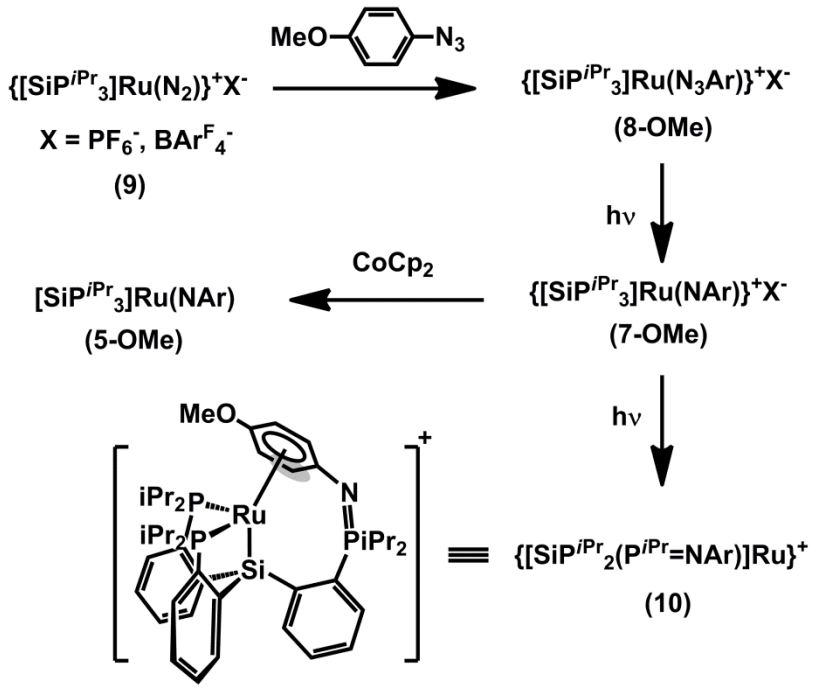

Scheme 5.5.

Interestingly, new signals at 86, 79, and 33 ppm in the $^{31}P\{^{1}H\}$ spectrum developed at the expense of the signal for **5.7-OMe** upon prolonged photolysis. The conversion was complete after two days and X-ray diffraction studies (*vide infra*) revealed nitrene insertion into the Ru−P bond of **5.7-OMe** and binding of the aryl ring in the nitrene moiety to the metal center in an η^6 mode (complex **5.10**, Scheme 5.5). The ^{1}H NMR spectrum of the nitrene insertion product **5.10** exhibits three resonances between 6.7 and 5.3 ppm that correspond to the resonances of the η^6 arene moiety. The $^{31}P\{^{1}H\}$ resonance at 33 ppm is attributed to the oxidized phosphine center. For ease of purification, subsequent studies utilized the PF_6^- anion for **5.7-OMe**, **5.8-OMe**, and **5.9**. These were synthesized in the same manner as the $BAr^F{}_4^-$ anion complexes (Scheme 5.5), except for **5.9-PF$_6$**, which was synthesized by oxidation of **5.4** with $AgPF_6$ (see experimental section).

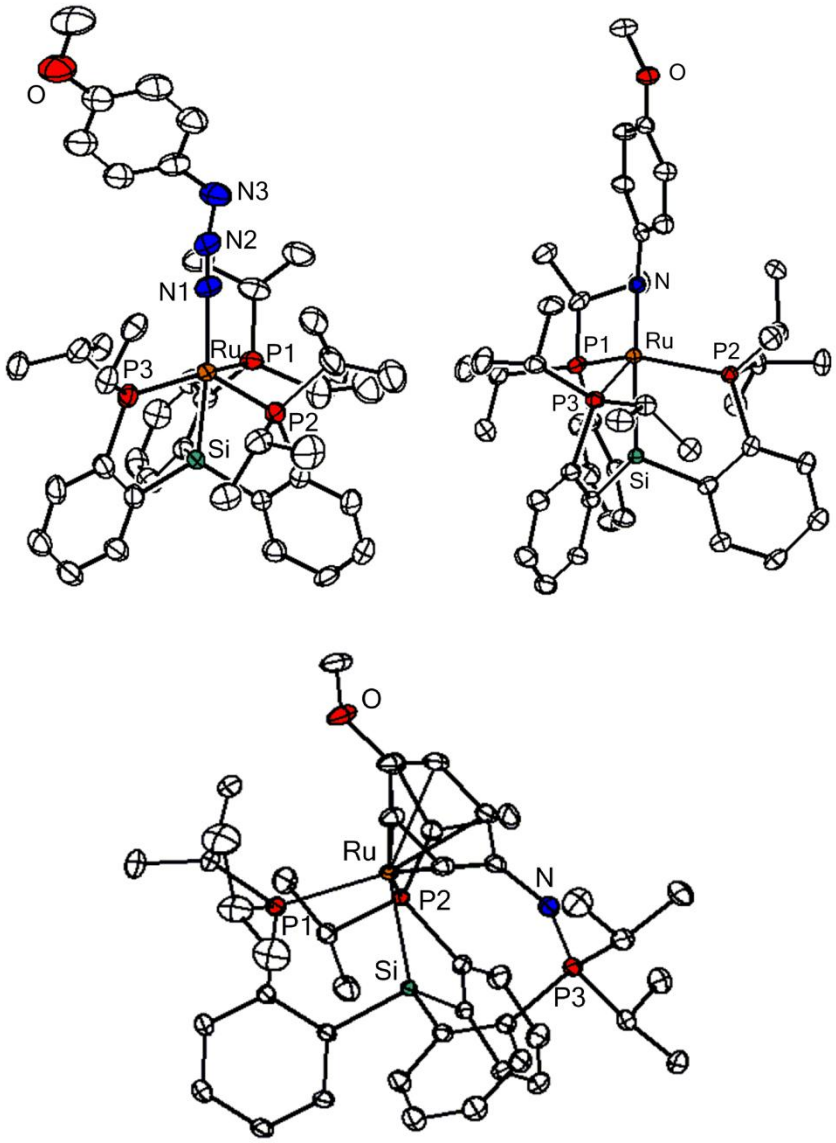

Figure 5.2. Solid-state structure of **5.8-OMe** (top, left), **5.7-OMe** (top, right), and **5.10** (bottom). Anions, hydrogen atoms, and solvent molecules are removed for clarity.

5.2.3 Solid-State Structures of 5.8-OMe, 5.7-OMe, and 5.10

The solid-state structures of **5.8-OMe**, **5.7-OMe**, and **5.10** have been obtained and are shown in Figure 5.2. The geometry about the metal center in **5.8-OMe** is in between that of a trigonal bipyramid and a square pyramid with a τ value[20] of 0.39. The N(1)−N(2) and N(2)−N(3) distances of 1.107(5) and 1.254(6) Å are short and similar to the values of crystallographically characterized free organic azides.[21] The N(1)−N(2) distance in **5.8-OMe** is significantly shorter than the bond distance in the Fe(I) azide adduct,[10] **5.2-Ad** (1.27(1) Å), suggesting little activation of the azide ligand. The near linear N(1)−N(2)−N(3) angle of 168.3(6) is also in contrast to **5.2-Ad** (147(4)^{o}) but similar to the value of 173.1(3)^{o} observed in a Cu(I) azide complex, [HB(3,5-$(CF_3)_2Pz)_3$]Cu(N_3Ad) ([HB(3,5-$(CF_3)_2Pz)_3$]$^-$ = hydridotris(3,5-bis(trifluoromethyl)pyrazolyl)borate).[8f] Interestingly, **5.8-OMe** appears to be the only crystallographically characterized ruthenium alkyl or aryl azide complex reported to date.

The solid-state structure of **5.7-OMe** features a metal center with a τ value of 0.90, approximating a trigonal bipyramidal geometry. The ruthenium is significantly displaced out of the plane of the phosphines, however, and the three P−Ru−P angles sum to 340.93(5)°. The Ru−Si bond length of 2.491(1) Å is accordingly much longer than typically observed distances in other [SiP$^{i\text{Pr}}_3$]RuX complexes, where X is a neutral or anionic ligand *trans* to the Si anchor in the [SiP$^{i\text{Pr}}_3$] scaffold (Table 5.2).[16] The elongation of the Ru−Si bond reflects an approach of the metal center towards a pseudotetrahedral geometry, with a corresponding weakening of the Ru−Si bond. This change in geometry has significant consequences towards its electronic structure (see section 5.2.8). The Ru−N distance of 1.802(3) Å, while significantly shorter than in **5.5-CF$_3$**, is longer than

the two other structurally characterized Ru(IV) imide complexes (1.716(3) and 1.785(6) Å).[18] The solid-state structure of **5.7-CF_3** is very similar to **5.7-OMe** (see appendix).

	[SiP^{iPr}_3]RuI*	4*	8-OMe	**7-OMe**
Ru−Si (Å)	2.284(1)	2.319(1)	2.305(1)	**2.491(1)**
∑(P−Ru−P)	353.3(1)	352.7(1)	352.1(1)	**340.9(1)**

Table 5.2. Comparison of Ru−Si bond lengths (Å) and sum of P−Ru−P angles (°) for representative 5-coordinate Ru(I) and Ru(II) complexes relative to **5.7-OMe**. *from reference 16.

Finally, the solid state structure of **5.10** features a phosphinimide moiety resulting from NAr insertion of **5.7-OMe** into one of the M−P bonds. This complex is best described as a three-legged piano stool complex. Dechelation of one P atom results from its oxidation to a formally pentavalent phosphorus atom, and an η^6 interaction between the aryl ring and the metal center is observed with Ru−C distances ranging between 2.23 and 2.40 Å. These distances are within, if not slightly longer, than reported Ru−C(aryl) distances for ruthenium complexes with an η^6 coordinated anisole ligand.[22]

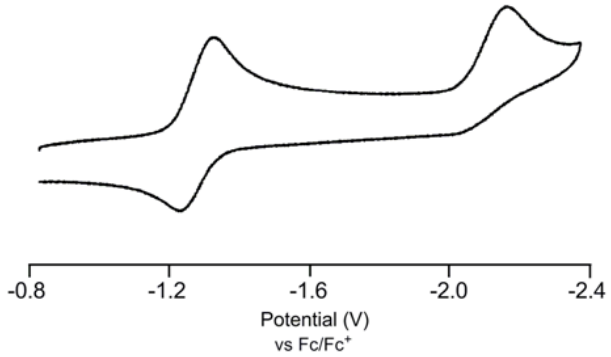

Figure 5.3. Cyclic voltammogram of **5.7-OMe** in 0.3 M $TBAPF_6$ in THF.

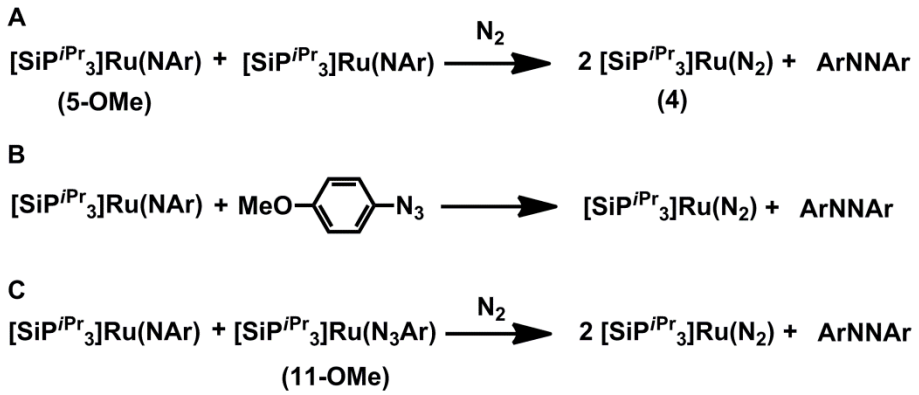

Scheme 5.6.

5.2.4 Synthesis of 5.5-OMe and Mechanistic Studies

The cyclic voltammetry of **5.7-OMe** is shown in Figure 5.3 and displays a reversible reduction event at −1.24 V and an irreversible reduction event at −2.17 V. The first wave is assigned to a formal Ru(IV) to Ru(III) reduction, as this wave is close to the formal Ru(IV)/Ru(III) couple of **5.7-CF_3**. The irreversible wave is assigned to a Ru(III)/Ru(II) redox event. The reversible nature of the first redox event indicates that the product resulting from one electron reduction of **5.7-OMe** is stable on the electrochemical timescale. Chemical reduction was accomplished by addition of one equivalent of $CoCp_2$ to **5.7-OMe**, which caused a color change from green to red/brown. Removal of $[CoCp_2]PF_6$ and extraction into pentane led to the isolation of **5.5-OMe** in moderate yield. While its solid-state structure was not be obtained, the ^{1}H NMR of **5.5-OMe** is reminiscent of the spectrum of **5.5-CF_3**. The room temperature (RT) EPR spectrum (*vide infra*) of **5.5-OMe** is also similar to that of **5.5-CF_3**, corroborating its assignment. Interestingly, **5.5-OMe** is relatively stable at room temperature, showing signs of decomposition only after several hours in solution. Further, **5.5-OMe** does not

produce azoanisole upon decay. These observations rule against a mechanism in common with the related Fe system, in which two imide species undergo N−N coupling (Scheme 5.6, A).[10]

Other plausible mechanisms that involve **5.5-OMe** in the catalytic cycle are shown in Scheme 5.6, B and C. In mechanism B, **5.5-OMe** reacts with free azide to yield azoanisole and **5.4**. This mechanism is related to one recently reported for a nickel system,[12b] in which azide addition to a nickel imide results in 1,3-dipolar addition to yield a tetrazene type intermediate/transition state that releases azoarene after N_2 extrusion. In mechanism C, **5.5-OMe** reacts with a transient Ru(I) azide adduct, $[SiP^{iPr}_3]Ru(N_3Ar)$ (**5.11-OMe)**, to release azoanisole and regenerate **5.4**. To test the validity of mechanism B *p*-$MeOC_6H_4N_3$ was added to **5.5-OMe**. Neither decay of **5.5-OMe** nor azoanisole formation was observed, ruling it out. To test mechanism C, a crossover experiment was designed with *p*-$EtOC_6H_4N_3$. First, a control experiment, in which a 1:1 mixture of *p*-$MeOC_6H_4N_3$ and *p*-$EtOC_6H_4N_3$ was added to **5.4,** was conducted. This reaction produced a statistical mixture of 1:2:1 = ArNNAr: ArNN'Ar: Ar'NNAr' (Ar = *p*-$MeOC_6H_4$, Ar' = *p*-$EtOC_6H_4$) (Scheme 5.7). Next, one equivalent of *p*-$EtOC_6H_4N_3$ was added to one equivalent each of **5.4** and **5.5-OMe**. If mechanism C was responsible for azoarene formation, the hetero azoarene, ArNNAr', would be expected to form to some extent. In contrast, only the homocoupled azoarene, Ar'N=NAr' (Ar' = *p*-$EtOC_6H_4$) was observed (Scheme 5.8). This series of experiments rules out all three mechanisms that are shown in Scheme 5.6 and establish that the formally Ru(III) imide complex **5.5-OMe** is not involved in the catalytic cycle.

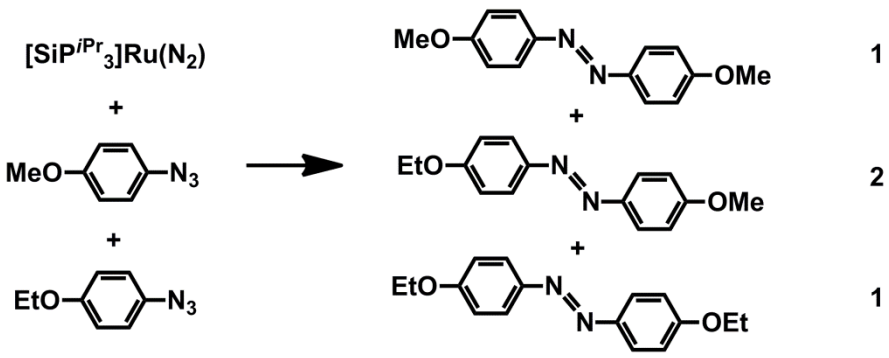

Scheme 5.7.

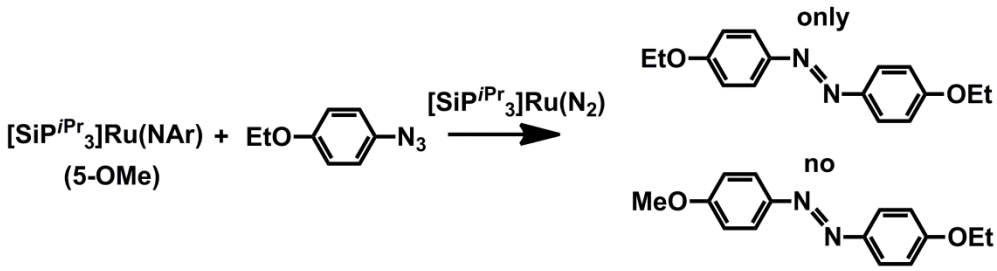

Scheme 5.8.

5.2.5 Considering the Release of Free Aryl Nitrene.

An interesting alternative to the mechanistic scenarios shown in Schemes 5.4 and 5.6 is the release of aryl nitrene during the catalytic cycle from a ruthenium aryl azide precursor, **5.11-OMe**. It is well established that aryl nitrenes have triplet ground states[23] that react at near diffusion controlled rates with either themselves or with free aryl azide to produce azoarenes.[24] This reactivity is unique to the triplet state; singlet aryl nitrene is not known to form azoarene. In the present Ru system under consideration, because **5.4** and **5.11-OMe** both have doublet ground states, both singlet and triplet nitrene could be released from **5.11-OMe** (Scheme 5.9). If triplet nitrene is released, rapid recombination with itself or with free azide would yield azoanisole. If singlet nitrene is released, it could

undergo intersystem crossing (ISC) to triplet nitrene to then produce azoanisole. This mechanism would be consistent with the absence of involvement of **5.5-OMe** and also with the results summarized in Scheme 5.7, where a statistical mixture of the three azoarenes is produced upon addition of a 1:1 mixture of two similar aryl azides to **5.4**.

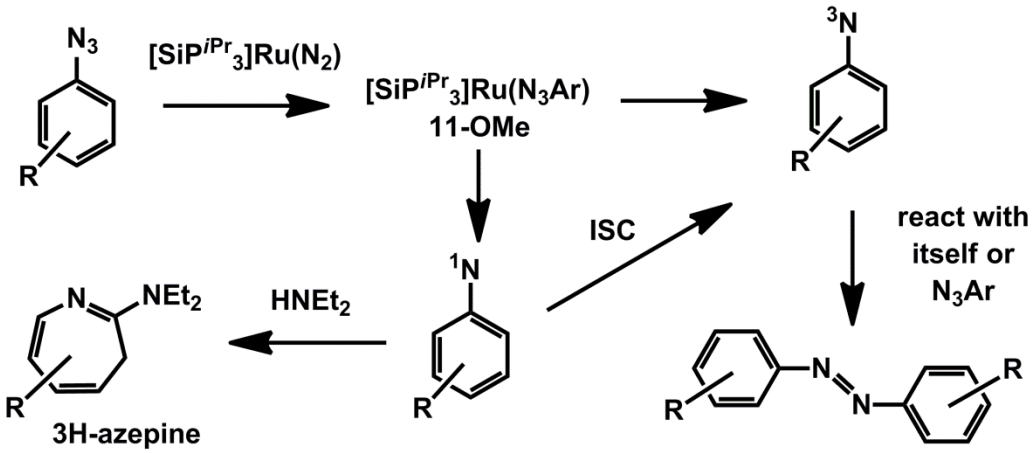

Scheme 5.9.

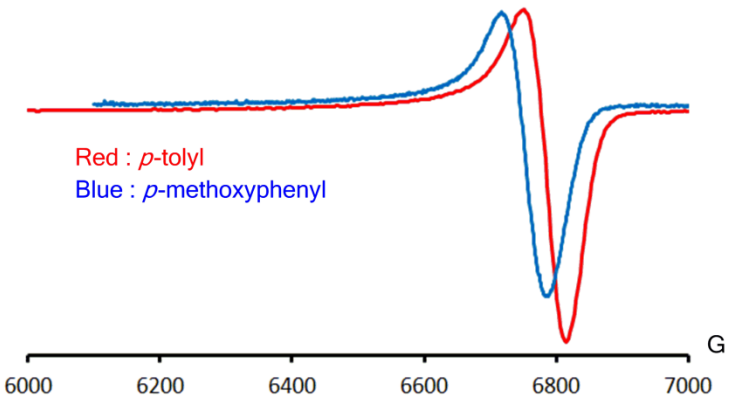

Figure 5.4. X-Band EPR spectra of triplet *p*-tolyl nitrene (red) and triplet *p*-methoxyphenyl nitrene (blue).

Singlet aryl nitrenes have been trapped with nucleophiles such as diethyamine to yield azepine (Scheme 5.9).[25] Indeed, in our hands generation of singlet nitrene by room

temperature photolysis of tolylazide in neat diethylamine produced azepine as the major product as judged by GC-MS and ^{1}H NMR spectroscopy. A similar trapping experiment with *p*-$MeOC_6H_4N_3$ produced little, if any, azepine, possibly due to the >100 fold greater rate of ISC for this nitrene relative to singlet tolylnitrene.[23b] Thus, for the trapping experiment with **5.4**, tolyl azide was used instead of *p*-$MeOC_6H_4N_3$. Addition of tolyl azide to **5.4** in neat diethylamine, however, produced no azepine but only azotoluene. Thus, if singlet nitrene is released by **5.11-Me**, it must be undergoing ISC to the triplet state sooner than it is being trapped by diethylamine. In this case, ISC would have to be assumed to be accelerated by the influence of a nearby ruthenium center, since efficient trapping was established without the presence of ruthenium. Trapping of triplet nitrene is more difficult since most of the conventional triplet nitrene traps, such as nitrosobenzene,[26] would react with metalloradical **5.4**. Direct observation of triplet nitrene during the reaction by EPR spectroscopy was also considered. While photolysis of both tolylazide and *p*-$MeOC_6H_4N_3$ at 77 K in a frozen glass produced the EPR signal characteristic of triplet nitrene (Figure 5.4),[27] thawing at −78 ^{o}C resulted in rapid loss of the signal within seconds. Thus, no buildup of triplent nitrene is expected, since the ruthenium catalyzed azoarene reaction is known only to take place at higher temperatures (*vide supra*).

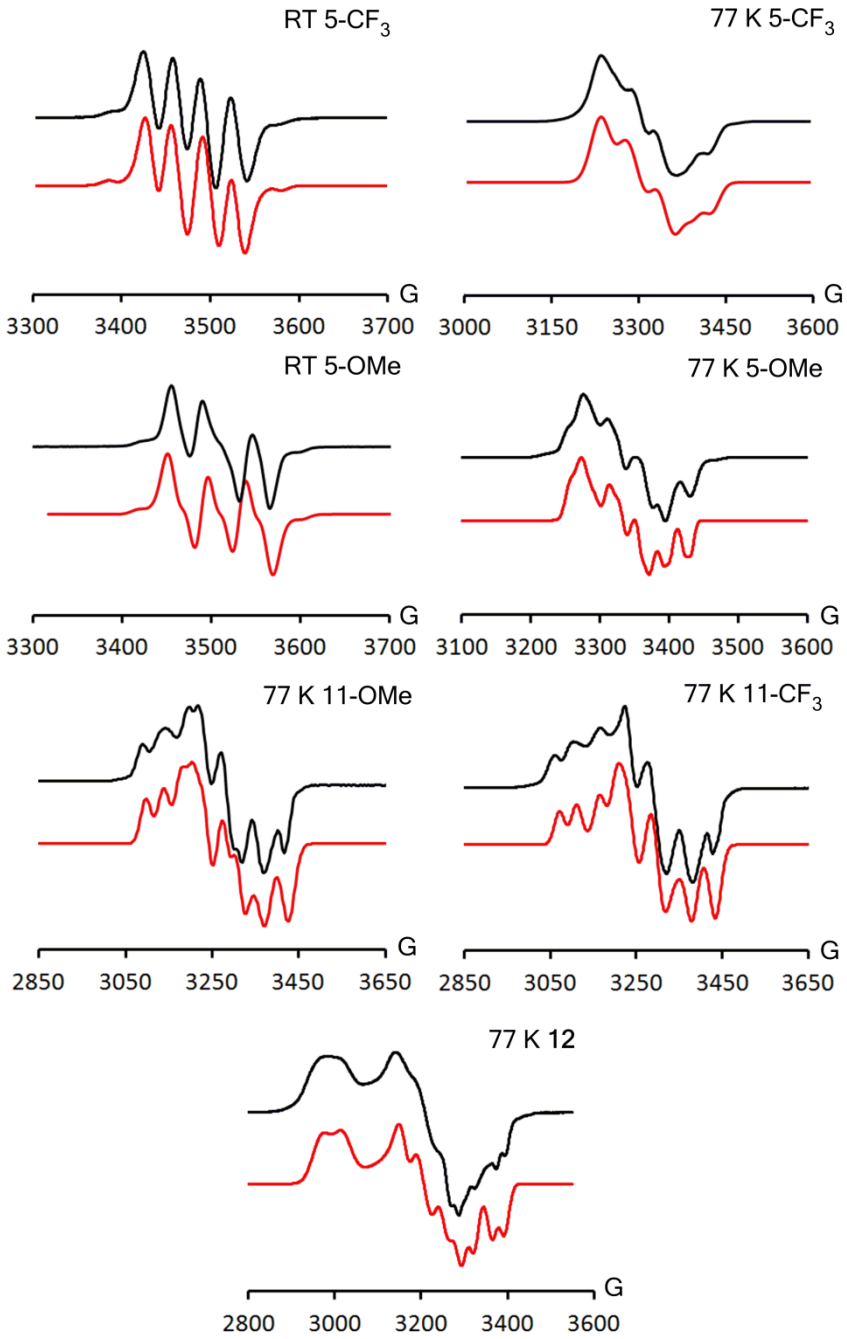

Figure 5.5. A, B: EPR spectra of **5.5-CF$_3$** (A: RT, B: 77 K). C, D: EPR spectra of **5.5-OMe** (C: RT, D: 77 K). E: 77 K EPR spectrum of **5.11-OMe**. F: 77 K EPR spectrum of **5.11-CF$_3$**. G: 77 K EPR spectrum of **5.12**. For simulation parameters see appendix.

5.2.6 EPR Spectroscopy on 5.5-R and 5.10-R

The room temperature and 77 K EPR spectra of **5.5-OMe** are shown in Figure 5.5. The room temperature spectrum depicts a three-line pattern due to large coupling of 119 MHz to the nitrogen of the NAr moiety and smaller coupling of 48 MHz to one phosphorus atom. The N hyperfine coupling in **5.5-OMe** is larger relative to **5.5-CF_3** while the P coupling is smaller, which yields a combined effect of creating a three line pattern for **5.5-OMe** instead of a four-line pattern as in **5.5-CF_3**.[16] Also worthy of note is the smaller Ru hyperfine coupling of 38 MHz in **5.5-OMe** relative to **5.5-CF_3** (48 MHz). Taken together, the hyperfine coupling to N and Ru indicate a greater spin density on the NAr moiety for **5.5-OMe** relative to **5.5-CF_3**. By analogy to the assignment of **5.5-CF_3** containing a $NAr^{\bullet-}$ radical moiety, we assign **5.5-OMe** as also possessing a $NAr^{\bullet-}$ radical.[4k,18b,28] The radical character on the NAr moiety is also supported from the isotropic g-value, g_{iso}, of 2.002, which shows little deviation from the value of the free electron, 2.0023. Further, the anisotropy in the g-values ($\Delta g = 0.063$) at 77 K is to be contrasted with the value for the Ru(I) metalloradical **5.4** (0.135**)** or the Ru(III) complex, {[SiP^{iPr}_3]RuCl}PF_6 (**5.12**), which shows a $\Delta g = 0.242$. The latter complex was synthesized by oxidation of previously reported [SiP^{iPr}_3]RuCl[16] with $AgPF_6$ and represents a formally Ru(III) metalloradical.

Measuring the RT EPR spectrum of the crude mixture from the stoichiometric reaction between **5.4** and *p*-$MeOC_6H_4N_3$ (Section **5.2.1**) yielded a complicated spectrum. Deconvolution of the spectrum was performed by subtracting out the contribution from **5.4** and provided a spectrum of nearly pure **5.5-OMe**. This result suggests that although

5.5-OMe is not responsible for the catalysis of azoanisole formation, it is nevertheless formed under the reaction conditions. To probe whether complexes **5.5-R** (R = OEt, Me, Mes) were also formed during stoichiometric reactions, the RT EPR spectra of crude reaction mixtures were also measured (see Figure 5.6 for R = Me). Again, a complicated pattern was observed (Figure 5.6, SI), but similar deconvolution resulted in spectra similar to that of **5.5-OMe**. The results again point to distinct pathways that give rise to **5.5-R** and azoarene, in which the azoarene formation step is favored for more electron donating substituents.

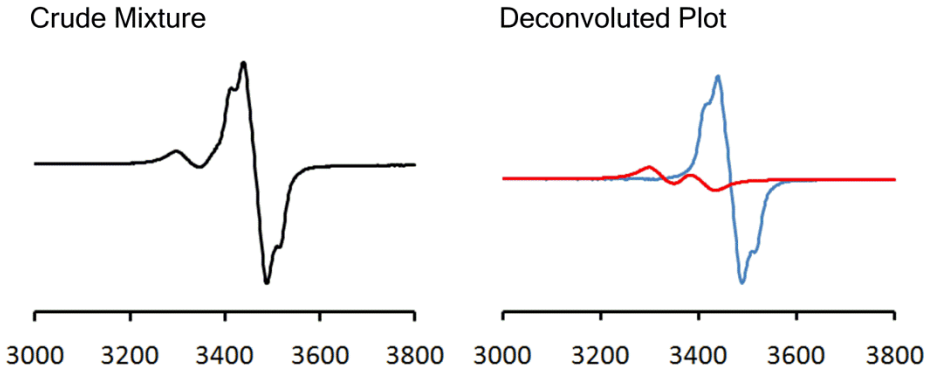

Figure 5.6. (Left) RT EPR spectrum of crude mixture from reaction between **5.4** and tolylazide. (Right) Contribution of **5.4** (red) and **5.5-Me** (blue) to crude spectrum.

As EPR proved to be a convenient tool in detecting minor amounts of paramagnetic products for this system, attempts were made to detect transient Ru(I) azide adducts, **5.11-R**, en route to either **5.5-R** or azoarene at low temperature. To this end, a solution of one equivalent of *p*-$CF_3C_6H_4N_3$ was layered over a frozen solution of **5.4**. The resulting layered frozen solution was rapidly thawed in a dry ice/isopropanol bath, quickly mixed, and frozen again for analysis by EPR spectroscopy. The EPR spectrum

showed new signals that were distinct from **5.4**, but conversion was not complete. Addition of excess azide (>50 equivalents) resulted in complete conversion to a new signal that was assigned as **5.11-CF_3 (**Figure 5.5**)**. Notably, the anisotropy in the g-values in this spectrum ($\Delta g = 0.17$) indicate significant metalloradical character (Figure 5.5). Similarly, addition of one equivalent of tolylazide was enough to see new features attributable to **5.11-Me**, although excess was required for full conversion. In contrast, addition of one equivalent of *p*-$MeOC_6H_4N_3$ led to unnoticeable changes in the EPR signatures of **5.4**, indicating the presence of an equilibrium between **5.4** and **5.11-OMe** that strongly favored **5.4**. Indeed, addition of over 50 equivalents of *p*-$MeOC_6H_4N_3$ and evacuation of N_2 from the EPR tube was necessary for the signals of **5.11-OMe** to be observed. The direction of the equilibrium in this case appears to be dictated by the π-accepting properties of the aryl azide, since *p*-$MeOC_6H_4N_3$ is expected to be a better σ-donor than *p*-$CF_3C_6H_4N_3$.

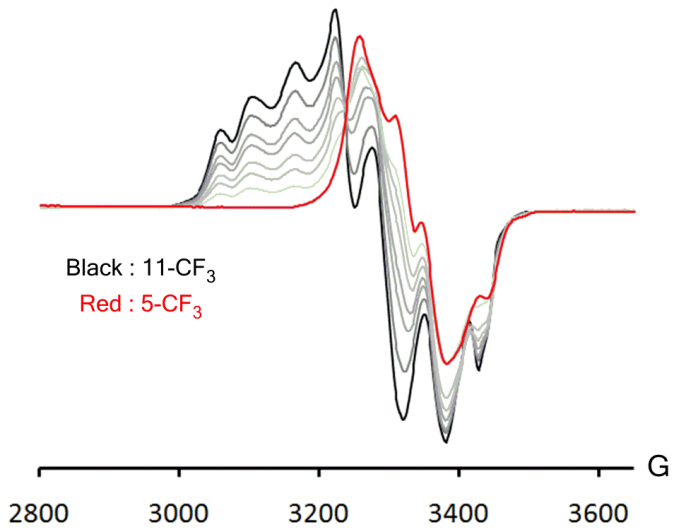

Figure 5.7. Decay of **5.11-CF_3** to **5.5-CF_3**. Black curve, **5.11-CF_3**. Red curve, **5.5-CF_3.**

Thawing a frozen solution of freshly prepared **5.11-CF$_3$** at −76 ^{o}C and recording the EPR spectrum as a function of time led to decay of **5.11-CF$_3$** to **5.5-CF$_3$** as shown in Figure 5.7. The decay followed first-order kinetics with a half-life of 23 min at −76 ^{o}C (Figure 5.8), and was independent of the concentration of *p*-CF_3-$C_6H_4N_3$. The kinetics are consistent with N_2 extrusion from a transient Ru(I) azide adduct, and corroborate the assignment of **5.11-CF$_3$**, as well as the assignment of **5.11-OMe**, which has similar EPR signatures.

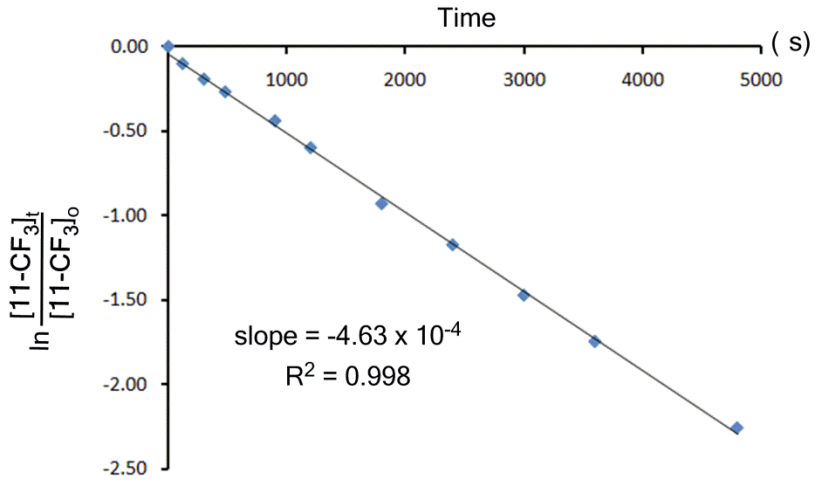

Figure 5.8. First-order decay plot of **5.11-CF$_3$** (3.4 mM) in 2-MeTHF at −76 °C.

5.2.7 DFT Calculations on 5.5-OMe and 5.11-OMe.

DFT calculations on **5.5-OMe** and **5.11-OMe** were performed to further probe their electronic structures. The optimized structure of **5.5-OMe** is very similar to that of structurally characterized **5.5-CF$_3$**[16] and features a geometry that is between a TBP and SQP with τ = 0.44 (Figure 5.9). One of the P−Ru−P angles is considerably larger (133.1^{o}) than the other two and the NAr moiety is found to slightly slant into the pocket created by this large angle, giving rise to the observed distorted structure. The Ru−N distance is

1.887 Å, close to the optimized value for **5.5-CF$_3$** (1.872 Å). Previous DFT calculations on **5.5-CF$_3$** supported the EPR simulations that assigned a significant amount of spin density on the NAr moiety. The calculation on **5.5-OMe** also points to a similar conclusion. In fact, larger delocalization of spin density is seen on the NAr moiety (70%) for **5.5-OMe** relative to **5.5-CF$_3$** (54%).[16] Conversely, the spin density on the metal center is lower (26% for **5.5-OMe** vs 40% for **5.5-CF$_3$**). These values are qualitatively consistent with the Ru and N hyperfine coupling constants found in the simulations of the RT EPR spectrum for **5.5-OMe** (section 5.2.6).

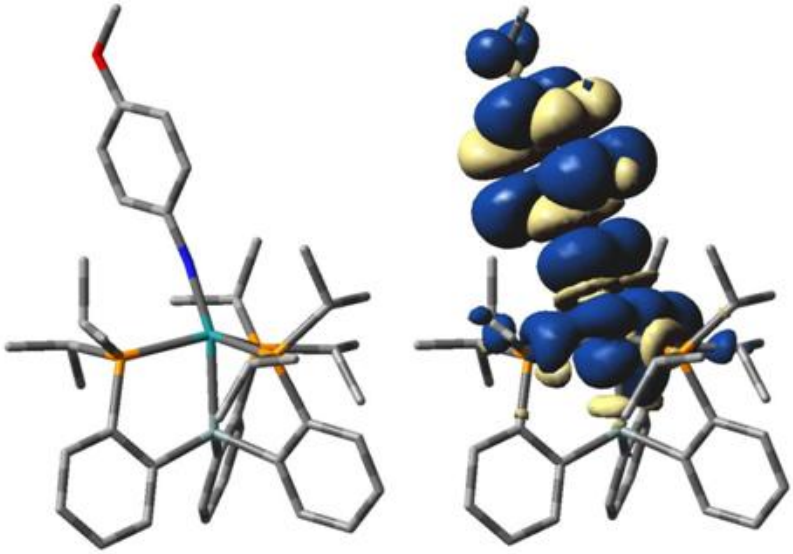

Figure 5.9. DFT optimized structure of **5.5-OMe** (left) and spin density plot (right).

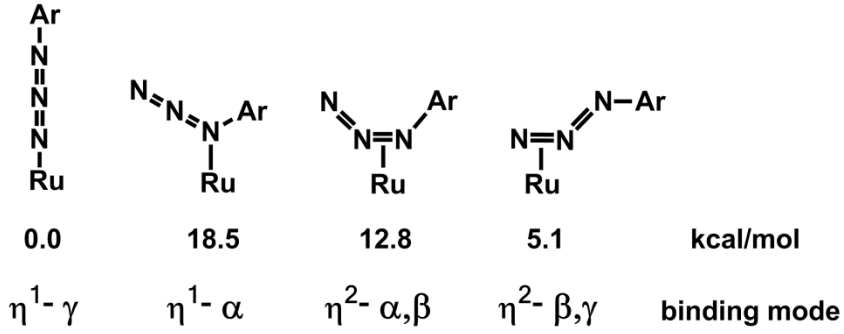

Figure 5.10. Energies of DFT optimized structures of **5.11-OMe.**

The calculations on **5.11-OMe**, in contrast, support the EPR simulations that point to a metalloradical species. As the azide adduct may bind in several different modes, two η^1−bound structures (α and γ−bound) and two η^2−structures (α,β and β,γ−bound) were examined (Figure 5.10). Of these four isomers, the γ−bound azide adduct is found to be the most stable structure, but is only slightly more stable than the β,γ−bound η^2 structure. The γ−bound structure shows localization of spin on the metal center, with little spread among the NAr moiety. In the optimized geometry, one P atom contains a much greater amount of spin density relative to the other two P atoms in the equatorial plane of the trigonal bipyramid. This feature is consistent with the Ru(I) metalloradicals, **5.4** and $[SiP^{iPr}_3]Ru(PMe_3)$,[16] and the Group 9 metalloradicals, $\{[SiP^{iPr}_3]M(PMe_3)\}^+$ (M = Co, Rh, Ir).[29] The unequal spread in spin is reflected in the 77 K EPR spectrum, where only one P atom is found to be largely responsible for the fine features (Figure 5.5). The γ-bound azide adduct was more favorable than the α-bound adduct by 18.5 kcal/mol (Figure 5.10), which must largely reflect the steric mismatch between the $[SiP^{iPr}_3]$ scaffold and the aryl substituent; the unfavorable nature of the α-N binding mode is reflected in the long Ru−N distance of 2.568 Å. Of the two η^2−bound structures, the β,γ−structure is more stable and only 5.1 kcal/mol above the energy of the γ−structure. This binding mode is rare but has precedent.[9] The geometry about the metal center is also rather close to that of the γ−structure, and the spin density distribution is found to be very similar. As a result, conclusive assignment of the ground state structure is difficult to make, and an equilibrium may even exist. The α,β−structure, in turn, is 12.8 kcal/mol above the γ−structure, and exhibits large spin density (76%) on the unbound γ−N atom, while only 3% is found on the metal center. This electronic structure is inconsistent with the EPR

spectrum, which exhibits large g−anisotropy and is suggestive of metalloradical character. We can therefore with confidence discard the alpha/beta structural isomer, which finds no literature precedent in any case.

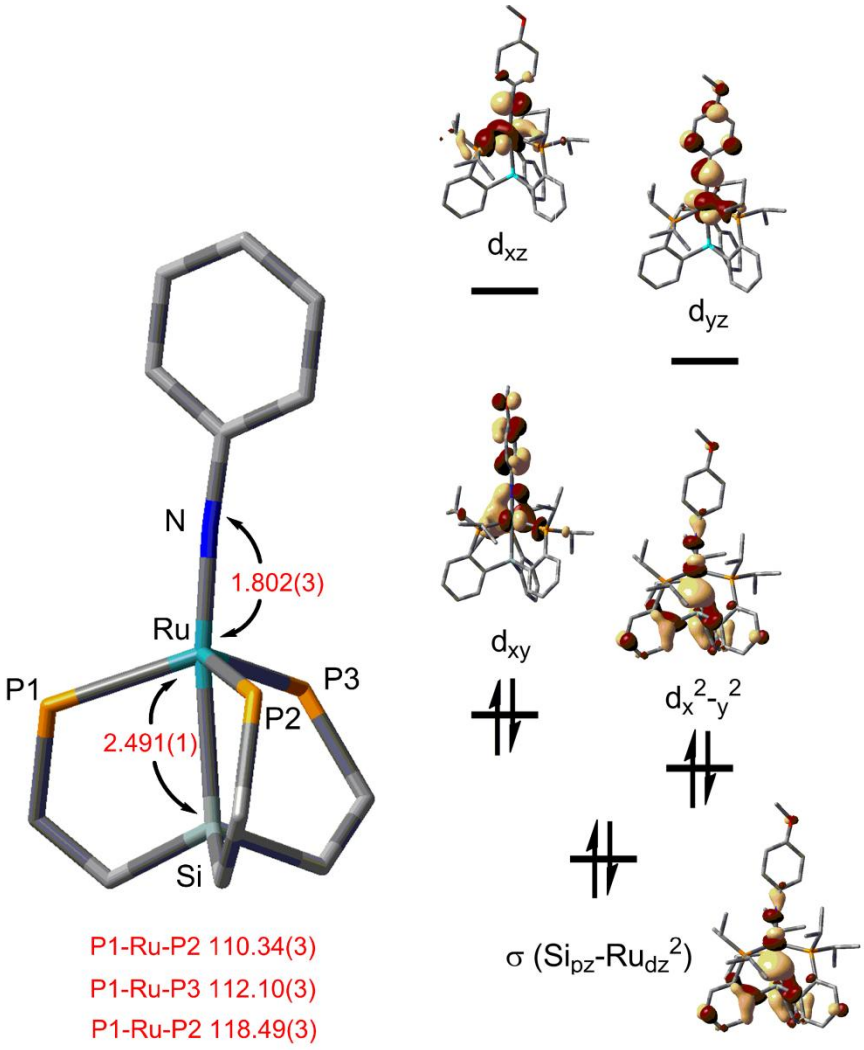

Figure 5.11. (Left) Core atoms of **5.7-OMe** with relevant bond lengths (Å) and angles (°). (Right) MO diagram of **5.7-OMe** obtained from a single point calculation on X-ray coordinates. The energy levels are drawn to scale. Calculated using the B3LYP functional with the LANL2TZ(f) for Ru and 6-311G** for all other atoms.

5.2.8 Electronic Structure of 7-OMe

Complex **5.7-OMe** is a trigonal bipyramidal, formally Ru(IV) complex with a d^4 electronic configuration. The thermal stability of this compound is striking given that a simplified molecular orbital diagram for a trigonal bipyramid (TBP) would place 4 electrons in π* d_{xz} and d_{yz} orbitals, yielding a formal Ru−N bond order of 1. DFT calculations were thus performed to analyze the frontier orbitals of **5.7-OMe**. These calculations indicate that in contrast to a typical TBP MO diagram, the π*orbitals, d_{xz} and d_{yz}, lie above the σ* orbitals d_{xy} and $d_{x^2-y^2}$ (Figure 5.11). Accordingly, four electrons are placed in the d_{xy}/$d_{x^2-y^2}$ instead of the d_{xz}/d_{yz} orbitals, conserving a formal bond order of 3 for the Ru−N bond. The stability of **5.7-OMe** and the origin of the reversal of orbital ordering are likely due to the pyramidalization of the ruthenium center. The ruthenium is displaced out of the plane of the three phosphines, which leads to decreased P−Ru−P angles, an increased Ru−Si bond length (Table 5.2), and an approach of the complex towards a pseudotetrahedral geometry. The ample precedent for stabilization of multiply bonded metal complexes in late transition metals under pseudotetrahedral metal centers supports this argument.[30] Interestingly, the orbital located directly below the π* orbitals possesses significant Si p_z and Ru d_z^2 character. The overall MO diagram is very reminiscent of that of the recently reported [TPB]Fe(NAr) complex ([TPB] = (2-*i*Pr$_2$C$_6$H$_4$)$_3$B), Ar = *p*-C$_6$H$_4$OMe),[31] which features an iron center chelated by a tris(phosphino)borane ligand that is topologically related to the [SiP$^{i\text{Pr}}_3$] ligand. The metal center in this complex is more pyramidal than **5.7-OMe** (340.9°), with P−M−P angles summing to 330.0°. That the two complexes exhibit similar MO diagrams is perhaps expected as the [Fe−B] unit in [TPB]Fe(NAr) is valence isoelectronic to the [Ru−Si]$^+$

unit in **5.7-OMe** (Figure 5.12). One difference between these units is the nature of the anchoring ligand; traditionally, silyl ligands are thought of as anionic electron donating ligands while boranes are considered neutral electron accepting ligands. While we continue to denote **5.7-OMe** as a formally Ru(IV) complex, the thought of the silicon atom acting as an electron acceptor (Si^{+}) in **5.7-OMe** is not unreasonable given the particularly low Ru(IV/III) redox potential of −1.24 V.

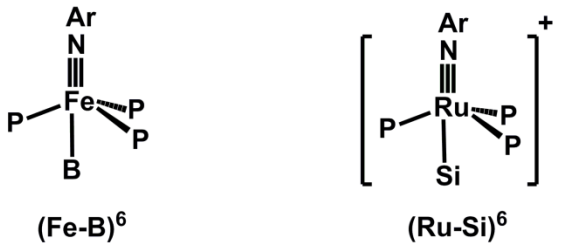

Figure 5.12. A comparison of [TPB]Fe(NAr) with **5.7-OMe.**

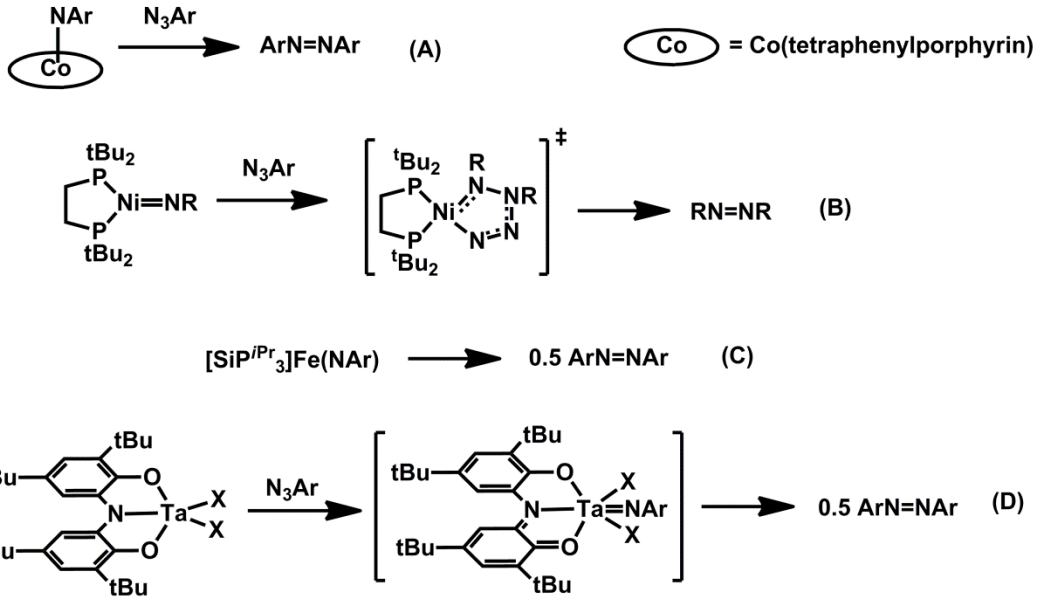

Scheme 5.10.

5.3. Mechanistic Considerations

Catalytic formation of azoarenes from aryl azides has little precedent. To our knowledge, the only example prior to our recent work on the [SiP$^{i\text{Pr}}_3$]Fe system was reported by Cenini as a side reaction of catalytic C−H amination with Co porphyrins.[13] Recently, Heyduk[32] has reported a similar reaction. The work herein adds to the library of catalytic group transfer of two nitrene moieties to form azoarenes and showcases the first reaction chemistry mediated by the unusual Ru(I) oxidation state. Importantly, the mechanistic analysis in this work illustrates that the mechanism responsible for azoarene formation is distinct from the [SiP$^{i\text{Pr}}_3$]Fe system. In Cenini's work, the azoarene is believed to form through the reaction between an imide complex of a cobalt porphyrin and a free organic azide (Scheme 5.10, A). This mechanism is akin to the reactivity observed in the stoichiometric azoarene formation mediated by a phosphine-supported Ni(II) center reported by Hillhouse (Scheme 5.10, B).[12b] In contrast, the [SiP$^{i\text{Pr}}_3$]Fe system invokes bimolecular coupling of two Fe(III) imide complexes; Heyduk's system also appears to operate through a related mechanism (Scheme 5.10, C and D).[10,32] The experimental studies described in the present work rule out either of these mechanisms for the [SiP$^{i\text{Pr}}_3$]Ru system. If a metal imide were involved, the catalytic cycle would involve a formal Ru(I)−N_2/Ru(III) NAr redox cycle, as in the [SiP$^{i\text{Pr}}_3$]Fe system. This redox cycle is inconsistent with the mechanistic studies performed in this work, since **5.5-OMe** was detected in stoichiometric reactions and found to be stable over hours in solution, while the catalytic azoarene formation in this system proceeds within seconds at room temperature. Moreover, independent synthesis of **5.5-OMe** as described above demonstrated that the decay product of **5.5-OMe** did not contain azoanisole. The

Cenini-type mechanism was also ruled out by observing that *p*-$MeOC_6H_4N_3$ does not yield any azoanisole on addition of **5.5-OMe**. Finally, crossover experiments described in section 5.2.4 also ruled out a mechanism that involves a transient Ru(I) azide adduct, **5.11-OMe**, reacting with **5.5-OMe**. *Thus, **5.5-OMe** does not appear to be responsible for azoarene formation at all.*

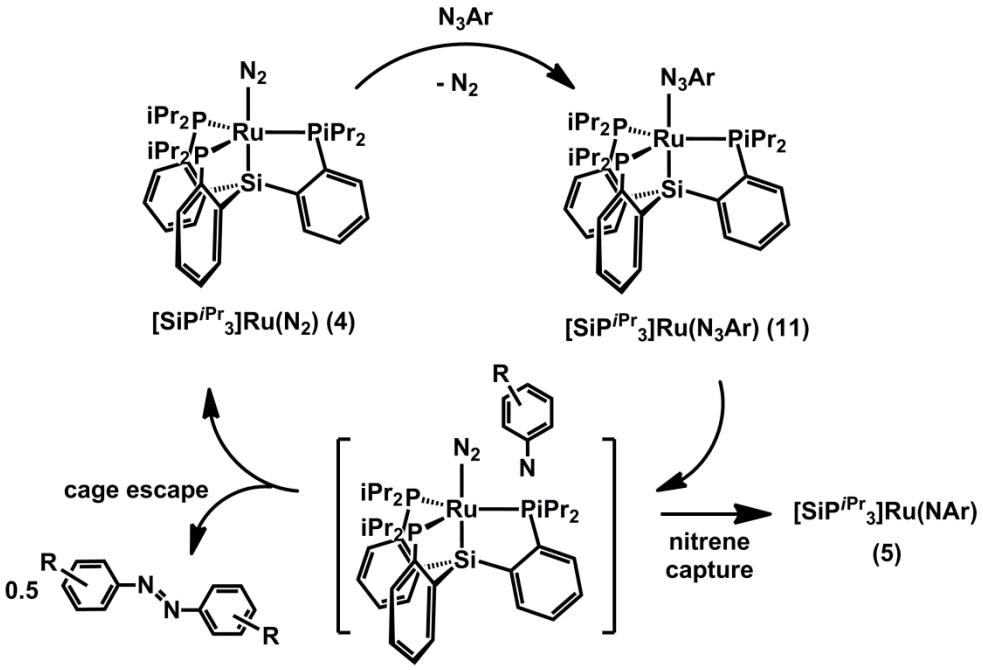

Scheme 5.11.

Another alternative to consider is the release of free triplet nitrene from **5.11-OMe** (Scheme 5.11). After release of free triplet nitrene from **5.11-OMe** it could react with itself or with free azide and yield azoanisole while regenerating **5.4** (Scheme 5.11). Such a mechanism would be consistent with the results in Scheme 5.7. The presence of **5.5-OMe** in the reaction mixture can be reconciled by the formation of a transient cage complex where the free nitrene is in the vicinity of the ruthenium. If the rate of nitrene capture by the metal fragment is rapid relative to nitrene escape from the cage, then the imide species, **5.5-R**, would be the major product. If cage escape is rapid, however,

nitrene will escape and rapidly form azoarene. The different product distributions (**5.5-R** and azoarene) from altering the R group, from CF_3 to OMe, could be explained by the differing rates of nitrene capture. The observation that **5.5-CF_3** is the sole product when *p*-$CF_3C_6H_4N_3$ is used is intuitively consistent with rapid nitrene capture, as nitrene capture formally involves a two-electron oxidation of the metal center, which is expected to be facilitated by electron withdrawing groups on the aryl moiety.

One last mechanism to consider involves the reaction between **5.11-OMe** with itself or with free *p*-$MeOC_6H_4N_3$. This mechanism is conceptually related to the "third oxidant" mechanism, as described by Goldberg in the oxygen atom transfer from iodosylarene to substrate by manganese corralazine complexes.[33] In this study, the often-invoked Mn(V) oxo functionality was not found to be the source of the oxygen atom transferred to substrate; instead, the oxygen atom was transferred directly from a coordinated iodosylarene ligand. While we cannot rule this mechanism out, we disfavor it since the electronic polarization between the two reactants that exists in the Mn system does not exist in our system. Specifically, in the Mn corralazine study, the coordinated iodosylbenzene acts as the electrophile and substrate (olefin, sulfide) acts as the nucleophile, and thus a distinct electronic polarization exists between the two. In our system, the transient Ru(I) azide adduct would need to act as both the nucleophile and electrophile, where such polarization is expected to be minimal. We thus favor the nitrene release mechanism.

5.4. Conclusions

In conclusion, we have demonstrated facile catalytic N−N coupling of aryl azides to yield azoarenes mediated by the Ru(I) metalloradical, [SiP$^{i\text{Pr}}_3$]Ru(N_2) (**5.4**). Studies aimed at probing the viability of a bimolecular coupling mechanism of metal imide species as found in the related iron system have led to the isolation of several structurally unusual complexes, including the ruthenium imides, **5.5-OMe** and **5.7-OMe**, as well as the azide adduct **5.8-OMe**. Mechanistic studies showed that **5.5-OMe** is not involved in the catalytic cycle and demonstrated the influence of the metal center on the mechanism of reaction. Instead, we favor a mechanism in which free aryl nitrene is released during the catalytic cycle and combines with itself or with free aryl azide to yield the azoarene.

5.5. Experimental Section

5.5.1 General Considerations

All manipulations were carried out using standard Schlenk or glovebox techniques under an atmosphere of dinitrogen. Unless otherwise noted, solvents were degassed and dried by thoroughly sparging with N_2 gas followed by passage through an activated alumina column. Hexamethyldisiloxane was dried over CaH_2 and distilled. Pentane, hexamethyldisiloxane, benzene, toluene, tetrahydrofuran, and diethylether were tested with a standard purple solution of sodium benzophenone ketyl in tetrahydrofuran. Unless noted otherwise, all reagents were purchased from commercial vendors and used without further purification. Celite (Celite® 545) was dried at 150 °C overnight before use. Complexes **5.4**, **5.5-CF$_3$**, **5.9-BAr$^F_4$**, [SiP$^{i\text{Pr}}_3$]RuCl were previously reported.[16] [(C_6H_6)$RuCl_2$]$_2$,[34], tris(2-(diisopropylphosphino)phenyl)silane ([SiP$^{i\text{Pr}}_3$]H),[11] aryl azides,[35]

and KC_8[36] were synthesized according to literature procedures. Triethylamine was dried over calcium hydride and distilled. Deuterated solvents were purchased from Cambridge Isotope Laboratories, Inc., degassed, and stored over 3 Å molecular sieves prior to use. Elemental analyses were performed by Midwest Microlabs. Varian Mercury-300 and Varian Inova-500 were used to collect ^{1}H, ^{13}C, ^{29}Si, and ^{31}P spectra at room temperature unless otherwise noted. ^{1}H and ^{13}C spectra were referenced to residual solvent resonances. ^{29}Si spectra were referenced to external tetramethylsilane (δ = 0 ppm), and ^{31}P spectra were referenced to external 85% phosphoric acid (δ = 0 ppm). IR measurements were obtained on samples prepared as KBr pellets using a Bio-Rad Excalibur FTS 3000 spectrometer. X-band EPR spectra were obtained on a Bruker EMX spectrometer. Spectra were simulated using *Easyspin*[37] program.

5.5.2 Crystallographic Details

X-ray diffraction studies were carried out at the Beckman Institute Crystallography Facility on a Brüker KAPPA APEX II diffractometer and at the MIT Department of Chemistry X-Ray Diffraction Facility on a Bruker three-circle Platform APEX II diffractometer solved using SHELX v. 6.14. The crystals were mounted on a glass fiber with Paratone-N oil. Data was collected at 100 K using Mo Kα (λ = 0.710 73 Å) radiation and solved using SHELXS[38] and refined against F^2 on all data by full-matrix least squares with SHELXL. X-ray quality crystals were grown as described in the experimental procedures.

5.5.3 Electrochemical Details

Electrochemical measurements were carried out in a glovebox under a dinitrogen atmosphere in a one-compartment cell using a CH Instruments 600B electrochemical analyzer. A glassy carbon electrode was used as the working electrode and platinum wire was used as the auxillary electrode. The reference electrode was $Ag/AgNO_3$ in THF. The ferrocene couple Fc+/Fc was used as an external reference. Solutions (THF) of electrolyte (0.3 M tetra-*n*-butylammonium hexafluorophosphate) and analyte were also prepared under an inert atmosphere.

5.5.4 Synthetic Details

Synthesis of {[SiP$^{iPr}_3$]Ru(NAr)}OTf (Ar = *p*-$C_6H_4CF_3$) (5.7-CF_3). [SiP$^{iPr}_3$]Ru(N_2) (100 mg, 0.14 mmol) was dissolved in 10 mL of Et_2O and cooled to −78 ^oC. *p*-$CF_3C_6H_4N_3$ (26 mg, 0.14 mmol) was diluted with 2 mL Et_2O and also cooled to −78 ^oC. The azide solution was added dropwise to the solution of [SiP$^{iPr}_3$]Ru(N_2), resulting in an immediate color change from green to red/purple. The solution was stirred for 10 min at −78 ^oC and for 10 min at room temperature. The solution was cooled to −78 ^oC again, and AgOTf (36 mg, 0.14 mmol) was added in one portion. The solution gradually precipitated a green solid, along with black Ag metal. The mixture was filtered through celite, and the green product was extracted into THF. The dark green solution was concentrated, and the product was recrystallized from layering pentane over a concentrated THF solution of green **5.7-CF_3** to yield crystals suitable for X-ray diffraction (82 mg, 59%). ^{1}H NMR (d_8-THF, δ): 8.31 (d, *J* = 8.0 Hz, 2H), 8.11 (d, *J* = 7.5 Hz, 3H), 7.77 (m, 3H), 7.59 (d, *J* = 8.5 Hz, 2H), 7.52 (t, *J* = 8.0 Hz, 3H), 7.41 (t, *J* = 7.5

Hz, 3H), 2.76 (br, 6H), 1.11 (dd, J = 14.5, 6.5 Hz, 18H), 0.52 (m, 18H). $^{13}C\{^1H\}$ NMR (d_8-THF, δ): 156.1, 141.2, 133.7, 132.0, 130.4, 129.2, 128.3, 120.8, 32.4, 19.5, 19.2. $^{19}F\{^1H\}$ NMR (d_8-THF, δ): −62.3, −77.3. $^{31}P\{^1H\}$ NMR (d_8-THF, δ): 109.8. Anal. Calcd for $C_{44}H_{58}NO_3F_6SiP_3SRu$: C, 51.96; H, 5.75; N. 1.38. Found: C, 51.59; H, 5.76; N, 1.25.

Synthesis of {[SiP$^{iPr}_3$]Ru(N$_3$Ar)}BAr$^F_4$ (5.8-OMe, Ar = C$_6$H$_4$OMe). **{**[SiP$^{iPr}_3$]Ru(N$_2$)}BAr$^F_4$ (46 mg, 0.029 mmol) was dissolved in 4 mL Et_2O and cooled to −78 ^{o}C. p-$MeOC_6H_4N_3$ (4.4 mg, 0.029 mmol) was dissolved in 1 mL Et_2O and also cooled to −78 ^{o}C. The azide solution was added dropwise to the **{**[SiP$^{iPr}_3$]Ru(N$_2$)}BAr$^F_4$ solution, which resulted in an immediate color change from orange to red. The solution was stirred at room temperature for 10 min and concentrated to yield red **5.8-OMe** (44 mg, 89%). Crystals suitable for X-ray diffraction were grown from layering pentane over a concentrated ether solution of **5.8-OMe** at −35 ^{o}C. ^1H NMR (d_8-THF, δ): 8.34 (d, J = 7.2 Hz, 3H), 7.79 (s, 8H), 7.64 (br, 3H), 7.57 (s, 4H), 7.47 (t, J = 7.2 Hz, 3H), 7.38 (t, J = 7.5 Hz, 3H), 7.16 (d, J = 9.0 Hz, 2H), 7.00 (d, J = 9.0 Hz, 2H), 3.78 (s, 3H), 2.10 (br, 6H), 1.17 (br, 18H), 0.83 (br, 18H). $^{13}C\{^1H\}$ NMR (d_8-THF, δ): 163.8 (m), 160.4, 154.4, 144.0, 136.5, 134.9,131.6, 131.0, 130.8, 130.0, 129.6, 127.4, 123.1, 123.0, 119.1, 117.1, 67.2, 56.5, 20.8 (br), 16.5. $^{19}F\{^1H\}$ NMR (d_8-THF, δ): −61.2. $^{31}P\{^1H\}$ NMR (d_8-THF, δ): 72.9.

Synthesis of {[SiP$^{iPr}_3$]Ru(NAr)}BAr$^F_4$ (5.7-OMe). {[SiP$^{iPr}_3$]Ru(N$_3$Ar)}BAr$^F_4$ (8-OMe, Ar = C_6H_4OMe) (40 mg, 0.023 mmol) was dissolved in 2 mL THF and charged in a 4 mL quartz cuvette. Excess p-$MeOC_6H_4N_3$ (4 mg, 0.027 mmol) was added to the cuvette and the red solution was photolyzed. The progress of the conversion was monitored by $^{31}P\{^1H\}$ NMR spectroscopy. After the conversion was complete (approximately 1 h), the green solution was concentrated, and the oily material was triturated with pentane (5 x 3

mL) to yield the green **5.7-OMe** (32 mg, 83%). Crystals suitable for X-ray diffraction were grown by layering pentane over a concentrated ether solution of **5.7-OMe** at −35 °C. ^{1}H NMR (d_8-THF, δ): 8.14 (d, *J* = 7.5 Hz, 3H), 7.78 (s, 8H), 7.77 (m, 3H), 7.57 (s, 4H), 7.44-6.85 (m, 10H), 3.83 (s, 3H), 2.74 (br, 6H), 1.12 (m, 18H), 0.55 (m, 18H). ^{13}C{^{1}H} NMR (d_8-THF, δ): 163.6 (m), 162.1, 157.2 (m), 142.6 (m), 136.5, 134.9, 133.0, 131.0, 130.8, 130.5, 130.2, 129.6, 127.5, 125.3, 125.2, 123.1, 119.1, 117.6, 57.1, 33.3, 20.5, 20.3.). ^{19}F{^{1}H} NMR (d_8-THF, δ): −61.4. ^{31}P{^{1}H} NMR (d_8-THF, δ): 106.4.

Synthesis of {[SiP$^{iPr}_3$]Ru(N$_2$)}PF$_6$ (5.9-PF$_6$), {[SiP$^{iPr}_3$]Ru(N$_3$Ar)}PF$_6$ (5.8-OMe), and {[SiP$^{iPr}_3$]Ru(NAr)}PF$_6$ (Ar = C$_6$H$_4$OMe) (5.7-OMe). 5.9-PF$_6$: [SiP$^{iPr}_3$]Ru(N$_2$) (35 mg, 0.048 mmol) was dissolved in 5 mL THF. AgPF$_6$ (12 mg, 0.048 mmol) was dissolved in 1 mL THF and both solution were cooled to −78 °C. The AgPF$_6$ solution was added dropwise to the solution of [SiP$^{iPr}_3$]Ru(N$_2$), causing an immediate darkening of the solution. The solution was stirred for 10 min, filtered through celite, and concentrated. The solid was washed with Et$_2$O and dried to yield **5.9-PF$_6$** (31 mg, 74%). ^{1}H NMR (d_8-THF, δ): 8.25 (d, *J* = 6.9 Hz, 3H), 7.64 (d, *J* = 7.2 Hz, 3H), 7.42 (t, *J* = 6.9 Hz, 3H), 7.33 (t, *J* = 6.6 Hz, 3H), 2.44 (br, 6H), 1.22 (s, 18H), 0.86 (s, 18H). %). ^{13}C {1H} NMR (d_8-THF, δ): 155.2, 144.7, 134.2, 131.8, 131.0, 129.4, 29.3, 21.3, 20.5. ^{19}F{^{1}H} NMR (d_8-THF, δ): −72.9 (d, *J* = 715 Hz). ^{31}P{^{1}H} NMR (d_8-THF, δ): 67.5, −142.1 (sep, *J* = 715 Hz). **5.8-OMe, PF$_6^-$ anion:** {[SiP$^{iPr}_3$]Ru(N$_2$)}PF$_6$ (17 mg, 0.020 mmol) was dissolved in 6 mL THF and cooled to −78 °C. *p*-MeOC$_6$H$_4$N$_3$ (2.9 mg, 0.020 mmol) was added to the solution in one portion, resulting in an immediate color change to red. The solution was stirred for 10 min, and concentrated to yield red **5.8-OMe** (18 mg, 94%). ^{1}H NMR (d_8-THF, δ): 8.26 (d, *J* = 7.0 Hz, 3H), 7.61 (br, 3H), 7.41 (t, *J* = 8.0 Hz, 3H), 7.32 (t, *J* = 8.0

Hz, 3H), 7.07 (d, *J* = 9.0 Hz, 2H), 6.97 (t, *J* = 9.0 Hz, 3H), 3.74 (s, 3H), 2.15 (br, 6H), 1.13 (s, 18H), 0.78 (s, 18H). $^{13}C\{^{1}H\}$ NMR (d_8-THF, δ): 159.8, 155.1, 144.5, 134.6, 132.8, 131.7, 131.3, 129.6, 122.6, 117.2, 56.6, 30.4, 21.2, 20.7. $^{19}F\{^{1}H\}$ NMR (d_8-THF, δ): −71.7 (d, *J* = 711 Hz). $^{31}P\{^{1}H\}$ NMR (d_8-THF, δ): 72.6, −142.9 (sep, *J* = 711 Hz). **5.7-OMe, PF_6^- anion:** The synthesis of **5.7-OMe** was performed in a three-step sequence, without isolation of intermediate products, **5.9-PF_6** and **5.8-OMe**. [SiP^{iPr}_3]Ru(N_2) (50 mg, 0.068 mmol) was dissolved in 8 mL THF. $AgPF_6$ (17 mg, 0.068 mmol) was dissolved in 2 mL THF. Both were cooled to −78 °C and the $AgPF_6$ solution was added dropwise to the solution of [SiP^{iPr}_3]Ru(N_2), leading to an immediate color change from green to dark brown. The mixture was stirred at −78 °C for 5 min, and stirred at room temperature for 10 min The mixture was filtered through celite, and the filtrate was cooled to −78 °C. A THF solution of *p*-$MeOC_6H_4N_3$ (20 mg, 0.14 mmol) was added dropwise to the filtrate, resulting in a color change to red. The red solution of **5.8-OMe** was stirred for 10 min, and charged into a 100 mL quartz flask. The solution was photolyzed, and the progress of the reaction was monitored by $^{31}P\{^{1}H\}$ NMR spectroscopy. After the conversion was complete (approximately 1h), the solution was concentrated, and the residues were washed with Et_2O to yield green **5.7-OMe** (57 mg, 86% overall). Recrystallization by layering pentane over a THF solution of **5.7-OMe** yielded crystals suitable for X-ray diffraction. ^{1}H NMR (d_8-THF, δ): 8.18 (d, *J* = 8.4 Hz, 2H), 8.12 (d, *J* = 7.2 Hz, 3H), 7.77 (m, 3H), 7.52 (t, *J* = 7.2 Hz, 3H), 7.41 (t, *J* = 6.9 Hz, 3H), 6.93 (d, *J* = 9.0 Hz, 2H), 3.85 (s, 3H), 2.76 (m, 6H), 1.11 (m, 18H), 0.55 (m, 18H). ^{13}C NMR (d^8-THF, δ): 162.3 (m), 157.3(m), 142.7 (m), 134.8 (m), 132.8, 131.2, 130.1, 125.5, 117.9, 57.3, 33.4 (m), 20.6, 20.3. ^{31}P NMR (d_8-THF, δ): 106.5, −143.6 (sep, *J* =

738 Hz). Anal. Calcd for $C_{43}H_{61}NOF_6SiP_4Ru$: C, 52.97; H, 6.31; N. 1.44. Found: C, 52.23; H, 6.18; N, 1.32.

Synthesis of [SiP$^{iPr}_2$P(=NAr)Ru]PF$_6$ (5.10). [SiP$^{iPr}_3$]Ru(N_2) (17 mg, 0.023 mmol) was dissolved in 5 mL THF. $AgPF_6$ (5.8 mg, 0.023 mmol) was dissolved in 1 mL THF. Both solutions were cooled to −78 ^oC and the $AgPF_6$ solution was added dropwise to the [SiP$^{iPr}_3$]Ru(N_2) solution, resulting in an immediate darkening of the solution. The mixture was stirred for 2 min at low temperature and then stirred for 2 min at room temperature. The mixture was filtered through celite, and the filtrate was cooled to −78 ^oC again. *p*-$MeOC_6H_4N_3$ (6.9 mg, 0.046 mmol) in 1 mL THF was added to the solution dropwise, leading to a color change to red. The solution was stirred for 5 min and charged into a 100 mL quartz flask. The solution was photolyzed for two days. The solution was concentrated and washed with Et_2O to yield **5.10** (14 mg, 62%). Crystals suitable for X-ray diffraction were obtained by vapor diffusion of pentane into a concentrated solution of **5.10**. ^{1}H NMR (d_8-THF, δ): 7.92-7.83 (m, 2H), 7.66 (dd, *J* = 7.5, 4.2 Hz, 2H), 7.49 (d, *J* = 7.2 Hz, 2H), 7.43-7.23 (m, 6H), 6.66 (d, *J* = 6.0 Hz, 1H), 5.47 (d, *J* = 6.0 Hz, 1H), 5.31 (t, *J* = 6.9 Hz, 2H), 3.88 (s, 3H), 3.19 (sep, *J* = 6.6 Hz, 1H), 3.07 (sep, *J* = 5.7 Hz, 1H), 2.51-2.11 (m, 3H), 1.70-0.81 (m, 30H), 0.68 (dd, *J* = 14.7, 7.2 Hz, 3H), -0.33 (dd, *J* = 12.9, 7.8 Hz, 3H). ^{13}C{^{1}H} NMR (d_8-THF, δ): 155.2, 149.4 (d, *J* = 45.1 Hz), 148.1 (d, *J* = 15.7 Hz), 144.8 (d, *J* = 43.9 Hz), 142.4 (d, *J* = 13.2 Hz), 140.8, 137.3 (d, *J* = 17.3 Hz), 136.2 (d, *J* = 18.6 Hz), 134.2 (m), 132.7, 132.1 (d, *J* = 17.1 Hz), 131.1, 130.8, 130.3, 129.8, 129.1, 126.2, 116.0 (br), 90.9, 84.9, 81.8, 81.3, 81.2, 57.6, 56.6 (br), 35.9 (d, *J* = 29.2 Hz), 33.5 (d, *J* = 12.4 Hz), 32.3 (*J* = 18.9 Hz), 31.0, 30.4, 28.3, 27.9, 27.2, 24.4, 23.8,

23.4, 23.0, 21.4, 20.8, 20.0, 17.8, 17.7, 16.3, 2.2. $^{31}P\{^{1}H\}$ NMR (d_8-THF, δ): 85.4 (d, J = 28.3 Hz), 73.9 (d, J = 28.3 Hz), 32.4.

Synthesis of [SiP$^{iPr}_3$]Ru(NAr) (Ar = C_6H_4OMe, 5.5-OMe). {[SiP$^{iPr}_3$]Ru(NAr)}PF_6 (Ar = C_6H_4OMe, 7-OMe) (11 mg, 0.011 mmol) was dissolved in 4 mL THF and cooled to −78 °C. $CoCp_2$ (2.0 mg, 0.011 mmol) was added in one portion and the resulting solution was stirred at −78 °C for 15 min The solution was warmed to room temperature and stirred for an additional 15 min The solution was concentrated, and the product was extracted into pentane. The pentane solution was filtered through celite. The extraction process was repeated once more to yield red/brown **5.5-OMe** (4.6 mg, 52%). ^{1}H NMR (C_6D_6, δ): 9.0, 7.8, 6.8, 5.9, 4.0 (extending from 8 to 0 ppm). μ_{eff} (Evan's Method, C_6D_6/C_6H_6) = 1.5 μ_B. UV-VIS(in THF): (nm, ε [mol^{-1} cm^{-1}]), 473 (4200), 737 (1700).

Synthesis of {[SiP$^{iPr}_3$]RuCl}PF_6 (5.12). [SiP$^{iPr}_3$]RuCl (30 mg, 0.040 mmol) was dissolved in 6 mL THF. $AgPF_6$ (10 mg, 0.040 mmol) was dissolved in 1 mL THF. Both were cooled to −78 °C and the $AgPF_6$ solution was added to the [SiP$^{iPr}_3$]RuCl solution. A gradual color change from red to brown took place. The solution was stirred at −78 °C for 15 min and was subsequently stirred at room temperature for 30 min The mixture was filtered through celite, and the filtrate was concentrated. The residues were washed with ether and benzene, and the product was extracted into THF and filtered through celite. Concentration of the purple filtrate yielded **5.12** (22 mg, 61%). ^{1}H NMR (CD_2Cl_2, δ): 12 (extending from 16 to 8 ppm), 9.7, 6.7, 6.4. μ_{eff} (Evan's Method, CD_2Cl_2) = 1.73 μ_B. UV-VIS(in CH_2Cl_2): (nm, ε [mol^{-1} cm^{-1}]), 454 (290), 494 (1300). Anal. Calcd for $C_{36}H_{54}F_6SiP_4RuCl$: C, 48.62; H, 6.12; N, 0. Found: C, 47.95; H, 6.05; N, 0.00.

Preparation of EPR samples for detecting Ru(I) azide adducts, 5.11-R. A solution of [SiP$^{iPr}_3$]Ru(N_2) (0.7 mg in 0.1 mL 2-MeTHF) was added to an EPR tube and the solution was frozen inside the glovebox using the glovebox cold well. A solution of azide (>30 equivalents in 0.1 mL 2-MeTHF) was layered above the frozen [SiP$^{iPr}_3$]Ru(N_2) solution and also frozen. The tube was quickly taken out of the glovebox, and immersed in liquid nitrogen. The tube was immersed in a dry ice/isopropanol bath quickly to thaw the solution, and the tube was rapidly shaken to homogenize the solution. The tube was reimmersed in liquid nitrogen and frozen, and was placed inside the EPR cavity for measurement. For detecting **5.11-OMe**, several freeze-pump-thaw cycles were additionally applied to remove N_2 to favor formation of **5.11-OMe**.

5.5 References Cited.

1 Selected reviews: a) Müller, P.; Fruit, C. *Chem. Rev.* **2003**, *103*, 2905. b) Che, C. –M.; Lo, V. K. -Y.; Zhou, C.-Y.; Huang, J.-S. *Chem. Rev. Soc.* **2011**, *40*, 1950.

2 Selected examples: a) Breslow, R.; Gellman, S. H. *J. Chem. Soc., Chem. Commun.* **1982**, 1400. b) Breslow, R.; Gellman, S. H. *J. Am. Chem. Soc.* **1983**, *105*, 6728. c) Mansuy, D. Mahy, J. –P.; Dureault, A.; Bedi, G.; Battioni, P. *J. Chem. Soc., Chem. Commun.* **1984**, 1161. d) Mahy, J. P.; Battioni, P.; Mansuy, D. *Tetrahedron Lett.* **1988**, *29*, 1927. e) Evans, D. A.; Faul, M. M.; Bilodeau, M. T. *J. Org. Chem.* **1991**, *56*, 6744. f) Müller, P.; Baud, C.; Jacquier Y. *Tetrahedron* **1996**, *52*, 1543. g) Albone, D. P.; Aujla, P. S.; Taylor, P. C.; Challenger, S.; Derrick, A. M. *J. Org. Chem.* **1998**, *63*, 9569. h) Zhou, X. -G.; Yu, X. -Q.; Huang, J. –S.; Che, C. -M. *Chem. Commun.* **1999**, 2377. i) Au, S. –M.; Huang, J. –S.; Yu, W. –Y.; Fung, W. –H.; Che, C. –M. *J. Am. Chem. Soc.* **1999**, *121*, 9120. j) Kohmura, Y.; Katsuki, T. *Tetrahedron Lett.* **2001**, *42*, 3339. k) Simkhovich, L.; Gross, Z. *Tetrahedron Lett.* **2001**, *42*, 8089. l) Espino, C. G; Du Bois, J. *Angew. Chem. Int. ed.* **2001**, *40*, 598. m) Mar Díaz-Requejo, M.; Belderraín, T. R.; Carmen Nicasio, M.; Trofimenko, S.; Pérez, P. J. *J. Am. Chem. Soc.* **2003**, *125*, 12078. n) Cui, Y.; He, C. *Angew. Chem. Int. ed.* **2004**, *43*, 4210. o) Zdilla, M. J.; Abu-Omar, M. M. *J. Am. Chem. Soc.* **2006**, *128*, 16971. p) Milczek, E.; Boudet, N.; Blakey, S. *Angew. Chem. Int. Ed.* **2008**, *47*, 6825.

3 A recent report describes the use of a hypervalent bromine reagent for the amination of unactivated C-H bonds. See Ochiai, M.; Miyamoto, K.; Kaneaki, T.; Hayashi, S.; Nakanish, W. *Science* **2011**, *332*, 448.

4 Selected examples; a) Kwart, H.; Khan, A. A. *J. Am. Chem. Soc.* **1965**, *89*, 1951. b) Cenini, S.; Tollari, S.; Penoni, A.; Cerada, C. *J. Mol. Cat. A.* **1999**, *137*, 135. c) Cenini, S.; Gallo, E.; Penoni, A.; Ragaini, F.; Tollari, S. d) Omura, K.; Murakami, M.; Uchida, T.; Irie, R.; Katsuki, T. *Chem. Lett.* **2003**, *32*, 354. e) Omura, K.; Uchida, T.; Irie, R.; Katsuki, T. *Chem. Commun.* **2004**, 2060. f) Li, Z.; Quan, R. W.; Jacobsen, E. N. *J. Am. Chem. Soc.* **1995**, *117*, 5889. g) Liu, Y.; Che, C.-M. *Chem. –Eur. J.* **2010**, *16*, 10494. h) Bach, T.; Körber, C. *Eur. J. Org. Chem.* **1999**, 1033. i) Bach, T.; Körber, C. *Tetrahedron Lett.* **1998**, *39*, 5015. j) Goa, G.-Y.; Jones, J. E.; Vyas, R.; Harden, J. D.; Zhang, X. P. *J. Org. Chem.* **2006**, *71*, 6655. k) Badiei, Y. M.; Dinescu, A.; dai, X.; Palomino, R. M.; Heinemann, F. W.; Cundari, T. R.; Warren, T. H. *Angew. Chem. Int. Ed.* **2008**, *47*, 9961. l) Stokes, B. J.; Dong, H.; Leslie, B. E.; Pumphrey, A. L.; Driver, T. G. *J. Am. Chem. Soc.* **2007**, *129*, 7500.

5 a) Proulx, G.; Bergman, R.G. *J. Am. Chem. Soc.* **1995**, *117*, 6382.b) Proulx, G.; Bergman, R. G. *Organometallics* **1996**, *15*, 684.

6 Gololobox, Yu. G.; Zhmurova, I. N.; Kasukhin, L. F. *Tetrahedron* **1981**, *37*, 437.

7 Fickes, M. G.; Davis, W. M.; Cummins, C. C. *J. Am. Chem. Soc.* **1995**, *117*, 6384.

8 γ-N bound azide complexes: a) Guillemot, G.; Solari, E.; Floriani, C. *Organometallics* **2001**, *20*, 607. b) Evans, W. J.; Mueller, T. J.; Ziller, J. W. *J. Am. Chem. Soc.* **2009**, *131*, 2678. c) Hanna, T. A.; Baranger, A. M.; Bergman, R. G. *Angew. Chem., Int. Ed. Engl.* **1996**, *35*, 653. α-N bound azide complex: d) Barz, M.; Herdtweck, E.; Thiel, W. R. *Angew. Chem., Int. Ed. Engl.* **1998**, *37*, 2262. e) Albertin, G.; Antonuitti, S.; Baldan, D.; Castro, J.; García-Fontán, S. *Inorg. Chem.* **2008**, *47*, 742. For a Cu complex that binds 1-adamantyl azide at the γ-N and a Ag complex that binds it at the α-N using the

same ancillary ligand see f) Rasika Dias, H. V.; Polach, S. A.; Goh, S.-K.; Archibong, E. F.; Marynick, D. S. *Inorg. Chem.* **2000**, *39*, 3894.

9 Waterman, R.; Hillhouse, G. L. *J. Am. Chem. Soc.* **2008**, *130*, 12628.

10 Mankad, N. P.; Müller, P.; Peters, J. C. *J. Am. Chem. Soc.* **2010**, *132*, 4083.

11 a) Mankad, N. P.; Whited, M. T.; Peters, J. C. *Angew. Chem. Int. Ed.* **2007**, *46*, 5768. b) Whited, M. T.; Mankad, N. P.; Lee, Y.; Oblad, P. F.; Peters, J. C. *Inorg. Chem.* **2009**, *48*, 2507. c) Lee, Y.; Mankad, N. P.; Peters, J. C. *Nat. Chem.* **2010**, *2*, 558.

12 a) Hansert, B.; Vahrenkamp, H. *J. Organomet. Chem.* **1993**, *459*, 265. b) Harrold, N. D.; Waterman, R.; Hillhouse, G. L.; Cundari, T. R. *J. Am. Chem. Soc.* **2009**, *131*, 12872.

13 The only prior report was by Cenini, in which azoarene was a minor product of catalysis. See Ragaini, F.; Penoni, A.; Gallo, E.; Tollari, S.; Gotti, C. L.; Lapadula, M.; Mangioni, E.; Cenini, S. *Chem. -Eur. J.* **2003**, *9*, 249.

14 N−N coupling to yield azobenzenes from metal imide complexes: Zarkesh, R. A.; Ziller, J. W.; Heyduk, A. F. *Angew. Chem. Int. Ed.* **2008**, *47*, 4715.

15 a) Schröder, D.; Shaik, S.; Schwarz, H. *Acc. Chem. Res.* **2000**, *33*, 139. b) Shaik, S.; Hirao, J.; Kumar, D. *Acc. Chem. Res.* **2007**, *40*, 532.

16 Takaoka, A.; Gerber, L. C. H.; Peters, J. C. *Angew. Chem., Int. Ed.* **2010**, *49*, 4088.

17 Dhuri, S. N.; Seo, M. S; Lee, Y.-M.; Hirao, H.; Wang, Y.; Nam, W.; Shaik, S. *Angew. Chem. Int. Ed* **2008**, *47, 3356.*.

18 a) Danopoulos, A. A.; Wilkinson, G.; Hussain-Bates, B.; Hursthouse, M. B. *Polyhedron* **1992**, *11*, 2961. b) Walstron, A. N.; Fullmer, B. C.; Fan, H.; Pink, M.; Buschhorn, D. T.; Caulton, K. G. *Inorg. Chem.* **2008**, *47*, 9002.

19 Takaoka, A.; Mendiratta, A.; Peters, J. C. *Organometallics* **2009**, *28*, 3744.

20 Addison, A. W.; Rao, T. N.; Van Rijn, J. J.; Verschoor, G. C. *J. Chem. Soc., Dalton Trans.* **1984**, 1349.

21 Select examples: a) Klapötke, T. M.; Krumm, B.; Piotrowski, H.; Polborn, K.; Holl, G. *Chem. –Eur. J.* **2003**, *9*, 687. b) Kawano, M.; Takayama, T.; Uekusa, H.; Ohashi, Y.; Ozawa, Y.; Matsubara, K.; Imabayashi, H.; Mitsumi, M.; Toriumi, K. *Chem. Lett.* **2003**, *32*, 922.

22 Selected examples: a) Hayashida, T.; Nagashima, H. *Organometallics*, **2002**, *21*, 3884. b) Kondo, T.; Tsunawaki, F.; Ura, Y.; Sadaoka, K.; Iwasa, T.; Wada, K.; Mitsudo, T. *Organometallics* **2005**, *24*, 905.

23 a) Schuster, G. B.; Platz, M. S. Photochemistry of Phenyl Azide. In *Advances in Photochemistry*; Volman, D.; Hammond, G.; Neckers, D., Ed.; John Wiley & Sons, Inc.; NJ, 1992; Vol. 17; p 69. b) Platz, M. S. Nitrenes. In *Reaction Intermediate Chemistry*; Moss, R. A.; Platz, M. S.; Jones, M. Jr., Ed.; John Wiley & Sons, Inc.; NJ, 2004; p 501.

24 Reiser, A.; Willets, F. W.; Terry, G. C.; Williams, V.; Marley, R. *Trans. Faraday Soc.* **1968**, *64*, 3265.

25 Borden, W. T.; Gritsan, N. P.; Hadad, C. M.; Karney, W. L.; Kemnitz, C. R.; Platz, M. S. *Acc. Chem. Res.* **2000**, *33*, 765.

26 Liang, T.-Y.; Schuster, G. B. *J. Am. Chem. Soc.* **1987**, *109*, 7803.

27 a) Smolinsky, G.; Wasserman, E.; Yager, W. A. *J. Am. Chem. Soc.* **1962**, *84*, 3220. b) Herbert Hall, J..; Fargher, J. A.; Gisler, M. R. *J. Am. Chem. Soc.* **1978**, *100*, 2029.

28 Other complexes assigned as containing a radical on the NAr ligand: a) Kogut, E.; Wiencko, H. L.; Zhang, L.; Cordeau, D. E.; Warren, T. H. *J. Am. Chem. Soc.* **2005**, *127*,

11248. b) Lu, C. C.; George, S. D.; Weyhermüller, Bill, E.; Bothe, E. Wieghardt, K. *Angew. Chem. Int. Ed.* **2008**, *47*, 6384. c) King, E. R.; Hennessy, E. T.; Betley, T. A. *J. Am. Chem. Soc.* **2011**, *133*, 4917.

29 Takaoka, A.; Peters, J. C. *Inorg. Chem.*, ASAP.

30 Sauouma, C.; Peters, J. C. *Coord. Chem. Rev.* **2011**, *255*, 920.

31 Moret, M. –E.; Peters, J. C. *Angew. Chem., Int. Ed.* **2011**, *50*, 2063.

32 Heyduk, A. F.; Zarkesh, R. A.; Nguyen, A. I. *Inorg. Chem.* **2011**, *50*, 9849.

33 Wang, S. H.; Mandimutsira, B. D.; Todd, R.; Ramdhanie, B.; Fox, J. P.; Goldberg, D. P. *J. Am. Chem. Soc.* **2004**, *126*, 18.

34 Palmer, M. J.; Kenny, J. A.; Walsgrove, T.; Kawamoto, A. M.; Wills, M. J. *J. Chem. Soc., Perkin Trans. 1* **2002**, 416.

35 Hu, M.; Li, J.; Yao, S. Q. *Org. Lett.* **2008**, *10*, 5529.

36 Weitz, I. S.; Rabinovitz, M. *J. Chem. Soc., Perkin Trans. 1* **1993**, 117.

37 S. Stoll, A. Schweiger, *J. Magn. Reson.* **2006**, *178*, 42.

38 Sheldrick, G. M. *Acta. Cryst.* **2008**, *A64*, 112.

Chapter 6: Dinitrogen Complexes of Sulfur-Ligated Iron

Reproduced in part with permission from

Takaoka, A.; Mankad, N. P.; Peters, J. C.

Journal of the American Chemical Society **2011**, *133*, 8440-8443.

6.1 Introduction

The intimate mechanism of nitrogen fixation by the nitrogenase enzymes remains a fascinating puzzle. Recent theoretical and experimental studies on the FeMo nitrogenase cofactor (FeMoco) have suggested N_2 binding at iron (Figure 6.1),[1] resulting in a growing interest in model complexes of iron with nitrogenous ligands (N_xH_y).[2] To date, such nitrogenase model chemistry has been dominated by complexes with phosphorus and nitrogen donors because of their propensity to afford N_2 complexes. This situation is striking given the sulfur-rich environment of the iron centers in the cofactor of FeMo nitrogenase.[3] Noteworthy in this context is the work by Sellmann[4] and more recently by Qu,[5] who have reported a number of iron complexes ligated by multiple sulfur donors and nitrogenous ligands.[6] Dinitrogen as a ligand remains a notable exception in these systems. In general, synthetic transition metal complexes with sulfur atom donors rarely afford N_2 adduct complexes; examples are known but remain comparatively uncommon.[7] With the exception of a single tetrahydrothiophene adduct of an Fe–N_2 complex,[8] the S–Fe–N_2 linkage is unknown, regardless of the number of S–Fe interactions.

Relative to phosphines and amines, π-donating sulfides and thiolates are weak-field ligands[9] that typically yield high-spin complexes with long Fe–L bonds.[10] Such a scenario is undesirable with respect to the favorable π back-bonding needed for a metal center to coordinate N_2. Accordingly, terminal N_2 adducts of transition metals do not populate high-spin states. In this regard, an electron-releasing and sulfur-containing ancillary ligand that yields low-spin metal centers may prove useful. Such scaffolds may help stabilize sulfur-ligated N_2 adducts of iron, especially in cases where N_2 is terminally

bonded. Thioethers are particularly appealing since they are σ-donating and (weakly) π-accepting[11] and thus would favor states with lower spin relative to thiolates and sulfides. To test this idea, we targeted hybrid thioether/phosphine relatives of a tetradentate tris(phosphino)silyl ligand, $(2\text{-}R_2PC_6H_4)_3Si$ ($[SiP^R_3]$; R = Ph, *i*Pr), that has proven exceptionally successful in stabilizing terminal trigonal-bipyramidal $\{[SiP^R_3]Fe–N_2\}^n$ complexes (n = −1, 0, +1).[12] Herein we present a new class of iron complexes featuring the S–Fe–N_2 linkage supported by such hybrid ligands.

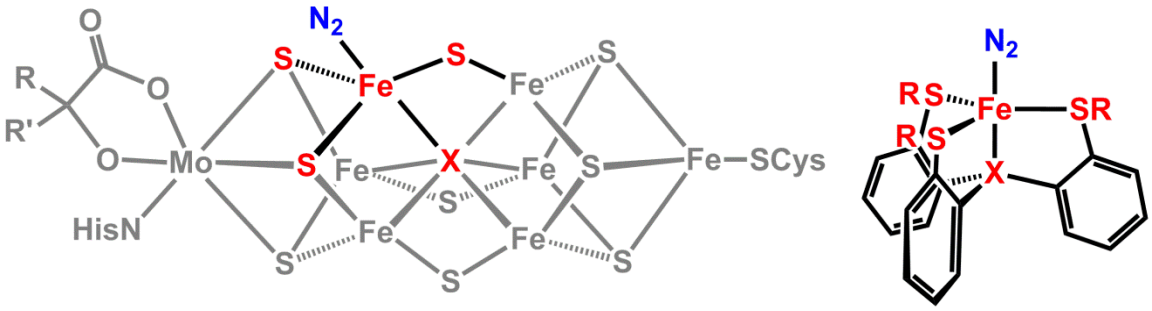

Figure 6.1. Hypothetical binding mode of N_2 at the FeMoco (left) and a hypothetical model complex (right). Whether any of the S-atoms shown in red for FeMoco (left) are protonated during catalysis is unknown.

6.2 Results and Discussion

Precursors of the desired ligands were conveniently synthesized by lithiation of the aryl bromides 2-*i*$Pr_2P(C_6H_4Br)$ (**6.1**) and 2-Ad$S(C_6H_4Br)$ (**6.2**) with *n*-BuLi followed by quenching with 0.5 equiv of $HSiCl_3$, which yielded the chlorosilanes $(2\text{-}iPr_2PC_6H_4)_2Si(H)(Cl)$ (**6.3**) and $(AdSC_6H_4)_2Si(H)(Cl)$ (**6.4**) in quantitative yield (Scheme **6.1**). Addition of another equivalent of the lithiation product of **6.2** and **6.1** to **6.3** and **6.4**, respectively, afforded the hybrid ligands $(2\text{-}iPr_2PC_6H_4)_2(2\text{-}AdSC_6H_4)SiH$ ($[SiP^{iPr}_2S^{Ad}]H$,

6.5) and (2-*i*Pr$_2$PC$_6$H$_4$)(2-AdSC$_6$H$_4$)$_2$SiH ([SiP$^{i\text{Pr}}$S$^{\text{Ad}}{}_2$]H, **6.6**) in high yield. The tris(thioether)silane ligand (2-AdSC$_6$H$_4$)$_3$SiH, ([SiS$^{\text{Ad}}{}_3$]H, **6.7**) was also synthesized by addition of 0.33 equiv of $HSiCl_3$ to the lithiation product of **2**.[13]

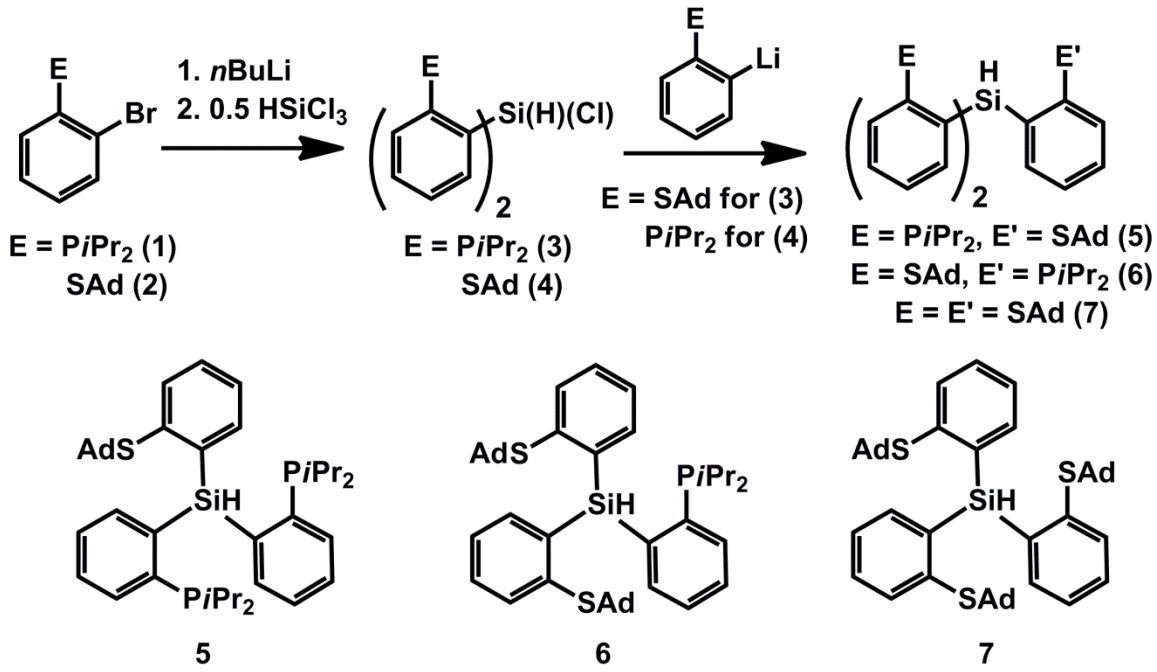

Scheme 6.1.

Metalation with iron was found to be facile for **6.5** and **6.6**. Addition of 2 equiv of MeMgCl to a solution of $FeCl_2$ and **6.5** or **6.6** at −78 °C yielded the paramagnetic (S = 1) iron(II) methyl complex [SiP$^{i\text{Pr}}{}_2$S$^{\text{Ad}}$]FeMe (**6.8**) or [SiP$^{i\text{Pr}}$S$^{\text{Ad}}{}_2$]FeMe (**6.9**), respectively (Scheme 6.2). The tris(thioether)silane **6.7** was not metalated under similar conditions, perhaps underscoring the need of a phosphine donor to aid the chelate-assisted Si–H bond activation.[12b]

Complexes **6.8** and **6.9** served as convenient entry points into the Fe–N_2 chemistry of interest. Protonation of the methyl ligand in **6.8** and **6.9** with HBAr$^{\text{F}}{}_4$ [BAr$^{\text{F}}{}_4$ = tetrakis(3,5-trifluoromethylphenyl)borate] in Et_2O resulted in loss of methane. For complex **6.8**, loss of methane was followed by binding of N_2 to yield the cationic,

paramagnetic (S = 1) dinitrogen complex {[SiP$^{iPr}_2$S^{Ad}]Fe(N$_2$)}BAr$^F_4$ (**6.10**), as evident from the N_2 stretch in its IR spectrum at ν_{N2} = 2156 cm^{-1}. Consistent with the high IR frequency, the N_2 ligand was appreciably labile, and a rapid color change from green to orange occurred under reduced pressure.

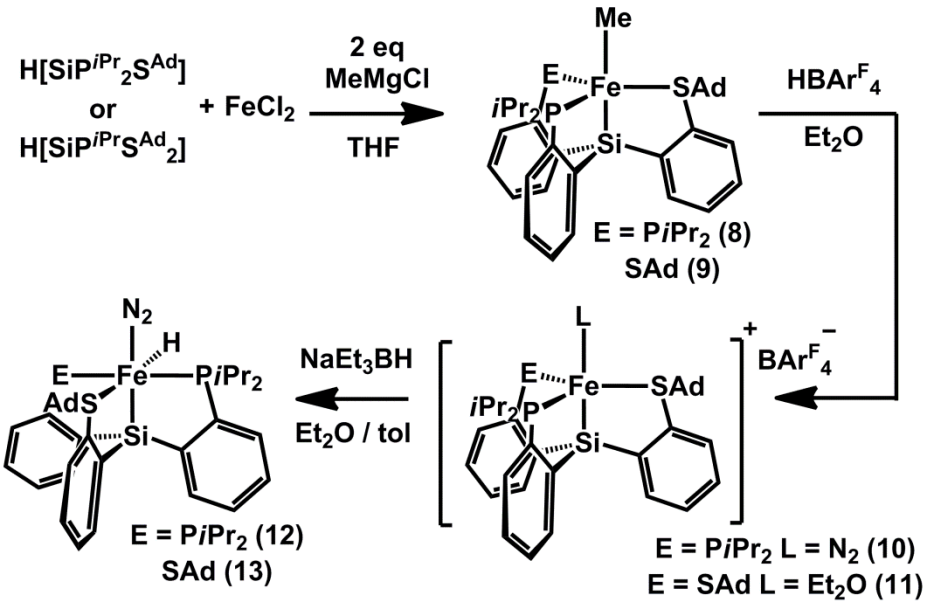

Scheme 6.2.

The solid-state structure of **10** (Figure 6.2 left) reveals a distorted trigonal-bipyramidal (TBP) geometry (τ = 0.73[14]) with a terminal N_2 ligand.[15] The distorted structure is in contrast to that of the corresponding {[SiP$^{iPr}_3$]Fe(N$_2$)}[BAr$^F_4$] complex, which exhibits a more rigorous TBP geometry.[12d] This difference likely reflects the smaller steric influence of a thioether relative to a phosphine donor, resulting in expansion of the P–Fe–P angle in **6.10** relative to {[SiP$^{iPr}_3$]Fe(N$_2$)}[BAr$^F_4$].

For the bis(thioether) complex **6.9**, protonation in Et_2O led instead to the solvent adduct {[SiP^{iPr}S$^{Ad}_2$]Fe(Et$_2$O)}BAr$^F_4$ (**6.11**). The lack of N_2 binding is likely dictated by the slightly reduced electron density at the iron center chelated by **6.6** relative to that by

6.5 due to the smaller number of phosphine donors. To increase the electron-richness of the iron center, the addition of a hydride donor was explored.

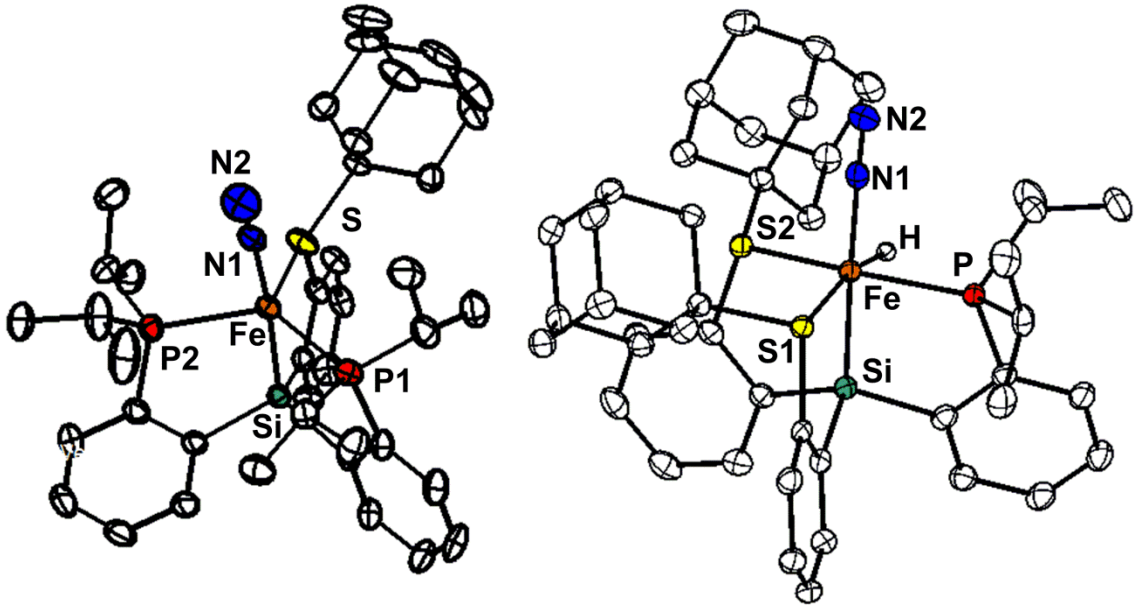

Figure 6.2. Solid-state structures of **6.10** and **6.13** (50% probability; H atoms and solvent for **6.10** and **6.13**, $BAr^{F}_{4}{}^{-}$ for **6.10** removed). Selected bond lengths (Å) and angles (°): **6.10**: Fe-N1; 1.954(3), Fe-Si; 2.3106(9), Fe-P1; 2.353(1), Fe-P2; 2.3542(9), Fe-S; 2.2941(9), Si-Fe-N1; 173.66(9), S-Fe-P1; 119.42(4), S-Fe-P2; 104.80; P1-Fe-P2; 129.76(4). **6.13**: Fe-N1; 1.828(2), Fe-Si; 2.2157(8), Fe-P; 2.185(7), Fe-S1; 2.3002(7), Fe-S2; 2.2887(7), N1-N2; 1.116(3), Si-Fe-N1; 177.79(7).

Accordingly, addition of $NaEt_3BH$ to **6.10** and **6.11** resulted in clean conversion to the corresponding neutral and diamagnetic hydride–N_2 complexes $[SiP^{iPr}{}_2S^{Ad}]Fe(H)(N_2)$ (**6.12**) and $[SiP^{iPr}S^{Ad}{}_2]Fe(H)(N_2)$ (**6.13**), which exhibited ν_{N2} values of 2055 and

2060 cm^{-1}, respectively. While isomers in which the hydride ligand is *trans* to either a thioether or a phosphine are conceivable, only one hydride signal (triplet for **6.12** and doublet for **6.13**) was observable in their respective ^{1}H NMR spectra at ca. −19 ppm. The solid-state structure of **6.13** featuring two thioether donors (Figure 6.2, right) exhibits a hydride ligand *trans* to one of the thioether ligands, as would be expected on the basis of the greater *trans* influence of a phosphine.[16] Density functional theory calculations indicated an energy difference of 17.5 kcal/mol in favor of the observed isomer (see the experimental section). The structure of **6.12** is presumed to be similar in light of the equivalence of the P atoms in the $^{31}P\{^{1}H\}$ spectrum.

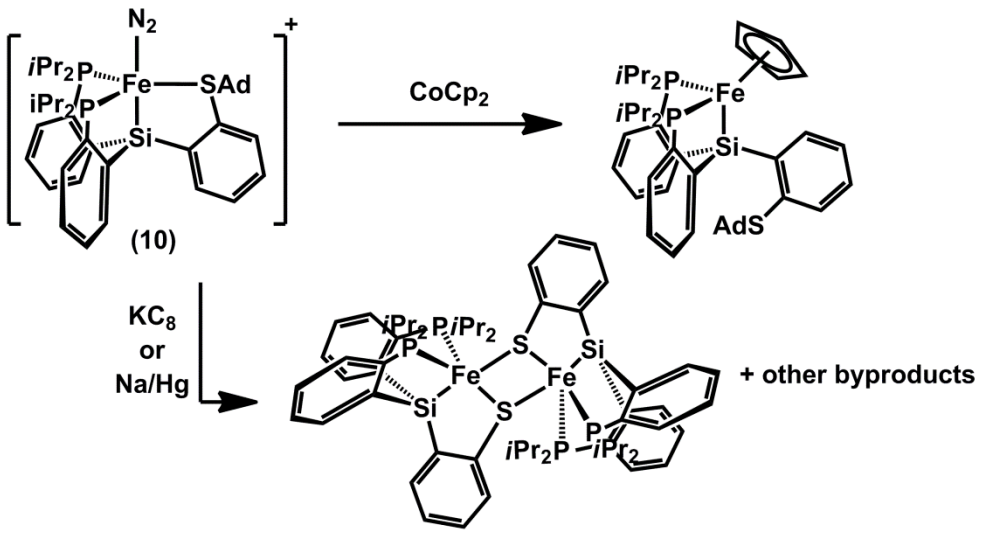

Scheme 6.3.

Despite the stability of $[SiP^{iPr}_{3}]Fe^{I}(N_2)$,[12a,b,d] the corresponding iron(I) complexes using ligands **6.5** and **6.6** did not prove to be accessible. For **6.10**, strong reductants such as KC_8 and Na/Hg resulted in a mixture of products. One of these products was determined by X-ray diffraction to be a dimeric complex formed by cleavage of the S–C(alkyl) bond of the thioether arm to yield a thiolate ligand that bridges two iron centers (Scheme 6.3). Related dimeric iron cores with bridging thiolates that are chelated by

tripodal tris(thiolate) ligands have been reported elsewhere.[17] In contrast, addition of $CoCp_2$ to **6.10** unexpectedly led to transmetalation of one Cp ligand with concomitant displacement of a thioether arm (see the appendix). These observations underscore some of the problems associated with stabilizing dinitrogen complexes using thiolates/thioethers, as thiolates tend to bridge metal centers and occupy sites that may otherwise be available for N_2 binding while thioethers can be labile in comparison with phosphines or undergo reductive S–C cleavage.

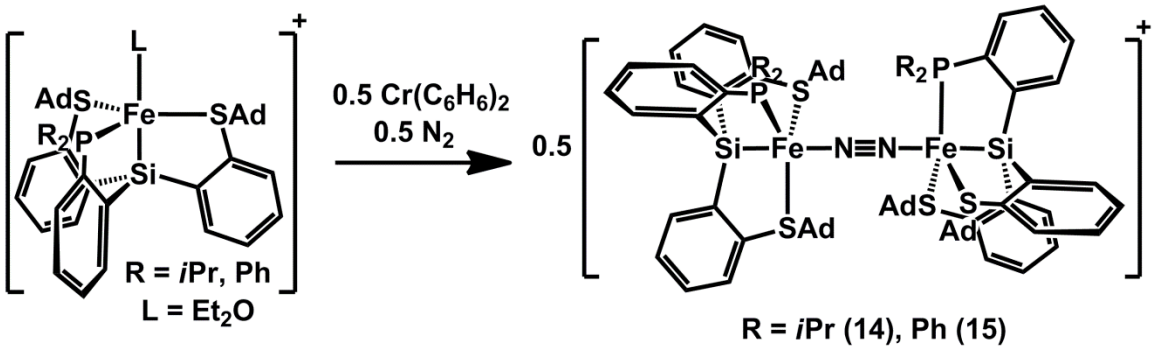

Scheme 6.4.

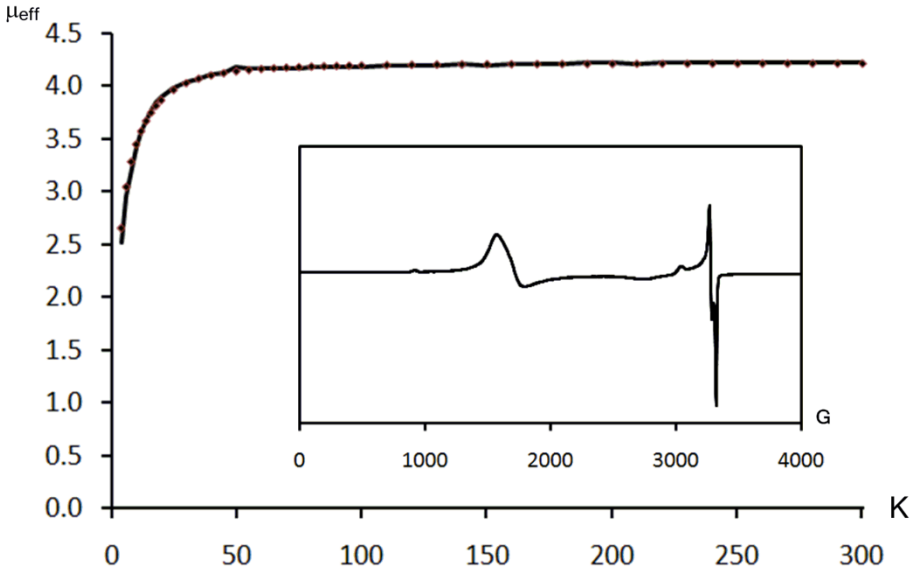

Figure 6.3. Variable temperature SQUID data (fit in black), and EPR data (20 K, 2-Me-THF), for **6.14**.

Reduction of the solvent adduct **6.11** using $CoCp_2$ or $Cr(C_6H_6)_2$ proved to be more interesting and led to a mixed-valent Fe(II)/Fe(I) complex with a bridging dinitrogen ligand, $[\{[SiP^{iPr}S^{Ad}_2]Fe\}_2(N_2)]BAr^F_4$ (**6.14**) (Scheme 6.4).[18] The combustion analysis data and stoichiometry of the reaction were consistent with our formulation of **6.14**, the latter requiring 0.5 equiv each of reductant and N_2 (Toepler pump analysis) per Fe center. While crystals suitable for X-ray diffraction invariably led to disorder/twinning problems arising from crystallization in a cubic space group, insights into the precise coordination environment of **6.14** were gained through its spectroscopic properties. Complex **6.14** exhibited a weak IR stretch at 1881 cm^{-1} that shifted to 1819 cm^{-1} when the reaction was performed under $^{15}N_2$ (calcd harmonic oscillator model: 1818 cm^{-1}). This ν_{N2} stretch was much lower in energy and significantly weaker in intensity than that for the terminal Fe(I) dinitrogen complex $[SiP^{iPr}_3]Fe(N_2)$ (2008 cm^{-1}); the frequency was closer to the value for the corresponding Fe(0) complex $[(SiP^{iPr}_3)Fe^0(N_2)]^-$ (1891 cm^{-1}), highlighting the influence of a second metal center.[12d] Since a molecule with an inversion center cannot yield an IR-active N_2 stretch, complex **6.14** must be asymmetric on the IR timescale, presumably via an asymmetric orientation of the phosphine/thioether arms (Scheme 6.4). Additionally, an intervalence charge-transfer band, characteristic of a mixed-valent species, was observed at 1360 nm in the NIR spectrum of **6.14** in Et_2O, and its assignment was supported by the observation of a solvent-dependent λ_{max}. The 20 K EPR spectrum of **6.14** exhibited features at g = 4.23, 3.98, and 2.02 due to the Kramer's doublet transition in an $S > {}^1/_2$ spin system (Figure 6.3). Indeed, the solution and solid-state magnetic moments were consistent with the EPR spectrum, supporting an $S = {}^3/_2$ spin state arising from ferromagnetic coupling between the S = 1 Fe(II) and $S = {}^1/_2$ Fe(I)

centers [or two Fe(1.5) centers].[19] The temperature independence of the solid-state data suggests an $S = {}^3/_2$ state that is largely separated from the other spins states. The N_2-bridged diiron complex $\{[SiP^{Ph}S^{Ad}{}_2]Fe\}_2(N_2)\}[BAr^F{}_4]$ (**6.15**) ($[SiP^{Ph}S^{Ad}{}_2]H$ = (2-$Ph_2PC_6H_4$)(2-$AdSC_6H_4)_2SiH$) featuring phenyl groups on the phosphine donors was synthesized analogously to **6.14** and exhibited similar spectroscopic features (see the appendix).

6.3 Conclusion

To conclude, a class of dinitrogen complexes of iron chelated by hybrid silyl ligands that include sulfur and phosphine donors has been characterized. Noteworthy are the iron–N_2 adducts **6.13**, **6.14**, and **6.15**, which possess multiple sulfur donors per Fe; these complexes are unique in this regard. Additionally, **6.14** and **6.15** represent unusual examples of formally Fe(I)/Fe(II) mixed-valent dinitrogen complexes. The work herein illustrates that mononuclear and dinuclear dinitrogen complexes of sulfur-ligated iron are accessible in various spin states ($S = {}^3/_2$, $S = 1$, and $S = 0$) using sulfur-containing scaffolds that induce relatively electron-rich metal centers. The structural relevance of thioether donors as models of the local environment of the iron centers in the FeMo cofactor in part depends on whether inorganic sulfide is protonated during catalytic turnover,[20] which in turn could result in HS → Fe dative interactions (Figure 6.1). Regardless, the use of thioethers in the present synthetic context provides steric protection while conserving a low-valent iron center.

6.4 Experimental Section

6.4.1 General Considerations

All manipulations were carried out using standard Schlenk or glovebox techniques under an atmosphere of dinitrogen. Unless otherwise noted, solvents were degassed and dried by thoroughly sparging with N_2 gas followed by passage through an activated alumina column. Hexamethyldisiloxane was dried over CaH_2 and distilled. Pentane, hexamethyldisiloxane, benzene, methylcyclohexane, toluene, tetrahydrofuran, and diethylether were tested with a standard purple solution of sodium benzophenone ketyl in tetrahydrofuran. Unless noted otherwise, all reagents were purchased from commercial vendors and used without further purification. Celite (Celite® 545) was dried at 150 °C overnight before use. Compounds **1**[21] and $HBAr^F_4 \cdot 2Et_2O$[22] were prepared according to literature procedures. Deuterated solvents were purchased from Cambridge Isotope Laboratories, Inc., degassed, and stored over 3-Å molecular sieves prior to use. Elemental analyses were performed by Midwest Microlabs.

6.4.2 X-ray Crystallography Procedures

X-ray diffraction studies were carried out at the Beckman Institute Crystallography Facility on a Brüker KAPPA APEX II diffractometer and solved using SHELX v. 6.14. The crystals were mounted on a glass fiber with Paratone-N oil. Data was collected at 100 K using Mo Kα (λ = 0.71073 Å) radiation and solved using SHELXS[23] and refined against F^2 on all data by full-matrix least squares with SHELXL.[23] X-ray quality crystals were grown as described in the experimental procedures.

6.4.3 SQUID Measurements

Measurements were recorded using a Quantum Designs SQUID magnetometer running MPMSR2 software (Magnetic Property Measurement System Revision 2). The samples were prepared under dinitrogen atmosphere in a polycarbonate capsule and suspended in the magnetometer in a plastic straw.recorded at 50,000 G.

6.4.4 Spectroscopic Measurements

A Varian Mercury 300 MHz spectrometer equipped with an autoswitchable probe and a Varian Inova 500 MHz spectrometer equipped with an auto-x pfg broad band probe were used to collect ^{1}H, ^{13}C, ^{29}Si, and ^{31}P spectra at room temperature. ^{1}H and ^{13}C spectra were referenced to residual solvent resonances. ^{29}Si spectra were referenced to external tetramethylsilane (δ = 0 ppm), and ^{31}P spectra were referenced to external 85% phosphoric acid (δ = 0 ppm). UV-VIS measurements were taken on a Cary 50 UV/Vis Spectrophotometer using quartz cuvettes with a teflon screw cap. IR measurements were obtained on samples prepared as KBr pellets or using a KBr disk solution cell using a Bio-Rad Excalibur FTS 3000 spectrometer. NIR measurements were obtained using a Nicolet FT-NIR spectrometer using quartz cuvettes capped with a Teflon screw cap. X-band EPR spectra were obtained on a Bruker EMX spectrometer.

6.4.5 Electrochemistry

Electrochemical measurements were carried out in a glovebox under a dinitrogen atmosphere in a one-compartment cell using a CH Instruments 600B electrochemical analyzer. A glassy carbon electrode was used as the working electrode and platinum wire

was used as the auxillary electrode. The reference electrode was Ag/AgNO3 in THF. The ferrocene couple Fc+/Fc was used as an external reference. Solutions (THF) of electrolyte (0.3 M tetra-*n*-butylammonium hexafluorophosphate) and analyte were also prepared under an inert atmosphere.

6.4.6 DFT Calculations

Geometry optimization for **6.13** was run on the Gaussian03[24] suite of programs starting from solid-state coordinates with the B3LYP[25] level of theory with the 6-31G(d)[26] basis set for all atoms. An optimization of the isomer of **6.13**, in which the hydride ligand is *trans* to the phosphine ligand, was also conducted (Compound **6.13'**). Frequencies calculations on **6.13** and **6.13'** confirmed the optimized structures to be minima. The calculations were followed by additional energy calculations, which were run using the same functional but with the 6-311G(d,p)[27] basis set for all atoms.

6.4.7 Synthesis

Synthesis of 2-Ad(C_6H_4Br) (6.2). 2-bromothiophenol (7.6 g, 40 mmol) was added to a stirring solution of 1-adamantol (7.6 g, 50 mmol) in a 3:2 mixture of approximately 300 mL of H_2SO_4/H_2O. After sturring for 2 days, the solids were filtered and washed with water. The solids were extracted into ether, concentrated, and recrystallized from hot hexanes to yield the product, 2-Ad(C_6H_4Br) (8.2 g, 63 %). ^{1}H NMR ($CDCl_3$, δ): 7.68 (dd, *J* = 7.8 Hz, 1.5 Hz, 1H), 7.62 (dd, *J* = 7.8 Hz, 1.8 Hz, 1H), 7.29-7.16 (m, 2H), 2.02 (s, 3H), 1.91 (s, 6H), 1.63 (s, 6H). $^{13}C\{^1H\}$ NMR (C_6D_6, δ): 139.9, 133.4, 132.8, 129.8, 126.7, 50.4, 43.6, 35.9, 29.9. HR-MS: Calc., 324.0370: Found, 324.0378.

Synthesis of (2-*i*Pr$_2$C$_6$H$_4$)$_2$Si(H)(Cl) (**6.3**). 2-*i*Pr$_2$P(C$_6$H$_4$Br) (**6.1**) (63 mg, 0.23 mmol) was dissolved in 5 mL Et$_2$O in a vial. The solution was cooled at −78 ^{o}C inside the glovebox and nBuLi (0.15 ml, 0.23 mmol, 1.6 M soln.) was added dropwise. The resulting solution was stirred for 1 hr at −78 ^{o}C upon which white solids were observed to precipitate out of solution. The mixture was stirred at RT for 1 hr. Volatiles were removed, and the pale powder was redissolved in 3 mL toluene. HSiCl$_3$ (15 mg, 0.11 mmol) was weighed out and diluted with 2 mL toluene. Both toluene solutions were cooled to −78 ^{o}C in the glovebox cold well, and the HSiCl$_3$ solution was added dropwise to the lithiated thioether solution. The resulting mixture was allowed to warm up slowly overnight. The mixture was filtered through celite, and concentrated to yield (2-*i*Pr$_2$C$_6$H$_4$)$_2$Si(H)(Cl) (48 mg, 97%). This material was used in subsequent reactions without any further purification. ^{1}H NMR (C$_6$D$_6$, δ): 7.88 (dt, *J* = 10Hz, 2Hz, 2H), 7.30-7.26 (m, 2H), 7.14-7.07 (m, 5H), 1.93 (m, 2H), 1.85 (m, 2H), 1.06 (dd, *J* = 15Hz, 5Hz, 3H) 0.99 (dd, *J* = 15Hz, 5Hz, 3H) 0.86 (dd, *J* = 15Hz, 5Hz, 3H) 0.77 (dd, *J* = 15Hz, 5Hz, 3H). ^{13}C{^{1}H} NMR (C$_6$D$_6$, δ): 144.1 (d, *J* = 46 Hz), 143.2 (d, *J* = 19Hz), 135.6 (d, *J* = 16 Hz), 131.7, 129.5, 128.4, 25.3 (d, *J* = 12 Hz), 24.6 (d, *J* = 12 Hz), 20.23 (d, *J* = 12 Hz), 20.15 (d, *J* = 18 Hz), 19.9 (d, *J* = 19 Hz), 19.4 (d, *J* = 9 Hz). ^{29}Si{^{1}H} NMR (C$_6$D$_6$, δ): -21.3 (t, *J* = 32 Hz). ^{31}P NMR (C$_6$D$_6$, δ): 0.39. IR (KBr pellet, cm^{-1}): 2238, 2212 (ν[Si-H]). HR-MS: Calc., 450.1828: Found, 450.1841.

Synthesis of (AdSC$_6$H$_4$)$_2$Si(H)(Cl) (**6.4**). 2-AdS(C$_6$H$_4$Br) (**6.2**) (75 mg, 0.23 mmol) was dissolved in 4 mL Et$_2$O in a vial. The solution was cooled at −78 ^{o}C inside the glovebox and nBuLi (0.15 mL, 0.23 mmol, 1.6 M soln.) was added dropwise. The resulting solution was stirred for 1 hr at −78 ^{o}C upon which white solids were observed to

precipitate out of solution. The mixture was stirred at RT for 1 hr. Volatiles were removed, and the white powder was redissolved in 3 mL toluene. $HSiCl_3$ (15 mg, 0.11 mmol) was weighed out and diluted with 2 mL toluene. Both toluene solutions were cooled to −78 ^oC in the glovebox cold well, and the $HSiCl_3$ solution was added dropwise to the lithiated thioether solution. The resulting mixture was allowed to warm up slowly overnight. The mixture was filtered through celite, and concentrated to yield $(AdSC_6H_4)_2Si(H)(Cl)$ (59 mg, 96%). ^1H NMR (C_6D_6, δ): 7.84 (m, 2H), 7.52 (m, 2H), 7.07 (m, 4H), 6.84 (s, 1H), 1.95-1.82 (m, 18H), 1.44 (s, 12H). $^{13}C\{^1H\}$ NMR (C_6D_6, δ): 142.3, 138.0, 137.3, 126.8, 130.2, 128.0, 50.0, 43.8, 36.0 30.1. $^{29}Si\{^1H\}$ NMR (C_6D_6, δ): -20.4 IR (KBr pellet, cm^{-1}): 2222, 2172(sh) (ν[Si-H]). HR-MS: Calc., 515.2263: Found, 515.2240.

Synthesis of [SiP$^{iPr}_2$S^{Ad}]H (6.5). 2-*i*$Pr_2P(C_6H_4Br)$ (2.0 g, 7.4 mmol) was dissolved in 50 mL Et_2O. The flask was cooled to −78 ^oC and nBuLi (4.6 mL, 7.4 mmol) was added dropwise. The flask was stirred for 30 min upon which a pale precipirate formed. The flask was stirred at RT for 1 hr, and volatiles were removed. The pale solid was redissolved in toluene and cooled to −78 ^oC. $HSiCl_3$ (480 mg, 3.5 mmol) was diluted with 6 mL toluene and also cooled to −78 ^oC. The silane was added dropwise to the cold solution of phosphine, and the resulting mixture was allowed to warm to RT slowly over several hours to form $(2\text{-}iPr_2C_6H_4)_2Si(H)(Cl)$ (**6.3**). This solution containing **6.3** was used directly in the subsequent reaction without any purification, *vide infra*.

In a separate flask, $2\text{-}AdS(C_6H_4Br)$ (1.15 g, 3.5 mmol) was dissolved in 20 mL ether. The flask was cooled to −78 ^oC, and nBuLi (2.2 mL, 3.5 mmol, 1.6 M soln.) was added dropwise. The resulting solution was stirred for 30 min, at which time a white precipitate

formed. Volatiles were removed, and the white solid was redissolved in 10 mL toluene. This solution was cooled to −78 ^{o}C and added dropwise to a solution of **6.3** at −78 ^{o}C. The resulting mixture was allowed to warm to RT overnight. The pale yellow solution was filtered through celite, concentrated, and washed with a small amount of pentane (2 x 2 mL) to afford analytically pure **[SiP$^{iPr}_2$S^{Ad}]H** (1.8 g, 78% overall yield). ^{1}H NMR (C_6D_6, δ): 7.76 (d, *J* = 7.5 Hz, 1H), 7.38 (d, *J* = 6.9 Hz, 2H), 7.29-6.92 (m, 10H), 2.11 (s, 6H), 2.03 (m, 2H), 1.95 (s, 3H), 1.55 (s, 6H), 1.13 (m, 12H), 0.94 (s, 12H). ^{13}C{^{1}H} NMR (C_6D_6, δ): 146.5 (d, *J* = 5 Hz), 146.1 (d, *J* = 5 Hz), 145.8 (d *J* = 5 Hz), 144.5 (d, *J* = 21 Hz), 139.6, 139.4, 138.7, 138.6, 138.4, 132.3, 129.5, 128.8, 128.4, 127.8, 50.7, 44.9, 37.0, 30.9, 25.7, 20.9 (m). ^{29}Si{^{1}H} NMR (C_6D_6, δ): -32.9 (t, *J* = 26 Hz). ^{31}P{^{1}H} NMR (C_6D_6, δ): 2.0. IR (KBr pellet, cm^{-1}): 2218 (ν[Si-H]). HR-MS: Calcd, 659.3426: Found, 659.3404. Anal. Calcd for $C_{40}H_{56}SiP_2S$: C, 72.91; H, 8.57; N. 0.00. Found: C, 73.02; H, 8.57; N, 0.00.

Synthesis of [SiP^{iPr}S$^{Ad}_2$]H (6.6). 2-AdS(C_6H_4Br) (2.4 g, 7.4 mmol) was dissolved in 50 mL Et_2O. The flask was cooled to −78 ^{o}C and nBuLi (4.6 mL, 7.4 mmol, 1.6 M soln.) was added dropwise. The flask was stirred for 30 min, at which time a white precipirate formed. The flask was stirred at RT for 1 hr, and volatiles were removed. The white solid was redissolved in 50 mL toluene and cooled to −78 ^{o}C. $HSiCl_3$ (500 mg, 3.7 mmol) was diluted with 5 mL toluene and also cooled to −78 ^{o}C. The silane was added dropwise to the cold solution of phosphine, and the resulting mixture was allowed to warm to RT slowly over several hours to form ($AdSC_6H_4)_2$Si(H)(Cl) (**6.4**). This solution containing **6.4** was used directly in the subsequent reaction without any purification, *vide infra*.

In a separate flask, 2-*i*Pr$_2$P(C$_6$H$_4$Br) (1.0 g, 3.7 mmol) was dissolved in 30 mL ether. The flask was cooled to −78 ^{o}C, and nBuLi (2.3 mL, 3.7 mmol, 1.6 M soln.) was added dropwise. The resulting solution was stirred for 30 min, at which time a pale precipitate formed. Volatiles were removed, and the pale solid was redissolved in 10 mL toluene. This solution was cooled to −78 ^{o}C and added dropwise to a solution of **6.4** at −78 ^{o}C. The resulting mixture was allowed to warm to RT overnight. The pale yellow solution was filtered through celite, concentrated, and washed with a small amount of pentane (2 x 2 mL) to afford analytically pure [SiP^{iPr}S$^{Ad}_2$]H (2.0 g, 77% overall yield). ^{1}H NMR (C$_6$D$_6$, δ): 7.70 (d, *J* = 8.1 Hz, 2H), 7.41 (d, *J* = 6.3 Hz, 1H), 7.25-7.10 (m, 7H), 6.95 (t, *J* = 7.5 Hz, 3H), 2.16 (s, 12H), 2.06 (m, 2H), 1.98 (s, 6H), 1.59 (s, 12H), 1.17 (dd, *J* = 14 Hz, 6.9 Hz, 6H), 1.00 (dd, *J* = 12 Hz, 7.2 Hz, 6H). ^{13}C{^{1}H} NMR (C$_6$D$_6$, δ): 145.5, 145.2, 144.9, 143.6 (d, *J* = 13 Hz), 138.6, 138.4, 138.1, 137.4 (d, *J* = 14 Hz,) 131.7, 128.9, 128.5, 128.2, 127.9, 50.0, 44.2, 36.3, 30.3, 25.1, 20.3, 20.21, 20.20, 20.1. ^{29}Si{^{1}H} NMR (C$_6$D$_6$, δ): -30.3 (d, *J* = 26 Hz). ^{31}P{^{1}H} NMR (C$_6$D$_6$, δ): 1.9. IR (KBr pellet, cm^{-1}): 2221 (ν[Si-H]). HR-MS: Calcd, 709.3487: Found, 709.3488. Anal. Calcd for C$_{44}$H$_{57}$SiPS$_2$: C, 74.53; H, 8.10; N. 0.00. Found: C, 74.24; H, 7.99; N, 0.00.

Synthesis of [SiS$^{Ad}_3$]H (6.7). 2-AdS(C$_6$H$_4$Br) (320 mg, 0.98 mmol) was dissolved in 10 mL Et$_2$O. The solution was cooled to −78 ^{o}C and nBuLi (0.61 mL, 0.98 mmol, 1.6 M soln.) was added dropwise. The solution was stirred for 30 min, upon which a white precipitate was observed. The mixture was stirred for 1 hr at RT. Volatiles were removed, and the white solid was dissolved in 10 mL toluene. HSiCl$_3$ (40 mg, 0.30 mmol) was diluted with 2 mL of toluene and cooled to −78 ^{o}C. The HSiCl$_3$ was added dropwise to a solution of the lithiated thioether at −78 ^{o}C dropwise. The mixture was allowed to warm

to RT overnight. The mixture was filtered through celite, and concentrated to yield a white powder. Washing with 3 mL of pentane afforded analytically pure [SiS^{Ad}_3]H (0.22 g, 88%). ^{1}H NMR (C_6D_6, δ): 7.72 (d, *J* = 7.6 Hz, 3H), 7.21-7.11 (m, 6H), 7.00 (s, 1H), 6.93 (t, *J* = 7.6 Hz, 3H), 2.18 (s, 12H), 1.98 (s, 6H), 1.58 (s, 12H). $^{13}C\{^1H\}$ NMR (C_6D_6, δ): 144.6, 138.3, 138.0, 137.9, 129.0, 127.9, 49.8, 44.1, 36.2, 30.2. $^{29}Si\{^1H\}$ NMR (C_6D_6, δ): -31.0 IR (KBr pellet, cm^{-1}): 2250 (ν[Si-H]). HR-MS: Calcd, 758.3454: Found, 758.3470. Anal. Calcd for $C_{48}H_{58}SiS_3$: C, 75.93; H, 7.70; N. 0.00. Found: C, 75.71; H, 7.80; N, 0.00.

Synthesis of [SiP$^{iPr}_2$S^{Ad}]FeMe (6.8). [$SiP^{iPr}_2S^{Ad}$]H (490 mg, 0.75 mmol) and $FeCl_2$ (95 mg, 0.75 mmol) were dissolved in approximately 50 mL of THF. The flask was cooled to −78 ^{o}C and MeMgCl (0.50 mL, 1.5 mmol, 3 M soln.) diluted with 10ml THF was added dropwise via cannula. A color change to dark red took place upon addition. The resulting mixture was allowed to warm up slowly overnight. Volatiles were removed. The solids were washed with a small amount of pentane, extracted into 25 mL of benzene, and filtered through celite. The red solution was concentrated, and the extraction with benzene was repeated. Removal of volatiles and washing with pentane yielded red **[SiP$^{iPr}_2$S^{Ad}]FeMe** (0.34 g, 59%). This material was used without any further purification in subsequent reactions. ^{1}H NMR (C_6D_6, δ): 8.8, 6.8, 5.8, 5.0, 3.2, 0.5, 0.2, −0.8, −1.8, −5.2, −8.5.μ_{eff} (Evans' method, C_6D_6, 23 ^{o}C) = 3.2 μ_B. UV-VIS (in THF): (nm, ε [mol^{-1} cm^{-1}]), 349 (4100, sh), 477 (2200, sh), 802 (140).

Synthesis of [SiP$^{iPr}_2$S^{Ad}]FeCl. [$SiP^{iPr}_2S^{Ad}$]FeMe (0.32 g, 0.44 mmol) was dissolved in 50 mL THF. The flask was cooled to −78 ^{o}C and HCl (0.44 mL, 0.44 mmol, 1 M soln.) was added dropwise. The resulting solution was stirred overnight and allowed to warm to

room temperature. The volatiles were removed, and the residues were washed with pentane. The product was extracted into benzene, and the orange mixture was filtered through celite. Concentration of the dark orange solution yielded [SiP$^{i\text{Pr}}_2$S$^{\text{Ad}}$]FeCl as an orange powder (0.28 g, 85%). Crystals suitable for X-ray diffraction were grown from layering pentane over a benzene solution of [SiP$^{i\text{Pr}}_2$S$^{\text{Ad}}$]FeCl. ^{1}H NMR (C_6D_6, δ): 8.7, 6.6, 6.4, 6.1, 1.7, 0.6, 0.0, −2.6, −5.0, −8.1. μ_{eff} (Evans' method, C_6D_6, 23 ^{o}C) = 2.5 μ_B. UV-VIS (in THF): (nm, ε [mol^{-1} cm^{-1}]), 426 (2500), 475 (3200), 818 (80). Anal. Calcd for $C_{40}H_{55}SiP_2SFeCl$: C, 64.12; H, 7.40; N. 0.00. Found: C, 63.93.71; H, 7.14; N, 0.00.

Synthesis of [SiP$^{i\text{Pr}}$S$^{\text{Ad}}_2$]FeMe (6.9). [SiP$^{i\text{Pr}}$S$^{\text{Ad}}_2$]H (0.50 g, 0.71 mmol) and $FeCl_2$ (110 mg, 0.85 mmol) was dissolved in 80 mL THF and the flask was cooled to −78 ^{o}C. MeMgCl (0.56 mL, 1.7 mmol, 3 M soln.) diluted with 10 mL THF was added dropwise to the solution via cannula. A color change to brown/dark red took place. The flask was allowed to warm to room temperature slowly overnight. Volatiles were removed, and the mixture was extracted into pentane and filtered through celite. This filtrate contains the product, [SiP$^{i\text{Pr}}$S$^{\text{Ad}}_2$]FeMe (**6.9**), in addition to small amounts of free ligand, adamantane, and other products. Concentrating the filtrate to 20 mL and cooling at −35 ^{o}C overnight precipitates out a red solid that contains most of the free ligand, as well as **6.9**. Concentration of the mother liquor to 15 mL and cooling at −35 ^{o}C over several days yields analytically pure **6.9**. (0.25 g, 45%). ^{1}H NMR (C_6D_6, δ): 5.6, 5.5, 4.3, 1.1, 0.1, −1.8, −4.8. μ_{eff} (Evans' method, C_6D_6, 23 ^{o}C) = 2.9 μ_B. UV-VIS (in THF): (nm, ε [mol^{-1} cm^{-1}]), 345 (5400, sh), 410 (3200, sh), 481 (1900, sh), 815 (70). Anal. Calcd for $C_{45}H_{59}SiPS_2Fe$: C, 69.38; H, 7.63; N. 0.00. Found: C, 69.76; H, 8.01; N, 0.00.

Synthesis of {[SiP$^{iPr}_2$S^{Ad}]Fe(N$_2$)}BAr$^F_4$ (6.10). [SiP$^{iPr}_2$S^{Ad}]FeMe (100 mg, 0.14 mmol) was dissolved in a 2:1 mixture of Et_2O and benzene in a vial. The vial was cooled in the glovebox cold well (dry ice/acetone bath). HBAr$^F_4$·2Et_2O (140 mg, 0.14 mmol) was dissolved in 2 mL Et_2O and also placed in the cold well. The HBAr$^F_4$·2Et_2O solution was added dropwise to the solution of [SiP$^{iPr}_2$S^{Ad}]FeMe, resulting in a color change to green. The reaction mixture was stirred for 15 min in the cold well, after which it was stirred at room temperature for 15 min The mixture was filtered through celite, concentrated, and recrystallized by layering a concentrated solution in Et_2O over a solution of 1:1 = hexamethyldisiloxane: pentane to yield green plates of [SiP$^{iPr}_2$S^{Ad}]Fe(N$_2$)}BAr$^F_4$ (88 mg, 41%) suitable for x-ray diffraction. The ^{1}H NMR spectrum of this compound was taken in 10:1 = C_6H_6:d_8-THF, due to the limited solubility of **6.10** in C_6D_6. Consequently, the reported NMR shifts are those of the solvento adduct, [SiP$^{iPr}_2$S^{Ad}]Fe(THF)}BAr$^F_4$. Room temperature magnetic moments were obtained by Evans method, in which the measurement was taken in C_6D_6/C_6H_6 with a drop of Et_2O to dissolve **6.10** (Et_2O does not appear to displace N_2 to a significant degree, if at all). ^{1}H NMR (d_8-THF, δ): 11.5, 8.4, 7.7, 5.9, 4.4, 0.7, 0.0, −0.6, −2.6, −3.2, −4.5, −6.7, −8.4. μ_{eff} (Evans' method, C_6D_6, 23 ^oC) = 3.2 μ_B. UV-VIS (in Et_2O): (nm, ε [mol^{-1} cm^{-1}]), 433 (1100, sh), 516 (630), 621 (310, sh), 855 (95, sh). IR (KBr liquid cell, Et_2O, cm^{-1}): 2156 (ν[N_2]).

Synthesis of [SiP$^{iPr}_2$S^{Ad}]Fe(Cp). {[SiP$^{iPr}_2$S^{Ad}]Fe(N$_2$)}BAr$^F_4$ (17 mg, 0.011 mmol) was dissolved in 3 mL Et_2O in a vial and placed inside the glovebox cold well (dry ice/acetone). $CoCp_2$ (2.0 mg, 0.011 mmol) was added. The color of the solution gradually changed from brown/green to red. The solution was stirred for 30 min inside the cold well, after which it was stirred at room temperature for 30 min Volatiles were removed,

and the product was extracted into pentane and filtered through celite. Volatiles were removed, and the extraction was repeated once more. Concentration of the solution resulted in yellow [SiP$^{i\text{Pr}}_2$S$^{\text{Ad}}$]Fe(Cp) (4.6 mg, 56%). Crystals suitable for X-ray diffraction were grown from slow evaporation of a concentration pentane solution, in a small vial inside a larger vial with hexamethyldisiloxane. ^{1}H NMR (C_6D_6, δ): 7.94 (d, *J* = 6.9 Hz, 1H), 7.88 (d, *J* = 6.9 Hz, 1H), 7.78 (m, 1H), 7.54 (m, 1H), 7.26-6.95 (m, 8H), 4.58 (s, 5H), 2.87 (m, 1H), 2.50 (m, 1H), 2.13-0.74 (m, 38H), −0.35 (s, 3H). ^{31}P{^{1}H}NMR (C_6D_6, δ): 110.3 (d, *J* = 30 Hz, 1P), 92.3 (d, *J* = 30 Hz, 1P).

Synthesis of {[SiP$^{i\text{Pr}}_2$S$^{\text{Ad}}$]Fe(L)}BAr$^{\text{F}}_4$ (6.11). [SiP$^{i\text{Pr}}$S$^{\text{Ad}}_2$]FeMe (8.0 mg, 0.010 mmol) was dissolved in 6 mL of Et_2O in a vial and placed in the glovebox cold well (dry ice/acetone). HBAr$^{\text{F}}_4$·2Et_2O (10 mg, 0.010 mmol) was dissolved in 2 mL Et_2O and also cooled in the cold well. The HBAr$^{\text{F}}_4$·2Et_2O solution was added dropwise to the [SiP$^{i\text{Pr}}$S$^{\text{Ad}}_2$]FeMe solution, which resulted in a color change from red to organge. The solution was stirred in the well for 15 min, after which it was stirred at room temperature for an additional 15 min Removals of volatiles yielded an orange film of {[SiP$^{i\text{Pr}}_2$S$^{\text{Ad}}$]Fe(Et_2O)}BAr$^{\text{F}}_4$ (16 mg, 94%). The ^{1}H NMR spectrum and magnetic moment by Evans method of this compound were measured in d_8-THF, due to the limited solubility of **6.10** in C_6D_6. Consequently, the reported NMR shifts and magnetic moment are those of the solvento adduct, [SiP$^{i\text{Pr}}$S$^{\text{Ad}}_2$]Fe(THF)}BAr$^{\text{F}}_4$. ^{1}H NMR (d_8-THF, δ): 7.79, 7.57, 6.5, −0.1, −3.7, −6.2. μ_{eff} (Evans' method, d_8-THF, 23 $^{\text{o}}$C) = 2.8 μ_B. UV-VIS (in THF): (nm, ε [mol^{-1} cm^{-1}]), 431 (2200), 501 (2000), 870 (170).

Synthesis of [SiP$^{i\text{Pr}}_2$S$^{\text{Ad}}$]Fe(H)(N$_2$) (6.12). {[SiP$^{i\text{Pr}}_2$S$^{\text{Ad}}$]Fe(N_2)}BAr$^{\text{F}}_4$ (80 mg, 0.050 mmol) was dissolved in 15 mL of 1:1 = Et_2O:toluene in a vial. The vial was placed inside

the glovebox cold well (dry ice/acetone). $NaEt_3BH$ (50 μL, 0.050 mmol, 1M sln) was added via syringe, and the resulting mixture was stirred in the cold well for 1 hr. The vial was subsequently stirred at room temperature for 10 min and volatiles were removed. The product was extracted into pentane and filtered through celite. The solution was concentrated, and the extraction was repeated once more. Removal of volatiles yielded $[SiP^{iPr}{}_2S^{Ad}]Fe(H)(N_2)$ (33 mg, 89%). ^1H NMR (C_6D_6, δ): 8.38 (d, *J* = 7.2 Hz, 2H), 8.14 (dd, *J* = 7.0 Hz, 1.5 Hz, 1H), 7.53 (d, *J* = 7.8 Hz, 1H), 7.28-6.84 (m, 8H), 2.64 (m, 2H), 2.37 (s, 6H), 1.96 (s, 3H), 1.62-1.38 (m, 12H), 1.25-0.81 (m, 20H), −20.3 (t, *J* = 67 Hz). $^{13}C\{^1H\}$ NMR (C_6D_6, δ): 155.5 (m), 149.0, 148.6, 148.4, 147.6, 140.8, 132.6, 132.0, 126.4, 126.0, 124.7, 57.6, 44.3, 36.3, 32.1, 30.7, 29.2 (m), 19.6, 19.3, 18.6. ^{31}P NMR (C_6D_6, δ): 88.9 (m). IR (KBr liquid cell, Et_2O, cm^{-1}): 2055 (ν[N_2]),1910 (ν[Fe-H]).

Synthesis of $[SiP^{iPr}S^{Ad}{}_2]Fe(H)(N_2)$ (6.13). $[SiP^{iPr}S^{Ad}{}_2]FeMe$ (12 mg, 0.015 mmol) was dissolved in 4 mL Et_2O in a vial and cooled inside the glovebox cold well (dry ice/acetone). $HBAr^F{}_4\cdot 2Et_2O$ (15 mg, 0.015 mmol) was dissolved in 2 mL Et_2O and also cooled. The $HBAr^F{}_4\cdot 2Et_2O$ solution was added dropwise to the solution of $[SiP^{iPr}S^{Ad}{}_2]FeMe$, which resulted in a color change from red to orange. The solution was stirred inside the cold well for 20 min and subsequently stirred at room temperature for 15 min Volatiles were removed, and the orange oil was redissolved in 5 mL of 2:1 = toluene:Et_2O and replaced inside the cold well. $NaEt_3BH$ (15 μL, 0.015 mmol, 1 M soln.) was added via syringe, and the resulting mixture was stirred inside the well for 30 min The mixture was stirred at room temperature for 20 min, which resulted in a color change from orange to brown/orange. Volatiles were removed, and the product was extracted into pentane, and filtered through celite. The orange solution was concentrated, and the

extraction was repeated once more to yield [SiP^{iPr}S$^{Ad}_2$]Fe(H)(N_2) (7.9 mg, 66%). Crystals suitable for X-ray diffraction were obtained by slow evaporation of a concentrated solution of **6.13** in a small vial into a larger vial with hexamethyldisiloxane. ^{1}H NMR (C_6D_6, δ): 8.28 (d, *J* = 7.2 Hz, 2H), 7.80 (d, *J* = 7.2 Hz, 1H), 7.62 (d, *J* = 7.8 Hz, 1H), 7.46 (d, *J* = 7.5 Hz, 1H), 7.30-7.03 (m, 5H), 6.94 (t, *J* = 7.2 Hz, 1H), 6.82 (t, *J* = 7.5 Hz, 1H), 2.65 (m, 1H), 2.22-1.13 (m, 40H), 0.50 (dd, *J* = 14Hz, 7.2 Hz, 3H), −18.7 (d, *J* = 97 Hz, 1H). ^{13}C{^{1}H} NMR (C_6D_6, δ): 155.2, 154.8 (d, *J* = 38 Hz), 151.8, 151.3 (d, *J* = 46 Hz), 145.2, 144.3, 133.3 (d, *J* = 43 Hz), 131.40, 131.9 (t, *J* = 8.8 Hz), 127.2, 126.5, 125.5, 57.3, 56.5, 41.9, 41.6, 36.0, 30.3 (d, *J* = 20 Hz), 20.9, 19.8, 19.6, 19.4. ^{31}P{^{1}H} NMR (C_6D_6, δ): 92.8 (d, *J* = 81 Hz). IR (KBr pellet, cm^{-1}): 2060 (ν[N_2]). Anal. Calcd for $C_{44}H_{57}SiPS_2FeN_2$: C, 66.65; H, 7.24; N. 3.53. Found: C, 66.31; H, 7.51; N, 3.36.

Synthesis of {[SiP^{iPr}S$^{Ad}_2$]Fe}$_2$(N_2)}BAr$^F_4$ (6.14). [SiP^{iPr}S$^{Ad}_2$]FeMe (0.10 g, 0.13 mmol) was dissolved in 13 mL Et_2O in a vial and placed inside the glovebox cold well (dry ice/acetone). HBAr$^F_4$·2Et_2O (0.13 g, 0.13 mmol) was dissolved in 3 mL Et_2O and also cooled. The HBAr$^F_4$·2Et_2O solution was added dropwise to the solution of [SiP^{iPr}S$^{Ad}_2$]FeMe, which resulted in a color change from red to orange. The solution was stirred for 30 min inside the cold well, and then stirred at room temperature for 10 min Benzene (3 mL) was added and the solution was replaced inside the well. Cr(C_6H_6)$_2$ (13 mg, 0.64 mmol) was added in one portion, and the mixture was stirred inside the cold well for 1.5 hr. The dark orange/red solution was subsequently stirred at room temperature for 40 min, and the volatiles were removed. The product was extracted into benzene, and separated from the yellow solids by filtration through celite. The solution was concentrated, and the extraction procedure was repeated once more. Layering a 1:1

mixture of methylcyclohexane:pentane over a concentrated Et_2O solution of the product at −35 °C resulted in formation of small microcrystals that analyzed for $\{[SiP^{iPr}S^{Ad}_2]Fe\}_2(N_2)\}BAr^F_4\cdot$MeCy (0.11 g, 65 %). ^{1}H NMR (C_6D_6, δ): 11.6, 7.9, 6.2, 2.7, −0.5, −4.0, −4.7, −9.3, −11.8, −15.5. μ_{eff} (Evans' method, C_6D_6, 23 °C) = 4.3 μ_B. IR (KBr pellet, cm^{-1}): 1881 (ν[N_2]). UV-VIS (in Et_2O): (nm, ε [mol^{-1} cm^{-1}]), 500 (3200, sh), 608 (1200, sh), 899 (1100). NIR (in Et_2O): (nm, ε [mol^{-1} cm^{-1}]), 1360 (2780). Anal. Calcd for $C_{127}H_{138}N_2BF_{24}Si_2P_2S_4Fe_2$: C, 60.60; H, 5.52; N. 1.11. Found: C, 60.78; H, 5.74; N, 0.86.

Synthesis of $[SiP^{Ph}S^{Ad}_2]H$. 2-AdS(C_6H_4Br) (1.5 g, 4.4 mmol) was dissolved in 100 mL Et_2O. The flask was cooled to −78 °C and nBuLi (2.8 mL, 4.4 mmol, 1.6 M soln.) was added dropwise. The flask was stirred for 30 min, upon which a white precipirate formed. The flask was stirred at RT for 1 hr, and volatiles were removed. The white solid was redissolved in 80 ml toluene and cooled to −78 °C. $HSiCl_3$ (300 mg, 2.2 mmol) was diluted with 4 mL toluene and also cooled to −78 °C. The silane was added dropwise to the cold solution of phosphine, and the resulting mixture was allowed to warm to RT slowly over several hours to form $(AdSC_6H_4)_2Si(H)(Cl)$ (**6.4**). This solution containing **6.4** was used directly in the subsequent reaction without any purification, *vide infra*.

In a separate flask, 2-$Ph_2P(C_6H_4Br)$ (0.75 g, 2.2 mmol) was dissolved in 60 mL ether. The flask was cooled to −78 °C, and nBuLi (1.4 mL, 2.2 mmol, 1.6 M soln.) was added dropwise. The resulting solution was stirred for 30 min, upon which a pale precipitate formed. The mixture was stirred at room temperature for 1 hr. Volatiles were removed, and the pale solid was redissolved in 15 mL toluene. This solution was cooled to −78 °C and added dropwise to a solution of **6.4** at −78 °C. The resulting mixture was allowed to warm to RT overnight. The pale orange solution was filtered through celite, concentrated,

and washed with a small amount of pentane (5 x 2 mL) to afford analytically pure [SiP^{Ph}S$^{Ad}_2$]H (1.4 g, 81 % overall yield). ^{1}H NMR (C_6D_6, δ): 7.68 (d, *J* = 7.5 Hz, 2H), 7.40 (m, 6H), 7.30 (br, 2H), 7.10-6.99 (m, 10H), 6.93 (t, *J* = 8.0 Hz, 1H), 6.84 (dd, *J* = 7.5 Hz, 2.5 Hz, 1H), 1.97 (s, 12H), 1.90 (s, 6H), 1.51 (s, 12H). ^{13}C{^{1}H} NMR (C_6D_6, δ): 142.0 (d, *J* = 3.3 Hz), 141.6, 141.24, 141.16, 141.08, 136.4, 135.5 (d, *J* = 12.9 Hz), 135.0 (d, *J* = 14.1 Hz), 131.4, 131.3 (d, *J* = 19.2 Hz), 127.0, 126.7, 125.9, 125.7 (d, *J* = 6.5 Hz), 125.5, 125.3, 47.4, 41.4, 33.7, 27.8. ^{29}Si{^{1}H} NMR (C_6D_6, δ): -20.5 (d, *J* = 27 Hz). ^{31}P{^{1}H} NMR (C_6D_6, δ): −9.6. IR (KBr pellet, cm^{-1}): 2220 (ν[Si-H]). Anal. Calcd for $C_{50}H_{53}SiPS_2$: C, 77.28; H, 6.87; N. 0.00. Found: C, 76.95; H, 6.72; N, 0.00.

Synthesis of [SiP^{Ph}S$^{Ad}_2$]FeMe. [SiP^{Ph}S$^{Ad}_2$]H (0.50 g, 0.64 mmol) and $FeCl_2$ (98 mg, 0.77 mmol) was dissolved in 80 mL THF and the flask was cooled to −78 ^{o}C. MeMgCl (0.52 mL, 1.5 mmol, 3 M soln.) diluted with 10 mL THF was added dropwise to the solution via cannula. A color change to dark red took place. The flask was allowed to warm to room temperature slowly overnight. Volatiles were removed, and the mixture was washed with 40 mL pentane, 15 mL Et_2O. The product was extracted into benzene and filtered through celite. The red solution was concentrated. The washing/extraction procedure was repeated once more and the red solution concentrated to yield analytically pure [SiP^{Ph}S$^{Ad}_2$]FeMe (0.30 g, 57%). ^{1}H NMR (C_6D_6, δ): 8.5, 5.5, 4.6, 4.3, −0.4, −0.6. μ_{eff} (Evans' method, C_6D_6, 23 ^{o}C) = 3.2 μ_B. UV-VIS (in THF): (nm, ε [mol^{-1} cm^{-1}]), 405 (5400, sh), 485 (2700, sh), 820 (40). Anal. Calcd for $C_{51}H_{55}SiPS_2Fe$: C, 72.32; H, 6.54; N. 0.00. Found: C, 73.01; H, 6.65; N, 0.00.

Synthesis of {[SiP^{Ph}S$^{Ad}_2$]Fe}$_2$(N$_2$)}BAr$^F_4$ (6.15). [SiP^{Ph}S$^{Ad}_2$]FeMe (41 mg, 0.048 mmol) was dissolved in a 1:1 mixture of C_6H_6 : Et_2O in a vial and placed inside the glovebox

cold well (dry ice/acetone). $HBAr^F_4 \cdot 2Et_2O$ (49 mg, 0.048 mmol) was dissolved in 1.5 mL Et_2O and also cooled. The $HBAr^F_4 \cdot 2Et_2O$ solution was added dropwise to the solution of $[SiP^{Ph}S^{Ad}_2]FeMe$. The solution was stirred for 30 min inside the cold well, and then stirred at room temperature for 10 min Et_2O (5 mL) was added and the solution was replaced inside the well. $Cr(C_6H_6)_2$ (5.0 mg, 0.024 mmol) was added in one portion, and the mixture was stirred inside the cold well for 1.5 hr. The red solution was subsequently stirred at room temperature for 3 hr., and the volatiles were removed. The product was extracted into a mixture of 1:1 pentane : benzene, and separated from the yellow solids by filtration through celite. The solution was concentrated, and the extraction procedure was repeated once more. Slow evaporation of a solution of 4:1 Et_2O : at −35 ^oC resulted in formation of small microcrystals that analyzed for $\{[SiP^{Ph}S^{Ad}_2]Fe\}_2(N_2)\}BAr^F_4 \cdot MeCy$ (41 mg, 64%). ^1H NMR (C_6D_6, δ): 15.5, 10.2, 9.7, 8.5, 8.1, 6.2, 5.4, 5.2, 4.5, 3.1, 2.7, 2.0, 0.5, −0.1, −0.6, −0.9, −2.9, −3.2, −3.4, −4.1, −4.6, −11.1. μ_{eff} (Evans' method, C_6D_6, 23 ^oC) = 4.5 μ_{eff}. IR (KBr pellet, cm^{-1}): 1898 (ν[N_2]). UV-VIS (in Et_2O): (nm, ε [mol^{-1} cm^{-1}]), 500 (5100, sh), 601 (1790, sh), 921 (1650). NIR (in Et_2O): (nm, ε [mol^{-1} cm^{-1}]), 1310 (2330). Anal. Calcd for $C_{139}H_{120}N_2BF_{24}Si_2P_2S_4Fe_2$: C, 62.92; H, 4.93; N. 1.06. Found: C, 63.32; H, 5.38; N, 0.88.

References Cited.

1 a) Kästner, J.; Blöchl, P. E. *J. Am. Chem. Soc.* **2007**, *129*, 2998. b) Hinnemann, B.; Nørskov, J. K. *J. Am. Chem. Soc.* **2005**, *126*, 3920. c) Hoffman, B. M.; Dean, D. R.; Seefeldt, L. C. *Acc. Chem. Res.* **2009**, *42*, 609. d) Peters, J. C.; Mehn, M. P. *Activation of Small Molecules*; Tolman, W. B., ed.; Wiley-VCH **2006**, 81. e) Crossland, J. L.; Tyler, D. R. *Coord. Chem. Rev.* **2010**, *254*, 1883. f) Holland, P. L. *Can. J. Chem.* **2005**, *83*, 296.

2 a) Verma, A. K.; Nazif, T. N.; Achim, C.; Lee S. C. *J. Am. Chem. Soc.* 2000, *122*, 11013. b) Brown, S. D.; Betley, T. A. Peters, J. C. *J. Am. Chem. Soc.* **2003**, *125*, 322. c) Betley, T. A.; Peters, J. C. *J. Am. Chem. Soc.* **2004**, *126*, 6252. d) Saouma, C. T.; Müller, P.; Peters, J. C. *J. Am. Chem. Soc.* **2009**, *131*, 10358. e) Scepaniak, J. J.; Young, J. A.; Bontchev, R. P.; Smith, J. M. *Angew. Chem. Int. Ed.* **2009**, *48*, 3158. f) Vogel, C.; Heinemann, F. W.; Sutter, J.; Anthon, C.; Meyer, K. *Angew. Chem. Int. Ed.* **2008**, *47*, 2681. g) Holland, P. L. *Acc. Chem. Res.* **2008**, *41*, 905. h) Crossland, J. L.; Tyler, D. R. *Coord. Chem. Rev.* **2010**, *254*, 1883. i) Field, L. D.; Li, H. L.; Dalgarno, S. J.; Turner, P. *Chem. Commun.* **2008**, 1680.

3 Einsle, O.; Tezcan, F. A.; Andrade, S. L. A.; Schmid, B.; Yoshida, M.; Howard, J. B.; Rees, D. C. *Science* **2002**, *297*, 1696.

4 Sellmann, D.; Sutter, J. *Acc. Chem. Res.* **1997**, *30*, 460.

5 a) Chen, Y.; Liu, L.; Peng, Y.; Chen, P.; Luo, Y.; Qu, J. *J. Am. Chem. Soc.* **2011**, *133*, 1147. b) Chen, Y.; Zhou, Y.; Chen, P.; Tao, Y.; Li, Y.; Qu, J. *J. Am. Chem. Soc.* **2008**, *130*, 15250.

6 For a bridging sulfide coordinated diiron complex that also binds phenylhydrazine, see Vela J.; Stoian, S.; Flaschenriem, C. J.; Münck, E.; Holland, P. J. *J. Am. Chem. Soc.* **2004**, *126*, 4522.

7 Selected examples; a) Mori, H.; Seino, H.; Hidai, M.; Mizobe, Y. *Angew. Chem. Int. Ed.* **2007**, *46*, 5431. b) Dilworth, J. R.; Henderson, R. A.; Hills, A.; Hughes, D. L.; Macdonald, C.; Stephens, A. N.; Walton, D. R. M. *J. Chem. Soc., Dalton Trans.* **1990**, 1077. c) Yoshida, T.; Adachi, T.; Kaminaka, M.; Ueda, T. *J. Am. Chem. Soc.* **1988**, *110*, 4872. d) Morris, R. H.; Ressner, J. M.; Sawyer, J. F.; Shiralian, M. *J. Am. Chem. Soc.* **1984**, *106*, 3683.

8 Bart, S.; Lobkovsky, E.; Bill, E.; Wieghardt, K.; Chirik, P. J. *Inorg. Chem.* **2007**, *46*, 7055.

9 Lane, R. W.; Ibers, J. A.; Frankel, R. B.; Papaefthymiou, G. C.; Holm, R. H. *J. Am. Chem. Soc.* **1977**, *99*, 84.

10 a) Lee, S. C.; Holm, R. H. *Chem. Rev.* **2004**, *104*, 1135. b) Malianak, S. M.; Coucouvanis, D. *Prog. Inorg. Chem.* **2001**, *49*, 599.

11 a) Mullen, G. E. D.; Went, M. I.; Wocadlo, S.; Powell, A. K.; Blower P. I. *Angew. Chem. Int. Ed.* 1997, 36, 1205. b) Kraatz, H.-B.; Jacobsen, H.; Ziegler, T.; Boorman, P. M. *Organometallics* **1993**, *12*, 76.

12 a) Mankad, N. P.; Whited, M. T.; Peters, J. C. *Angew. Chem. Int. Ed.* **2007**, *129*, 5768. b) Whited, M. T.; Mankad, N. P.; Lee, Y.; Oblad, P. F.; Peters, J. C. *Inorg. Chem.* **2009**, *48*, 2507. c) Takaoka, A.; Gerber, L. C. H.; Peters, J. C. *Angew. Chem. Int. Ed.* **2010**, *49*, 4088. d) Lee, Y.; Mankad, N. P.; Peters, J. C. *Nat. Chem.* **2010**, *2*, 558. e) Moret, M. E., Peters, J. C. *Angew. Chem. Int. Ed.* **2011**, *50*, 2063.

13 A related tris(thioether)silyl ligand has been recently reported. See Takeda, N.; Watanabe, D.; Nakamura, T.; Unno, M. *Organometallics* **2010**, *29*, 2839.

14 Addison, A. W.; Rao, T. N.; Van Rijn, J. J.; Verschoor, G. C. *J. Chem. Soc., Dalton Trans.* **1984**, 1349.

15 The N-N bond length is 1.037(4) Å. This anomalously short N-N distance is likely due to disorder. Multiple data sets did not provide a more reasonable N-N distance.

16 Connolly, J.; Forder, R. J.; Reid, G. *Inorg. Chim. Acta.* **1997**, *264*, 137.

17 a) Niemoth-Anderson, J. D.; Clark, K. A.; George, T. A.; Ross, C. C. R. II. *J. Am. Chem. Soc.* **2000**, *122*, 3977. b) Davis, S. C.; Evans, D. J.; Hughes, D. L.; Konkol, M.; Richards, R. L.; Sanders, J. R.; Sobota, P. *J. Chem. Soc., Dalton. Trans.* **2002**, 2473.

18 For examples of N_2 bridged iron dimers see; a) Betley, T. A.; Peters, J. C. *J. Am. Chem. Soc.* **2003**, *125*, 10782; b) Field, L. D.; Guest, R. W.; Turner, P. *Inorg. Chem.* **2010**, *49*, 9086. c) Smith, J. M.; Sadique, A. R.; Cundari, T. R.; Rodgers, K. R.; Lukat-Rodgers, G.; Lachicotte, R. J.; Flaschenriem, C. J.; Vela, J.; Holland, P. L. *J. Am. Chem. Soc.* **2006**, *128*, 756. d) Chomitz, W. A.; Arnold, J. *Chem. Commun.* **2007**, 4797. e) Berke, H.; Bankhardt, W.; Huttner, G.; Von Seyeri, J.; Zsolnai, L. *Chem. Ber.* **1981**, *114*, 2754.

19 Such behavior has been observed previously. See Drüke, S.; Chaundhuri, P.; Pohl, K.; Wieghardt, K.; Ding, X.-Q.; Bill, E.; Sawaryn, A.; Trautwein, A. X.; Winkler, H.; Gurman, S. J. *J. Chem. Soc., Chem. Commun.* **1989**, 59.

20 a) Sellmann, D.; Fürsattel, A.; Sutter, J. *Coord. Chem. Rev.* **2000**, *200*, 545. b) Peters, J. W.; Szilagyi, R. K. *Curr. Opin. Chem. Bio.* **2006**, *10*, 101.

21 a) R. Talay, D. Rehder, *Zeit. f. Natur, B: Anorg. Chem.*, **1981**, *36*, 451. b) M. Tamm, B. Dreβel, K. Baum, T. Lügger, T. Pape, *J. Organomet. Chem.*, **2003**, *677*, 1.

22 Brookhart, M.; Grant, B.; Volpe, A. F., Jr. *Organometallics* **1992**, *11*, 3920.

23 Sheldrick, G. M. *Acta. Cryst.* **2008**, *A64*, 112.

24 Gaussian 03, Revision C.02, Frisch, M. J.; Trucks, G. W.; Schlegel, H. B.; Scuseria, G. E.; Robb, M. A.; Cheeseman, J. R.; Montgomery, Jr., J. A.; Vreven, T.; Kudin, K. N.; Burant, J. C.; Millam, J. M.; Iyengar, S. S.; Tomasi, J.; Barone, V.; Mennucci, B.; Cossi, M.; Scalmani, G.; Rega, N.; Petersson, G. A.; Nakatsuji, H.; Hada, M.; Ehara, M.; Toyota, K.; Fukuda, R.; Hasegawa, J.; Ishida, M.; Nakajima, T.; Honda, Y.; Kitao, O.; Nakai, H.; Klene, M.; Li, X.; Knox, J. E.; Hratchian, H. P.; Cross, J. B.; Bakken, V.; Adamo, C.; Jaramillo, J.; Gomperts, R.; Stratmann, R. E.; Yazyev, O.; Austin, A. J.; Cammi, R.; Pomelli, C.; Ochterski, J. W.; Ayala, P. Y.; Morokuma, K.; Voth, G. A.; Salvador, P.; Dannenberg, J. J.; Zakrzewski, V. G.; Dapprich, S.; Daniels, A. D.; Strain, M. C.; Farkas, O.; Malick, D. K.; Rabuck, A. D.; Raghavachari, K.; Foresman, J. B.; Ortiz, J. V.; Cui, Q.; Baboul, A. G.; Clifford, S.; Cioslowski, J.; Stefanov, B. B.; Liu, G.; Liashenko, A.; Piskorz, P.; Komaromi, I.; Martin, R. L.; Fox, D. J.; Keith, T.; Al-Laham, M. A.; Peng, C. Y.; Nanayakkara, A.; Challacombe, M.; Gill, P. M. W.; Johnson, B.; Chen, W.; Wong, M. W.; Gonzalez, C.; and Pople, J. A.; Gaussian, Inc., Wallingford CT, 2004.

25 a) Becke, A.D. *J. Chem. Phys.* **1993**, *98*, 5648. b) Lee, C.; Yang, W.; Parr, R. G. *Phys. Rev. B.* **1988**, *37*, 785.

26 a) Hariharan, P. C.; Pople, J. A. *Theoret. Chimica Acta.* **1973**, *28*, 213. b) Francl, M. M.; Petero, W. J.; Hehre, W. J.; Binkley, J. S.; Gordon, M. S.; DeFrees, D. J.; Pople, J.

A. *J. Chem. Phys.* **1982**, *77*, 3654. c) Rassolov, V.; Pople, J. A.; Ratner, M.; Windus, T. L. *J. Chem. Phys.* **1998**, *109*, 1223.

27 a) Krishnan, R.; Binkley, J. S.; Seeger, R.; Pople, J. A. *J. CHem. Phys.* **1980**, *72*, 650. b) McLean, A. D.; Chandler, G. S. *J. Chem. Phys.* **1980**, *72*, 5639.

Appendix 1: Supplementary Data for Chapter 2

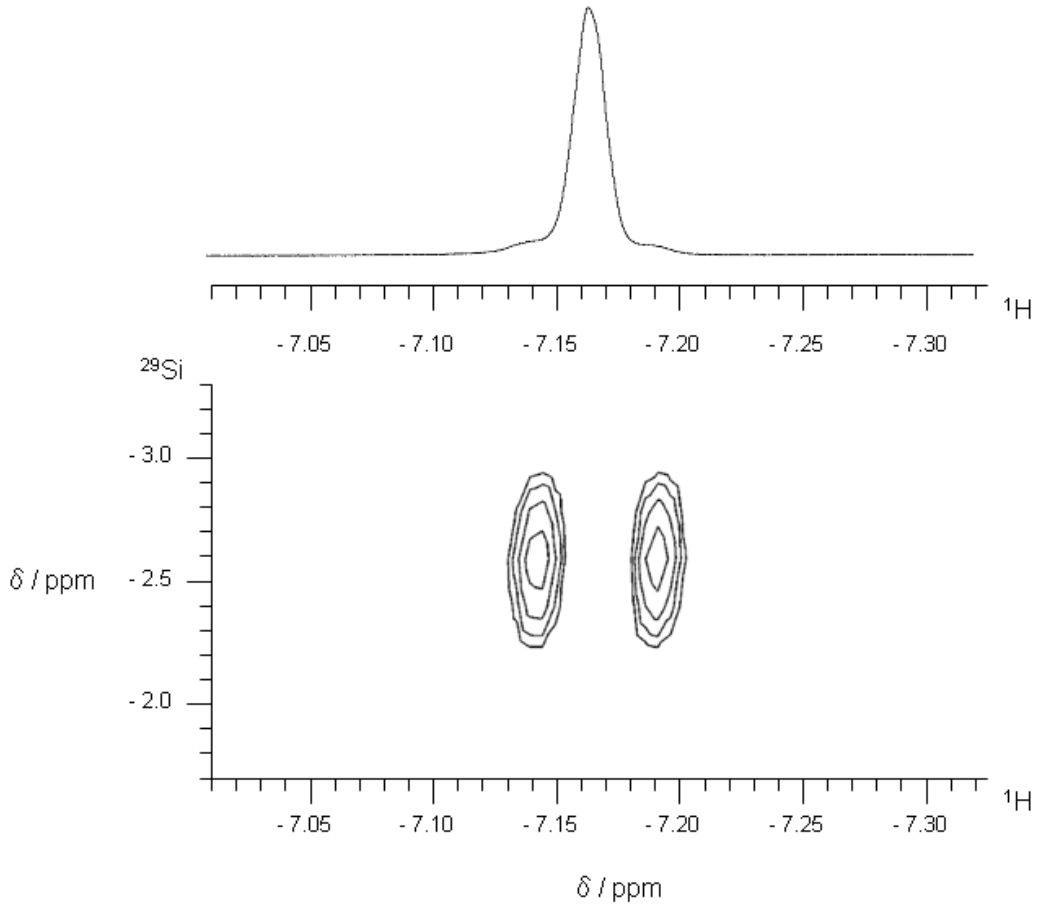

Figure A1.1. ^{1}H–^{29}Si HSQC spectrum of **2.13** of upfield peak in d_8-THF.

T(K)	rate constant(/hr)
298.2	0.0164(4)
308.2	0.0463(15)
318.2	0.138(4)
328.2	0.393(17)

Table A1.1. Kinetic data for Eyring plot.

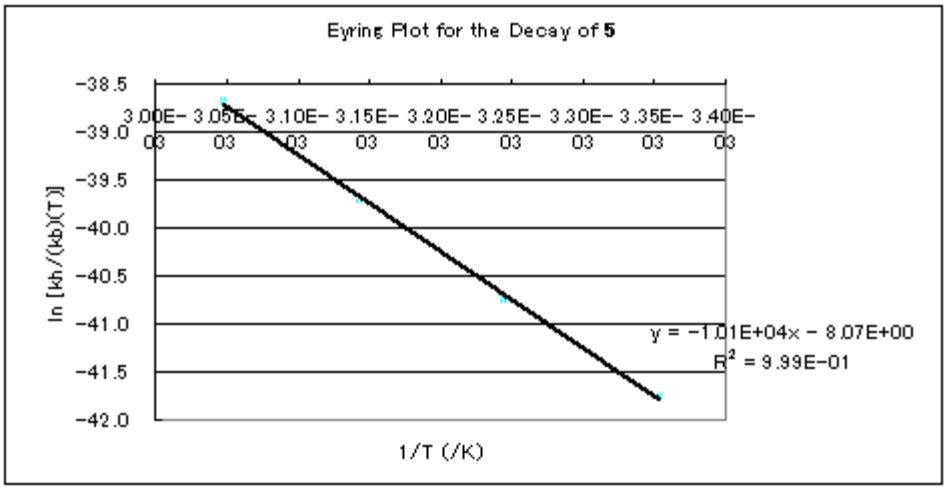

Figure A1.2. Eyring plot for the decay of **2.5**.

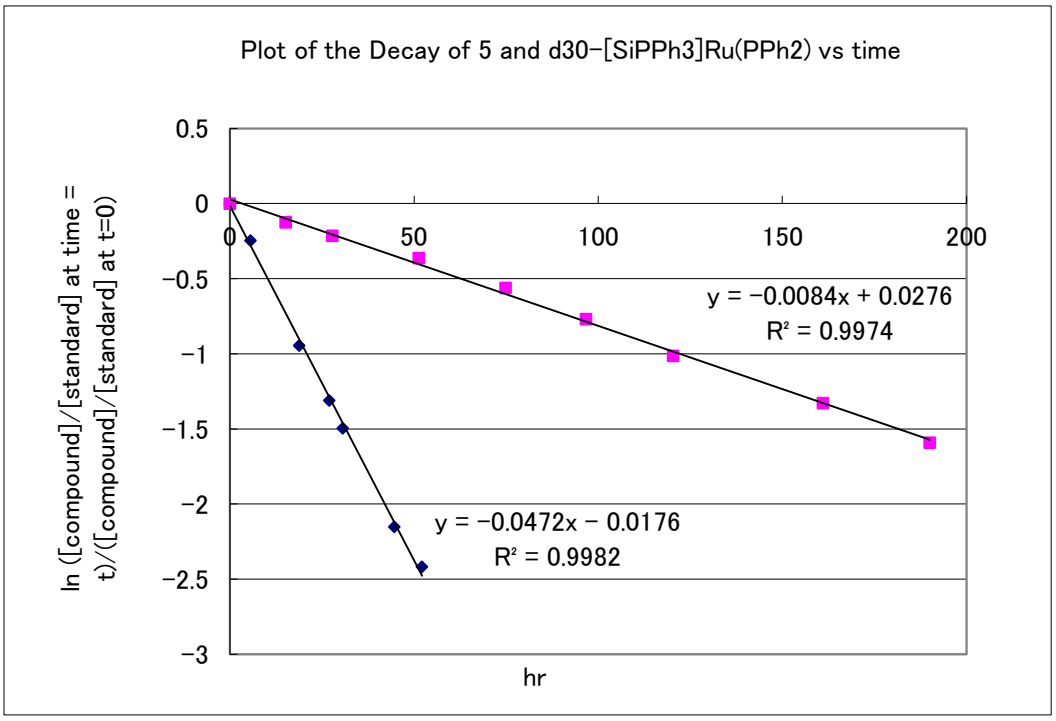

Figure A1.3. Typical decay behavior of **2.5** vs d_{30}-[SiP$^{Ph}_3$]Ru(PPh$_2$) at 35°C.

Blue: **2.5**

Pink: ***d*$_{30}$-[SiP$^{Ph}_3$]Ru(PPh$_2$)**

Appendix 2: Supplementary Data for Chapter 3

	Opt. M	P(total)	X-ray# M	P(total)				
3.3	76	16	64	25				
3.4	69	15	58	26				
3.5	84	13	73	24				
3.6	79	13	N/A	N/A				
	Opt. M	**P(total)**	**N**	**Ar(total)**	**X-ray# M**	**P(total)**	**N**	**Ar(total)**
3.11	38*	7*	29*	28*	33	8	31	28
3.12	39+	5+	24+	30+	38	7	27	27

Table A2.1. Spin densities calculated from optimized and solid-state structures.

* Optimized using PBE1PBE. Using B3LYP instead gives M(%), 40; P(total, %), 5.4; N(%), 27; Ar(total, %), 27. $^{+}$ Optimized using B3LYP. $^{\#}$ Coordinates from X-ray structure.

Table A2.2. Crystal data and structure refinement for [SiP^{iPr}_3]RuN_2 (**3.3**).

Identification code	08275	
Empirical formula	C36 H54 N2 P3 Ru Si	
Formula weight	736.88	
Temperature	100(2) K	
Wavelength	0.71073 Å	
Crystal system	Orthorhombic	
Space group	Pbca	
Unit cell dimensions	a = 16.117(3) Å	α = 90°.
	b = 17.264(3) Å	β = 90°.
	c = 25.583(5) Å	γ = 90°.
Volume	7118(2) $Å^3$	
Z	8	
Density (calculated)	1.375 Mg/m^3	
Absorption coefficient	0.637 mm^{-1}	
F(000)	3096	
Crystal size	0.20 x 0.15 x 0.10 mm^3	
Theta range for data collection	1.59 to 29.57°.	
Index ranges	-22≤h≤22, -23≤k≤23, -35≤l≤35	
Reflections collected	180260	
Independent reflections	9979 [R(int) = 0.0771]	
Completeness to theta = 29.57°	100.0%	
Absorption correction	Semi-empirical from equivalents	
Max. and min transmission	0.9390 and 0.8832	
Refinement method	Full-matrix least-squares on F^2	
Data / restraints / parameters	9979 / 0 / 400	
Goodness-of-fit on F^2	1.029	
Final R indices [I > 2sigma(I)]	R1 = 0.0474, wR2 = 0.1174	
R indices (all data)	R1 = 0.0650, wR2 = 0.1308	
Largest diff. peak and hole	3.218 and -1.209 e.$Å^{-3}$	

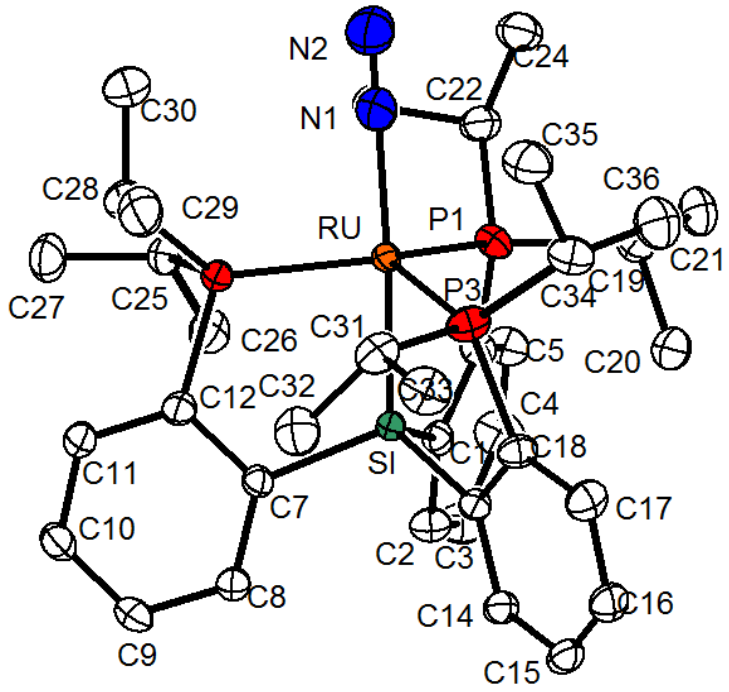

Figure A2.1. Solid-state structure of [SiP$^{iPr}_3$]RuN$_2$ (**3.3**).

Table A2.3. Crystal data and structure refinement for $[SiP^{iPr}_3]OsN_2$ (**3.4**).

Identification code	d8-09074	
Empirical formula	C36 H54 N2 Os P3 Si	
Formula weight	826.01	
Temperature	100(2) K	
Wavelength	1.54178 Å	
Crystal system	Monoclinic	
Space group	P2(1)/c	
Unit cell dimensions	a = 11.1140(3) Å	α = 90°.
	b = 16.0189(4) Å	β = 102.523(2)°.
	c = 20.6455(6) Å	γ = 90°.
Volume	3588.16(17) $Å^3$	
Z	4	
Density (calculated)	1.529 Mg/m^3	
Absorption coefficient	8.498 mm^{-1}	
F(000)	1676	
Crystal size	0.20 x 0.10 x 0.05 mm^3	
Theta range for data collection	3.52 to 68.68°.	
Index ranges	$-13\leq h\leq 13$, $0\leq k\leq 19$, $0\leq l\leq 24$	
Reflections collected	7142	
Independent reflections	7142 [R(int) = 0.0000]	
Completeness to theta = 68.68°	99.2%	
Absorption correction	Semi-empirical from equivalents	
Max. and min transmission	0.6760 and 0.2813	
Refinement method	Full-matrix least-squares on F^2	
Data / restraints / parameters	7142 / 0 / 403	
Goodness-of-fit on F^2	1.037	
Final R indices [I > 2sigma(I)]	R1 = 0.0314, wR2 = 0.0822	
R indices (all data)	R1 = 0.0331, wR2 = 0.0861	
Largest diff. peak and hole	1.376 and -2.818 $e.Å^{-3}$	

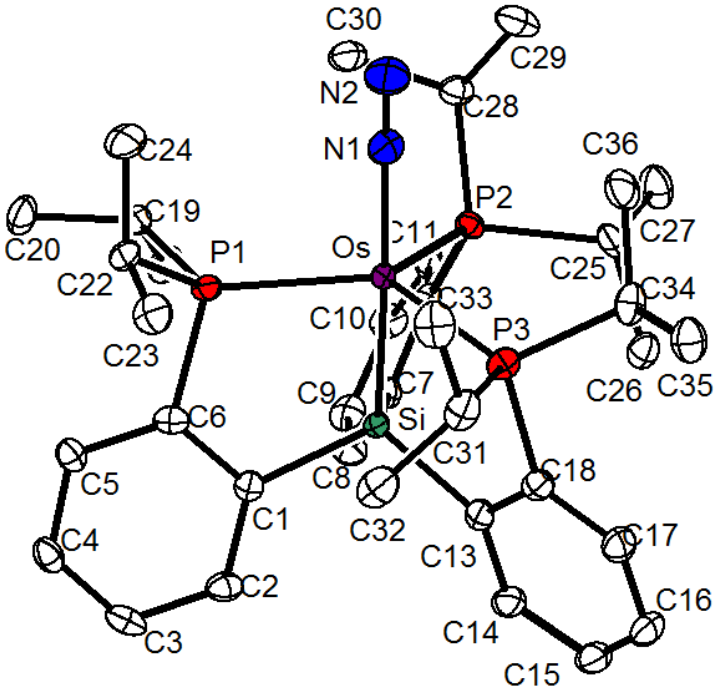

Figure A2.2. Solid-state structure of [SiP$^{iPr}_3$]OsN$_2$ (**3.4**).

Table A2.4. Crystal data and structure refinement for [SiP^{iPr}_3]Ru(PMe_3) (**3.5**).

Identification code	d8-08083finalfull	
Empirical formula	C39 H63 P4 Ru Si	
Formula weight	784.93	
Temperature	100(2) K	
Wavelength	1.54178 Å	
Crystal system	Monoclinic	
Space group	P2(1)/n	
Unit cell dimensions	a = 12.5281(4) Å	α = 90°.
	b = 19.2082(7) Å	β = 90.860(2)°.
	c = 16.4422(6) Å	γ = 90°.
Volume	3956.2(2) $Å^3$	
Z	4	
Density (calculated)	1.318 Mg/m^3	
Absorption coefficient	5.211 mm^{-1}	
F(000)	1660	
Crystal size	0.35 x 0.30 x 0.02 mm^3	
Theta range for data collection	3.54 to 65.08°.	
Index ranges	-14≤h≤14, -22≤k≤22, -15≤l≤19	
Reflections collected	47128	
Independent reflections	6540 [R(int) = 0.0425]	
Completeness to theta = 65.08°	96.9%	
Absorption correction	Semi-empirical from equivalents	
Max. and min transmission	0.9030 and 0.2628	
Refinement method	Full-matrix least-squares on F^2	
Data / restraints / parameters	6540 / 0 / 421	
Goodness-of-fit on F^2	1.036	
Final R indices [I > 2sigma(I)]	R1 = 0.0284, wR2 = 0.0740	
R indices (all data)	R1 = 0.0319, wR2 = 0.0767	
Largest diff. peak and hole	1.092 and -0.338 e.$Å^{-3}$	

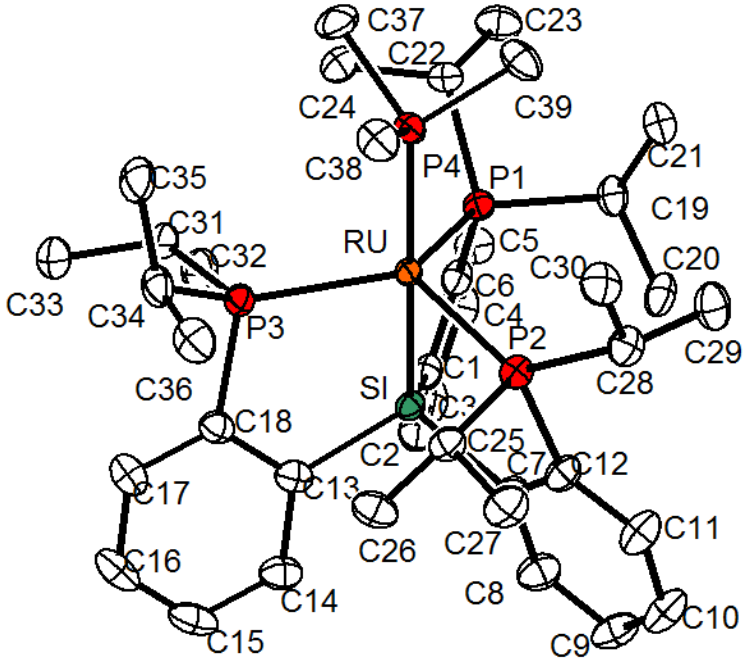

Figure A2.3. Solid-state structure of [SiP$^{iPr}_3$]Ru(PMe$_3$) (**3.5**).

Table A2.5. Crystal data and structure refinement for $\{[SiP^{iPr}_3]Ru(N_2)\}^+BAr^F_4^-$ (**3.7**)

Identification code	d9-09004	
Empirical formula	C69.50 H69 B Cl3 F24 N2 P3 Ru Si	
Formula weight	1727.50	
Temperature	100(2) K	
Wavelength	0.71073 Å	
Crystal system	Monoclinic	
Space group	P2(1)/n	
Unit cell dimensions	a = 18.9178(17) Å	α = 90°.
	b = 14.7491(13) Å	β = 97.260(2)°.
	c = 26.802(2) Å	γ = 90°.
Volume	7418.3(11) $Å^3$	
Z	4	
Density (calculated)	1.547 Mg/m^3	
Absorption coefficient	0.504 mm^{-1}	
F(000)	3500	
Crystal size	0.30 x 0.20 x 0.10 mm^3	
Theta range for data collection	1.41 to 29.57°.	
Index ranges	-26≤h≤26, -20≤k≤20, -37≤l≤37	
Reflections collected	194723	
Independent reflections	20830 [R(int) = 0.0611]	
Completeness to theta = 29.57°	100.0%	
Absorption correction	Semi-empirical from equivalents	
Max. and min transmission	0.9514 and 0.8636	
Refinement method	Full-matrix least-squares on F^2	
Data / restraints / parameters	20830 / 2122 / 1052	
Goodness-of-fit on F^2	1.042	
Final R indices [I > 2sigma(I)]	R1 = 0.0421, wR2 = 0.1033	
R indices (all data)	R1 = 0.0578, wR2 = 0.1149	
Absolute structure parameter		
Largest diff. peak and hole	0.976 and -0.901 e.$Å^{-3}$	

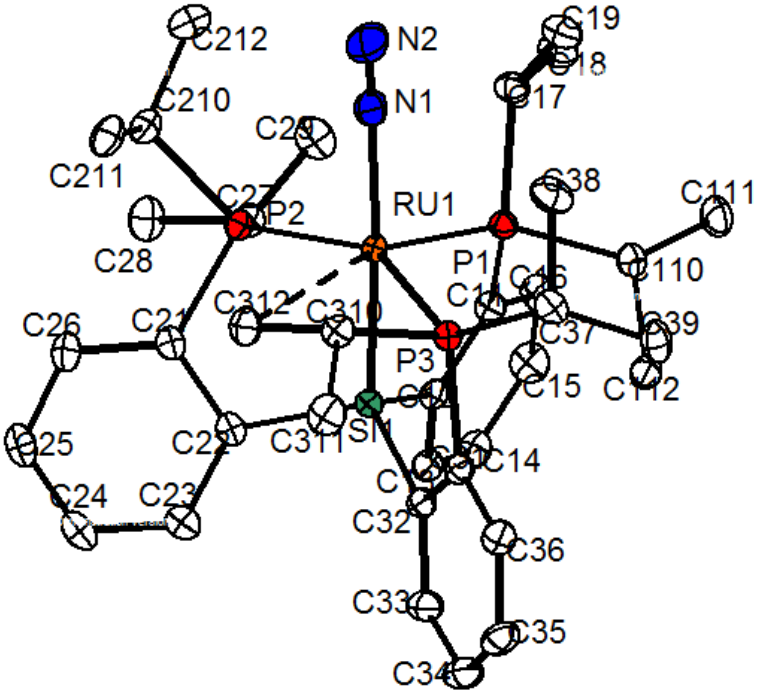

Figure A2.4. Solid-state structure of $\{[SiP^{iPr}_3]Ru(N_2)\}^+BAr^F_4^-$ (**3.7**).

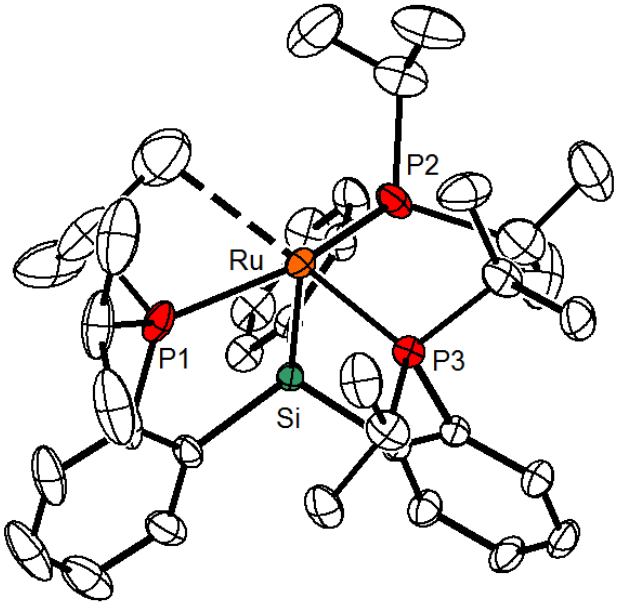

Figure A2.5. A crystal grown at RT by layering a concentrated THF solution of **3.7** over pentane.

Ru-Si1	2.2662(9)	Ru-P1	2.3695(9)
Ru-P2	2.4138(9)	Ru-P3	2.2576(8)
Ru-C21	2.615(3)	τ = 0.31 (distorted SQP)	

Table A2.6. Crystal data and structure refinement for {[SiP$^{iPr}_3$]Ru(N_2)}$^-K^+(THF)_2$ (**3.8**).

Identification code	08353	
Empirical formula	C44 H77 K N2 O2 P3 Ru Si	
Formula weight	917.17	
Temperature	100(2) K	
Wavelength	0.71073 Å	
Crystal system	Triclinic	
Space group	P-1	
Unit cell dimensions	a = 10.5052(10) Å	α = 97.113(2)°.
	b = 11.4116(11) Å	β = 97.168(2) °.
	c = 19.7474(18) Å	γ = 95.718(2)°.
Volume	2314.8(4) Å^3	
Z	1	
Density (calculated)	1.316 Mg/m^3	
Absorption coefficient	0.595 mm^{-1}	
F(000)	966	
Crystal size	0.40 x 0.15 x 0.10 mm^3	
Theta range for data collection	1.05 to 28.28°.	
Index ranges	-13≤h≤13, -15≤k≤15, -26≤l≤26	
Reflections collected	56515	
Independent reflections	11454 [R(int) = 0.0400]	
Completeness to theta = 66.59°	99.8%	
Absorption correction	Semi-empirical from equivalents	
Max. and min transmission	0.9429 and 0.7969	
Refinement method	Full-matrix least-squares on F^2	
Data / restraints / parameters	11454 / 487 / 578	
Goodness-of-fit on F^2	1.179	
Final R indices [I > 2sigma(I)]	R1 = 0.0411, wR2 = 0.1029	
R indices (all data)	R1 = 0.0490, wR2 = 0.1080	
Absolute structure parameter		
Largest diff. peak and hole	1.222 and -1.159 e.Å^{-3}	

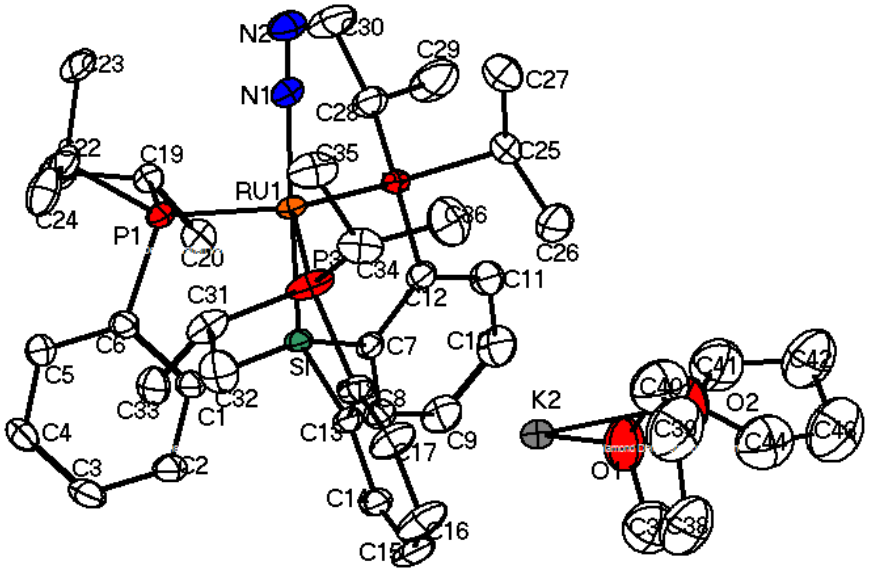

Figure A2.6. Solid-state structure of $\{[SiP^{iPr}_3]Ru(N_2)\}^{-}K^{+}(THF)_2$ (**3.8**).

Table A2.7. Crystal data and structure refinement for {[SiP^{iPr}_3]Os(N_2)}$^-K^+(THF)_2$ (**3.9**).

Identification code	09096b	
Empirical formula	C44 H70 K N2 O2 Os P3 Si	
Formula weight	1009.32	
Temperature	100(2) K	
Wavelength	0.71073 Å	
Crystal system	Triclinic	
Space group	P-1	
Unit cell dimensions	a = 10.5143(16) Å	α = 97.110(3)°.
	b = 11.4249(17) Å	β = 97.274(2)°.
	c = 19.698(3) Å	γ = 95.651(2)°.
Volume	2313.4(6) $Å^3$	
Z	2	
Density (calculated)	1.449 Mg/m^3	
Absorption coefficient	3.012 mm^{-1}	
F(000)	1036	
Crystal size	0.35 x 0.30 x 0.08 mm^3	
Theta range for data collection	1.05 to 30.03°.	
Index ranges	-14≤h≤14, -16≤k≤16, -27≤l≤27	
Reflections collected	63054	
Independent reflections	13444 [R(int) = 0.0338]	
Completeness to theta = 66.59°	99.5%	
Absorption correction	Semi-empirical from equivalents	
Max. and min transmission	0.7946 and 0.4187	
Refinement method	Full-matrix least-squares on F^2	
Data / restraints / parameters	13444 / 389 / 550	
Goodness-of-fit on F^2	1.194	
Final R indices [I > 2sigma(I)]	R1 = 0.0324, wR2 = 0.0853	
R indices (all data)	R1 = 0.0364, wR2 = 0.0878	
Absolute structure parameter		
Largest diff. peak and hole	2.387 and -1.960 e.$Å^{-3}$	

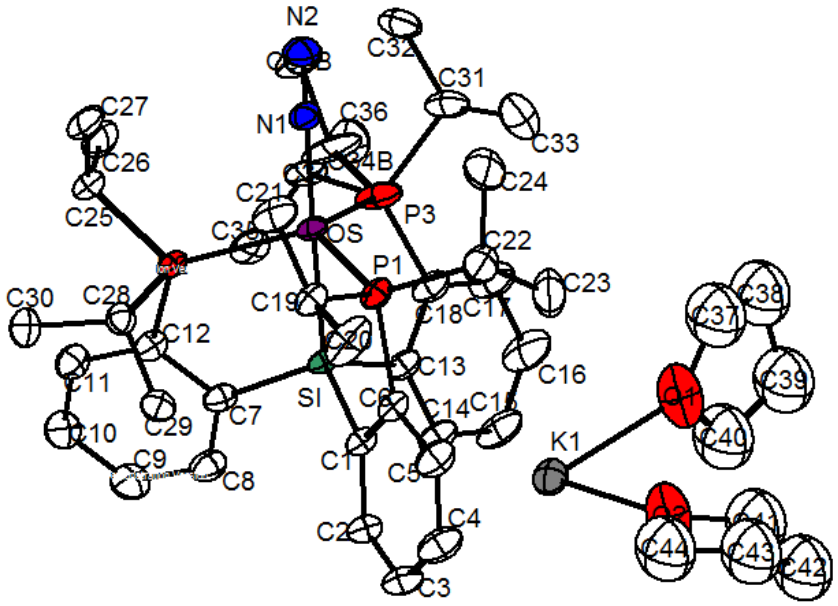

Figure A2.7. Solid-state structure of {[SiP$^{iPr}_3$]Os(N_2)}$^-K^+(THF)_2$ (**3.9**).

Table A2.8. Crystal data and structure refinement for [SiP^{iPr}_3]Ru(H)(N_2) (**3.10**).

Identification code	08293	
Empirical formula	C36 H55 N2 P3 Ru Si	
Formula weight	737.89	
Temperature	100(2) K	
Wavelength	0.71073 Å	
Crystal system	Orthorhombic	
Space group	P2(1)2(1)2(1)	
Unit cell dimensions	a = 11.1005(6) Å	α = 90°.
	b = 15.6559(8) Å	β = 90°.
	c = 20.9624(11) Å	γ = 90°.
Volume	3643.0(3) $Å^3$	
Z	4	
Density (calculated)	1.345 Mg/m^3	
Absorption coefficient	0.622 mm^{-1}	
F(000)	1552	
Crystal size	0.30 x 0.20 x 0.15 mm^3	
Theta range for data collection	1.62 to 29.57°.	
Index ranges	-15≤h≤15, -21≤k≤21, -29≤l≤29	
Reflections collected	77775	
Independent reflections	10226 [R(int) = 0.0630]	
Completeness to theta = 29.57°	100.0%	
Absorption correction	Semi-empirical from equivalents	
Max. and min transmission	0.9124 and 0.8353	
Refinement method	Full-matrix least-squares on F^2	
Data / restraints / parameters	10226 / 0 / 403	
Goodness-of-fit on F^2	0.733	
Final R indices [I > 2sigma(I)]	R1 = 0.0281, wR2 = 0.0853	
R indices (all data)	R1 = 0.0324, wR2 = 0.0918	
Absolute structure parameter	-0.027(17)	
Largest diff. peak and hole	0.667 and -0.387 e.$Å^{-3}$	

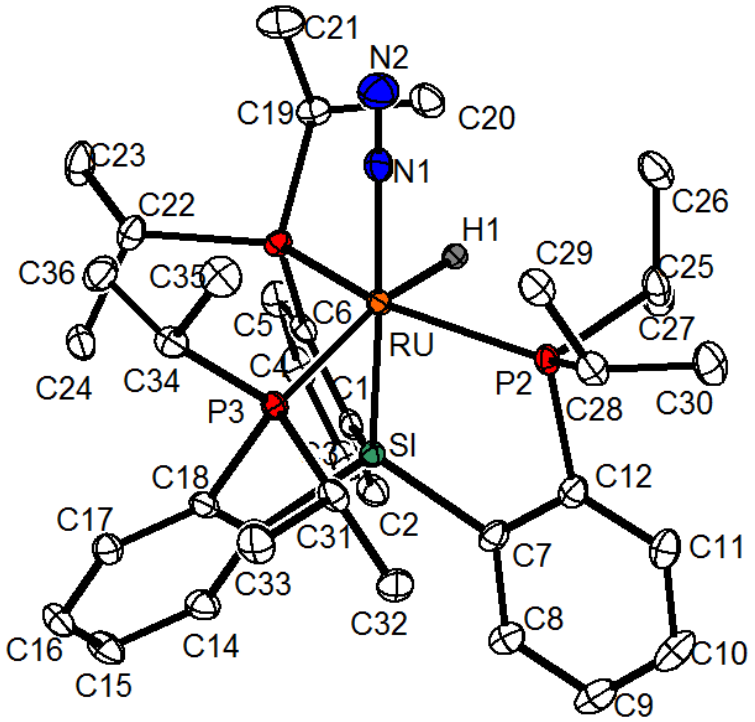

Figure A2.8. Solid-state structure of [SiP$^{iPr}_3$]Ru(H)(N_2) (**3.10**).

Table A2.9. Crystal data and structure refinement for [SiP$^{i\text{Pr}}_3$]Ru(NAr) Ar = *p*-$C_6H_4CF_3$ (**3.11**).

Identification code	d8-09008	
Empirical formula	C43 H58 F3 N P3 Ru Si	
Formula weight	868.01	
Temperature	100(2) K	
Wavelength	1.54178 Å	
Crystal system	Orthorhombic	
Space group	P2(1)2(1)2(1)	
Unit cell dimensions	a = 13.1112(3) Å	α = 90°.
	b = 15.1411(3) Å	β = 90°.
	c = 21.0181(4) Å	γ = 90°.
Volume	4172.47(15) Å^3	
Z	4	
Density (calculated)	1.431 Mg/m^3	
Absorption coefficient	5.135 mm^{-1}	
F(000)	1872	
Crystal size	0.10 x 0.10 x 0.01 mm^3	
Theta range for data collection	3.60 to 66.59°.	
Index ranges	-15≤h≤13, -18≤k≤18, -25≤l≤25	
Reflections collected	79209	
Independent reflections	7365 [R(int) = 0.0564]	
Completeness to theta = 66.59°	99.9%	
Absorption correction	Semi-empirical from equivalents	
Max. and min transmission	0.9504 and 0.6277	
Refinement method	Full-matrix least-squares on F^2	
Data / restraints / parameters	7365 / 0 / 481	
Goodness-of-fit on F^2	1.012	
Final R indices [I > 2sigma(I)]	R1 = 0.0232, wR2 = 0.0549	
R indices (all data)	R1 = 0.0257, wR2 = 0.0561	
Absolute structure parameter	-0.020(5)	
Largest diff. peak and hole	0.355 and -0.394 e.Å^{-3}	

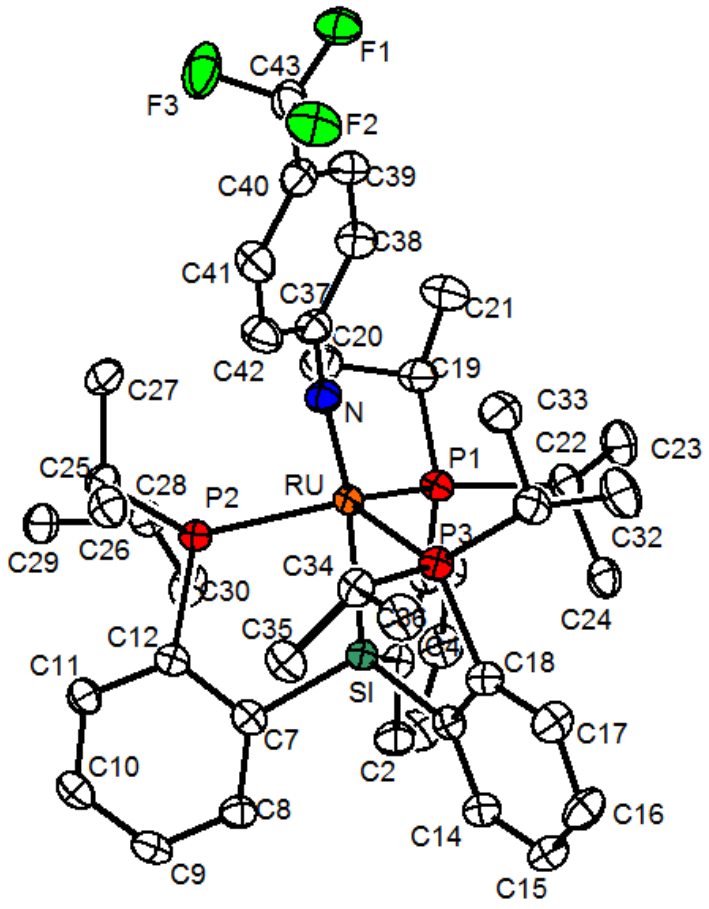

Figure A2.9. Solid-state structure of [SiP$^{iPr}_3$]Ru(NAr) Ar = *p*-$C_6H_4CF_3$ (**3.11**).

Table A2.10. Crystal data and structure refinement for [SiP^{iPr}_3]Os(NAr) Ar = *p*-$C_6H_4CF_3$ (**3.12**).

Identification code	09349	
Empirical formula	C43 H58 F3 N P3 Os Si	
Formula weight	957.10	
Temperature	100(2) K	
Wavelength	0.71073 Å	
Crystal system	Orthorhombic	
Space group	P2(1)2(1)2(1)	
Unit cell dimensions	a = 13.1221(13) Å	α = 90°.
	b = 15.1093(15) Å	β = 90°.
	c = 20.964(2) Å	γ = 90°.
Volume	4156.4(7) $Å^3$	
Z	4	
Density (calculated)	1.529 Mg/m^3	
Absorption coefficient	3.257 mm^{-1}	
F(000)	1940	
Crystal size	0.10 x 0.10 x 0.01 mm^3	
Theta range for data collection	1.66 to 30.03°.	
Index ranges	-18≤h≤18, -21≤k≤21, -28≤l≤29	
Reflections collected	96801	
Independent reflections	12162 [R(int) = 0.0956]	
Completeness to theta = 30.03°	100.0%	
Absorption correction	Semi-empirical from equivalents	
Max. and min transmission	0.7365 and 0.6408	
Refinement method	Full-matrix least-squares on F^2	
Data / restraints / parameters	12162 / 0 / 481	
Goodness-of-fit on F^2	1.071	
Final R indices [I > 2sigma(I)]	R1 = 0.0373, wR2 = 0.0706	
R indices (all data)	R1 = 0.0505, wR2 = 0.0764	
Absolute structure parameter	-0.014(5)	
Largest diff. peak and hole	2.127 and -1.324 e.$Å^{-3}$	

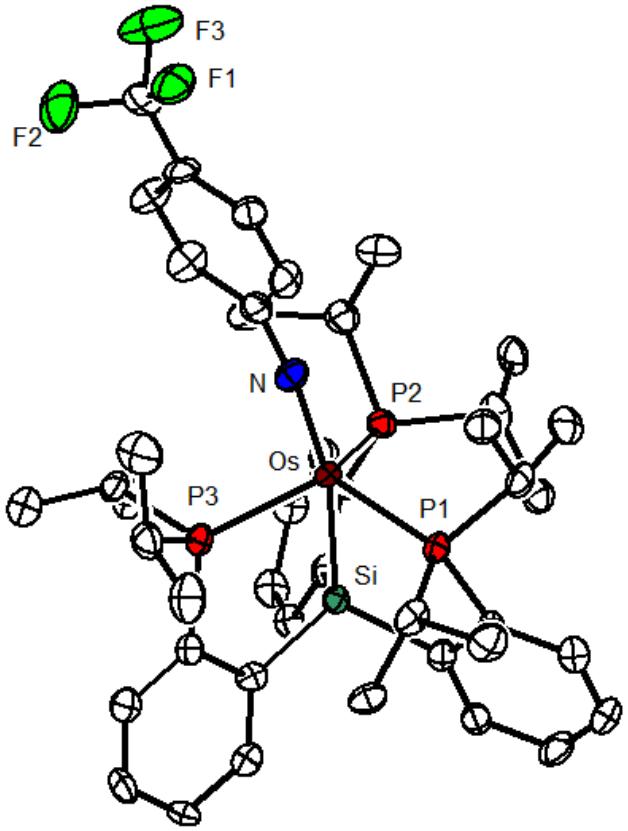

Figure A2.10. Solid-state structure of [SiP$^{iPr}_3$]Os(NAr) Ar = *p*-$C_6H_4CF_3$ (**3.12**).

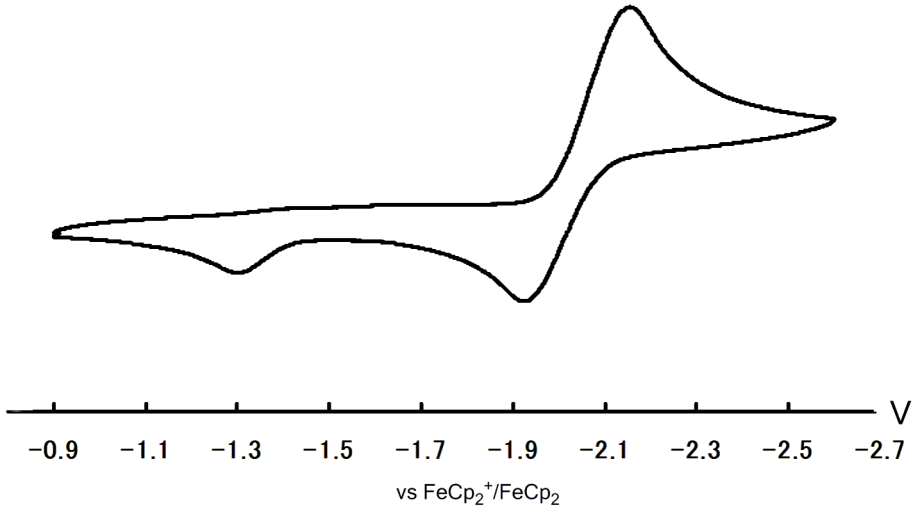

Figure A2.11. CV of [SiP$^{i\text{Pr}}_3$]RuCl (**3.1**) (50 mV/s).

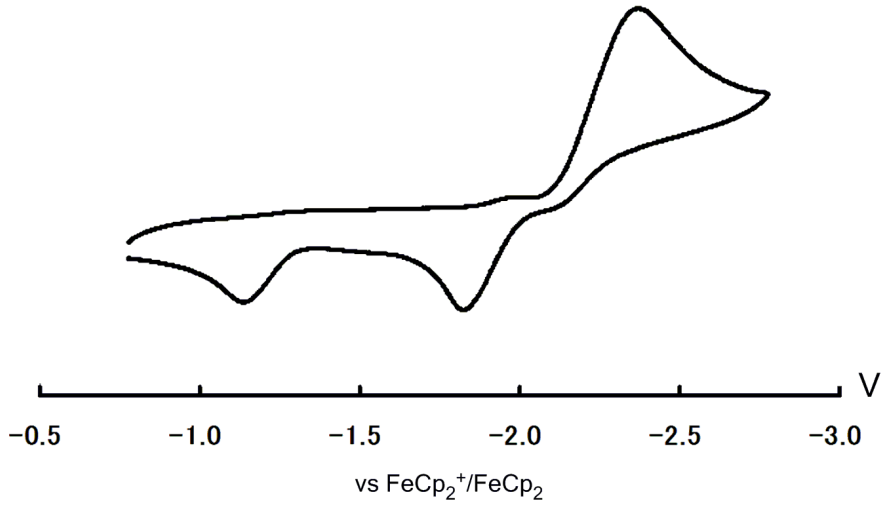

Figure A2.12. CV of [SiP$^{i\text{Pr}}_3$]OsCl (**3.2**) (50 mV/s).

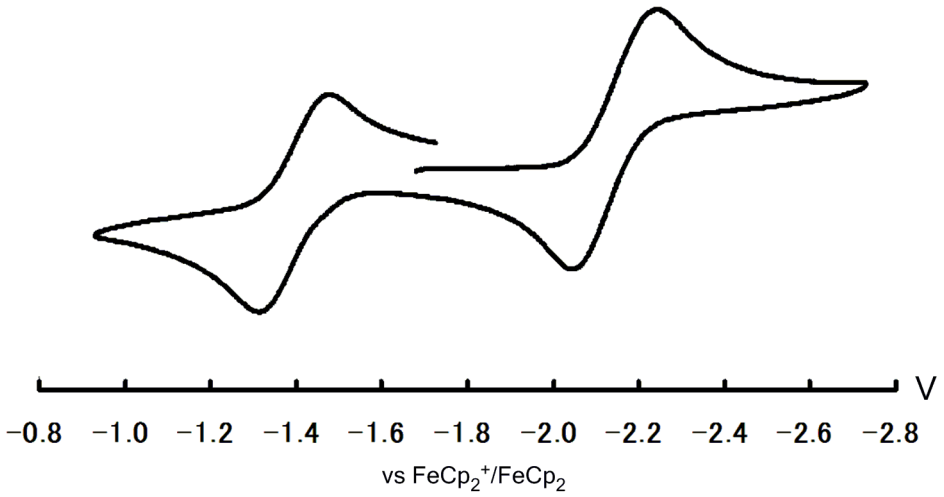

Figure A2.13. CV of $[SiP^{iPr}_3]RuN_2$ (**3.3**) (100 mV/s).

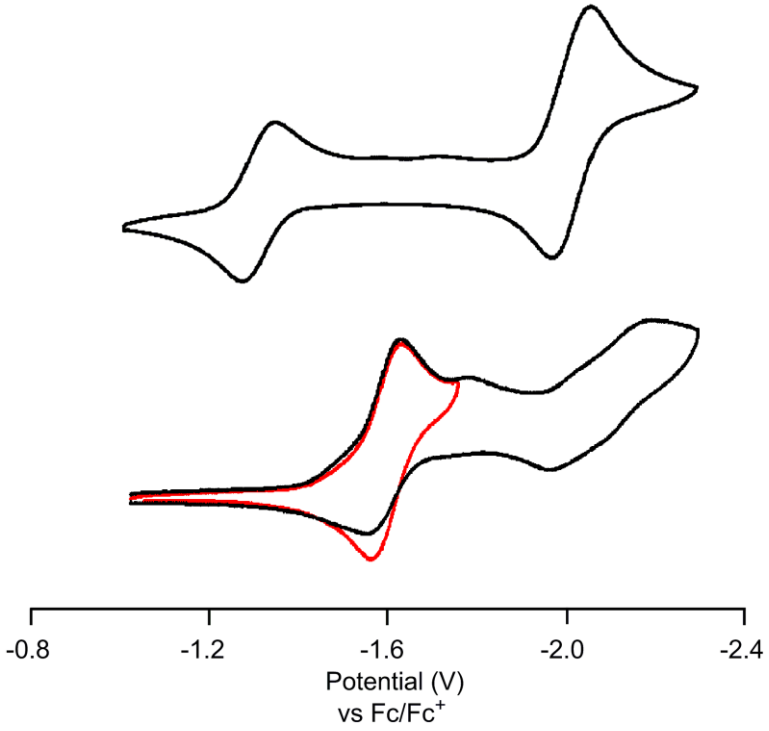

Figure A2.14. CV of $\{[SiP^{iPr}_3]RuN_2\}^+BAr^F_4^-$ (**3.7**) (100 mV/s).

Top: $\{[SiP^{iPr}_3]RuN_2\}^+BAr^F_4^-$ scanned cathodically.

Bottom: $\{[SiP^{iPr}_3]RuN_2\}^+BAr^F_4^-$ under Ar purge. Red curve represents curve when scan is stopped after the first reduction event.

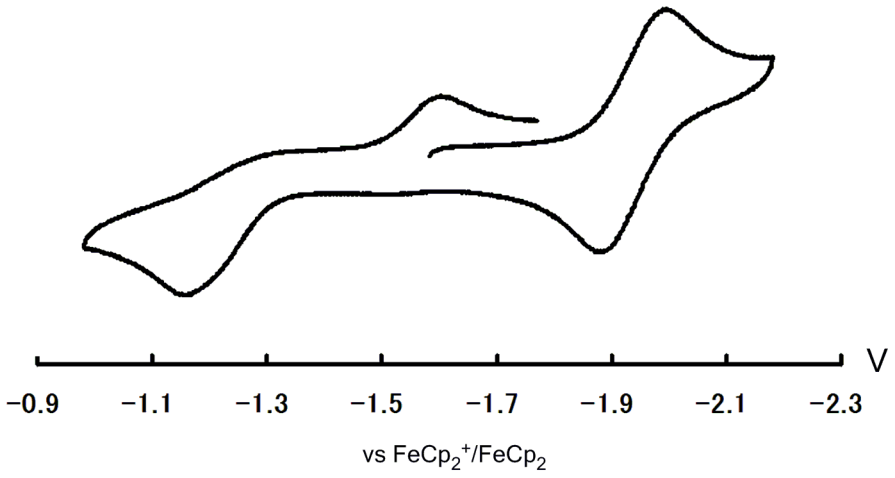

Figure A2.15. CV of [SiP$^{i\text{Pr}}_3$]OsN$_2$ (**3.4**) (50 mV/s).

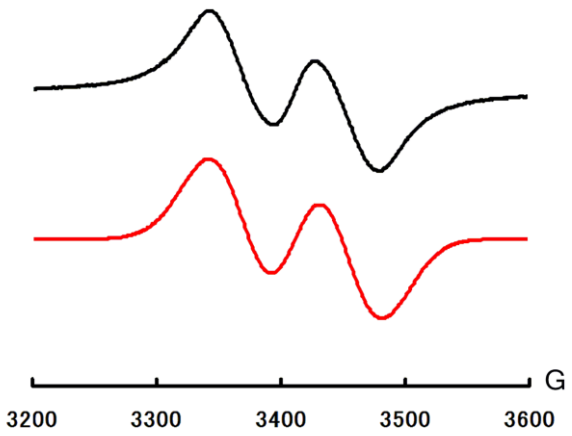

Figure A2.16. X-band RT EPR spectrum of [SiP$^{i\text{Pr}}_3$]RuN$_2$ (**3.3**) in toluene glass (red line: simulation).

Experimental parameters; Microwave power, 0.638 mW; microwave frequency, 9.860 GHz; modulation amplitude, 10 G; gain, 5020.
Simulation parameters: ν = 9.8604 GHz; g = 2.065; For one P atom, A(^{31}P) = 230 MHz; Linewidth, 59 G.

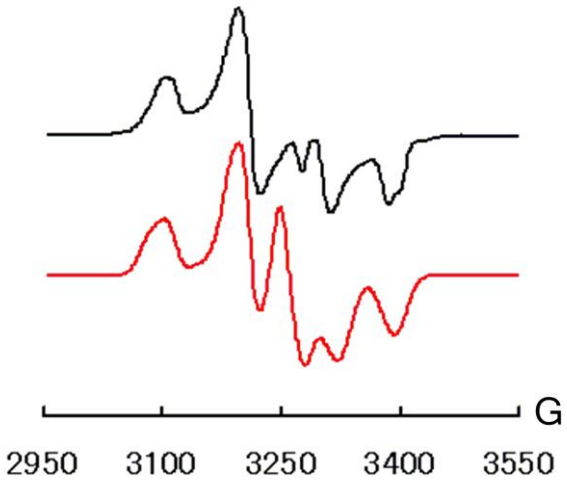

Figure A2.17. X-band 77K EPR spectrum of [SiP$^{i\text{Pr}}_3$]RuN$_2$ (**3.3**).

Experimental parameters; Microwave power, 0.202 mW; microwave frequency, 9.378 GHz; modulation amplitude, 10 G; gain, 1000.
Simulation parameters: ν = 9.378 GHz; g_x = 2.130, g_y = 2.076, g_z = 1.995; For one P atom, A_x(^{31}P) = 200 MHz, A_y(^{31}P) = 140 MHz, A_z(^{31}P) = 200 MHz; For two P atoms, A_x(^{31}P) = 70 MHz, A_y(^{31}P) = 45 MHz, A_z(^{31}P) = 40 MHz; Linewidth, W_x = 16 G, W_y = 11 G, W_z = 11 G.

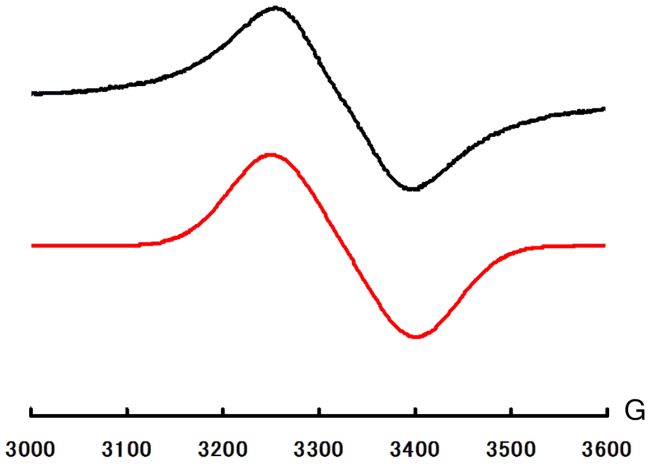

Figure A2.18. X-band RT EPR spectrum of [SiP$^{i\text{Pr}}_3$]OsN$_2$ (**3.4**) in toluene glass (red line: simulation).

Experimental parameters; Microwave power, 1.011 mW; microwave frequency, 9.860 GHz; modulation amplitude, 10 G; gain, 1000.
Simulation parameters: ν = 9.860 GHz; g = 2.118; For one P atom, A(^{31}P) = 220 MHz; Linewidth, 74 G.

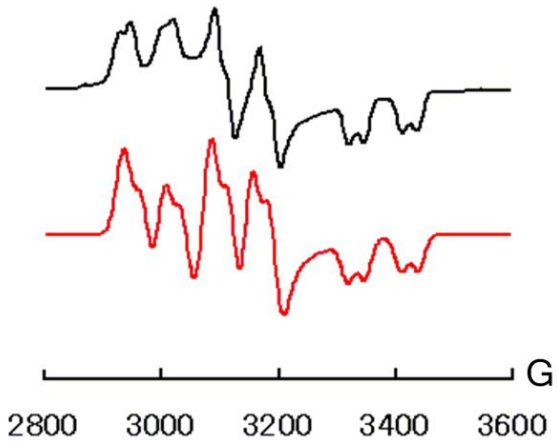

Figure A2.19. X-band 77K EPR spectrum of [SiP$^{i\text{Pr}}_3$]Os(N$_2$) (**3.4**).

Experimental parameters; Microwave power, 0.636 mW; microwave frequency, 9.377 GHz; modulation amplitude, 10 G; gain, 1000.
Simulation parameters: ν = 9.377 GHz; g_x = 2.239, g_y = 2.133, g_z = 1.982; For one P atom, $A_x(^{31}P)$ = 220 MHz, $A_y(^{31}P)$ = 210 MHz, $A_z(^{31}P)$ = 260 MHz; For one P atom, $A_x(^{31}P)$ = 90 MHz, $A_y(^{31}P)$ = 85 MHz, $A_z(^{31}P)$ = 80 MHz; Linewidth, W_x = 16 G, W_y = 15.5 G, W_z = 12.5 G.

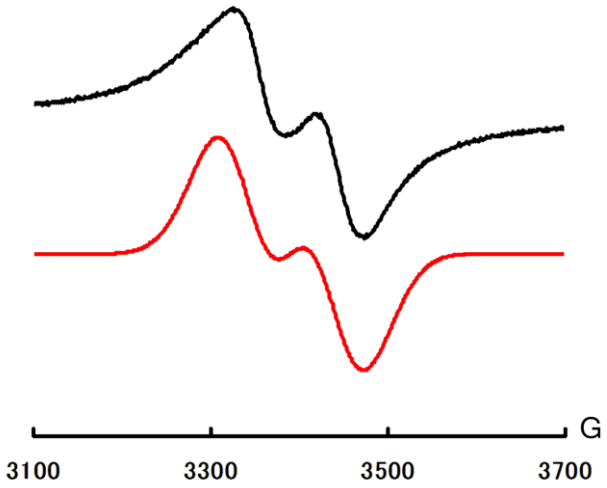

Figure A2.20. X-band RT EPR spectrum of [SiP$^{iPr}_3$]Ru(PMe$_3$) (**3.5**) in toluene glass (red line: simulation).

Experimental parameters; Microwave power, 1.598 mW; microwave frequency, 9.860 GHz; modulation amplitude, 10 G; gain, 22400.
Simulation parameters: ν = 9.8597 GHz; g = 2.078; For one P atom, A(^{31}P) = 260 MHz; Linewidth, 86 G.

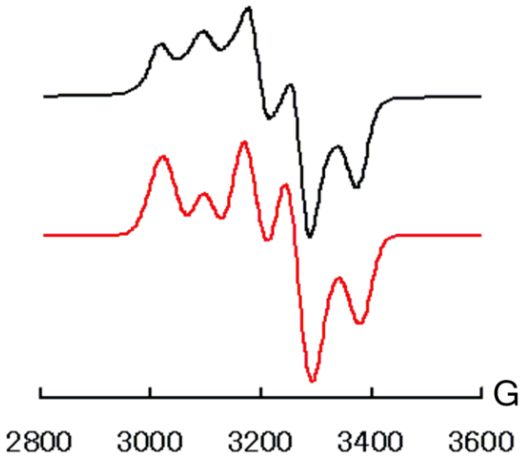

Figure A2.21. X-band 77K EPR spectrum of [SiP$^{iPr}_3$]Ru(PMe$_3$) (**3.5**).

Experimental parameters; Microwave power, 0.801 mW; microwave frequency, 9.375 GHz; modulation amplitude, 10 G; gain, 502.
Simulation parameters: ν = 9.375 GHz; g_x = 2.175, g_y = 2.075, g_z = 2.009; For one P atom, A_x(^{31}P) = 220 MHz, A_y(^{31}P) = 230 MHz, A_z(^{31}P) = 250 MHz ; For two P atoms, A_x(^{31}P) = 40 MHz, A_y(^{31}P) = 50 MHz, A_z(^{31}P) = 40 MHz; Linewidth, W_x = 28 G, W_y = 28 G, W_z = 20 G.

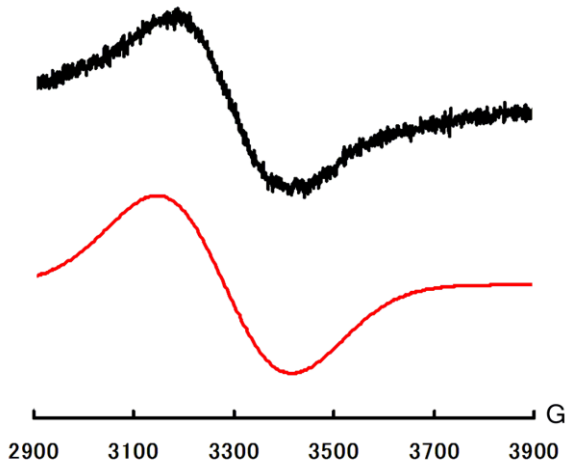

Figure A2.22. X-band RT EPR spectrum of [SiP$^{iPr}_3$]Os(PMe$_3$) (**3.6**) in toluene glass (red line: simulation).

Experimental parameters; Microwave power, 0.801 mW; microwave frequency, 9.860 GHz; modulation amplitude, 10 G; gain, 50200.
Simulation parameters: ν = 9.860 GHz; g = 2.147; Linewidth, 270 G.

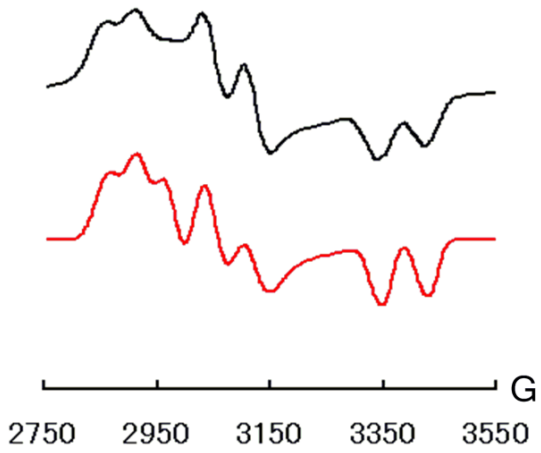

Figure A2.23. X-band 77K EPR spectrum of [SiP$^{iPr}_3$]Os(PMe$_3$) (**3.6**).

Experimental parameters; Microwave power, 0.801 mW; microwave frequency, 9.375 GHz; modulation amplitude, 10 G; gain, 1420.
Simulation parameters: ν = 9.377 GHz; g_x = 2.290, g_y = 2.200, g_z = 1.978; For one P atom, $A_x(^{31}P)$ = 190 MHz, $A_y(^{31}P)$ = 190 MHz, $A_z(^{31}P)$ = 230 MHz; For one P atom, $A_x(^{31}P)$ = 140 MHz, $A_y(^{31}P)$ = 230 MHz, $A_z(^{31}P)$ = 60 MHz; Linewidth, W_x = 27 G, W_y = 30 G, W_z = 15 G.

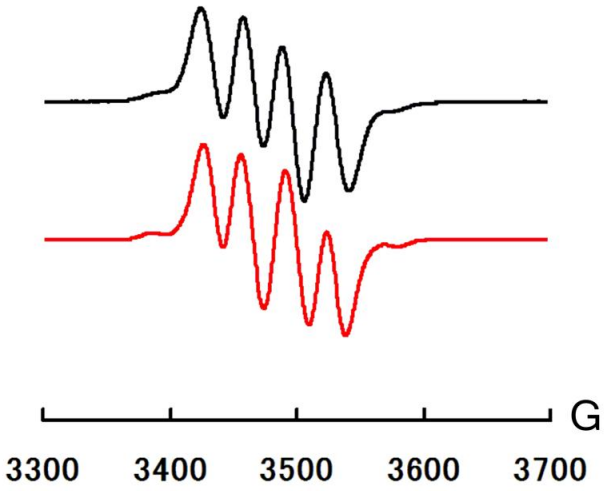

Figure A2.24. X-band RT EPR spectrum of [SiP$^{iPr}_3$]Ru(NAr) Ar = *p*-$C_6H_4CF_3$ (**3.11**) in toluene glass.

Experimental parameters; Microwave power, 3.188 mW; microwave frequency, 9.844 GHz; modulation amplitude, 10 G; gain, 1000.
Simulation parameters: ν = 9.844 GHz; g = 2.020; For one P atom, A(^{31}P) = 64 MHz; For one N atom, A(^{14}N) = 98 MHz; For one Ru atom, A(^{99}Ru, ^{101}Ru) = 48 MHz, Linewidth, 18.5 G.

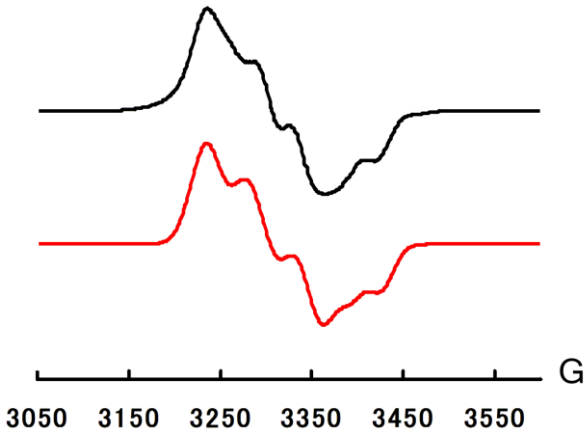

Figure A2.25. X-band EPR spectrum of [SiP$^{iPr}_3$]Ru(NAr) Ar = *p*-$C_6H_4CF_3$ (**3.11**) in toluene glass at 77 K.

Experimental parameters; Microwave power, 1.279 mW; microwave frequency, 9.374 GHz; modulation amplitude, 10 G; gain, 502.
Simulation parameters: ν = 9.374 GHz; g_x = 2.045, g_y = 2.037, g_z = 1.977; For one N atom, A_x(^{14}N) = 80 MHz, A_y(^{14}N) = 140 MHz, A_z(^{14}N) = 90 MHz; Linewidth, W_x = 20 G, W_y = 21 G, W_z = 16 G.

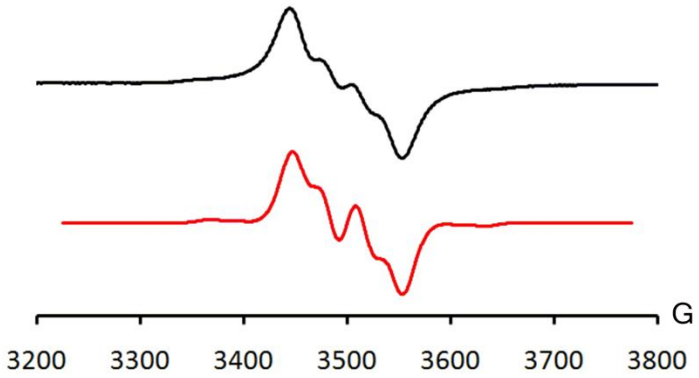

Figure A2.26. X-band RT EPR spectrum of [SiP$^{i\text{Pr}}_3$]Os(NAr) Ar = *p*-$C_6H_4CF_3$ (**3.12**) in toluene glass.

Experimental parameters; Microwave power, 0.127 mW; microwave frequency, 9.861 GHz; modulation amplitude, 10 G; gain, 1590.
Simulation parameters: ν = 9.861 GHz; g = 2.013; For one P atom, A(^{31}P) = 58 MHz; For one N atom, A(^{14}N) = 93 MHz; For one Os atom, A(^{189}Os) = 155 MHz, Linewidth, 25.5 G.

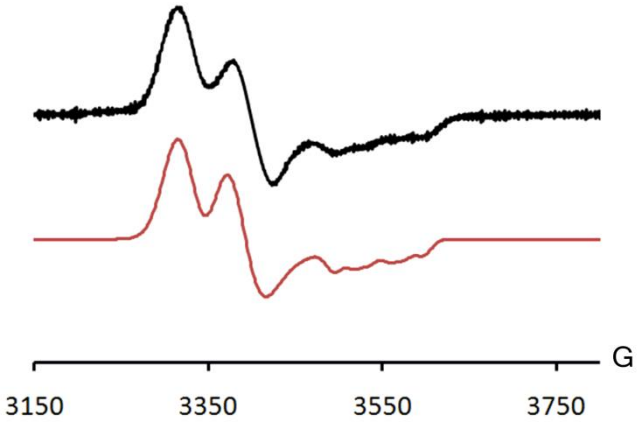

Figure A2.27. X-band EPR spectrum of [SiP$^{i\text{Pr}}_3$]Os (NAr) Ar = *p*-$C_6H_4CF_3$ (**3.12**) in toluene glass at 77 K.

Experimental parameters; Microwave power, 0.636 mW; microwave frequency, 9.654 GHz; modulation amplitude, 10 G; gain, 5020.
Simulation parameters: ν = 9.374 GHz; g_x = 2.073, g_y = 2.039, g_z = 1.945; For one N atom, A_z(^{14}N) = 110 MHz, A_z(^{31}P) = 60 MHz ; Linewidth, W_x = 23 G, W_y = 25 G, W_z = 11 G.

Appendix 3: Supplementary Data for Chapter 4

Table A3.1. Crystal data and structure refinement for {[SiP^{iPr}_3]Co(PMe_3)}BAr^F_4 (**4.1**).

Identification code	ayt17	
Empirical formula	C71 H75 B Co F24 P4 Si	
Formula weight	1606.02	
Temperature	100(2) K	
Wavelength	0.71073 Å	
Crystal system	Monoclinic	
Space group	C2/c	
Unit cell dimensions	a = 38.7112(11) Å	α = 90°.
	b = 14.8630(4) Å	β = 110.296(2).
	c = 29.3525(8) Å	γ = 90°.
Volume	4983.9(9) $Å^3$	
Z	8	
Density (calculated)	1.347 Mg/m^3	
Absorption coefficient	0.407 mm^{-1}	
F(000)	6584	
Crystal size	0.17 x 0.13 x 0.12 mm^3	
Theta range for data collection	2.17 to 24.89°.	
Index ranges	-48≤h≤47, -18≤k≤18, -36≤l≤36	
Reflections collected	150225	
Independent reflections	16140 [R(int) = 0.0918]	
Completeness to theta = 33.13°	99.6%	
Absorption correction	none	
Max. and min transmission		
Refinement method	Full-matrix least-squares on F^2	
Data / restraints / parameters	16140 / 415 / 1047	
Goodness-of-fit on F^2	1.127	
Final R indices [I > 2sigma(I)]	R1 = 0.0587, wR2 = 0.1510	
R indices (all data)	R1 = 0.1009, wR2 = 0.1763	
Largest diff. peak and hole	1.047 and -0.693 e.$Å^{-3}$	

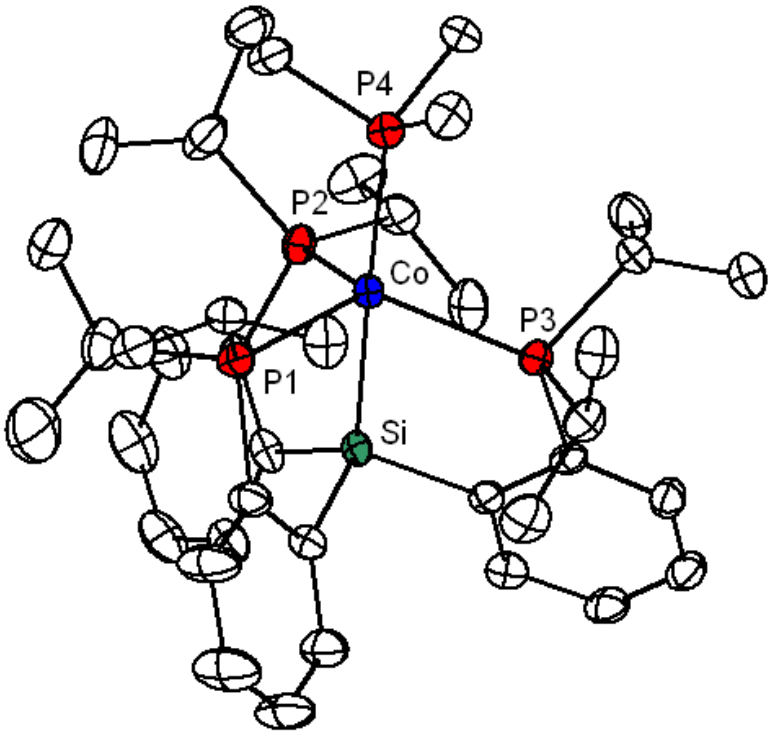

Figure A3.1. Solid-state Structure of {[SiP$^{i\text{Pr}}_3$]Co(PMe$_3$)}BAr$^{\text{F}}_4$ (**4.1**). Hydrogen atoms, BAr$^{\text{F}}_4$ anion, and solvent molecule removed for clarity.

Table A3.2. Crystal data and structure refinement for {[SiP^{iPr}_3]Rh(PMe_3)}BAr^F_4 (**4.2**).

Identification code	ayt16try2	
Empirical formula	C71 H75 B F24 P4 Rh Si	
Formula weight	1650.00	
Temperature	100(2) K	
Wavelength	0.71073 Å	
Crystal system	Monoclinic	
Space group	C2/c	
Unit cell dimensions	a = 38.898(2) Å	α = 90°.
	b = 14.9266(10) Å	β = 110.083(3)°.
	c = 29.4282(19) Å	γ = 90°.
Volume	16047.7(18) $Å^3$	
Z	8	
Density (calculated)	1.366 Mg/m^3	
Absorption coefficient	0.401 mm^{-1}	
F(000)	6728	
Crystal size	0.36 x 0.23 x 0.08 mm^3	
Theta range for data collection	2.16 to 27.83°.	
Index ranges	-55≤h≤55, -21≤k≤21, -42≤l≤42	
Reflections collected	211474	
Independent reflections	24573 [R(int) = 0.0691]	
Completeness to theta = 33.13°	99.7%	
Absorption correction	none	
Max. and min transmission		
Refinement method	Full-matrix least-squares on F^2	
Data / restraints / parameters	24573 / 816 / 1149	
Goodness-of-fit on F^2	0.918	
Final R indices [I > 2sigma(I)]	R1 = 0.0550, wR2 = 0.1662	
R indices (all data)	R1 = 0.0848, wR2 = 0.1931	
Largest diff. peak and hole	2.569 and -0.555 e.$Å^{-3}$	

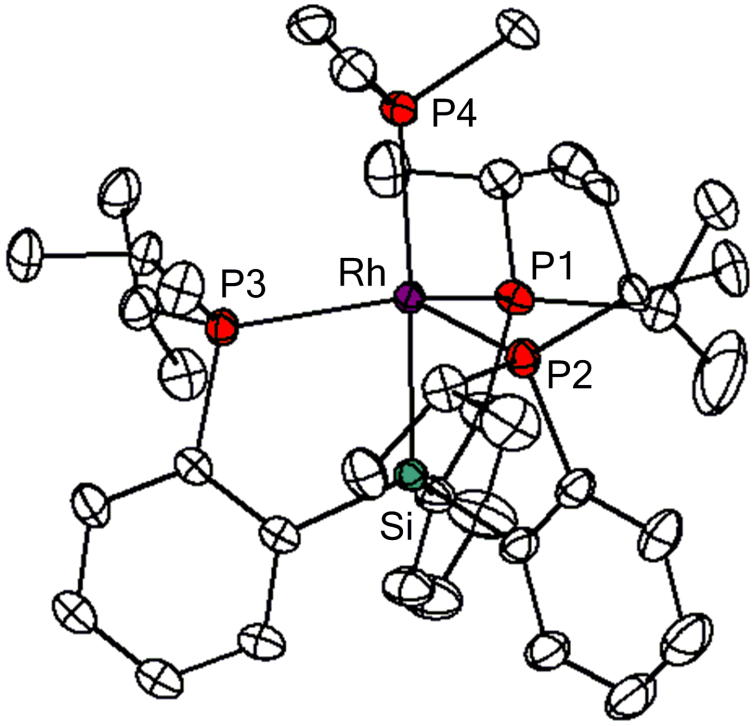

Figure A3.2. Solid-state Structure of {[SiP$^{iPr}_3$]Rh(PMe$_3$)}BAr$^F_4$ (**4.2**). BAr$^F_4$ anion and hydrogen atoms removed for clarity.

Table A3.3. Crystal data and structure refinement for {[SiP^{iPr}_3]Ir(PMe_3)}OTf (**4.3'**).

Identification code	09289	
Empirical formula	C40 H53 Cl4 F3 Ir O3 P4 S Si	
Formula weight	1156.85	
Temperature	100(2) K	
Wavelength	0.71073 Å	
Crystal system	Monoclinic	
Space group	P2(1)/c	
Unit cell dimensions	a = 10.7531(11)Å	α = 90°.
	b = 30.421(3) Å	β = 101.115(2)°.
	c = 15.5269(16) Å	γ = 90°.
Volume	4983.9(9) $Å^3$	
Z	4	
Density (calculated)	1.542 Mg/m^3	
Absorption coefficient	3.133 mm^{-1}	
F(000)	2316	
Crystal size	0.50 x 0.50 x 0.05 mm^3	
Theta range for data collection	2.23 to 28.51°.	
Index ranges	-14≤h≤14, -40≤k≤40, -20≤l≤20	
Reflections collected	101689	
Independent reflections	12377 [R(int) = 0.0637]	
Completeness to theta = 33.13°	100.0%	
Absorption correction	Semi-empirical from equivalents	
Max. and min transmission	0.8591 and 0.3034	
Refinement method	Full-matrix least-squares on F^2	
Data / restraints / parameters	12377 / 57 / 575	
Goodness-of-fit on F^2	1.091	
Final R indices [I > 2sigma(I)]	R1 = 0.0432, wR2 = 0.0973	
R indices (all data)	R1 = 0.0565, wR2 = 0.1044	
Largest diff. peak and hole	2.441 and -1.733 e.$Å^{-3}$	

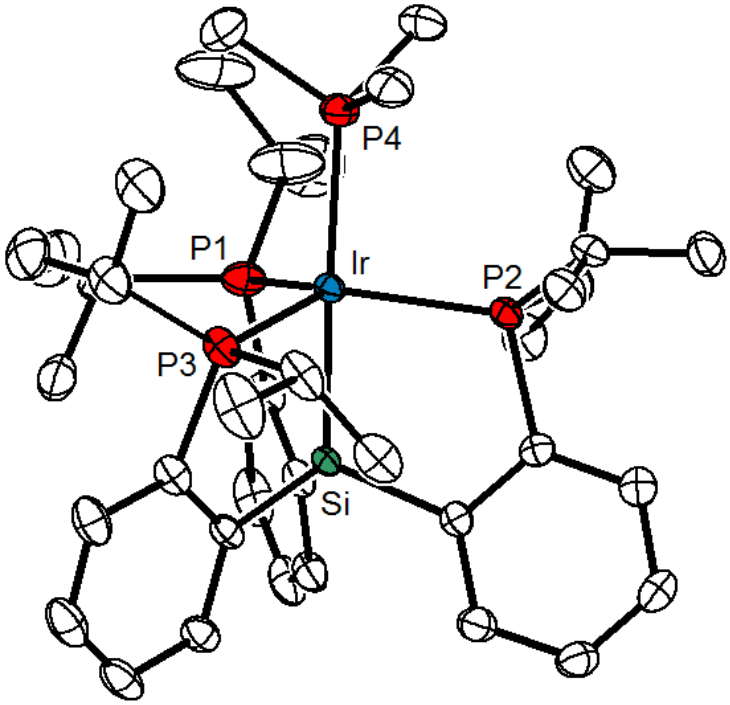

Figure A3.3. Solid-state Structure of {[SiP$^{iPr}_3$]Ir(PMe$_3$)}OTf (**4.3'**). Hydrogen atoms, OTf anion, and solvent molecules removed for clarity.

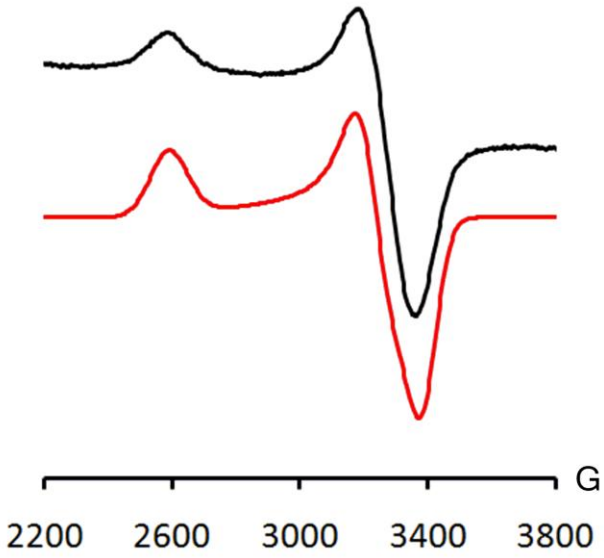

Figure A3.4. 77 K EPR spectrum of {[SiP$^{i\text{Pr}}_3$]Co(PMe$_3$)}BAr$^{\text{F}}_4$ (**4.1**).

Experimental parameters; Microwave power, 0.814 mW; microwave frequency, 9.418 GHz; modulation amplitude, 2 G; gain, 2000.

Simulation parameters: g_x = 2.60, g_y = 2.08, g_z = 1.99; Linewidth, lw = 1; HStrain; W_x = 500 MHz, W_y = 350 MHz, W_z = 300 MHz.

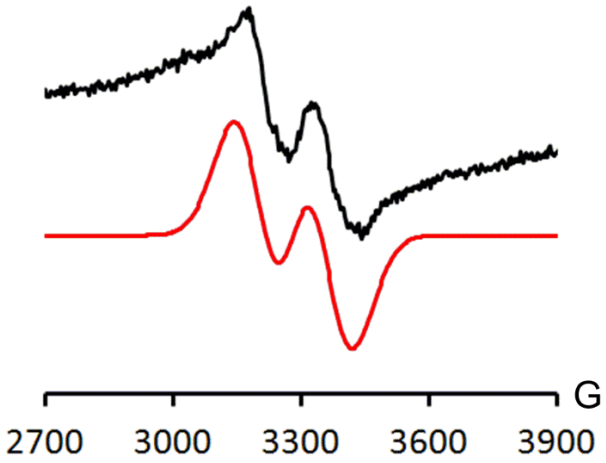

Figure A3.5. RT EPR spectrum of {[SiP$^{iPr}_3$]Rh(PMe$_3$)}BAr$^F_4$ (**4.2**).

Experimental parameters; Microwave power, 2.036 mW; microwave frequency, 9.647 GHz; modulation amplitude, 2 G; gain, 20000.
Simulation parameters: g = 2.10, g_y . Linewidth, lw =15; For 1 P atom, A(P) = 450 MHz.

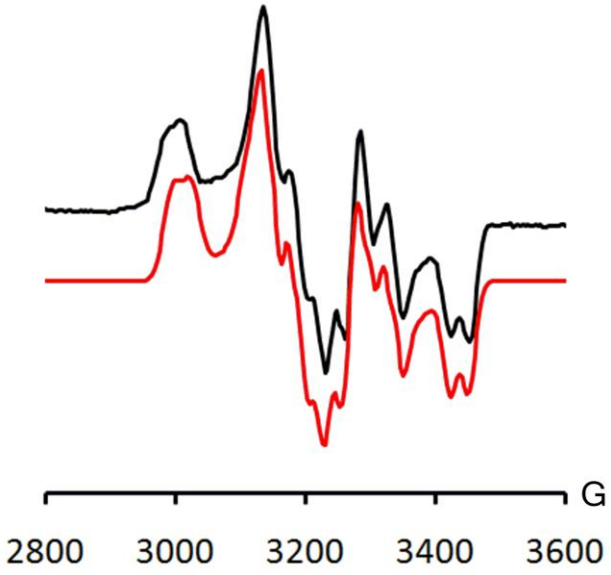

Figure A3.6. 77 K EPR spectrum of {[SiP$^{iPr}_3$]Rh(PMe$_3$)}BAr$^F_4$ (**4.2**).

Experimental parameters; Microwave power, 0.807 mW; microwave frequency, 9.417 GHz; modulation amplitude, 2 G; gain, 2000.
Simulation parameters: g_x = 2.205, g_y = 2.087, g_z = 2.025; For one P atom, A_x(^{31}P) = 360 MHz, A_y(^{31}P) = 430 MHz, A_z(^{31}P) = 550 MHz; For one atom of I = ½ (P or Rh), A_x = 90 MHz, A_y = 115 MHz, A_z = 80 MHz; For one atom of I = ½ (P or Rh), A_x = 1 MHz, A_y = 50 MHz, A_z = 1 MHz. Linewidth, lw =1, HStrain, W$_x$ = 95 MHz, W$_y$ = 50 MHz, W$_z$ = 68 MHz.

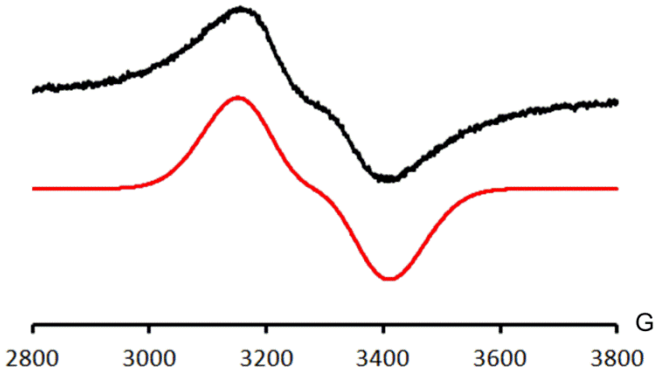

Figure A3.7. RT EPR spectrum of {[SiP$^{iPr}_3$]Ir(PMe$_3$)}BAr$^F_4$ (**4.3**).

Experimental parameters; Microwave power, 0.401 mW; microwave frequency, 9.855 GHz; modulation amplitude, 10 G; gain, 1000.
Simulation parameters: g = 2.145, g_y. Linewidth, lw =17; For 1 P atom, A(P) = 400 MHz.

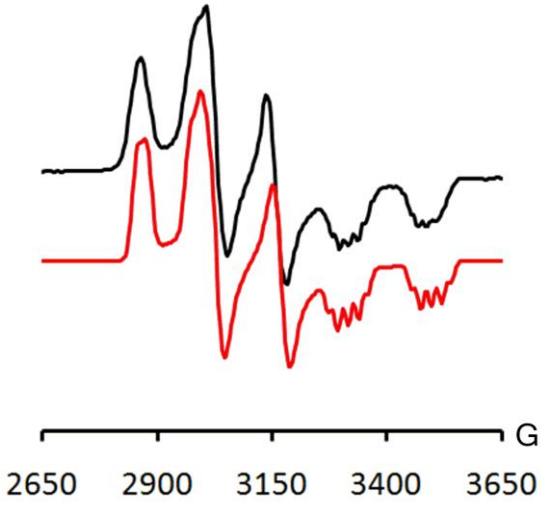

Figure A3.8. 77 K EPR spectrum of {[SiP$^{iPr}_3$]Ir(PMe$_3$)}BAr$^F_4$ (**4.3**).

Experimental parameters; Microwave power, 0.813 mW; microwave frequency, 9.419 GHz; modulation amplitude, 2 G; gain, 2000.
Simulation parameters: g_x = 2.300, g_y = 2.170, g_z = 1.975; For one P atom, A_x(^{31}P) = 370 MHz, A_y(^{31}P) = 430 MHz, A_z(^{31}P) = 500 MHz; For one P atom, A_x (^{31}P) = 70 MHz, A_y (^{31}P) = 30 MHz, A_z (^{31}P) = 50 MHz; For one Ir atom, A_x (Ir) = 1 MHz, A_y = 1 MHz, A_z = 65 MHz. Linewidth, lw =1, HStrain, W_x = 35 MHz, W_y = 90 MHz, W_z = 70 MHz.

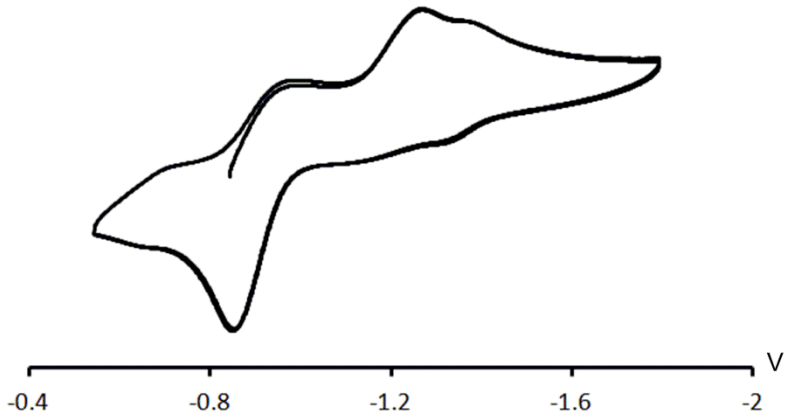

Figure A3.9. Cyclic Voltammogram of {[SiP$^{iPr}_3$]Co(PMe$_3$)}BAr$^F_4$ (**4.1**).

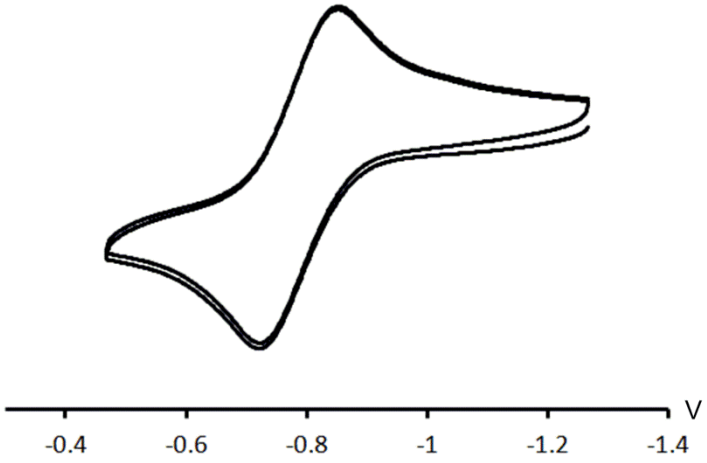

Figure A3.10. Cyclic Voltammogram of [SiP$^{iPr}_3$]Rh(PMe$_3$) (**4.2**).

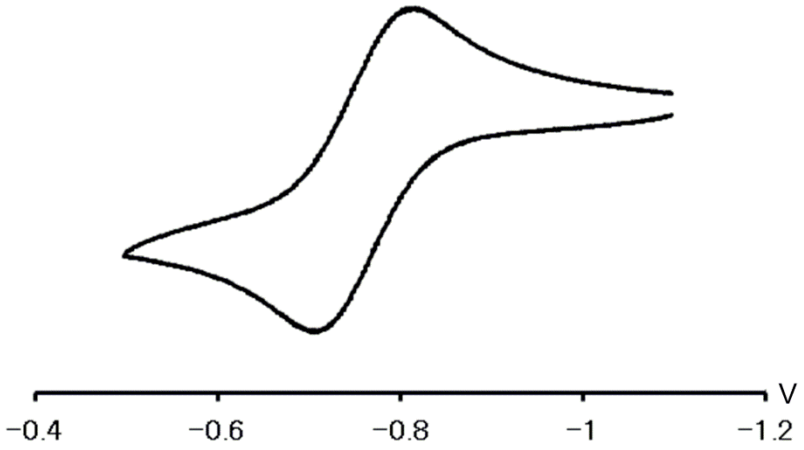

Figure A3.11. Cyclic Voltammogram of [SiP^{iPr}_3]Ir(PMe_3) (**4.3**).

Appendix 4: Supplementary Data for Chapter 5

Table A1.1. Crystal data and structure refinement for {[SiP$^{iPr}_3$]Ru(NAr)}OTf (Ar = $C_6H_4CF_3$, **5.7-CF$_3$**).

Identification code	d8-09018	
Empirical formula	C52 H66 F6 N O5 P3 Ru S Si	
Formula weight	1153.19	
Temperature	100(2) K	
Wavelength	1.54178 Å	
Crystal system	Monoclinic	
Space group	P2(1)/n	
Unit cell dimensions	a = 17.4556(4) Å	α = 90°.
	b = 15.9409(4) Å	β = 110.714(2)°.
	c = 20.2398(5) Å	γ = 90°.
Volume	5267.8(2) Å^3	
Z	4	
Density (calculated)	1.454 Mg/m^3	
Absorption coefficient	4.440 mm^{-1}	
F(000)	2392	
Crystal size	0.48 x 0.25 x 0.02 mm^3	
Theta range for data collection	2.88 to 68.11°.	
Index ranges	-20≤h≤20, -18≤k≤18, -23≤l≤23	
Reflections collected	93228	
Independent reflections	9433 [R(int) = 0.0427]	
Completeness to theta = 33.13°	97.2%	
Absorption correction	Semi-empirical from equivalents	
Max. and min transmission	0.9164 and 0.2244	
Refinement method	Full-matrix least-squares on F^2	
Data / restraints / parameters	8744 / 377 / 751	
Goodness-of-fit on F^2	1.051	
Final R indices [I > 2sigma(I)]	R1 = 0.0337, wR2 = 0.0974	
R indices (all data)	R1 = 0.0355, wR2 = 0.0995	
Largest diff. peak and hole	0.898 and -0.767 e.Å^{-3}	

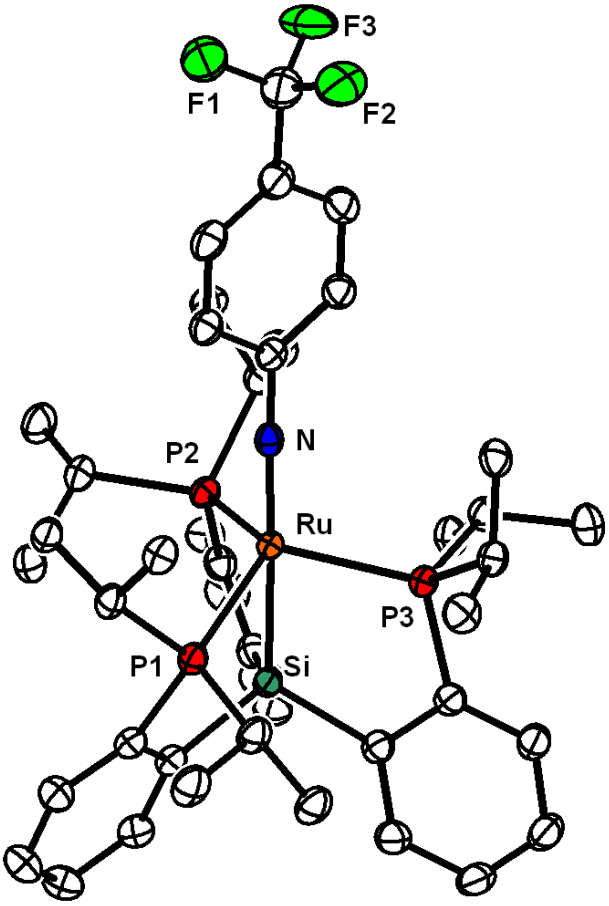

Figure A4.1. Solid-state structure of {[SiP$^{iPr}_3$]Ru(NAr)}OTf (Ar = $C_6H_4CF_3$, **5.7-CF$_3$**).

Anion, H-atoms, and solvent molecules removed for clarity.

Table A4.2. Crystal data and structure refinement for {[SiP^{iPr}_3]Ru(NAr)}BAr^F_4 (Ar = C_6H_4OMe, **5.7-OMe**).

Identification code	09117	
Empirical formula	C75 H66 B F24 N O P3 Ru S Si	
Formula weight	1686.17	
Temperature	100(2) K	
Wavelength	0.71073 Å	
Crystal system	Triclinic	
Space group	P-1	
Unit cell dimensions	a = 13.0069(10) Å	α = 104.3690(10)°.
	b = 15.6351(11) Å	β = 104.2060(10)°.
	c = 20.2288(15) Å	γ = 99.7600°.
Volume	3745.2(5) $Å^3$	
Z	2	
Density (calculated)	1.495 Mg/m^3	
Absorption coefficient	0.394 mm^{-1}	
F(000)	1710	
Crystal size	0.35 x 0.25 x 0.20 mm^3	
Theta range for data collection	2.25 to 29.64°.	
Index ranges	-17≤h≤17, -20≤k≤20, -26≤l≤26	
Reflections collected	89456	
Independent reflections	9920 [R(int) = 0.0490]	
Completeness to theta = 33.13°	99.6%	
Absorption correction	Semi-empirical from equivalents	
Max. and min transmission	0.9254 and 0.8744	
Refinement method	Full-matrix least-squares on F^2	
Data / restraints / parameters	18518 / 0 / 976	
Goodness-of-fit on F^2	1.201	
Final R indices [I > 2sigma(I)]	R1 = 0.0492, wR2 = 0.1511	
R indices (all data)	R1 = 0.0634, wR2 = 0.1654	
Largest diff. peak and hole	1.866and -1.097e.$Å^{-3}$	

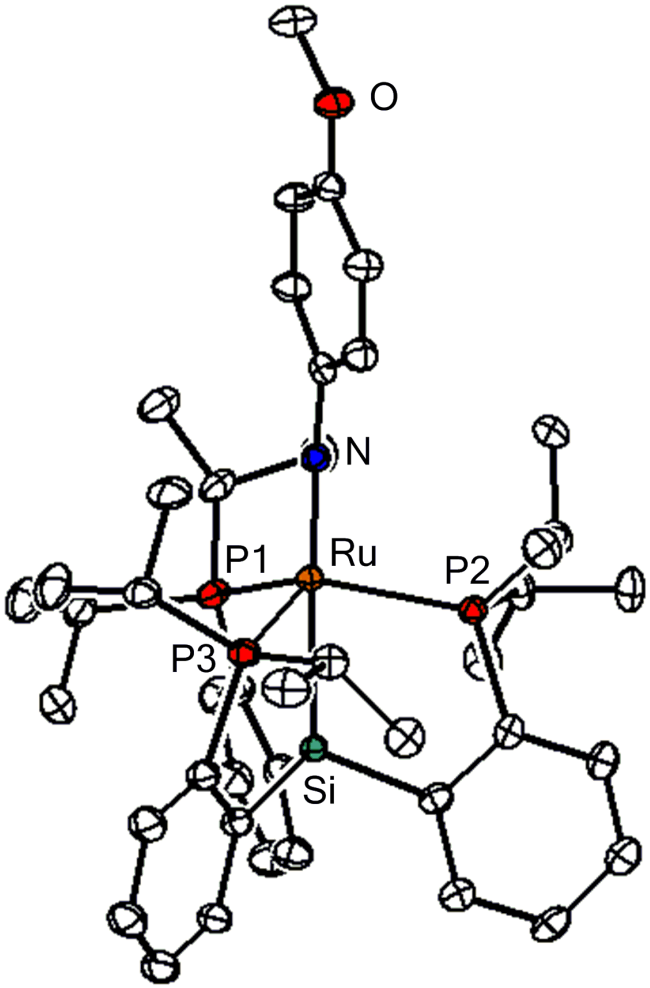

Figure A4.2. Solid-state structure of {[SiP$^{iPr}_3$]Ru(NAr)}OTf (Ar = C_6H_4OMe, **5.7-OMe**).

Anion, H-atoms, and solvent molecules removed for clarity.

Table A4.3. Crystal data and structure refinement for {[SiP^{iPr}_3]Ru(N_3Ar)}BAr^F_4 (Ar = C_6H_4OMe, **5.8-OMe**).

Identification code	09278	
Empirical formula	C75 H73 B F24 N3 O P3 Ru Si	
Formula weight	1721.24	
Temperature	100(2) K	
Wavelength	0.71073 Å	
Crystal system	Monoclinic	
Space group	P2(1)	
Unit cell dimensions	a = 15.1068(14) Å	α = 90.00°.
	b = 15.2076(12) Å	β = 110.504(3)°.
	c = 17.5911(16) Å	γ = 90.00°.
Volume	3785.3(6) $Å^3$	
Z	2	
Density (calculated)	1.510 Mg/m^3	
Absorption coefficient	0.392 mm^{-1}	
F(000)	1752	
Crystal size	0.20 x 0.15 x 0.12 mm^3	
Theta range for data collection	2.20 to 30.07°.	
Index ranges	-21≤h≤20, -21≤k≤21, -24≤l≤24	
Reflections collected	87565	
Independent reflections	9846 [R(int) = 0.0796]	
Completeness to theta = 33.13°	99.9%	
Absorption correction	Semi-empirical from equivalents	
Max. and min transmission	0.9545 and 0.9257	
Refinement method	Full-matrix least-squares on F^2	
Data / restraints / parameters	22047 / 1628 / 1055	
Goodness-of-fit on F^2	1.017	
Final R indices [I > 2sigma(I)]	R1 = 0.0595, wR2 = 0.1309	
R indices (all data)	R1 = 0.0964, wR2 = 0.1515	
Largest diff. peak and hole	1.062 and -0.477 e.$Å^{-3}$	

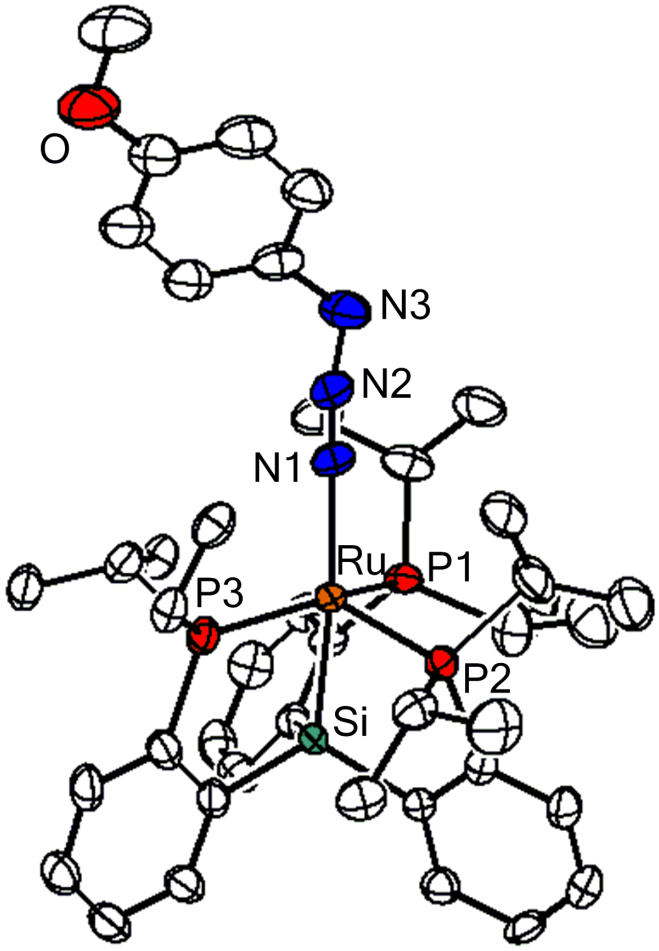

Figure A4.3. Solid-state structure of {[SiP$^{iPr}_3$]Ru(N$_3$Ar)}BAr$^F_4$ (Ar = C_6H_4OMe, **5.8-OMe**).

Anion, H-atoms, and solvent molecules removed for clarity.

Table A4.4. Crystal data and structure refinement for {[$SiP^{iPr}_2P^{iPr}$(=NAr)]Ru}PF_6 (Ar = C_6H_4OMe, **5.10**).

Identification code	ayt14	
Empirical formula	C47 H69 F6 N O2 P4 Ru Si	
Formula weight	1047.07	
Temperature	100(2) K	
Wavelength	0.71073 Å	
Crystal system	Monoclinic	
Space group	P2(1)/c	
Unit cell dimensions	a = 12.6608(6) Å	α = 90.00°.
	b = 13.3290(6) Å	β = 92.074(2)°.
	c = 28.9276(13) Å	γ = 90.00°.
Volume	4878.5(4) $Å^3$	
Z	4	
Density (calculated)	1.426 Mg/m^3	
Absorption coefficient	0.538 mm^{-1}	
F(000)	2184	
Crystal size	0.38 x 0.30 x 0.29 mm^3	
Theta range for data collection	2.35 to 44.31°.	
Index ranges	-25≤h≤25, -26≤k≤26, -56≤l≤57	
Reflections collected	350218	
Independent reflections	9918 [R(int) = 0.0428]	
Completeness to theta = 33.13°	99.5%	
Absorption correction	Semi-empirical from equivalents	
Max. and min transmission	0.8595 and 0.8215	
Refinement method	Full-matrix least-squares on F^2	
Data / restraints / parameters	40397 / 474 / 636	
Goodness-of-fit on F^2	1.062	
Final R indices [I > 2sigma(I)]	R1 = 0.0386, wR2 = 0.1005	
R indices (all data)	R1 = 0.0560, wR2 = 0.1133	
Largest diff. peak and hole	2.275 and -1.046 e.$Å^{-3}$	

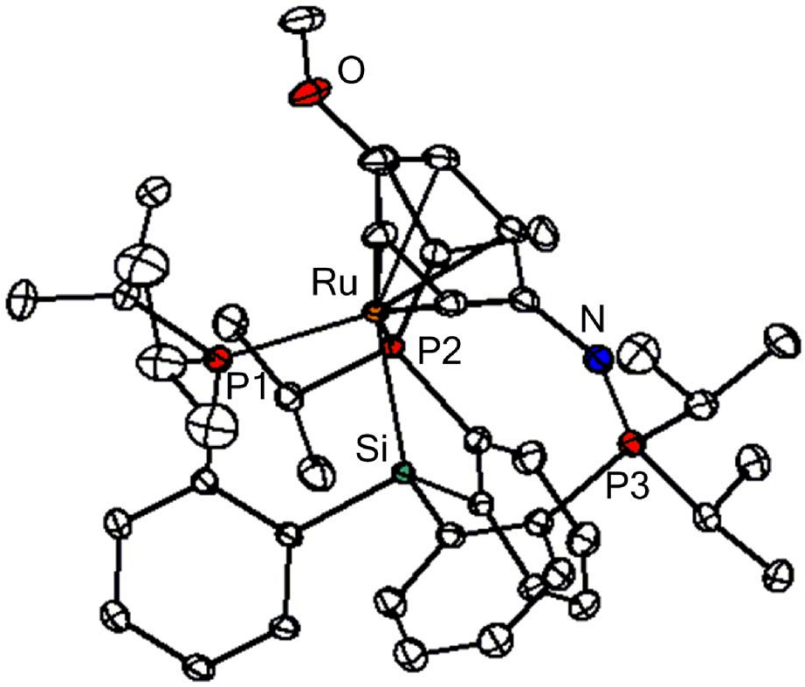

Figure A4.4. Solid-state structure of {[SiP$^{iPr}_2$P^{iPr}(=NAr)]Ru}PF_6 (Ar = C_6H_4OMe, **5.10**).

Anion, H-atoms, solvent molecules removed for clarity.

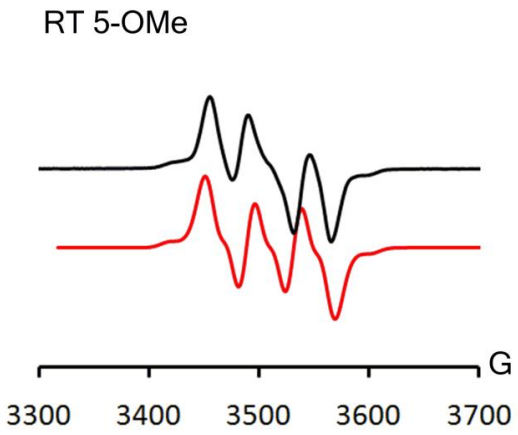

Figure A4.5. RT EPR spectrum of [SiP$^{i\text{Pr}}_3$]Ru(NAr), Ar = *p*-C_6H_4OMe (**5.5-OMe**).

Experimental parameters; Microwave power, 1.011 mW; microwave frequency, 9.847 GHz; modulation amplitude, 10 G; gain, 1000; time constant, 2.560 ms. Simulation parameters: g = 2.002. For 1 N atom, A(^{14}N) = 119 MHz. For 1 P atom, A(^{31}P) = 48 MHz. For 1 Ru atom, A(^{99}Ru) = A(^{101}Ru) = 38 MHz.

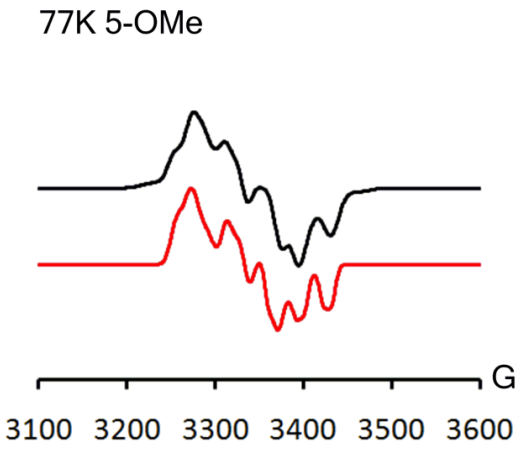

Figure A4.6. 77 K EPR spectrum of [SiP$^{i\text{Pr}}_3$]Ru(NAr), Ar = *p*-C_6H_4OMe (**5.5-OMe**)

Experimental parameters; Microwave power, 0.172 mW; microwave frequency, 9.373 GHz; modulation amplitude, 10 G; gain, 1000; time constant, 2.560.
Simulation parameters: g_x = 2.035, g_y = 2.014, g_z = 1.972; For one P atom, A_x(^{31}P) = 40 MHz, A_y(^{31}P) = 40 MHz, A_z(^{31}P) = 20 MHz; For one N atom, A(^{14}N)$_x$ = 80 MHz, A(^{14}N)$_y$ = 105 MHz, A(^{14}N)$_z$ = 90 MHz; lw =1, HStrain, W_x = 35 MHz, W_y = 35 MHz, W_z = 10 MHz.

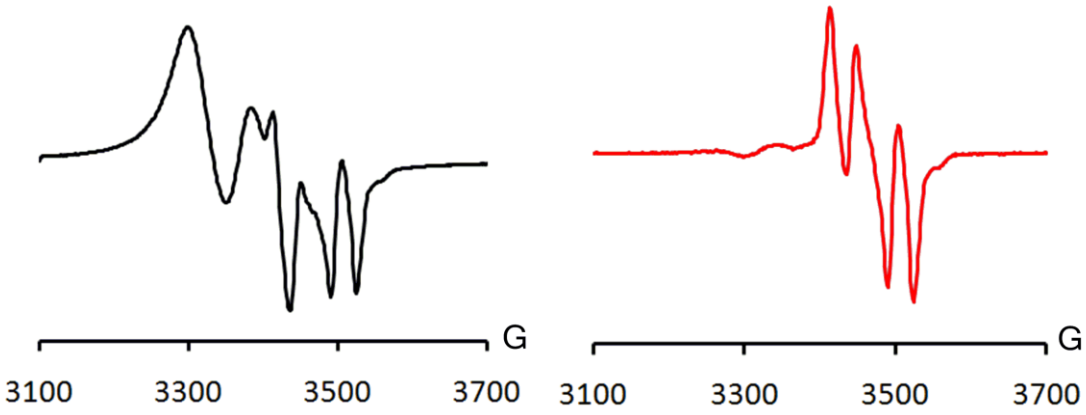

Figure A4.7. RT EPR spectra of crude mixture (left) of stoichiometric reaction between [SiP$^{i\text{Pr}}_3$]Ru(N_2) (**5.4**) and *p*-MeO$C_6H_4N_3$ and after subtraction of **5.4** (right).

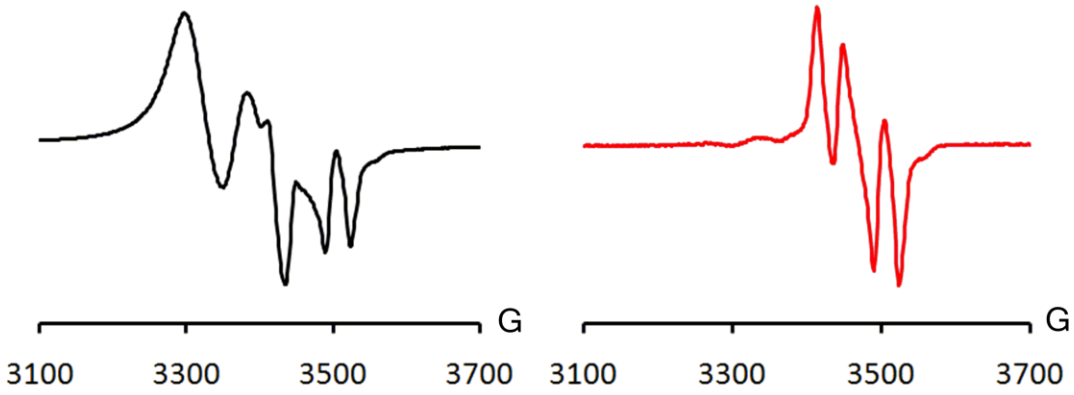

Figure A4.8. RT EPR spectra of crude mixture (left) of stoichiometric reaction between [SiP$^{i\text{Pr}}_3$]Ru(N_2) (**5.4**) and *p*-EtO$C_6H_4N_3$ and after subtraction of **5.4** (right).

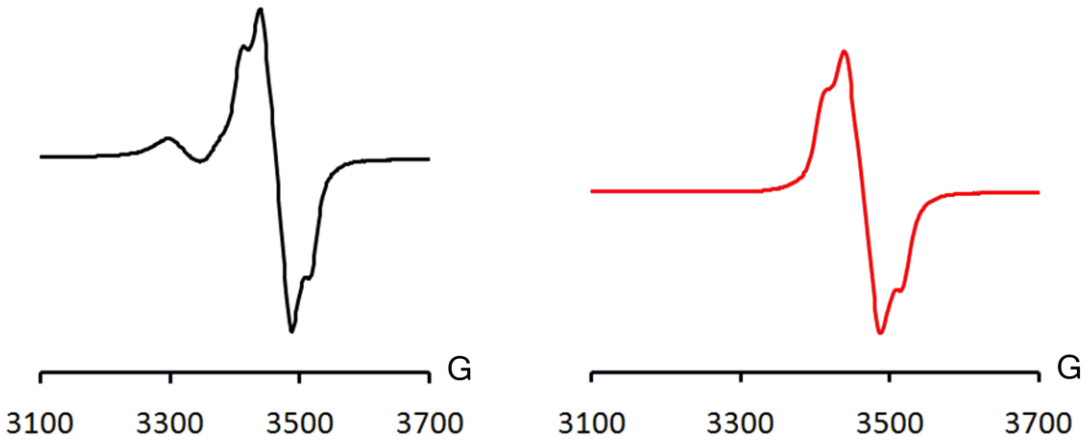

Figure A4.9. RT EPR spectra of crude mixture (left) of stoichiometric reaction between [SiP$^{i\text{Pr}}_3$]Ru(N_2) (**5.4**) and $MeC_6H_4N_3$ and after subtraction of **5.4** (right).

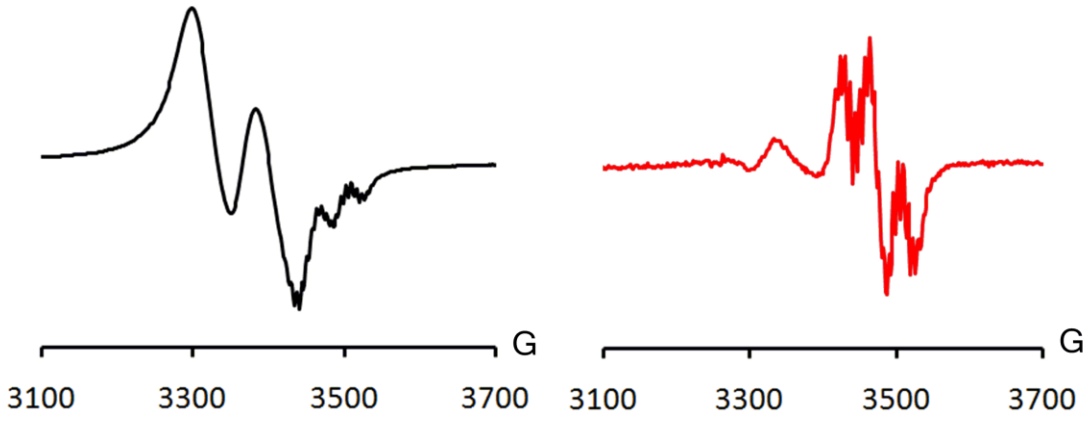

Figure A4.10. RT EPR spectra of crude mixture (left) of stoichiometric reaction between [SiP$^{i\text{Pr}}_3$]Ru(N_2) (**5.4**) and $MesN_3$ and after subtraction of **5.4** (right).

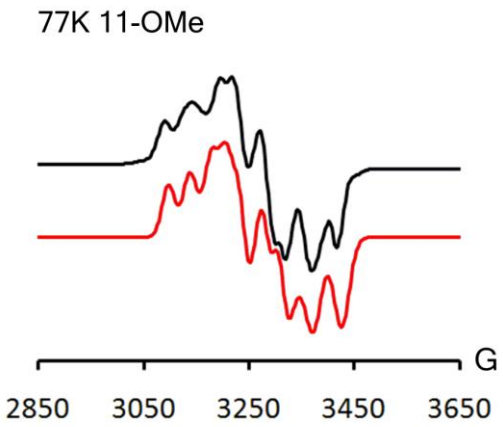

Figure A4.11. 77K EPR spectrum of [SiP$^{i\text{Pr}}_3$]Ru(N_3Ar), Ar = *p*-C_6H_4OMe (**5.11-OMe**).

Experimental parameters; Microwave power, 6.454 mW; microwave frequency, 9.421 GHz; modulation amplitude, 2 G; gain, 5020; time constant, 40.960.
Simulation parameters: g_x = 2.137, g_y = 2.068, g_z = 1.985; For one P atom, $A_x(^{31}P)$ = 240 MHz, $A_y(^{31}P)$ = 210 MHz, $A_z(^{31}P)$ = 150 MHz ; For one P atom, $A(^{31}P)_x$ = 120 MHz, $A(^{31}P)_y$ = 85 MHz, $A(^{31}P)_z$ = 1 MHz; lw =1, HStrain, W_x = 80 MHz, W_y = 70 MHz, W_z = 90 MHz.

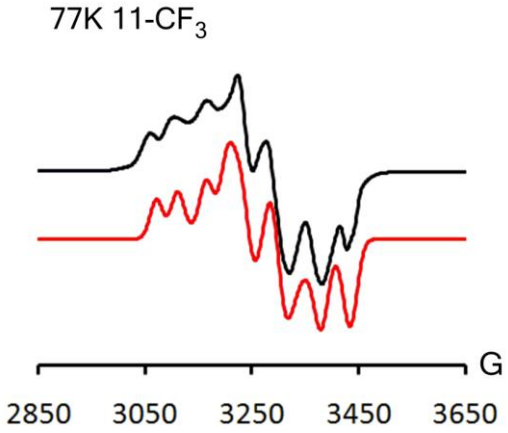

Figure A4.12. 77K EPR spectrum of [SiP$^{i\text{Pr}}_3$]Ru(N_3Ar), Ar = *p*-$C_6H_4CF_3$ (**5.11-CF_3**).

Experimental parameters; Microwave power, 6.423 mW; microwave frequency, 9.442 GHz; modulation amplitude, 2 G; gain, 5020; time constant, 40.960.
Simulation parameters: g_x = 2.15, g_y = 2.063, g_z = 1.988; For one P atom, $A_x(^{31}P)$ = 280 MHz, $A_y(^{31}P)$ = 170 MHz, $A_z(^{31}P)$ = 150 MHz; For one P atom, $A(^{31}P)_x$ = 120 MHz, $A(^{31}P)_y$ = 1 MHz, $A(^{31}P)_z$ = 1 MHz; For one P atom; lw =1, HStrain, W_x = 80 MHz, W_y = 95 MHz, W_z = 80 MHz.

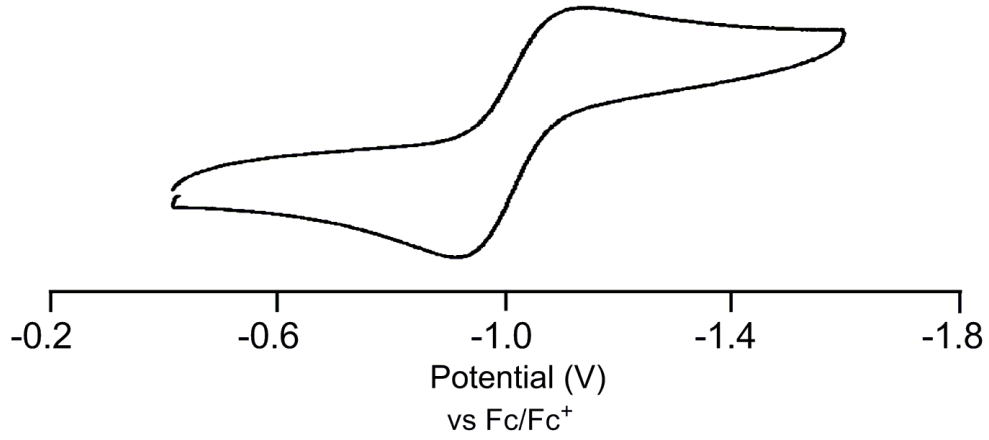

Figure A.13. Cyclic Voltammogram of [SiP$^{iPr}_3$]Ru(NAr), Ar = *p*-$C_6H_4CF_3$, (**5.7-CF_3**).

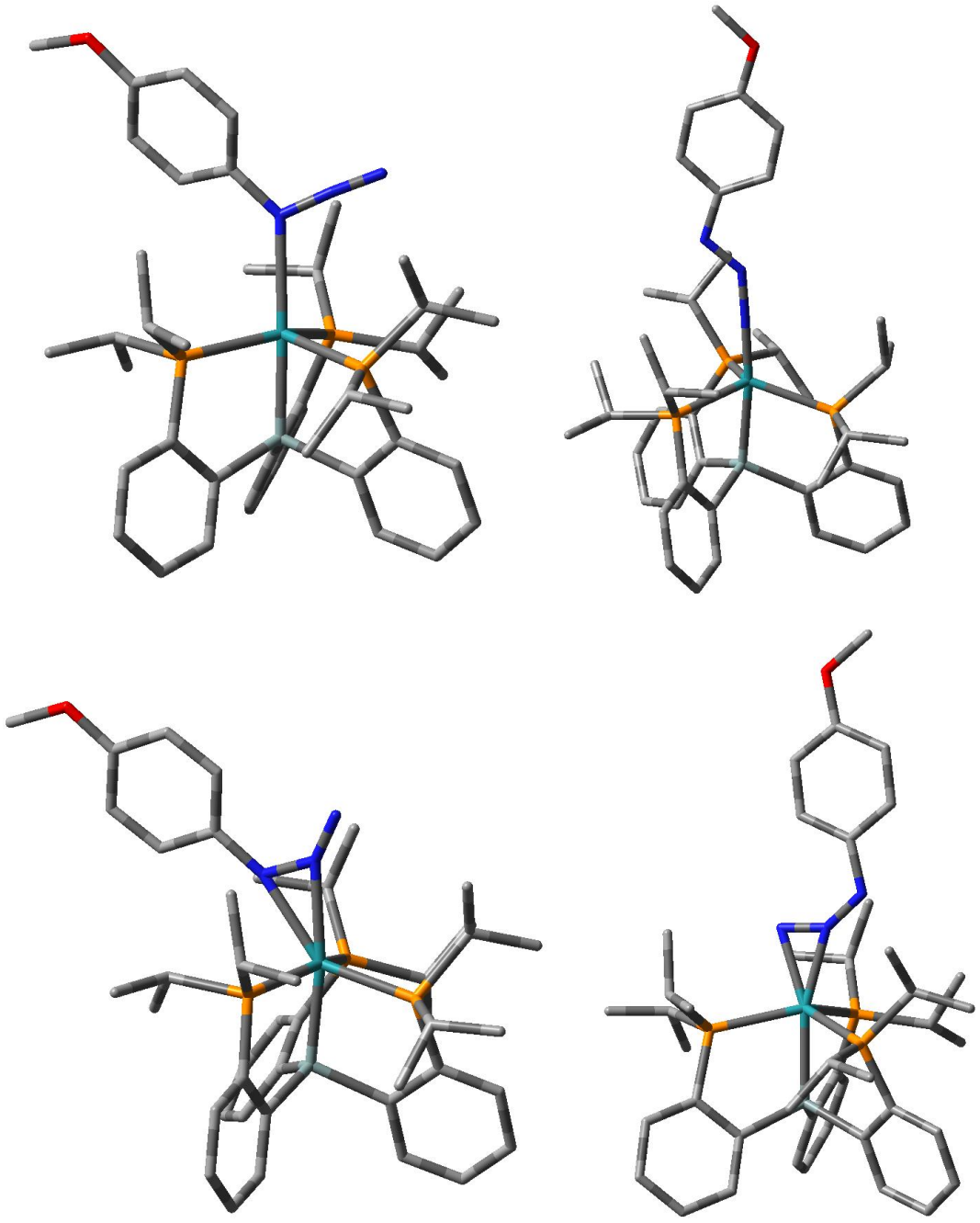

Figure A4.14. DFT optimized structure of γ (top left), α (top right), and η^2 bound azide adducts (bottom), [SiP$^{iPr}_3$]Ru(N_3Ar) (Ar = C_6H_4OMe) (**5.11-OMe**).

Table A4.5. DFT optimized coordinates of γ-bound azide adduct, [SiP$^{iPr}_3$]Ru(N_3Ar) (Ar = C_6H_4OMe) (**5.11-OMe**).

Ru	-0.153974	0.203551	-0.100873
Si	-2.523141	-0.177653	-0.017141
P	-0.502845	-1.425570	-1.884255
P	-0.358877	-0.869265	2.081444
P	-0.995985	2.470239	-0.169713
O	9.255831	1.111878	-0.023372
N	1.778993	0.260050	-0.123079
N	2.975716	0.268469	-0.139428
N	3.889926	-0.645884	-0.292656
C	-3.184424	-0.696089	-1.729743
C	-4.509973	-0.541657	-2.196263
H	-5.276951	-0.153011	-1.528519
C	-4.853645	-0.835250	-3.529594
H	-5.875704	-0.694865	-3.875190
C	-3.862407	-1.287619	-4.421111
H	-4.113056	-1.496006	-5.459021
C	-2.540506	-1.466909	-3.970885
H	-1.791801	-1.810130	-4.680157
C	-2.193638	-1.180651	-2.631223
C	-2.891508	-1.612255	1.190810
C	-4.094037	-2.359876	1.189323
H	-4.883734	-2.107881	0.483073
C	-4.284706	-3.447574	2.060857
H	-5.212338	-4.015373	2.033865
C	-3.262833	-3.800920	2.961849
H	-3.396212	-4.640947	3.640122
C	-2.061930	-3.068146	2.987106
H	-1.294943	-3.357330	3.695192
C	-1.855325	-1.983307	2.101704
C	-3.475899	1.399882	0.499040
C	-4.815665	1.444212	0.951303
H	-5.391774	0.523333	1.027250
C	-5.415681	2.655921	1.342655
H	-6.443148	2.666341	1.700303
C	-4.676837	3.853949	1.284801
H	-5.130821	4.792118	1.596332
C	-3.344721	3.834767	0.831638
H	-2.784573	4.766526	0.808101
C	-2.739659	2.618880	0.439442
C	-0.612136	-3.301695	-1.562667
H	-1.562171	-3.388081	-1.012661
C	-0.729703	-4.172478	-2.838840
H	0.193009	-4.154070	-3.431803
H	-1.562931	-3.865137	-3.478301
H	-0.907854	-5.216870	-2.546313
C	0.503260	-3.844310	-0.640090
H	0.352981	-4.922043	-0.483841
H	0.475969	-3.359482	0.336308
H	1.504038	-3.702275	-1.061274
C	0.660314	-1.254247	-3.359940
H	0.215916	-1.838536	-4.179055
C	0.739239	0.224427	-3.811713

H	1.190531	0.843446	-3.026406
H	-0.247220	0.637294	-4.052830
H	1.368422	0.302884	-4.709236
C	2.077787	-1.819164	-3.098621
H	2.728767	-1.564399	-3.946880
H	2.075572	-2.911007	-3.005348
H	2.539760	-1.405577	-2.195984
C	-0.631193	0.085776	3.710073
H	0.193421	0.812254	3.730831
C	-1.966180	0.865604	3.698948
H	-2.821685	0.179750	3.722220
H	-2.072459	1.503114	2.820673
H	-2.024781	1.504091	4.591825
C	-0.564868	-0.750264	5.014192
H	-0.659935	-0.073696	5.875946
H	0.373463	-1.298666	5.129668
H	-1.395391	-1.463282	5.068237
C	1.262488	-1.827179	2.405593
H	1.610326	-2.016441	1.384475
C	1.242503	-3.193490	3.133636
H	2.264511	-3.599148	3.136769
H	0.603093	-3.922878	2.625055
H	0.919071	-3.117960	4.177908
C	2.318993	-0.882175	3.042376
H	2.132120	-0.706043	4.107727
H	2.362250	0.085485	2.531043
H	3.310776	-1.342228	2.947988
C	-1.066332	3.254532	-1.908473
H	-0.085100	3.007176	-2.341401
C	-1.248288	4.793056	-1.952752
H	-1.279913	5.117559	-3.002448
H	-0.433074	5.340367	-1.468258
H	-2.197060	5.094678	-1.491514
C	-2.158044	2.596909	-2.785068
H	-3.160934	2.841721	-2.413584
H	-2.069755	1.509647	-2.819824
H	-2.079738	2.977972	-3.812910
C	-0.024895	3.787325	0.772710
H	-0.530038	4.747570	0.594720
C	0.003716	3.548194	2.297195
H	0.498560	2.599935	2.533155
H	-1.000731	3.532849	2.733264
H	0.570936	4.354234	2.783675
C	1.419439	3.880860	0.220914
H	1.970021	4.666152	0.757109
H	1.450183	4.123610	-0.847857
H	1.949986	2.933208	0.366213
C	5.208279	-0.150118	-0.217156
C	5.575660	1.208199	-0.007714
H	4.797769	1.958669	0.105970
C	6.921158	1.586563	0.050344
H	7.206932	2.622819	0.209027
C	7.940778	0.622557	-0.098215
C	7.597854	-0.728616	-0.306617
H	8.362322	-1.490755	-0.424834
C	6.243346	-1.102367	-0.364472

H	5.970303	-2.142114	-0.526134
C	10.348308	0.165509	-0.169217
H	10.326353	-0.597898	0.622186
H	11.261391	0.758606	-0.080037
H	10.323847	-0.327506	-1.152036

Table A4.6. DFT optimized coordinates of α -bound azide adduct, [SiP$^{iPr}_3$]Ru(N_3Ar) (Ar = C_6H_4OMe) (**5.11-OMe**).

Ru	-0.071564	-0.164751	-0.195077
Si	1.796941	0.712670	0.814207
P	0.573030	-2.041019	1.271889
P	1.472275	-0.280718	-2.084903
P	-0.851572	2.117706	0.035885
N	-2.057881	-2.270529	-1.715468
N	-1.807338	-3.201166	-2.327088
C	2.029291	-0.000632	2.563109
C	2.691549	0.618827	3.649627
H	3.090670	1.624995	3.533460
C	2.822595	-0.028203	4.891952
H	3.322191	0.469885	5.720581
C	2.299083	-1.325286	5.056839
H	2.396538	-1.839762	6.010620
C	1.639214	-1.956034	3.986925
H	1.242675	-2.955770	4.142821
C	1.483625	-1.302996	2.741065
C	3.378944	0.138024	-0.107502
C	4.676239	0.159554	0.459789
H	4.815401	0.547856	1.467626
C	5.792525	-0.340526	-0.234490
H	6.778452	-0.322327	0.225682
C	5.621698	-0.872876	-1.526311
H	6.475224	-1.265077	-2.075630
C	4.342873	-0.899047	-2.112643
H	4.243657	-1.306131	-3.111236
C	3.211635	-0.410829	-1.414258
C	1.777657	2.621017	0.884794
C	2.877371	3.436641	1.244918
H	3.818148	2.974924	1.540726
C	2.799387	4.840403	1.193718
H	3.660556	5.447401	1.465628
C	1.605180	5.454895	0.770465
H	1.536611	6.539345	0.714150
C	0.498674	4.663300	0.412023
H	-0.408172	5.160095	0.077528
C	0.569282	3.251162	0.467304
C	1.868034	-3.320974	0.675470
H	2.584199	-2.672351	0.151608
C	2.650705	-4.094811	1.764040
H	1.987783	-4.718493	2.380244
H	3.209730	-3.427794	2.425527
H	3.372165	-4.769109	1.279440
C	1.307733	-4.335942	-0.354161
H	2.136886	-4.771151	-0.929435
H	0.609216	-3.884146	-1.065037
H	0.793121	-5.164433	0.148784
C	-0.713755	-3.117232	2.182400
H	-0.143054	-3.874116	2.743507
C	-1.550314	-2.292400	3.193286
H	-2.102747	-1.497713	2.677938
H	-0.939176	-1.824356	3.969209

H	-2.286166	-2.946041	3.683722
C	-1.690263	-3.865720	1.240430
H	-2.292749	-4.572728	1.828979
H	-1.189821	-4.432593	0.452756
H	-2.383893	-3.160749	0.770899
C	1.761137	1.110828	-3.371429
H	0.753646	1.324695	-3.756389
C	2.304769	2.391284	-2.695131
H	3.341838	2.247778	-2.368758
H	1.720058	2.687355	-1.824079
H	2.291074	3.223186	-3.413885
C	2.675618	0.786239	-4.580912
H	2.697393	1.655879	-5.254622
H	2.337490	-0.072482	-5.166872
H	3.706396	0.602608	-4.257421
C	1.063659	-1.779597	-3.189782
H	0.575234	-2.444027	-2.467706
C	2.166224	-2.638793	-3.856879
H	1.688705	-3.487034	-4.370301
H	2.859218	-3.052497	-3.116781
H	2.746150	-2.088150	-4.605295
C	-0.022543	-1.378997	-4.227182
H	0.399976	-0.813854	-5.064713
H	-0.813551	-0.767000	-3.774070
H	-0.489834	-2.283645	-4.637736
C	-1.964856	2.342680	1.580937
H	-2.839991	1.715930	1.360143
C	-2.477326	3.774206	1.874743
H	-3.106872	3.755187	2.776682
H	-3.086115	4.186705	1.061808
H	-1.646479	4.461719	2.071326
C	-1.274119	1.775357	2.843470
H	-0.410825	2.389505	3.128673
H	-0.914838	0.753665	2.686091
H	-1.977658	1.773809	3.689110
C	-1.844686	3.148146	-1.215214
H	-2.039078	4.128352	-0.758174
C	-1.084380	3.390097	-2.536454
H	-0.866261	2.439643	-3.036348
H	-0.140039	3.921418	-2.382450
H	-1.704905	3.992396	-3.215814
C	-3.208995	2.484561	-1.517145
H	-3.774518	3.103297	-2.228345
H	-3.828531	2.356135	-0.622239
H	-3.067028	1.497281	-1.971923
N	-2.246222	-1.257816	-1.013850
C	-3.654555	-1.001618	-0.773077
C	-4.630514	-1.187702	-1.778551
C	-4.039688	-0.541085	0.492813
C	-5.975399	-0.912389	-1.509131
H	-4.342723	-1.535371	-2.768148
C	-5.389410	-0.259921	0.770520
H	-3.283071	-0.415375	1.258373
C	-6.361835	-0.445731	-0.233497
H	-6.740579	-1.045755	-2.267639
H	-5.663112	0.090419	1.760473

O	-7.725499	-0.200864	-0.072484
C	-8.201457	0.283904	1.216500
H	-7.748131	1.252613	1.468855
H	-9.280117	0.402553	1.098580
H	-7.994276	-0.441694	2.015280

Table A4.7. DFT optimized coordinates of (α,β)-N η^2-bound azide adduct, [SiP$^{iPr}_3$]Ru(N_3Ar) (Ar = C_6H_4OMe) (**5.11-OMe**).

Ru	0.037963	0.040541	-0.523882
Si	1.446582	0.235193	1.307733
P	0.321976	-2.389307	0.166460
P	2.064291	0.262706	-1.672576
P	-0.575027	2.260263	0.150511
N	-1.634280	-0.273527	-2.049917
N	-2.008278	-0.251533	-3.202644
C	1.016932	-1.090347	2.592566
C	1.170264	-0.992626	3.995432
H	1.525488	-0.061385	4.433857
C	0.852297	-2.069740	4.842458
H	0.963237	-1.971744	5.920365
C	0.390883	-3.277481	4.284493
H	0.149704	-4.121999	4.926232
C	0.234161	-3.392902	2.891767
H	-0.116101	-4.338389	2.487990
C	0.523111	-2.306431	2.032942
C	3.237013	-0.216448	0.782795
C	4.281929	-0.538738	1.681639
H	4.093125	-0.526024	2.754082
C	5.559574	-0.903385	1.220395
H	6.346868	-1.154236	1.928193
C	5.811631	-0.950232	-0.164631
H	6.794948	-1.234056	-0.533330
C	4.788805	-0.633601	-1.076695
H	5.008143	-0.680761	-2.136999
C	3.498623	-0.276343	-0.616433
C	1.511882	2.017890	1.991173
C	2.408043	2.485535	2.981496
H	3.079203	1.786539	3.478026
C	2.479061	3.849184	3.322443
H	3.181119	4.187021	4.081721
C	1.651088	4.777329	2.662336
H	1.709957	5.835386	2.908164
C	0.744831	4.334781	1.680877
H	0.114479	5.066408	1.181872
C	0.664383	2.964947	1.342165
C	1.867452	-3.423356	-0.322412
H	2.642874	-2.661668	-0.461553
C	2.388801	-4.407227	0.754972
H	1.653476	-5.188894	0.989042
H	2.657912	-3.901403	1.685600
H	3.288576	-4.909468	0.371185
C	1.718495	-4.199181	-1.657192
H	2.700924	-4.597090	-1.947313
H	1.356896	-3.579886	-2.482468
H	1.040323	-5.054063	-1.548965
C	-1.072696	-3.664343	-0.062164
H	-0.613802	-4.634062	0.193652
C	-2.308912	-3.457043	0.847063
H	-2.862589	-2.569733	0.538848
H	-2.063060	-3.357343	1.906956

H	-2.980190	-4.320918	0.735555
C	-1.574019	-3.732688	-1.530679
H	-2.279955	-4.569758	-1.628214
H	-0.778562	-3.884014	-2.262996
H	-2.106878	-2.815592	-1.793372
C	2.749732	1.905488	-2.343466
H	1.896098	2.357538	-2.862859
C	3.198521	2.849149	-1.201632
H	4.099114	2.461466	-0.710746
H	2.436813	2.988792	-0.434769
H	3.443643	3.835622	-1.619489
C	3.919863	1.802681	-3.357425
H	4.159729	2.814379	-3.714775
H	3.688571	1.193718	-4.234032
H	4.824516	1.406620	-2.883132
C	1.877655	-0.828897	-3.218633
H	1.162774	-1.578408	-2.859474
C	3.106586	-1.596775	-3.764434
H	2.774936	-2.247127	-4.586786
H	3.565356	-2.236655	-3.004272
H	3.877674	-0.931682	-4.167699
C	1.150383	-0.058628	-4.354660
H	1.794984	0.686236	-4.833909
H	0.240181	0.432673	-3.998518
H	0.841597	-0.774694	-5.128208
C	-2.099478	2.166225	1.293576
H	-2.866937	1.691829	0.673551
C	-2.650705	3.528226	1.785496
H	-3.501800	3.341070	2.455237
H	-3.017080	4.163328	0.971802
H	-1.900684	4.087331	2.358227
C	-1.847950	1.253594	2.516683
H	-1.108276	1.691970	3.197341
H	-1.494383	0.260793	2.226065
H	-2.785311	1.133297	3.077891
C	-1.100619	3.695962	-0.963003
H	-1.387795	4.521609	-0.297459
C	0.002820	4.221169	-1.905020
H	0.255957	3.469319	-2.659849
H	0.916114	4.505341	-1.372343
H	-0.366688	5.108567	-2.438046
C	-2.344732	3.290151	-1.795289
H	-2.659410	4.137804	-2.419888
H	-3.199199	3.001166	-1.173839
H	-2.116931	2.450689	-2.462529
N	-2.233891	-0.371460	-0.861613
C	-3.643016	-0.345297	-0.787283
C	-4.524190	-0.234498	-1.901745
C	-4.229663	-0.452133	0.501068
C	-5.914422	-0.229812	-1.719560
H	-4.122790	-0.156718	-2.905122
C	-5.620829	-0.447751	0.684243
H	-3.580538	-0.546518	1.365223
C	-6.474378	-0.335271	-0.432795
H	-6.582760	-0.146730	-2.572118
H	-6.019173	-0.535923	1.690697

O	-7.877469	-0.320253	-0.369817
C	-8.507839	-0.441388	0.933487
H	-8.228187	0.392283	1.594270
H	-9.582665	-0.410233	0.741076
H	-8.248024	-1.393829	1.418275

Table A4.8. DFT optimized coordinates of (β,γ)-N η^2-bound azide adduct, [SiP^{iPr}_3]Ru(N_3Ar) (Ar = C_6H_4OMe) (**5.11-OMe**).

Ru	0.047534	-0.185402	-0.197971
Si	-2.310867	0.078066	0.220060
P	-0.028357	0.382073	2.228762
P	-0.484363	1.849514	-1.473998
P	-0.860769	-2.316318	-0.981698
N	2.128994	-0.001492	-0.103216
N	3.138018	0.806052	-0.165610
C	-2.735560	-0.244517	2.048498
C	-4.011430	-0.615826	2.535908
H	-4.836330	-0.758768	1.840312
C	-4.228886	-0.846511	3.906106
H	-5.212296	-1.146856	4.261633
C	-3.162327	-0.700631	4.814894
H	-3.317360	-0.883691	5.875908
C	-1.890022	-0.325406	4.348622
H	-1.081889	-0.223414	5.067800
C	-1.665071	-0.099950	2.970526
C	-2.875018	1.876620	-0.091120
C	-4.090330	2.418966	0.392667
H	-4.767796	1.794665	0.972486
C	-4.430113	3.765335	0.171370
H	-5.363208	4.165845	0.561718
C	-3.550375	4.593656	-0.551269
H	-3.801828	5.636958	-0.729091
C	-2.340092	4.074482	-1.045197
H	-1.685428	4.730880	-1.604955
C	-1.984346	2.724653	-0.810023
C	-3.369090	-1.138015	-0.805174
C	-4.756119	-1.015794	-1.057124
H	-5.304618	-0.159361	-0.668787
C	-5.442361	-1.965627	-1.836297
H	-6.506571	-1.847604	-2.029026
C	-4.744748	-3.062914	-2.378567
H	-5.267407	-3.795904	-2.989099
C	-3.365749	-3.204518	-2.138414
H	-2.840484	-4.048167	-2.579033
C	-2.673522	-2.250271	-1.357886
C	0.019124	2.240360	2.637239
H	-0.754759	2.629191	1.958520
C	-0.382672	2.633679	4.079865
H	0.311324	2.215682	4.821978
H	-1.397123	2.312022	4.333185
H	-0.342795	3.727982	4.178811
C	1.364687	2.924323	2.267422
H	1.183880	3.978875	2.016848
H	1.874985	2.451300	1.423423
H	2.053218	2.910155	3.121125
C	1.189133	-0.425955	3.435886
H	0.908737	-0.039975	4.428997
C	1.021227	-1.966048	3.445320
H	1.268796	-2.378980	2.461038
H	0.007493	-2.279444	3.713566

H	1.714502	-2.401238	4.178812
C	2.683124	-0.084315	3.212030
H	3.266907	-0.515682	4.038051
H	2.885011	0.988068	3.187556
H	3.055726	-0.522665	2.283547
C	-0.964643	1.719088	-3.312972
H	-0.140927	1.147773	-3.764781
C	-2.276173	0.924324	-3.508471
H	-3.136238	1.487877	-3.127220
H	-2.259719	-0.042116	-3.004144
H	-2.440902	0.746949	-4.580624
C	-1.095068	3.065816	-4.070980
H	-1.275853	2.859236	-5.135750
H	-0.201252	3.690948	-4.004156
H	-1.951295	3.641934	-3.701750
C	1.049861	2.969351	-1.484544
H	1.556481	2.666999	-0.563951
C	0.891168	4.507453	-1.424469
H	1.892297	4.953550	-1.335497
H	0.312312	4.826801	-0.550920
H	0.426703	4.929176	-2.323729
C	2.014963	2.551872	-2.627226
H	1.674838	2.888654	-3.612961
H	2.167172	1.467595	-2.653126
H	2.997929	3.000498	-2.436821
C	-0.684284	-3.794699	0.192197
H	0.363534	-3.731173	0.521405
C	-0.925157	-5.193805	-0.428563
H	-0.766672	-5.957883	0.345558
H	-0.246737	-5.423795	-1.256313
H	-1.958406	-5.300397	-0.781954
C	-1.596122	-3.628791	1.430286
H	-2.653947	-3.727170	1.155872
H	-1.461686	-2.660539	1.914545
H	-1.364285	-4.412010	2.165047
C	-0.091870	-2.994821	-2.570861
H	-0.651795	-3.912034	-2.807230
C	-0.248061	-2.030741	-3.767131
H	0.270914	-1.084337	-3.575033
H	-1.297407	-1.812352	-3.990768
H	0.200625	-2.484056	-4.662075
C	1.399050	-3.371481	-2.386573
H	1.778466	-3.812007	-3.319372
H	1.558074	-4.098654	-1.582442
H	2.000653	-2.489214	-2.148794
N	1.902231	-1.218572	0.005718
C	4.435175	0.237825	-0.156018
C	5.492943	1.181198	-0.193958
C	4.777804	-1.143468	-0.125457
C	6.838495	0.784568	-0.200335
H	5.234098	2.236964	-0.218405
C	6.122154	-1.544428	-0.134038
H	3.995554	-1.892410	-0.095886
C	7.156916	-0.590783	-0.170472
H	7.616365	1.541843	-0.229526
H	6.388637	-2.597553	-0.111655

O	8.463882	-1.105025	-0.174657
C	9.572350	-0.166232	-0.209831
H	9.569830	0.491443	0.671663
H	10.474943	-0.781582	-0.204342
H	9.550465	0.447051	-1.12247

Appendix 5: Supplementary Data for Chapter 6

Table A5.1. Crystal data and structure refinement for [$SiP^{iPr}_2S^{Ad}$]FeCl.

Identification code	ayt03	
Empirical formula	C40 H55 Cl Fe P2 S Si	
Formula weight	749.23	
Temperature	100(2) K	
Wavelength	0.71073 Å	
Crystal system	Orthorhombic	
Space group	Pca2(1)	
Unit cell dimensions	a = 15.5224(6) Å	α = 90°.
	b = 14.0036(5) Å	β = 90°.
	c = 17.1234(6) Å	γ = 90°.
Volume	3722.1(2) $Å^3$	
Z	4	
Density (calculated)	1.337 Mg/m^3	
Absorption coefficient	0.680 mm^{-1}	
F(000)	1592	
Crystal size	2.33 x 1.55 x 1.48 mm^3	
Theta range for data collection	2.29 to 33.13°.	
Index ranges	-22≤h≤23, -20≤k≤16, -24≤l≤25	
Reflections collected	57143	
Independent reflections	9936 [R(int) = 0.0400]	
Completeness to theta = 33.13°	99.9%	
Absorption correction	Semi-empirical from equivalents	
Max. and min transmission	0.4328 and 0.3004	
Refinement method	Full-matrix least-squares on F^2	
Data / restraints / parameters	12714 / 1 / 423	
Goodness-of-fit on F^2	1.021	
Final R indices [I > 2sigma(I)]	R1 = 0.0351, wR2 = 0.0853	
R indices (all data)	R1 = 0.0406, wR2 = 0.0887	
Largest diff. peak and hole	1.489 and -0.539 $e.Å^{-3}$	

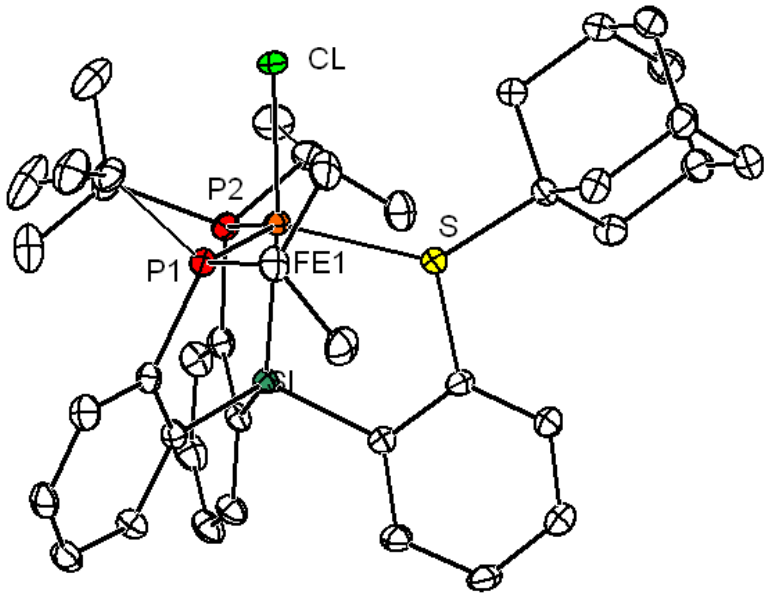

Figure A5.1. Solid-state structure of [SiP$^{i\text{Pr}}_2$S$^{\text{Ad}}$]FeCl.

Table A5.2. Crystal data and structure refinement for {[$SiP^{iPr}_2S^{Ad}$]Fe(N_2)}BAr^F_4 (**6.10**).

Identification code	ayt05	
Empirical formula	C72 H67 B Cl F24 Fe N2 P2 S Si	
Formula weight	1640.48	
Temperature	100(2) K	
Wavelength	0.71073 Å	
Crystal system	Monoclinic	
Space group	P2(1)/c	
Unit cell dimensions	a = 16.5522(7) Å	α= 90°.
	b = 15.7697(6) Å	β = 102.447(2)°.
	c = 28.0672(11) Å	γ = 90°.
Volume	7154.0(5) $Å^3$	
Z	4	
Density (calculated)	1.523 Mg/m^3	
Absorption coefficient	0.446 mm^{-1}	
F(000)	3348	
Crystal size	1.86 x 1.55 x 0.74 mm^3	
Theta range for data collection	2.50 to 24.69°.	
Index ranges	-20≤h≤20, -19≤k≤19, -35≤l≤35	
Reflections collected	78211	
Independent reflections	14505 [R(int) = 0.0573]	
Completeness to theta = 24.69°	99.0%	
Absorption correction	Semi-empirical from equivalents	
Max. and min transmission	0.7336 and 0.4907	
Refinement method	Full-matrix least-squares on F^2	
Data / restraints / parameters	14505 / 120 / 1039	
Goodness-of-fit on F^2	1.022	
Final R indices [I > 2sigma(I)]	R1 = 0.0547, wR2 = 0.1339	
R indices (all data)	R1 = 0.0835, wR2 = 0.1503	
Largest diff. peak and hole	1.249 and -0.746 e.$Å^{-3}$	

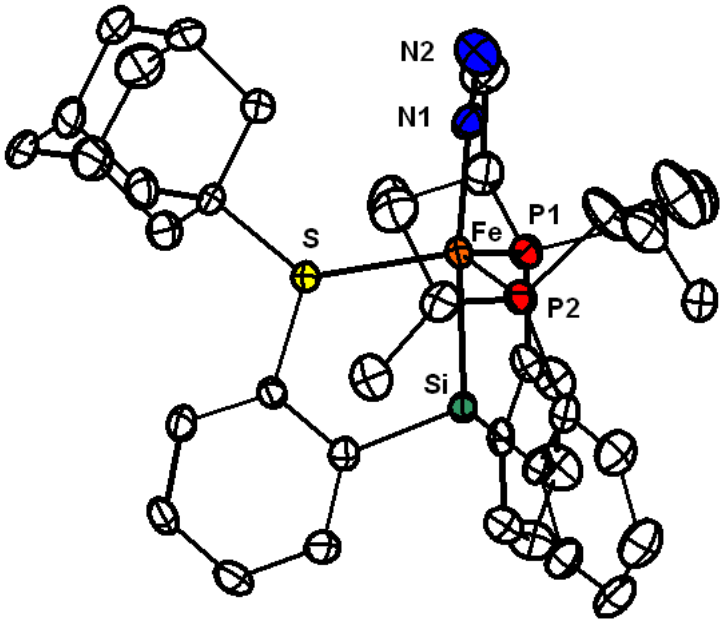

Figure A5.2. Solid-state structure of {[$SiP^{iPr}_2S^{Ad}$]Fe(N_2)}BAr^F_4 (**6.10**). $BAr^F_4{}^-$ anion excluded from figure.

Table A5.3. Crystal data and structure refinement for {[SiP$^{i\text{Pr}}_2$S$^{\text{Ad}}$]Fe(Cp).

Identification code	ayt06	
Empirical formula	C96 H120 Fe2 O P4 S2 Si4	
Formula weight	1701.98	
Temperature	100(2) K	
Wavelength	0.71073 Å	
Crystal system	Tetragonal	
Space group	I-4	
Unit cell dimensions	a = 27.2245(6) Å	α = 90°.
	b = 27.2245(6) Å	β = 90°.
	c = 13.8202(4) Å	γ = 90°.
Volume	10243.2(4) Å^3	
Z	4	
Density (calculated)	1.104 Mg/m^3	
Absorption coefficient	0.474 mm^{-1}	
F(000)	3616	
Crystal size	1.78 x 1.41 x 1.11 mm^3	
Theta range for data collection	2.37 to 26.85°.	
Index ranges	-38≤h≤38, -38≤k≤38, -19≤l≤19	
Reflections collected	78637	
Independent reflections	14977 [R(int) = 0.0639]	
Completeness to theta = 26.85°	99.9%	
Absorption correction	Semi-empirical from equivalents	
Max. and min transmission	0.6213 and 0.4859	
Refinement method	Full-matrix least-squares on F^2	
Data / restraints / parameters	14977 / 99 / 533	
Goodness-of-fit on F^2	1.077	
Final R indices [I > 2sigma(I)]	R1 = 0.0498, wR2 = 0.1376	
R indices (all data)	R1 = 0.0612, wR2 = 0.1455	
Largest diff. peak and hole	1.316 and -0.475 e.Å^{-3}	

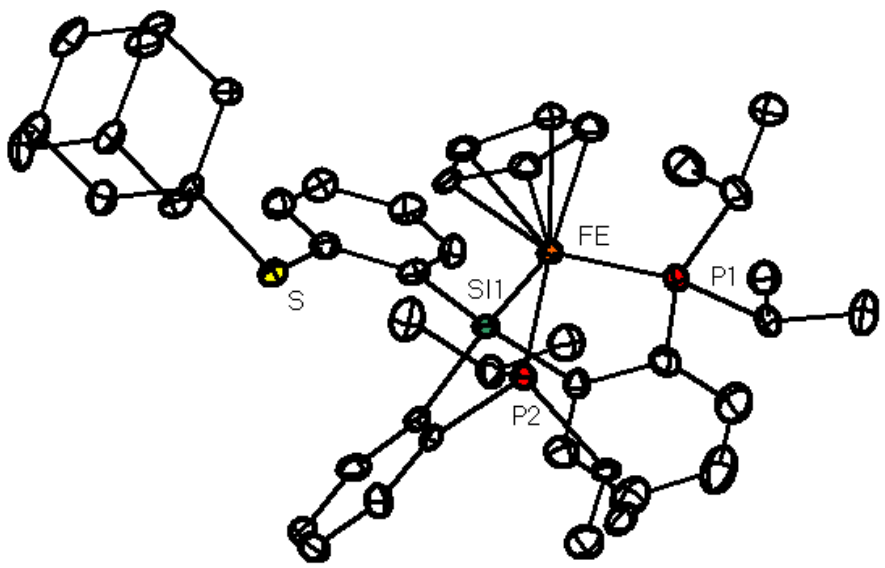

Figure A5.3. Solid-state structure of [SiP$^{iPr}_2$S^{Ad}]Fe(Cp).

Table A5.4. Crystal data and structure refinement for $\{[SiP^{iPr}{}_2S]Fe\}_2$.

Identification code	ayt072	
Empirical formula	C70 H104 Fe2 P4 S2 Si2	
Formula weight	1301.41	
Temperature	100(2) K	
Wavelength	0.71073 Å	
Crystal system	Monoclinic	
Space group	P2(1)/n	
Unit cell dimensions	a = 12.2792(14) Å	α = 90°.
	b = 18.8853(18) Å	β = 90.993°.
	c = 14.6011(19) Å	γ = 90°.
Volume	3385.4(7) $Å^3$	
Z	2	
Density (calculated)	1.277 Mg/m^3	
Absorption coefficient	0.660 mm^{-1}	
F(000)	1392	
Crystal size	0.26 x 0.11 x 0.11 mm^3	
Theta range for data collection	2.40 to 23.70°.	
Index ranges	-15≤h≤14, -23≤k≤23, -18≤l≤16	
Reflections collected	47126	
Independent reflections	6631 [R(int) = 0.2393]	
Completeness to theta = 23.70°	99.3%	
Absorption correction	Semi-empirical from equivalents	
Max. and min transmission	0.8471 and 0.9309	
Refinement method	Full-matrix least-squares on F^2	
Data / restraints / parameters	6631 / 47 / 348	
Goodness-of-fit on F^2	1.613	
Final R indices [I > 2sigma(I)]	R1 = 0.1426, wR2 = 0.3305	
R indices (all data)	R1 = 0.2502, wR2 = 0.3619	
Largest diff. peak and hole	1.881 and -1.043 e.$Å^{-3}$	

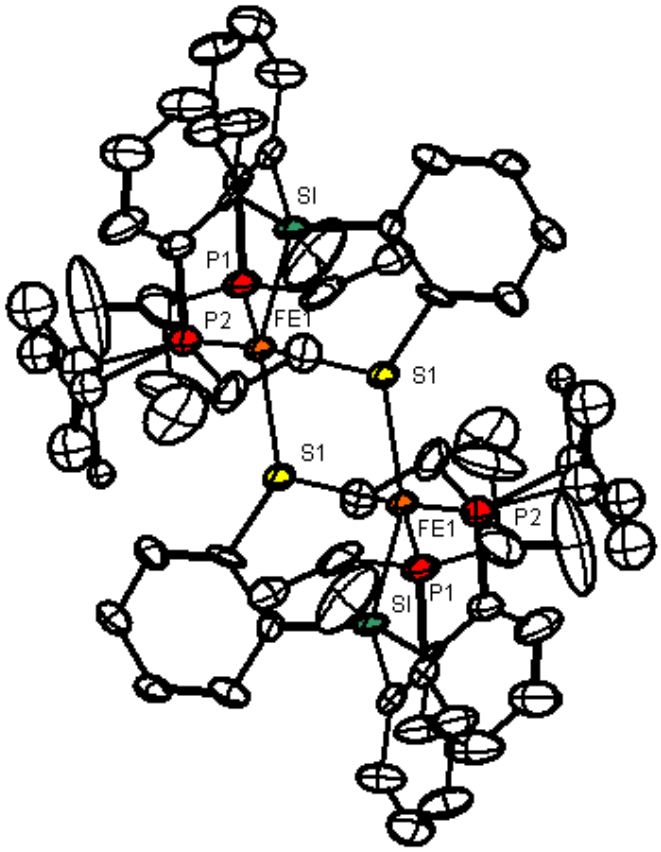

Figure A5.4. Solid-state structure of $\{[SiP^{iPr}{}_2S]Fe\}_2$.

The crystal for this data set was obtained from a reaction of **$\{[SiP^{iPr}{}_2S^{Ad}]Fe(N_2)\}BAr^F{}_4$** with KC_8. The reaction gives multiple products but a crystal was grown from the reaction mixture and the data collected. The crystal was of poor quality, and only connectivity could be determined.

Table A5.5. Crystal data and structure refinement for $[SiP^{iPr}S^{Ad}_2]Fe(H)(N_2)$ (**6.13**).

Identification code	ayt09
Empirical formula	C58 H80 Fe N2 P S2 Si
Formula weight	984.27
Temperature	100(2) K
Wavelength	0.71073 Å
Crystal system	Triclinic
Space group	P-1
Unit cell dimensions	a = 11.0806(5) Å α = 93.7520(10)°.
	b = 13.0186(6) Å β = 105.5990(10)°.
	c = 19.1039(10) Å γ = 91.5850(10)°.
Volume	2645.8(2) $Å^3$
Z	2
Density (calculated)	1.235 Mg/m^3
Absorption coefficient	0.456 mm^{-1}
F(000)	1058
Crystal size	0.21 x 0.19 x 0.11 mm^3
Theta range for data collection	2.22 to 31.45°.
Index ranges	-15≤h≤15, -18≤k≤18, -27≤l≤26
Reflections collected	58590
Independent reflections	16055 [R(int) = 0.0660]
Completeness to theta = 31.45°	99.4%
Absorption correction	Semi-empirical from equivalents
Max. and min transmission	0.9104 and 0.9516
Refinement method	Full-matrix least-squares on F^2
Data / restraints / parameters	16055 / 81 / 654
Goodness-of-fit on F^2	1.161
Final R indices [I > 2sigma(I)]	R1 = 0.0579, wR2 = 0.1453
R indices (all data)	R1 = 0.0926, wR2 = 0.1598
Largest diff. peak and hole	0.931 and -0.418 $e.Å^{-3}$

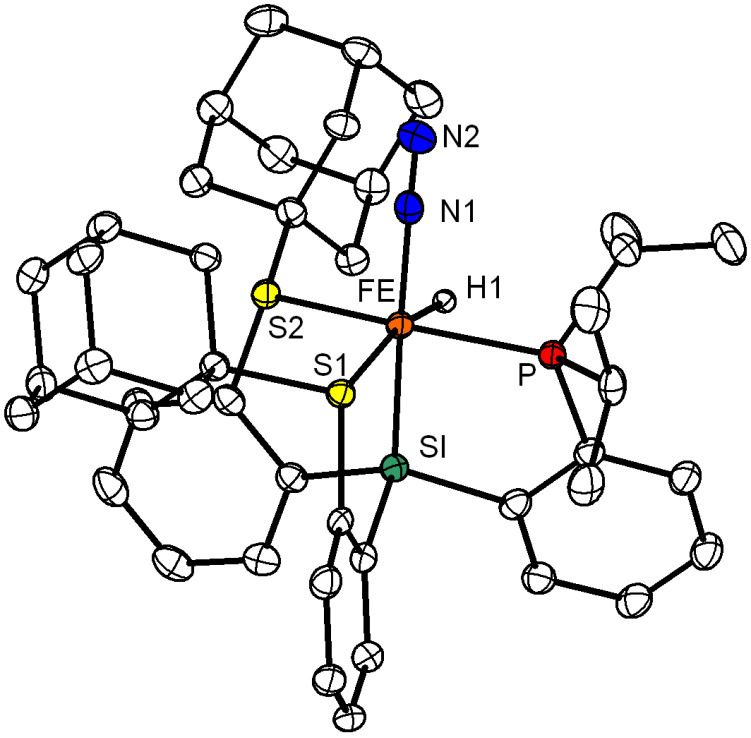

Figure A5.5. Solid-state structure of [SiP^{iPr}S$^{Ad}_2$]Fe(H)(N_2) (**6.13**).

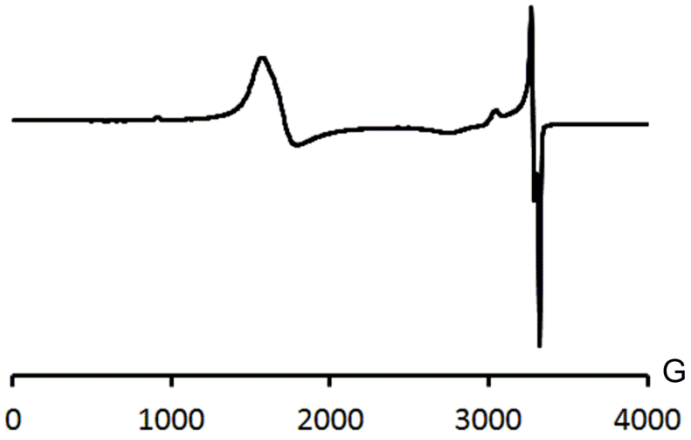

Figure A5.6. EPR spectrum of {[SiP^{iPr}S$^{Ad}{}_2$]Fe}$_2$(N$_2$)}BAr$^F{}_4$ (**6.14**). (20K in 2-MeTHF)

Experimental parameters; Microwave power, 6.439 mW; microwave frequency, 9.376 GHz; modulation amplitude, 4 G; gain, 7960; time constant, 40.960 ms.

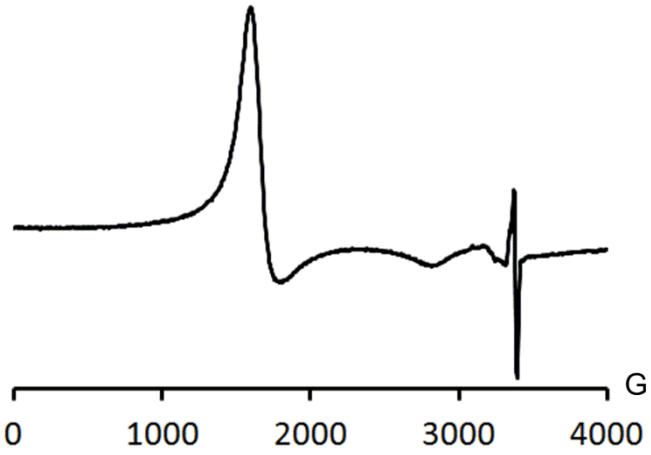

Figure A5.7. EPR spectrum of {[SiP^{Ph}S$^{Ad}{}_2$]Fe}$_2$(N$_2$)}BAr$^F{}_4$ (**6.15**). (20K in 2-MeTHF)

Experimental parameters; Microwave power, 6.439 mW; microwave frequency, 9.377 GHz; modulation amplitude, 4 G; gain, 7960; time constant, 40.960 ms.

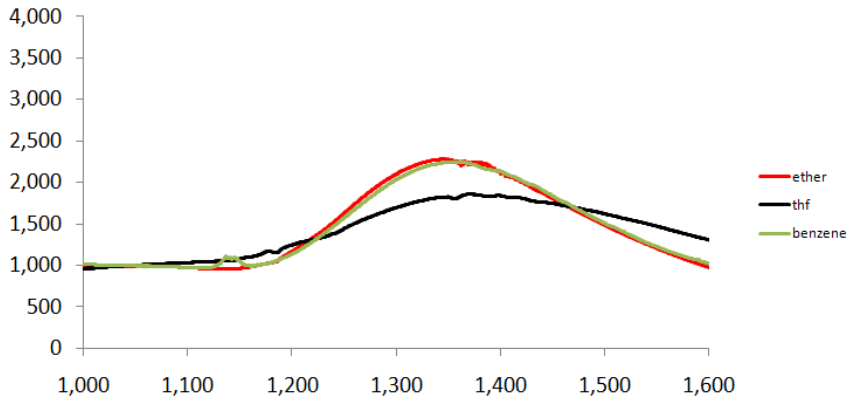

Figure A5.8. NIR spectrum of {[SiP^{iPr}S$^{Ad}{}_2$]Fe}$_2$(N$_2$)}BAr$^F{}_4$ (**6.14**). (ε (M^{-1} cm^{-1}) vs wavelength (nm))

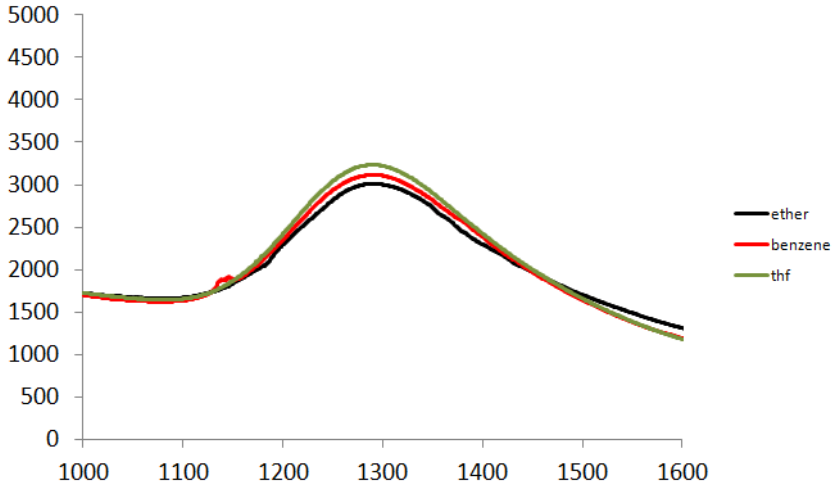

Figure A5.9. NIR spectrum of {[SiP^{Ph}S$^{Ad}{}_2$]Fe}$_2$(N$_2$)}BAr$^F{}_4$ (**6.15**). (ε(M^{-1} cm^{-1}) vs wavelength (nm))

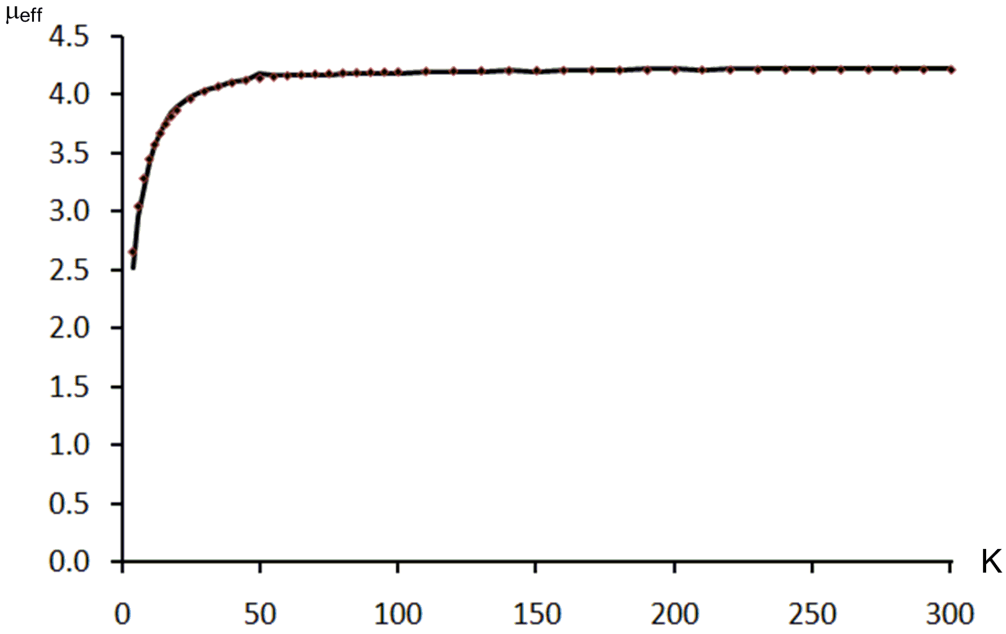

Figure A5.10. SQUID data for **6.14**.

Fitting parameters
Spin = 1.5; g = 2.178; D = $\left|17.3\right|$ cm^{-1}; E/D = 0.05
Field; 5T.